Εθνικό Μετσόβιο Πολυτεχνείο
Σχολή Πολιτικών Μηχανικών
Τομέας Γεωτεχνικής

National Technical University of Athens
School of Civil Engineering
Geotechnical Division

Διπλωματική Εργασία

Μαρκέλλα Κ. Σπάρη

Επιβλέποντες

Καθηγητής Γ. Γκαζέτας

Επικ. Καθ. Ι. Χ. Αναστασόπουλος

ΜΕΤΑΠΛΑΣΤΙΚΗ ΛΙΚΝΙΣΤΙΚΗ ΑΠΟΚΡΙΣΗ ΜΟΝΟΒΑΘΜΙΟΥ ΤΑΛΑΝΤΩΤΗ : ΕΞΑΙΤΗΣΗ ΣΕ ΔΥΟ ΔΙΕΥΘΥΝΣΕΙΣ

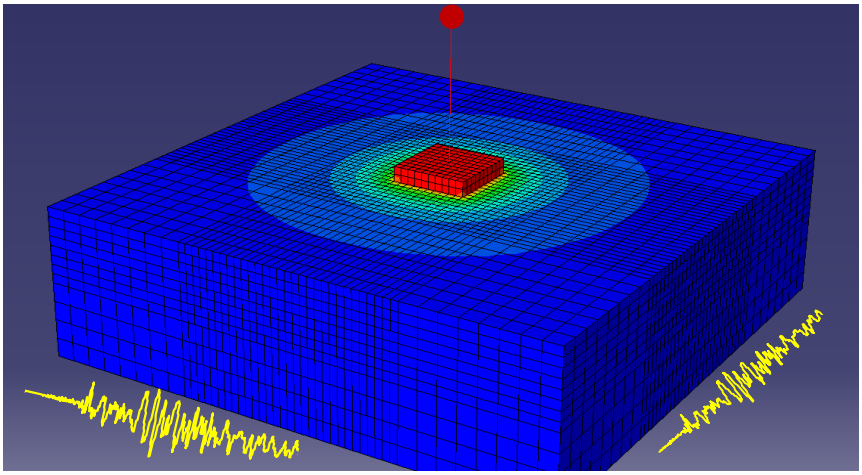

Metaplastic rocking response of SDOF oscillator under bi–directional seismic excitation

DIPLOMA THESIS

Markella K. Spari

Supervisors

Professor G. Gazetas

Assist. Prof. I. Anastasopoulos

Ιούνιος 2012

CONTENTS:

NOTATION :

g	acceleration of gravity
m	structural mass
$N=mg$	vertical load of the foundation
N_u	ultimate vertical load of the foundation
Q	horizontal load of the foundation
M	overturning moment of the foundation
M_{ult}	ultimate moment capacity of the foundation
B	width of a strip or rectangular foundation
b	half-width of a strip or rectangular foundation
J_o	moment of inertia about point O
$p = \sqrt{mgR/J_o}$	frequency parameter
$sgn()$	signum function of ()
$a_c = b/h$	static overturning acceleration
θ	angle of rocking rotation
θ_{max}	amplitude of rocking rotation
$\theta_c = \arctan(b/h)$	critical rocking angle of overturning
$\dot{\theta}$	angular velocity of rocking
δ	horizontal displacement of the deck (drift)
w	vertical displacement of the footing
A_{eff}	effective contact area of the footing
a_g	ground acceleration
a_{FF}	acceleration of the free field
a_m	acceleration of mass
$FS=N_u/N$	safety factor of footing against vertical loading
S_u	undrained shear strength of soil
E	Young modulus of soil
K	elastic stiffness
G	shear modulus of halfspace
ω	frequency of excitation

Introduction

1.1 SOIL-STRUCTURE INTERACTION IN SEISMIC DESIGN PHILOSOPHY

Over the last decades research on seismic soil-structure interaction assumed linear elastic soil behavior and fully bonded contact between footing and soil. In seismic design prevailed the ‘’capacity ‘’design philosophy that admitted yielding and inelastic response in controlled parts of the superstructure and was originally developed on fixed base systems . Plastic hinges in the superstructure allowed energy dissipation and reduced the overall seismic demand with respect to the elastic case. Foundations were designed in such way that they must remain structurally elastic(or nearly elastic) and the transmitted horizontal forces and overturning moments (increased by the ‘’ overstrength” factors would not mobilize bearing capacity soil failure mechanisms on induce sliding at the soil-foundation interface. It was also assumed that only limited uplift (restricted about to the half of the fully bonded contact area) would take place.

However the over-dimensioning of foundations in the name of safety in cases of high seismic demand , is not always a economically feasible decision. In seismic retrofit of existing buildings and bridges, allowing the soil and foundation yielding is often a rational alternative to much more expensive approaches. Thus , increasing the structural capacity of some elements implies that forces transmitted to the foundation would be increased.

In the last 20 years especially after the Northridge 1994 and Kobe 1995 earthquakes, accelerograms have revealed that very substantial ground motions can be expected in near fault zones. Since large ground acceleration levels are associated with even larger spectral acceleration levels would impose enormous ductility demands to structures. Furthermore under such strong seismic excitation it logical that nonlinear inelastic behavior cannot be assumed only at the structure but to the supporting soil as well. The aforementioned considerations articulated the

need for an alternative approach that would account for soil inelasticity. Today, a growing body of evidence suggests that soil-foundation plastic yielding under seismic excitation is not only unavoidable, but may even be beneficial (*Paolucci 1997; Pecker 1998, 2003; Martin and Lam 2000; FEMA 356 2000; Kutter et al. 2003; Faccioli et al. 2001; Gazetas et al. 2003; Gajan et al. 2005, 2008; Mergos and Kawashima 2005; Apostolou and Gazetas 2005; Paolucci et al. 2007; Kawashima et al. 2007; Gajan and Kutter 2008; Chatzigogos et al. 2009; Gerolymos et al. 2008, 2009*).
since soil yielding beneath foundations can be an effective energy dissipation mechanism. However, this benefit may come with the expected costs of excessive transient and permanent deformations. To realistically account for the systems' performance, these consequences of permanent settlement and rotation must be reasonably estimated and accounted for.

Tree types of non-linearity can take place at the soil-foundation level in the case of shallow foundation and can alter the overall structure-foundation response:

(a) Sliding at the soil foundation interface

(b) Seperation and uplift of the foundation from the resting soil

(c) Mobilization of bearing capacity failure mechanisms in the supporting soil.

1.2 OBJECTIVES OF THE STUDY

Our understanding of the earthquake phenomenon has improved significantly during the last years; however, there are many issues that require our attention regarding its effects on the response of structures. Energy released during an earthquake travels in the form of waves. They are measured in the form of two horizontal and one vertical translational acceleration time histories. When we analyze a structure, we generally apply either one assumed or recorded horizontal component along one of the two major axes of the structure. Slender structural systems are more prone to develop high levels of foundation moment even during moderate seismic shaking and the rocking component of motion is predominant. The scope of this study is to shed some light in the meta-plastic response of such

structures in case of multi-component earthquake excitation taking into account non-linear soil-structure interaction.

Non –linear features of soil-foundation systems may be summarized in:

(a) Mobilization of bearing capacity failure mechanisms under cyclic overturning moments. Especially in the vicinity of corner points due to the concentration of vertical stresses and the resulting accumulation of displacements plastification of the supporting soil takes place. (material non-linearity)

(b) Separation from the supporting soil of a footing undergoing rocking oscillations (''uplift'') creating P-δ effects.(geometric non-linearity)

At the same time several issues regarding multi-components seismic response analysis of structures are addressed in this work.

(a) The first issue is related to the rules used to estimate the combined effect of the individual components of earthquakes.

(b) The relative importance of the weak horizontal component compared to that of the strong horizontal component in terms of :

  (i) vertical settlements

  (ii) rotation accumulation

  (iii) horizontal drifts

  (iv) effective contact area

(c) The effect of the second horizontal component for cyclic, long duration sequences of pulses were the ''sinking'' effect (large vertical settlements) prevail.

1.3 OUTLINE OF THE STUDY

The first chapter is dedicated in the fundamental tools to address SSI effects and rocking response of slender structures. Methods of combining the components of earthquake are presented and code provisions are discussed in Chapter 2.

In Chapter 3 the method of analysis, assumptions and modeling details are presented.

Chapter 4 is dedicated in bi-directional static loading of the proposed system and moment interaction diagrams for different factors of safety are produced.

Chapter 5 focuses on the rocking regime of the system's response. Therefore Ricker type pulses are utilized in order to assess the effect of the second horizontal component. Frequency content and intensity are taken ito consideration. Furthermore attempt has been made to investigate the effect of phase difference between the applied excitation components. At the same time the rocking of the foundation is viewed under a holistic 3 dimensional perspective. Moment-rotation , vertical settlement-rotation, drift time histories are examined in both directions.

In Chapter 6 the effect of phase difference is further investigated with the use of sinusoidal pulses.

In Chapter 7 the effect of excitation content investigated with the use of harmonic wavelets of different frequencies.

Chapter 8 is dedicated to the cyclic nature of the earthquake, therefore Tsang[IXA] are employed.

Chapter 9 deals with the true nature of earthquake and for that reason recorded acceleration histories are applied. The scope of this chapter is to illuminate the importance of the second horizontal component on the systems performance, which is often disregarded.

Chapter 10 is dedicated to conclusions and suggestions for further examination.

Literature Review

2.1 SOIL-STRUCTURE INTERACTION

The phenomenon of soil structure interaction can be briefly described as follows: during earthquake shaking the soil deforms under the influence of the incident seismic waves and carries dynamically with it the foundation and the supported structure. The induced motion of the superstructure generates inertial forces that result in dynamic forces and moments that through dynamic pressures at the foundation are subsequently transmitted to the resting soil. Thus, superstructure induced deformations develop in the soil and additional waves emanate from the soil-foundation interface. In response, foundation and superstructure undergo further dynamic displacements which generate inertial forces and vice versa.

Although the above phenomena occur simultaneously and are intrinsically co-evolving it is convenient in sense of conception and computationally to assume the response of the soil-foundation-structure system as superposition of two interaction effects based on the Kausel superposition theorem (Whitman,1972; *Kausel et al.,1978 ; Gazetas and Mylonakis,1998)*:

a) 'Kinematic interaction' referring to the modification of the incident seismic waves (reflections, scattering) due to the presence of a massless foundation-structure. As a result the foundation develops curvatures and bending moments due to its different rigidity in respect to the compliant surrounding soil. No soil mass moves as a rigid body with the foundation. Instead shear and dilational waves emanate from the footing soil interface into the soil, causing oscillating soil deformations at the surface and carrying away some of the input energy. The main consequence of Kinematic interaction is that the foundation input motion is different (usually reduced in short period range) than the free field motion.

b) 'Inertial interaction' referring to the response of the soil-foundation-structure system subjected to excitation by D'Alembert inertia forces induced on superstructure in the presence of an input motion modified by Kinematic interaction and the additional loading imposed to the foundation and the resting soil.

For a linear soil-foundation-structure system the superposition theorem states that the equation of motion for the overall system in its matrix formulation,

$$[M]\{\ddot{u}\} + [K]\{u\} = -[M]\, a_r \qquad [2.1]$$

Can be decoupled in the following differential equations:

$$[M_{soil}]\{\ddot{u}_{kin}\} + [K]\{u_{kin}\} = -[M_{soil}]\, a_r \qquad [2.2a]$$

$$[M_{str}]\{\ddot{u}_{iner}\} + [K]\{u_{iner}\} = -[M_{str}](\{\ddot{u}_{kin}\} + a_r) \qquad [2.2b]$$

Where: {u} is the relative displacement vector of points in the soil or the structure, $\{u_{kin}\}$ and $\{u_{iner}\}$ are respectively the kinematic and the inertial relative displacements, [K] is the stiffness matrix of the system, [M] is the matrix of the system, $[M_{soil}]$ is the mass matrix assuming that only the soil and foundation have mass and $[M_{str}]$ is the mass matrix assuming that only the superstructure has mass. By definition :

$$[M]=[M_{soil}]+[M_{str}] \quad \text{and} \quad \{u\}=\{u_{kin}\}+\{u_{iner}\} \qquad [2.3\ a,b]$$

The analysis of inertial interaction for computational purposes is further decomposed into consecutive independent analytical steps:

b_1) Computation of the dynamic foundation impedances (springs and dashpots)

b_2) Analysis of the dynamic response of the superstructure resting on these springs and dashpots subjected to the kinematic interaction modified input motion of step a)

Although the superposition theorem is exact for linear soil, pile and structure, it can nevertheless be applied to moderately non linear systems. This can be achieved by choosing reduced soil characteristics which are compatible with the free

field strains induced by the propagating seismic waves: this is the basis of the equivalent linear method, pioneered by *Idriss and Seed (1968*). This engineering approximation implies that all the soil non linearities arise from the passage of the seismic waves and that additional non linearities, developed around the edges of a mat foundation or along the piles shafts, are negligible. Experience shows that it is a valid approximation in many situations where large soil instabilities do not occur.

The relative importance that kinematic and inertial interaction have on the response of the structure depends on the characteristics of the foundation and the incoming wave field *(Pecker and Pender,2000).* For some situations, kinematic interaction can be neglected and the second step of the multistep approach can be bypassed. It must be realized however that, if kinematic interaction is thought to be significant, there is no simple means for evaluating it; as a matter of fact, evaluation of kinematic interaction is almost as difficult as solving the complete SSI problem. Obviously kinematic interaction is exactly zero for shallow foundations in a seismic environment consisting exclusively of vertically propagating shear waves or dilatational waves. *Gazetas (1984)* has demonstrated that when the piles are flexible with respect to the surrounding soil, kinematic interaction is significant for small to medium frequencies. During the last decade, numerous solutions for the dynamic impedances of any shape foundations and of piles have been published (*Gazetas, 1990*). They are available for homogeneous soil deposits but also for moderately heterogeneous ones. In addition, simplified methods are available in the case of pile foundations to account for the group effect (*Dobry and Gazetas, 1988*).

Impedance functions represent the frequency-dependent stiffness and damping characteristics of foundation-soil interaction. A synthesis of available numerical solutions for impedance functions is given by Gazetas (1991). Those solutions generally utilize assumptions of foundation rigidity and uniform soil of infinite depth with a fixed hysteretic damping ratio. Under these conditions, the soil profile is referred to as a visco-elastic half-space. Additional formulations are available to account for a specified depth-variable shear stiffness (*Gazetas 1991; Vrettos 1999*), foundation embedment (*Apsel and Luco 1987*), and non-rigid foundations *(Iguchi and Luco 1982*). Dynamic impedance is defined the ratio

between the steady-state force or moment and the resulting displacement or rotation at the base of an associated rigid but massless foundation subjected to harmonic excitation of frequency ω. Impedance functions represent the stiffness and damping characteristics of foundation-soil interaction under cyclic loads. Since dynamic force and displacement are generally out of phase the impedances can be therefore written in complex notation (*Veletsos and Wei 1971; Gazetas 1991*) :

$$K = K_1 + iK_2 \qquad [2.4]$$

Where K_1, K_2 are dynamic impedance functions.

Reissner (1936) motivated by Lamb's studies on *the dynamic Boussinesq problem* (1904) demonstrated that a vertically loaded circular foundation vibrating on a halfspace could be represented with a 1-dof viscoelastic oscillator and showed that the equivalent lumped-mass system parameters should be frequency dependent. To express the vertical displacements u_v he established the displacement functions $f_1(\omega)$ and $f_2(\omega)$

$$u_v = \frac{P_o\, e^{-i\omega t}}{GR}(f_1 + if_2) \qquad [2.5]$$

in which , P_o is the amplitude of the total force applied to the circular contact area, G is the shear modulus of the halfspace and R is the radius of the circular contact area.

According to *Reissner's* findings the dynamic impedance components of eq.2.3 are functions of the vibrational frequency ω as well. *Hsieh (1962)* showed that in analogy with the 1-dof oscillator, the real part in eq.2.3 represents the stiffness and the inertia of the supporting soil whereas the imaginary part describes the absorption of energy within the medium through radiation damping. Combining eq2.3 the complex dynamic impedance of steady state vibration can be written :

$$K = K - m\omega^2 + i\omega C \qquad [2.6]$$

Where: $K = GR\frac{f_1}{f_1^2+f_2^2}$ and $C = -\frac{GR}{\omega}\frac{f_2}{f_1^2+f_2^2}$

The parameters *K* and *C* are the spring and damping terms respectively of the equivalent lumped system, both functions of the frequency of vibration. *Lysmer (1965)* , by multiplying the displacement function $f = f_1 + i f_2$ by a factor 4 / (1 – *v*), obtained a new displacement function $F = F_1 + i F_2$, independent of *v* . By adopting a dimensionless frequency factor , $a_o = \frac{\omega b}{V_s}$, he derived charts of F_1 and F_2 as functions solely determined by α_o.

2.2 ROCKING OF RIGID STRUCTURES

2.2.1 ROCKING ON A RIGID BASE

It was *Milner and Perry* (1881) the first who attempted to quantitatively correlate the intensity of ground motion by studying the overturning of rectangular columns and since then the uplift response and toppling of structures

The modern study of the mechanics of rocking objects are typically attributed to *Housner* (1963) who investigated in depth the rocking behavior of rigid block supported on a rigid base subjected to earthquake shaking uncovering the role of excitation frequency and block size to overturning potential. *Ishiyama* (1982) determined the possible modes of response for a rigid body on rigid floor and established transition criteria from one to another. *Spanos and Koh* (1984) studied in detail the dynamic behavior or rigid block structures subjected to harmonic steady-state excitation developing analytical methods to determine the predominant modes of the system and produce stability diagrams where safe and unsafe regions were identified.

Makris and coworkers (1998,1999,2000,2001) focused on the transient rocking response of rigid blocks under near-source ground shaking idealized as trigonometric pulses and derived the acceleration amplitude needed for overturning. In their study the parameters that control overturning (pulse acceleration and frequency content, block size and slenderness and the sequence of pulses) were identified. Using linear and non linear analysis they uncovered that under cycloidal

pulse excitation, a free standing rigid block may overturn either after one impact or without impact at all. I t was shown that a safe region emerges between the two modes, in other words while the block overturns for a certain level of shaking, it counter-intuitive remains standing for an increased amplitude.

2.2.1.1 DEFINITION OF PROBLEM AND EQUATIONS OF MOTION

Consider two different systems of rigid structures, with fairly similar rocking behavior, resting on rigid soil subjected to horizontal shaking. Both can pivot around the center of rotation, O and O', when set in motion. Depending on the value of ground acceleration the systems may translate with ground, slide , rock or slide-rock. *J.Zhang and N.Makris* showed that the required coefficient of friction in order to avoid sliding is an increasing function of the acceleration under the assumption that the coefficient of friction was sufficient to maintain solely rocking and prevent sliding at all times.

For relatively small amplitudes of ground acceleration, provided that the moment of inertia force ($ma_g b$) does not exceed gravitational moment (mgb) systems remain in full contact with base and translate with it.

If the overturning moment reaches the critical value (mgh) uplifting occurs setting the system on rocking motion. Under static conditions, once uplift is initiated the system overturns with no impact. Thus the critical acceleration for uplift equals the minimum acceleration required to overturn the block. Derived from the equilibrium equation,

$$a_{stat,over} = \tan\theta_c = \frac{b}{h} \qquad [2.7]$$

In contrast, for the case of dynamic base excitation reaching α_c doesn't imply overturning of the system. This is attributed to the transient oscillatory nature of earthquake excitation. Meaning that although the system exceeds the stability moment the reversal of loading direction causes it to rotate towards the opposite direction.

Under a positive horizontal base acceleration αg the rigid structure will initially rotate with negative rotation θ < 0 and provided it doesn't overturn it will rotate positively θ > 0 and so forth.

Apostolou et al. (2003) investigated the role of the vertical component of ground acceleration and showed it's insignificant effect on rocking response.

Neglecting vertical acceleration, the equation of motion of a standing rigid structure with mass *m* are:

$$I_o\ddot{\theta} + mgR\sin(-\theta_c - \theta) = -m\alpha_g R\cos(-\theta_c - \theta)\,,\ \theta < 0 \qquad [2.8a]$$

$$I_o\ddot{\theta} + mgR\sin(\theta_c - \theta) = -m\alpha_g R\cos(\theta_c - \theta)\,,\ \theta > 0 \qquad [2.8b]$$

Where: $= \sqrt{b^2 + h^2}$, I_o is the moment of inertia about it's pivot point (O and O') and the angle $\theta_c = \arctan\left(\frac{b}{h}\right)$

The above equations can be expressed in the compact form:

$$\ddot{\theta}(t) = -p^2\{\sin[\theta_c\,\mathrm{sgn}\theta(t) - \theta(t)] + \alpha_g(t)\cos[\theta_c\,\mathrm{sgn}\theta(t) - \theta(t)]\} \qquad [2.9]$$

Where the frequency parameter $p = \sqrt{mgR/J_O}$ is in rad/sec.

The frequency parameter *p* is not the eigenfrequency of the system, but is a measure of the dynamic characteristics of the system and plays an important role in its rocking response and overturning potential *(Spanos & Koh, 1986; Makris & Roussos, 2000; Apostolou et al., 2003*). The frequency parameter *p* is a decreasing function of the block size, hence the larger the block the smaller the value of *p,* and vice versa. For rectangular blocks, $p_{block} = \sqrt{\frac{3g}{4R}}$, whereas for a rigid 1-dof oscillator $p_{1-dof} = \sqrt{\frac{g}{R}}$. The 1-dof oscillator corresponds to a rigid rectangular block if $R_{1\text{-dof}} = 4/3\ R_{block}$ (*Apostolou et al., 2006*).

When a rigid body is rocking back and forth about its pivot point loses a part of its kinetic energy when impacts the rigid base even under purely elastic impact

conditions. So, the angular velocity after the impact is a fraction to its velocity prior to impact. This fraction is known in the literature as the coefficient of restitution and its upper bound neglecting energy loss during impact is :

$$r = (1 - \frac{3}{2}\sin^2 \theta_c)^2 \qquad [2.10]$$

Actually, some additional energy is lost depending on the nature of the materials and the impact surface.

The ultimate moment that can be applied to the foundation is $M_u = mgb = ma_g h$, thus the maximum acceleration that can be developed at the mass of the structure is $a_c = tan\vartheta_c$. This peak value is applied instantaneously, and as soon as the rigid body uplifts, a nonlinear behavior is revealed even for elastic impact conditions. Once rocking commences the moment-rotation relationship enters a softening behavior due to P-δ effects and the system's stiffness decreases until $\vartheta = \vartheta_c$. Thus, the oscillation period of the system during the rocking motion is not constant and depends on the angle of rotation.

2.2.3 OVERVIEW OF KEY-RESPONSE PARAMETERS

Under static conditions only the slenderness of the structure is a decisive factor for it's response. Under dynamic excitation though, due to the profoundly non-linear nature of rocking motion, the systems response is sensitive to a number of parameters that reflect the dynamic characteristics of the structure and the excitation. The most important factors are:

(a) The slenderness of the structure

The slenderness of the structure ϑ_c defines the initiation of rocking for a certain amplitude of excitation. The critical acceleration for uplifting for a block

resting on a rigid base depends only on the slenderness of the structure and the uplift criterion is $\alpha_{crit} > \arctan(\theta_c)$. Therefore , less slender blocks are in general more stable and experience smaller rotations. Hence the minimum energy loss during impact depends only on the slenderness of the structure and as a result, structures with large aspect the vibrations decay is faster than for less slender ones.

(b) The size of the block and the excitation frequency

The rocking response of a block is a sensitive function of both its size and excitation frequency content. It has been recognized by researchers (*Kirpatrick, 1927; Housner,1963; Makris et al,2000, 2001; Apostolou et al,2003, 2007; Gerolymos et al, 2005*) that increasing the size of the structure or the frequency of excitation while maintaining the same slenderness (ratio of base width and height) can play a beneficial role in terms of overturning prevention. In other words small structures display larger rotations and overturn more easily than larger ones of equal slenderness. Apparently, the existence of long duration excitation pulses plays a predominant role in the uplifting response and the overturning potential. Given a slenderness ratio and kept the f/p ratio constant the rocking response of a structure remains unchanged. Hence the rocking response of a system is defined by the excitation frequency in reference to frequency parameter *p*.

(c) Asymmetry and detailed sequence of excitation pulses

Makris and Zhang (2000) identified the the effect of asymmetry and exact sequence of pulses by uncovering outstanding differences in the rocking response under variant trigonometric pulses, including the half sine, one sine, and one-cosine pulses.

This work was extended by *Gerolymos et al (2005*) who demonstrated the effect of asymmetric pulses by employing Ricker type excitations to investigate the overturning potential.

2.4 ROCKING ON COMPLIANT SOIL

For some cases the model of a rocking body on a rigid base may be a reasonable approach, however in most civil engineering applications the foundations rest on a soil medium which may experience substantial deformations by transmitted loads. Due to soil compliance , a rigid structure may sustain rocking motion without uplift at low amplitudes or rotation. For sufficiently large amplitudes of rotation though, separation of the footing from underlying soil is unavoidable and the response alternates between full contact and uplift phases. For very stiff soil the systems experiences uplift at very low rotation levels and it's response resembles the rigid base one (full contact phase diminishes). On the contrary, for soft soil conditions, the deformations of the supporting soil especially near edges are significant. This acts as an energy dissipation mechanism and as a result uplift is limited and motion attenuates faster. Furthermore large deformations under the foundation are accompanied with bearing capacity mechanisms and plastification zones that further act as dissipative mechanisms. Apart from the aforementioned parameters that affect rocking response for the compliant soil case the following ought to be mentioned:

(a) The visco-elastic soil properties G, v and ξ considering an homogenous and isotropic medium

(b) The structural weight N in reference with the ultimate load capacity N_u

(c) The presence of bedrock at shallow depth or a stiff crust underneath the foundation.

Compliant soil modeling approaches can be sub-divided in the following categories:

- Winkler-based models
- Continuum models
- Macro-element type models
- Direct methods (i.e., finite elements or finite differences)

2.2.2.1 WINKLER-BASED MODELS

One of the most commonly used method is the beam-on-non-linear-Winkler –foundation (BNWF) approach. The BNWF generalization originates from *Winkler's* (1867) representation of a soil medium, which assumes a system of discrete , closely spaced independent linear elastic springs. This approach implies that the lateral reaction in the soil q per unit length at a given distance along the foundation is only related to the foundation deflection δ at that distance. BNWF methods combine springs, dashpots and gap elements allowing one to capture the salient features of rocking foundation including uplift and yielding of soil even settlement.

Wiessing (1979) used elastoplastic springs coupled with Coulomb slider elements and sub-divided the foundation in finite strips. Elastoplastic springs were considered to have only compression capacity while Coulomb slider elements captured the uplift of the foundation.

Phycharis and Jennings (1983) and *Koh et al.*(1986) used the well known Winkler model, assuming that the springs cannot have tension capacity and to capture the uplift behavior of a rigid block resting on elastic soil produced analytical expressions for each phase of the response (uplift, full contact). In details Phycharis considered to types of soil modelling using springs 1) a simple symmetric two-spring model and 2) the distributed Winkler system of springs. Non-linearity at the foundation interface was considered through three mechanisms 1) viscous dampers 2) elastic-perfectly plastic non linear springs and 3) an impact mechanism allowing dissipation of energy at every impact.

At the same time *Yim and Chopra* (1984,1985) evaluated the rocking response of single-degree of freedom (sdof) and multi-degree of freedom (mdof) systems, supported on a two-spring dashpot base. A primary conclusion of this work was that foundation flexibility and uplift have little effect on higher modes of vibration.

Nakaki and Hart (1987) used discretely placed vertical elastic springs with viscous dampers at the base of a shear wall structure to illustrate the beneficial role of uplift during an earthquake. This study unveiled that uplift resulted in a significant

reduction of ductility demands on the structure for some cases. This is primarily because the rocking response shifts the period range of a system to greater values than the fixed base one. It was also noticed that the frequency content of the excitation has an important effect on the ductility demands of the system.

More recent work on non-linear Winkler-based models can be attributed to *Chen and Lai* (2003), *Houlsby et al*.(2005), *Eivan and Cassidy* (2005*), Harden et al.*(2005), *Allotey and El Naggar* (2003, 2007). The latter in order to overcome the shortcomings of earlier studies derived analytical equations for the moment-rotation response of footings resting on elasto-plastic Winkler foundation neglecting P-δ effects though. Their study unveiled how the inverse safety factor is related to the predominant type of foundation response (uplift, mobilization of bearing capacity failure mechanisms or both).

Raychowdhurry and Hutchinson (2009) evaluated the performance of a non-linear Winkler-based shallow foundation model using centrifuge testing results. The same authors in (2010) evaluated the performance of seismically loaded shear-walls on nonlinear shallow foundations and their numerical study indicates that the force and drift demands to the shear-wall reduce significantly, when nonlinear foundation behavior is realized, while permanent settlement is well below the permissible limit.

Pender (2007) ,while comparing the response of linear elastic springs to continuum elastic medium,analyses that the ratio of rotational to vertical stiffness is found to decrease as the load of the footing increases, in other words the decrease of rotational stiffness is more rapid than the vertical stiffness decrease and probably that non-linear behavior of soil can be better captured by spring-models.

2.2.2.2 ELASTIC/INELASTIC CONTINUUM MODELS

Pender (2007) however highlights some of the deficiencies and arising from the Winkler-based models. In order to study vertical and rotational stiffness of shallow foundations he compares the response of linear elastic springs to continuum elastic medium. The conclusion is that, for given dimensions of a rigid rectangular foundation on ground surface the rotational stiffness for a bed of springs is less than that resting on a continuous elastic medium. The underlying reason is that for the spring foundation there is no interaction between neighboring springs and this concerns particularly edges.

Apostolou and his co-workers (2003,2007) used finite element analysis to treat the soil as an elastic continuum and simulate stress distributions under the foundation in a more realistic way than the linear distribution proposed by Winkler models. They showed that in the very stiff soil, the uplift regime dominates whereas as soil compliance increases the rocking motion exhibits a more full contact rotational vibration behavior, reducing the contribution of uplift to the total rotation. The role of soil compliance may vary from beneficial to detrimental depending on the excitation period (T_E) in reference to the rocking period of the system(T_R).

Apostolou and Gazetas (2007) investigated in detail the rocking response of shallow foundations on compliant soil. Using a macroscopic model which takes into account the non-linearities, they produced analytical equations for the moment, the rotation and the vertical displacement for both elastic and inelastic soil.

2.2.2.3 MACRO-ELEMENT TYPE MODELS

Macro-element type models are intended to capture near field behavior. A macro-element replaces the soil-foundation system and is located at the base of the superstructure. Thus the footing and the underlying soil are considered as either a 3-dof (2D analysis) or a 6-dof (3 translational and 3 rotational-3D analysis) element that can describe the force-displacement behavior of a point of the footing in the vertical, horizontal and rotational sense.

The evolution of macro-element concept follows a parallel path with the advances of plasticity theory. *Roscoe and Schofield (1956,1957*) based on the theory of plasticity dealt with the non linear behavior of shallow foundations. *Nova and Montrasio (1991*) developed a model for strip footings on sand under monotonic loading with an isotropic-hardening elasto-plastic law. The basic idea is firstly to represent the bearing capacity of the foundation under combined loading as a closed surface (*Salencon (1972);Butterfield(1980*)). This ultimate surface is the yield surface of the plasticity model and evolves in space according with the appropriate hardening law (isotropic,anisotropic). Secondly the displacements of the footing are calculated using a plastic flow rule calibrated by experimental data.

Pedretti(1998) and *Prisco (2003)* extended this idea to cyclic loading introducing bounding surfaces for unloading and reloading. *Paolucci* (1997) based on Nova and Montrasio formulation introduced macro-element models for earthquake engineering. *Le Pape et* al.(1999) and Le Pape and Sieffert (2001) developed a macro-element in a thermodynamic framework. *Cremer et al.(2001,2002*) first introduced the foundation uplift in the macro-element formulation dealing seperately with uplift and plasticity. *Wolf (1988)* and *Wolf and Song* (2002) deal with the uplift behavior differently. While Cremer modifies the initial stiffness matrix, Wolf uses the equivalent foundations dimensions (reduced due to uplift) to recalculate the static spring coefficient.

Paolucci (2007) introduced a degradation rule for the foundation stiffness parameters to account for the reduction of soil contact area under successive cycles of loading. Cremer's plasticity model was further modified by *Grande et al (2008)* and *Chatzigogos et al.(2009,2010*). In the work of the latter the ultimate surface of the foundation is obtained as a combined result of different non-linear mechanisms (plasticization, uplift, sliding).

2.2.2.4 DIRECT METHODS

Direct methods employ finite element or finite differences applications where boththe structure and the foundation-soil system are modeled [e.g., *Tan, 1990; Butterfield & Gottardi, 1995; Taiebat & Carter, 2000; Gourvenec, 2007; Anastasopoulos et al., 2009; 2011*]. Since this study is based on FEM direct method some aspects of FEM modeling are thoroughly discussed in the following chapter

2.3 FOUNDATION BEARING CAPACITY

INTRODUCTION

One of the prime issues in the design of a shallow foundation is to estimate the ultimate bearing capacity under combined vertical, horizontal and moment loading. Consequently, extensive analytical and experimental research has been conducted in the field. *Poulos et al.(2001*) have reviewed the most significant findings on foundation analysis and have presented a variety of equations for estimating the ultimate capacity under combined loading.

Bearing capacity failure of shallow foundations occurs when the supporting soil fails in shear. This may involve either a general failure mechanism or a punching shear failure. The former is a sudden, catastrophic type of failure and is common in soils that exhibit brittle stress-strain behavior. The latter can be seen in soils that exhibit compressible, plastic stress-strain behavior and is accompanied by progressive downward movement or punching of the foundation into the underlying soil.

2.3.1 BEARING CAPACITY UNDER VERTICAL LOAD

The static bearing capacity of a shallow foundation under central, vertical loading was initially calculated by *L.Prandtl* in 1921. Provided that soil medium is described as homogenous half-space under un-drained conditions ($c=S_U$, $\varphi=0$) the ultimate reaction stress p_u is:

$$p_u = (\pi+2)\, S_u \qquad [2.11]$$

Terzaghi (1943) introduced the general bearing capacity factors N_c, N_γ, N_q to calculate the bearing capacity of a soil described by strength parameters c and φ as follows:

$$p_u = cN_C + \frac{1}{2}B\gamma N_\gamma + qN_q \qquad [2.12]$$

where: γ is the unit weight of soil , B is the width of a rectangular footing and q is the overburden pressure.

Notably for a cohesive soil under undrained conditions $N_c = \pi+2$ and $N_\gamma = 0$. If the overburden pressure is neglected Terzaghi's solution leads to Prandtl's.

Meyerhof (1953) and *Vesic (1975)* have derived expressions of the ultimate capacity accounting for the foundation shape and load eccentricity and inclination introducing several loading factors.

2.3.2 BEARING CAPACITY UNDER COMBINED LOAD

Bearing capacity factors have been established in common engineering practice as a simple way to estimate the ultimate loading of a shallow foundation. However in some cases of eccentric inclined loads the empirical capacity factors may not provide reliable safety margins. The accuracy of ultimate bearing capacity is crucially important for foundation that undergo large lateral and moment loading as offshore structures (*Ukritchon et al.1999; Bransby and Randolph, 1997*)

In this respect, as mentioned earlier in the macro-element section, much research has been focused in the development of failure criteria for general planar loading conditions (N,Q,M). Following the reasoning initiated by *Salencon (1972)*

and *Butterfield and Ticof (1980*) and endorsed by experimental work *(Houlsby and Martin,1993; Gottardi and Butterfield,1995; Gottardi et al,1999; Houlsby and Puzrin,1999; Martin and Houlsby,2000,2001; Houlsby and Cassidy,2002; Cassidy et al,2005; Bienen et al, 2006*) , it has been found that for any foundation there is a unique closed surface in the generalized loading space N, Q, M containing all possible combinations of loads that could cause the foundation's failure. Hence this surface outlines a failure envelope representing the bearing capacity of the foundation under combined loading. It is described by the following function *f*:

$$f(N,Q,M) = 0 \qquad [2.13]$$

The failure envelope is independent of load path and encompasses all the possible combinations of loads which could impose only elastic deformations. It is also unrelated to soil characteristics (e.g. cohesion, homogeneity) and footing geometry (*Gottardi and Butterfield,1994; Taiebat and Carter,2002).*

Gottardi and Butterfield (1994) used experimental data to derive the analytical solution and showed that the failure loci in the N-M and N-Q plane can be represented by parabolic curves. For the H-M plane bearing capacity stands an eccentric ellipse.

$$Q = t_h \, x \, (N_u - N) \qquad [2.14]$$

$$M/B = t_m \, x \, (N_u - N) \qquad [2.15]$$

Where t_h (t_m) is the slope of the N-Q (N-M) parabola at the intersection points with the horizontal axis and x is the N/N_u ratio.

Houlsby and Puzrin (1999) utilized the lower bound theorem to produced a closed-form expression of the failure envelope in the M-N plane of strip footings on udrained cohesive soil :

$$\frac{N}{A} = (\pi + 2) S_U \, (1 - 2\frac{M}{NB}) \qquad [2.16]$$

2.3.3 CALCULATION OF N-M FAILURE LOCUS FOR WINKLER MODELLING

Under combined vertical, horizontal and moment loading foundation failure may also occur due to horizontal shear failure of soil (sliding) or excessive rotation (overturning). Slender structures are more vulnerable to the latter. A compliant soil under a rocking foundation, due to the combined earthquake loading and the additional loading from the cyclic response of the structure, undergoes significant plastic deformation. Particularly when uplift initiates due to accumulation of vertical stresses under the supporting edge inelastic behavior and even mobilization of bearing capacity failure mechanisms is often unavoidable even for moderately soft soils. There are two distinct types of overturning failure uplift and soil yielding. The dominant parameter that controls the interplay between those two during rocking is the vertical load N to ultimate vertical capacity N*u* ratio expressed as $x=N/Nu$. That was uncovered by *Allotey and El Naggar (2003*) who investigated the rocking response of footings on elasto-plastic Winkler and produced analytical moment-rotation expression for co-existing uplift and yield. For relatively heavy foundations ($x>0.5$) the soil yielding precedes the footing uplift. When relatively light foundation ($x<0.5$) are considered we have the inverse; uplift is followed by soil yielding.

Apostolou and Gazetas (2007) derived the analytical solution of the M-N plane failure :

$$M_u = Nb\,(1 - N/N_u) \rightarrow M_u = Nb\,(1 - x) \qquad [2.17]$$

The failure envelope calculated by this equation and the analytical curves for uplift-yield onset are plotted in figures.

More recently *Gourvenec (2007)* compares ultimate limit states under vertical (V), moment (M) and horizontal (H) loading of rectangular footings with varying breadth-to-length aspect ratios (B/L) with predictions for plane-strain conditions. Footing-soil interfaces are considered either unable to sustain tension or with unlimited tensile resistance. Results are presented as failure envelopes in VH, VM and VMH load space and a closed-form expression is proposed to describe the shape of the normalized VMH envelope:

$$(\frac{h}{h*})^2 + (\frac{m}{m*})^2 = 1 \qquad [2.18]$$

Where : $m*$ and $h*$ are functions of v (=N/N_u) and are derived from the shape of the failure envelopes in V-H and V-M plane respectively

$$h* = \frac{0.25 - (v - 0.5)^2}{0.25}$$

$$m* = 4(v - v^2)$$

2.15 illustrates the three dimensional failure envelope for *VMH loading* for a zero-tension interface. Failure envelopes in planes of *HM* at *v = 0.25*, *v = 0.5*, and *v = 0.75* for footings unable to sustain tension with varying aspect ratios are shown in figure 2.15. In normalized load space, the envelopes fall in a reasonably tight band and can be approximated as an eclipse symmetrical about *H* = 0, proving that their shape is independent of the footing aspect ratio.

2.4 MULTICOMPONENT EARTHQUAKE EXCITATION AND COMBINATIONAL RULES

INTRODUCTION

Following catastrophic damages in some recent earthquakes around the world, seismic analysis and design procedures in general and codified seismic design procedures in particular, have changed significantly. In the last 20 years especially after the Northridge 1994 and Kobe 1995 earthquakes, accelerograms have revealed that very substantial ground motions can be expected in near fault zones

There is no doubt that now we have a better understanding of the earthquake-related issues. The computational power has also increased significantly to address many advanced topics. We can now analyze and design seismic load-tolerant structures for given or assumed earthquake time histories. Unfortunately, at present if ever, we cannot predict with certainty the future earthquake time histories and this is the weakest point in the seismic design of structures. The question remains whether we can assure safety of structures designed following the current design practices against any future earthquakes.

Energy released during an earthquake travels in the form of waves. They are measured in the form of two horizontal and one vertical translational acceleration time histories. Although, earthquakes can cause rotational excitations (*Clough and Penzien, 2003*), we do not measure them and they are completely ignored in the analysis. In addition, the potential direction of the epicenter of an earthquake excitation is generally overlooked by the civil engineering profession.

Thus, earthquake resistant design must consider the structural response to the simultaneous action of three translational components of ground motion: two in the horizontal plane and one in the vertical direction. A structure is usually analyzed for the two horizontal components of ground motion applied along the structural axes , sometimes as mentioned before, ignoring or overlooking the potential location of the epicenter of the earthquake with respect to a specific site.

Although it is generally assumed that these components are of the same intensity, in reality they are not, and their combined response depends on the incident angle (the angle between the ground motion components and the structural

axes). Standard practice is to determine separately the three peak responses of the structure that are due to each component of ground motion—with the horizontal components applied along the structural axes—and combine these peak responses according to one of the multi-component combination rules:

(1) the Simplified Square-Root-of-Sum-of-Squares (SRSS)- rule,

(2) the 40%-rule per Newmark ,

(3) and the 30%-rule per Rosenblueth and Contreras.

2.4.1 LITERATURE REVIEW

Penzien and Watabe (1975) proposed that the three components of an earthquake were uncorrelated along the principal axes. They are generally denoted as the principal components. The major principal axis is horizontal and directed towards the epicenter, the intermediate axis is horizontal and perpendicular to the major component, and the minor principal axis is vertical. The critical response could be obtained when these components are applied.

Wilson and Button (1982) presented a simple method to determine the critical angle of structures with respect to the epicenter without considering any correlation between the horizontal ground motion components. *Smeby and Der Kiureghian (1985*) observed that, for response spectra analysis of linear structures, when the two horizontal principal components are not along the structural principal axes, the effect of correlation is small and that if the two horizontal components have identical or nearly identical intensities, then the effect of correlation disappears. *López and Torres (1997)* also proposed a method to estimate the critical angle of incidence.

Newmark (1975) and Rosenblueth and Contreras (1977) were among the first to propose combination rules. They proposed the *Percentage Rule*, which approximates the combined response as the sum of the 100% of the response resulting from one component and a percentage (λ) of the responses resulting from the other two components.

To combine the two horizontal components, *Newmark (1975)* suggested λ to be 40% and *Rosenblueth and Contreras (1977)* suggested λ to be 30%. More recently, many other studies attempted to combine the seismic responses due to two or three components *(Correnza and Hutchinson, 1994; Wilson et al., 1995; De Steffano and Faella, 1996). Wilson and Suharwardy (1995)* concluded that the Percentage Rule could underestimate the design forces in certain members.

For modal analysis, *Der Kiureghian (1981)* and *Wilson et al. (1981)* proposed the Complete Quadratic Combination (CQC) rule to combine modal responses due to a single seismic component. *Smeby and Der Kiureghian (1985)* proposed an extension of the CQC rule, known as the CQC3 rule, to combine modal responses due to the three seismic components. *Smeby and Der Kiureghian (1985*) and *Lopez and Torres (1996)* verified the application of the CQC3 rule by considering building-type structures with a rectangular geometry. *Menun and Der Kiureghian (1998)* extended these studies by considering more complex three-dimensional curved bridge structures subjected to two horizontal components. They compared the results of the CQC3 rule with those of the SRSS, the *30%* (λ = 0.3), and the *40%* (λ = 0.4) rules and examined the shortcomings of these three rules. *López et al. (2001)* conducted a similar study to combine the two horizontal components with a range of one-story systems with symmetrical and unsymmetrical plan, and two multi-story buildings. *Hernández and López (2003)* extended the work of *López et al. (2001)* by considering the effect of the vertical component.

Most of the previous studies on combination rules were limited to elastic analysis applied to simplified plane concrete frames connected by rigid diaphragms and only a few stories high.

Nonetheless the response of reinforced concrete elements under bi-axial loading has concerned numerous analytical and experimental studies. It is well known that interaction phenomena between axial and lateral forces influence strength and ductility demand of a structural system. As an example, for columns of framed buildings, the variation in axial force results in modifying yielding conditions, which may lead to smaller bending capacity and, then, to a greater ductility demand. Moreover, for framed structures, interaction phenomena may work against the

activation of the intended strong column - weak beam dissipation mechanism, since the reduction in column strength can modify the resistance hierarchy among structural members. The outcome of such studies is usually presented in the form of interaction diagrams.

This study is an attempt to address the multi-component nature of the earthquake and the ductility demands on structures accounting for soil-structure interaction and the non-linear behavior of the soil. More particularly a slender structure (bridge pier) with given dimensions that is susceptible to rocking undergoes by-axial loading (static, dynamic) and it's performance is evaluated in terms of accumulated vertical and rotational displacements, total drift and effective contact area.

2.4.2 DEFINITION OF THE PROBLEM

Seismic motion is described by two uncorrelated horizontal components along its principal directions **1** and **2** and oriented at an angle relative to the reference axes x and y of the structure; ϑ is defined as the seismic incident angle . Components of the ground motion along any other set of axes, for example, along structural axes x and y, are correlated. The principal components of ground motion are characterized by pseudo-acceleration design spectra with identical shape: $\mathbf{A(T_n)}$ and $\boldsymbol{\gamma}\mathbf{A(T_n)}$ are the design spectra for the ground motions along the major and minor principal axes, respectively, where the spectrum intensity ratio is $\gamma \leq 1$ and T_n is the natural vibration period of a single-degree-of-freedom system.

The response quantity **r** that can be expressed as a linear combination of the structural displacements. The peak value of this response due to the simultaneous application of the two seismic components **1** and **2** depends on the incident angle and is given by the **CQC3**-rule :

$$r(\theta) = \{ \left[(r_x)^2 + \left(\gamma\, r_y\right)^2 \right] \cos^2\theta + \left[(\gamma r_x)^2 + r_y^2 \right] \sin^2\theta + 2(1-\gamma^2) r_{xy} sin\theta cos\theta \}^{\frac{1}{2}}$$

[2.19]

where r_x and r_y are the peak values of r due to a single component of ground motion, defined by the spectrum **$A(T_n)$** applied first along the x- and then along the y-direction, respectively.

The responses r_k (k =x, y), are give n by the **CQC**-rule:

$$r_k = \left\{ \sum_i \sum_j \rho_{ij} r_{ki} r_{kj} \right\}^{1/2} \qquad [2.20]$$

Where r_{ki} is the peak response , taken with the respective algebraic sign , due to the vibration mode i, and ρ_{ij} is the modal correlation coefficient for modes i and j. The term r_{xy} in equation is a cross-term of the modal responses that contributes to r_x and r_y :

$$r_{xy} = \sum_i \sum_j \rho_{ij} r_{xi} r_{yj}$$

The critical response r_{cr} , defined as the largest of the responses r(θ) for all possible seismic incident angles θ , is given by :

$$r_{cr} = \left\{ (1+\gamma^2) \left(\frac{r_x^2 + r_y^2}{2} \right) + (1-\gamma^2) \sqrt{\left(\frac{r_x^2 + r_y^2}{2} \right) + r_{xy}^2} \right\}^{1/2} \qquad [2.22]$$

The critical response occurs when the incident angle is equal to the critical angle:

$$\theta = \theta_{cr} = 0.5 \, tan^{-1} \left\{ \frac{2 r_{xy}}{(r_x^2 + r_y^2)} \right\} \qquad [2.23]$$

2.4.3 OVERVIEW OF COMBINATIONAL RULES

The Simplified-SRSS-rule:

According to this rule, specified in two regulatory documents [,], the combined response is given by:

$$r_e = \left(r_x^2 + r_y^2\right)^{1/2} \quad [2.25]$$

Note that the above equation is a special case of Equation (4), obtained by setting γ=1. We denote Equation (5) as the Simplified-SRSS-rule because it is a simplified version of the general SRSS-rule that will be presented later.

The 30%-rule:

This rule was first developed by *Rosenblueth and Contreras* and is specified in several regulatory documents [1; 5–7]. Based on the assumption that the two horizontal components are uncorrelated Gaussian processes of equal intensity (γ=1) it gives the following equation for the combined response:

$$r_e = \max\{0.3\,r_x + r_y, r_x + 0.3r_y\} \quad [2.26]$$

The larger of the two estimates is to be used for design.

The 40%-rule:

Originally proposed by *Newmark* and adopted in various codes , this rule assumes equal intensity (γ=1) for the two horizontal components and generally is a more conservative estimate of the combined response:

$$r_e = \max\{0.4\,r_x + r_y, r_x + 0.4r_y\} \quad [2.27]$$

The SRSS-rule:

This rule determines the Square-Root-of-the-Sum-of-the-Squares of the individual responses considering the different intensities of the two uncorrelated horizontal components. This rule is:

$$r_e = \max\left\{\sqrt{r_x^2 + \left(\gamma r_y\right)^2},\ \sqrt{(\gamma r_x)^2 + r_y}\right\} \quad [2.28]$$

Observe that Eq. 2.28 is a special case of Eq.2.19 setting θ=0◦ and θ=90◦ gives the two estimates in Eq. 2.28.

2.4.4 CODE PROVISIONS

When we analyze a structure, we generally apply either one assumed / predicted or recorded horizontal component in a specific way or two components along the two major axes of the structure, sometimes ignoring or overlooking the potential location of the epicenter of the earthquake with respect to a specific site. These practices calculate the loads in a conservative way, satisfying the intent of the professional design guidelines.

INTERNATIONAL BUILDING CODE (IBC-2003) :

The conservatism may depend on the code being used and the country where the code originates. In International Building Code (2003), several methods with different degrees of sophistication have been suggested by including the equivalent lateral force procedure and several types of dynamic analysis procedures (modal response spectra analysis, linear time-history analysis, and nonlinear time-history analysis). The code also identifies the minimum requirements that need to be satisfied before applying a particular method.

In accordance with Article 1620.2.10 of the IBC code: “The direction of application of seismic forces used in design shall be that which will produce the most critical load effect in each component. The requirement will be deemed satisfied if the design seismic forces are applied separately and independently in each of the two orthogonal directions.” Later, in Article 1620.3.2 for the design of common structures with various plan irregularities belonging to Seismic Design Category C and D, IBC states that the critical direction requirement of Section 1620.2.10 will be deemed satisfied if: “One hundred percent of the forces in one direction is added to the 30 percent of the forces in the perpendicular direction. The combination requiring the maximum component strength shall be used. Alternatively, the effects of the two orthogonal directions are permitted to be combined on a square root of the sum of the squares (SRSS) basis. When the SRSS method of combining directional effects is used, each term computed shall be assigned the sign that will result in the most conservative result.”

GREEK ASEISMIC CODE (EAK-2000)

In accordance with the Greek Aseismic Code (EAK 2000, 3.5.3) for simultaneous structural action of the horizontal seismic loads Fi along the principal directions x, y of the building as well as that of the vertical seismic loads , the probable extreme values A_{ex} of any response variable A are calculated by the relation:

$$A_{ex} = \pm\sqrt{A_x^2 + A_y^2 + A_z^2} \quad [2.29]$$

Where Ax , Ay , Az are the values of the said variable (with their sign) for independent static loading of the building along the directions under consideration, x, y and z, respectively.

The probable value B_A , simultaneous to A_{ex} , of another response variable B is calculated by using the relation:

$$B_A = \frac{A_x}{A_{ex}} B_x + \frac{A_y}{A_{ex}} B_y + \frac{A_Z}{A_{ex}} B_z \quad [2.30]$$

where B_x , B_y , B_z are the values of variable B (with their sign) for independent static loading of the building along the directions under consideration, x, y and z, respectively.

Alternatively, instead of the previous methodology, dimensioning by using the least favorable of the following combinations of static loadings is permitted:

$$F = \pm F_x \pm \boldsymbol{\lambda}\cdot F_y \pm \boldsymbol{\mu}\cdot F_z \quad [2.31]$$

$$F = \pm \boldsymbol{\lambda}\cdot F_x \pm F_y \pm \boldsymbol{\mu}\cdot F_z \quad [2.32]$$

$$F = \pm \boldsymbol{\lambda}\cdot F_x \pm \boldsymbol{\mu}\cdot F_y \pm F_z \quad [2.33]$$

Where $\boldsymbol{\lambda} = \boldsymbol{\mu} = 0.30$. In these symbolic relations, F_x , F_y and F_z represent the vectors of seismic loads along directions x, y and z and F represents the “resultant” seismic loading.

In the usual case of ignoring the third vertical component of the earthquake the third combination is omitted and $\boldsymbol{\mu}$ is taken equal to 0 in the first two.

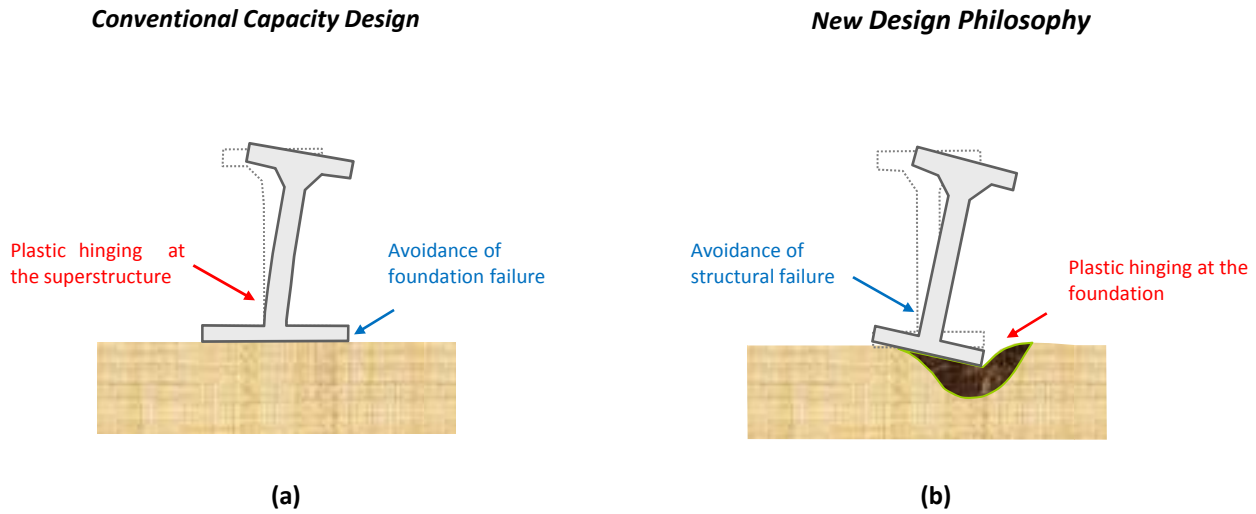

Figure 1.1. (a) Conventional Capacity Design compared with **(b)** New Design Philosophy introduced in Anastasopoulos et al. [2010].

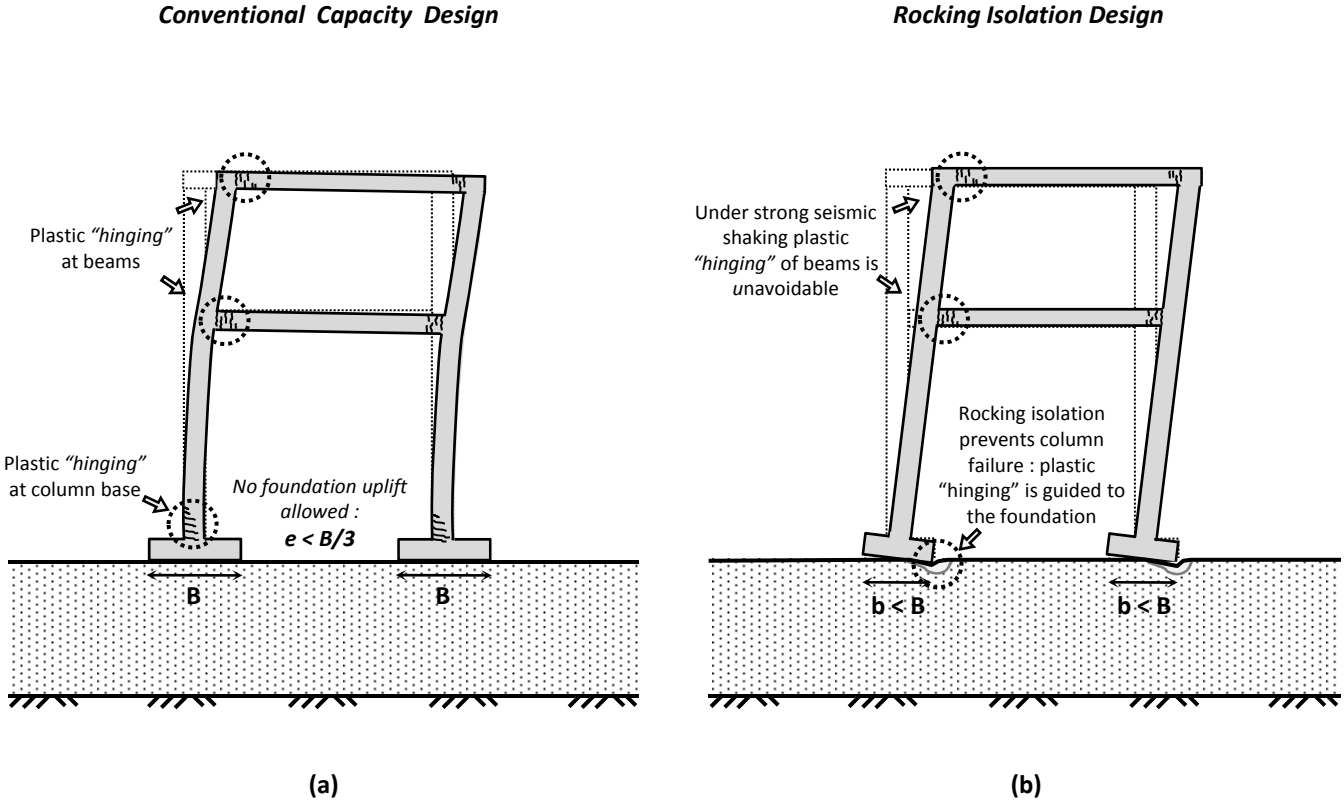

Figure 1.2. (a) Conventional Capacity Design compared with **(b)** Rocking–Isolation Design introduced in Gelagoti et al. [2010].

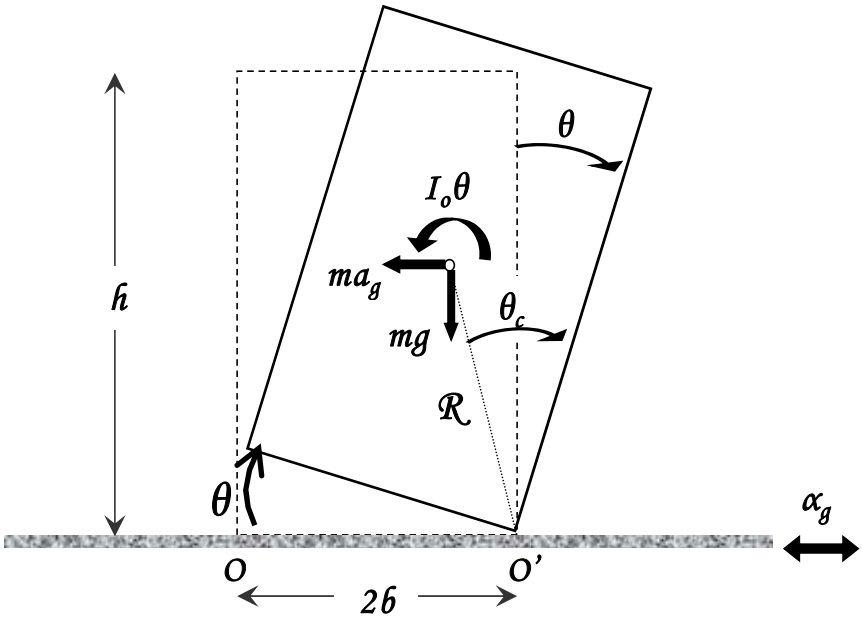

(a)

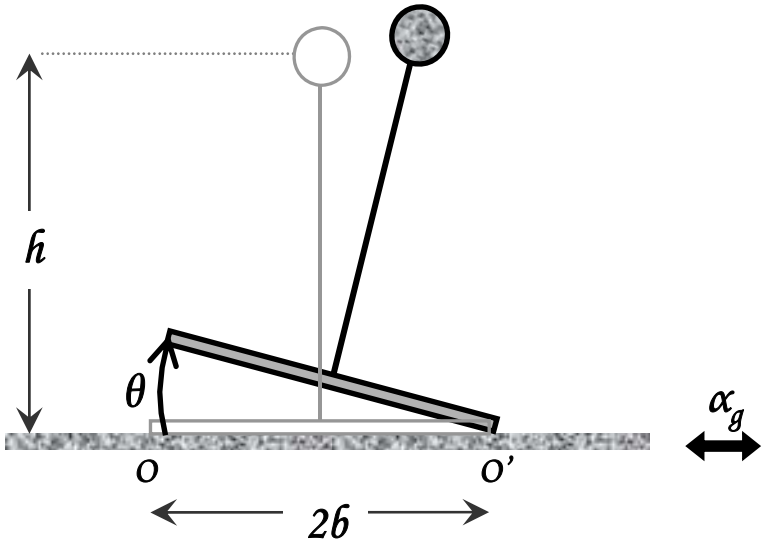

(b)

Figure 1.3. (a) A rectangular rigid block **(b)** a rigid 1-dof oscillator rocking on a rigid base.

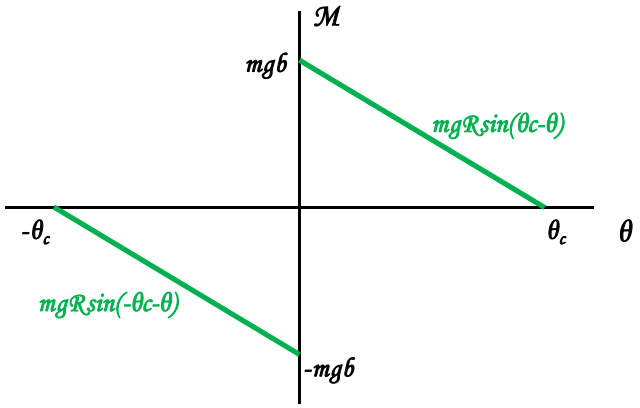

Figure 1.4. Moment rotation diagram of the rocking motion of a rigid body on a rigid base.

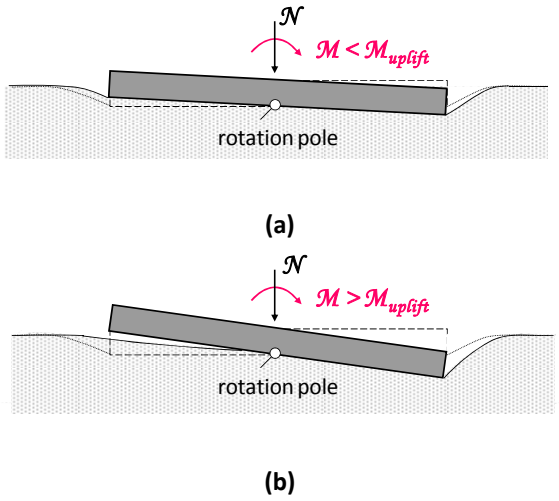

Figure 1.5. Rocking of a rigid footing on elastic soil **(a)** linear full contact phase **(b)** non-linear uplifting phase [Apostolou & Gazetas, 2007].

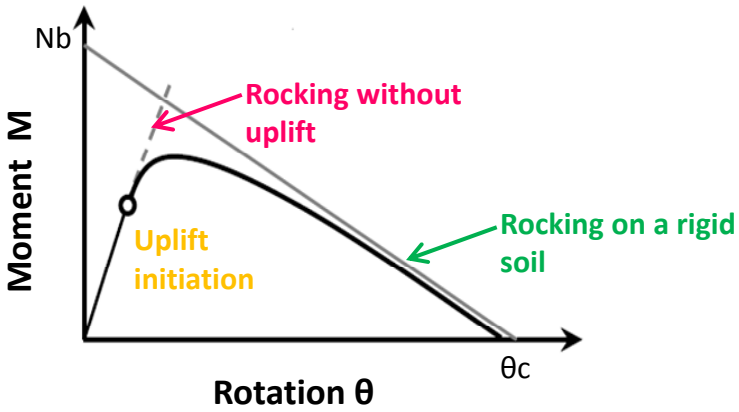

Figure 1.6. Moment-rotation curve of a shallow foundation with P-δ effects [Apostolou & Gazetas, 2005].

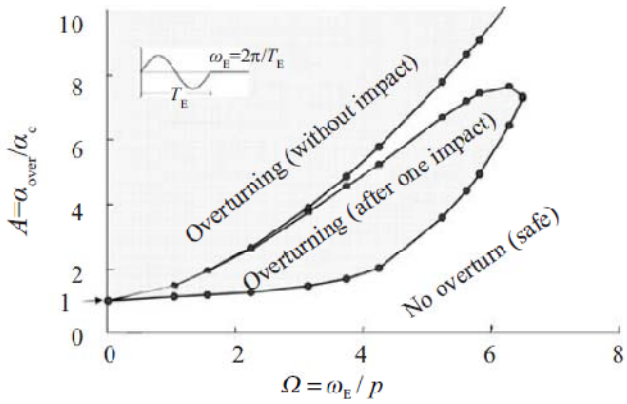

(a) One-cycle sinus

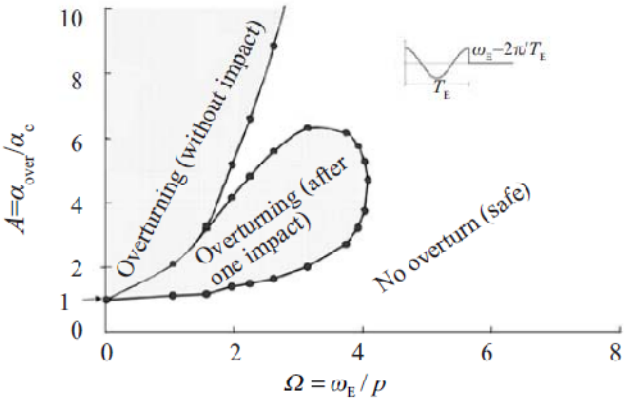

(b) One-cycle cosinus

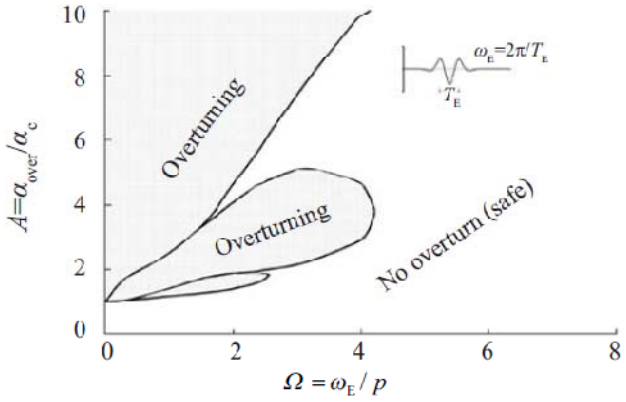

(c) Ricker pulse

Figure 1.7. Overturning amplification ratio for slender block under different pulses by numerical integration of equation of motion (circles) and analytical formula (solid lines) defined by Zhang and Makris [2001] for coefficient of restitution 0.8.

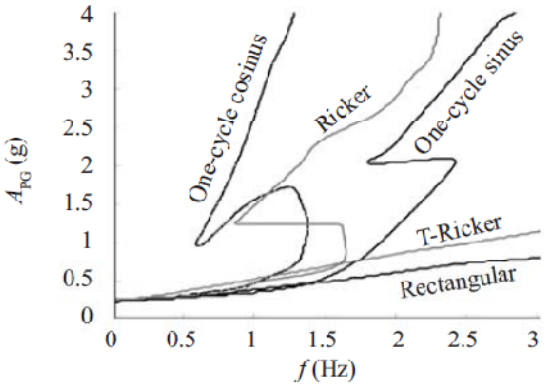

Figure 1.8. Overturning acceleration spectra of a free standing rigid block with semi - width b = 0.32m and semi - height h = 1.29m (a_c = 0.25g, p = 2.14 rad/s , coefficient of restitution r = 0.8) subjected to five acceleration pulses, computed by the artificial neural network [Gerolymos et al. 2005].

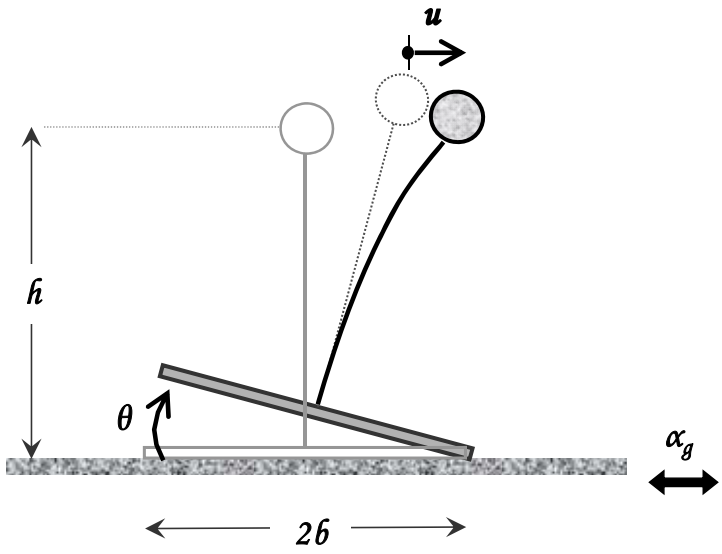

Figure 1.9. A flexible 1-dof oscillator rocking on a rigid base. The response is now described by the angle of rotation θ and the horizontal relative displacement of the mass center u.

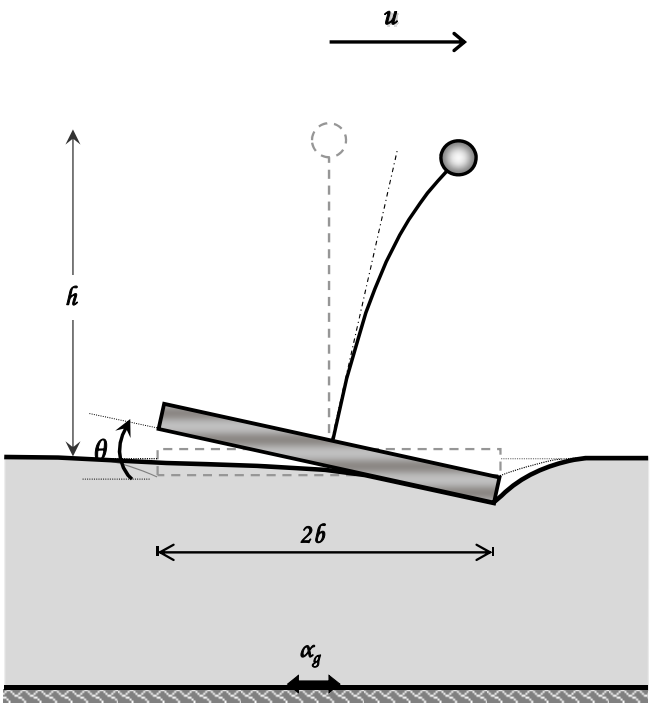

Figure 1.10. A flexible 1-dof oscillator rocking on a compliant soil. The response of the system consists of coupled flexural and rocking oscillations.

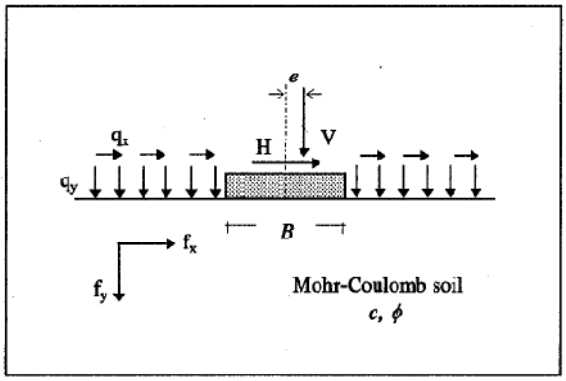

(a) Shallow foundation on a homogeneous Mohr - Coulomb soil .

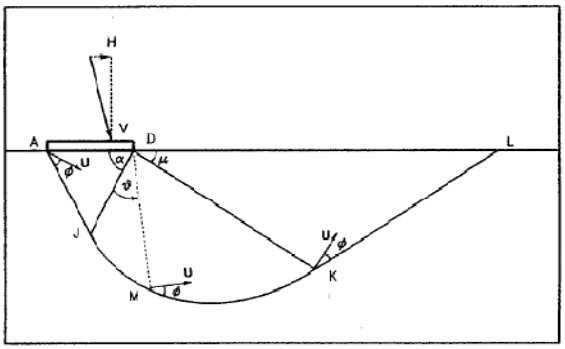

(b) Kinematic mechanism defined by two geometric parameters α and μ.

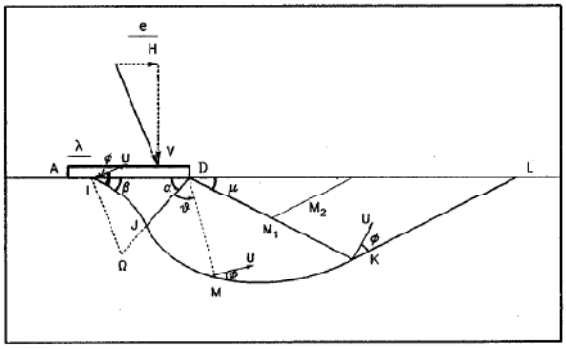

(c) Kinematic mechanism defined by four geometric parameters λ, β, α and μ.

Figure 1.11. Kinematic failure mechanism of shallow foundations when foundation uplift is considered after Paolucci & Pecker [1997] **.**

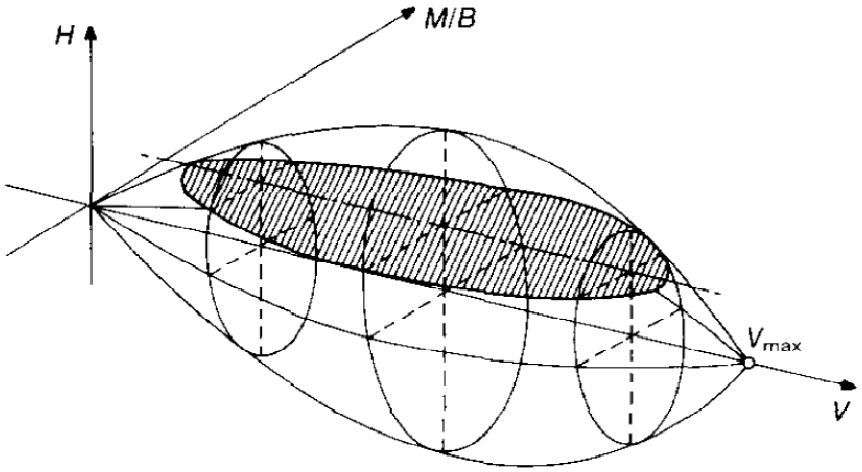

Figure 1.12. Three dimensional bearing capacity failure envelope of shallow foundation on sand after Butterfield & Gottardi [1994].

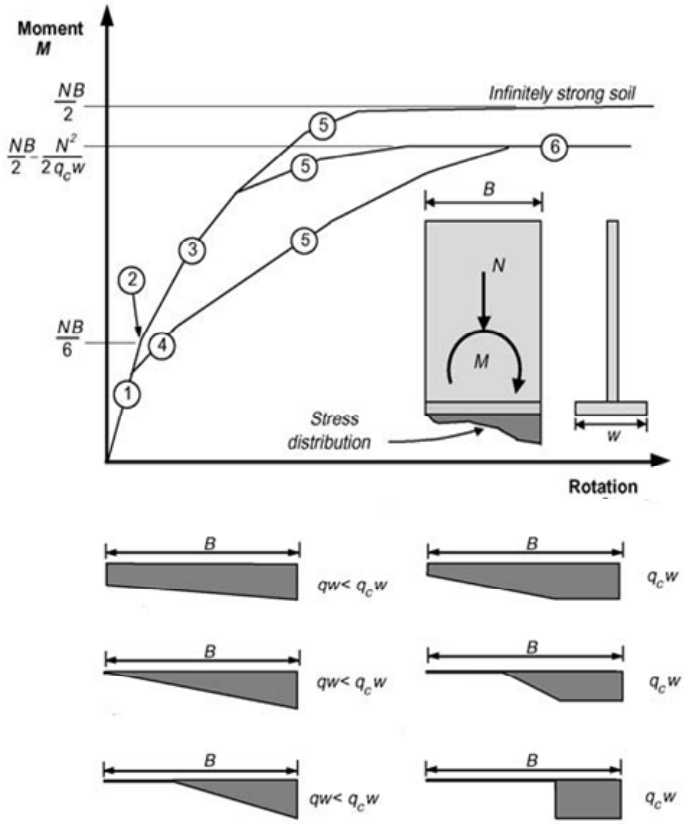

Figure 1.13. Rocking of a shear wall on strip footing : the different states of the M-theta curve under monotonic loading [FEMA 274].

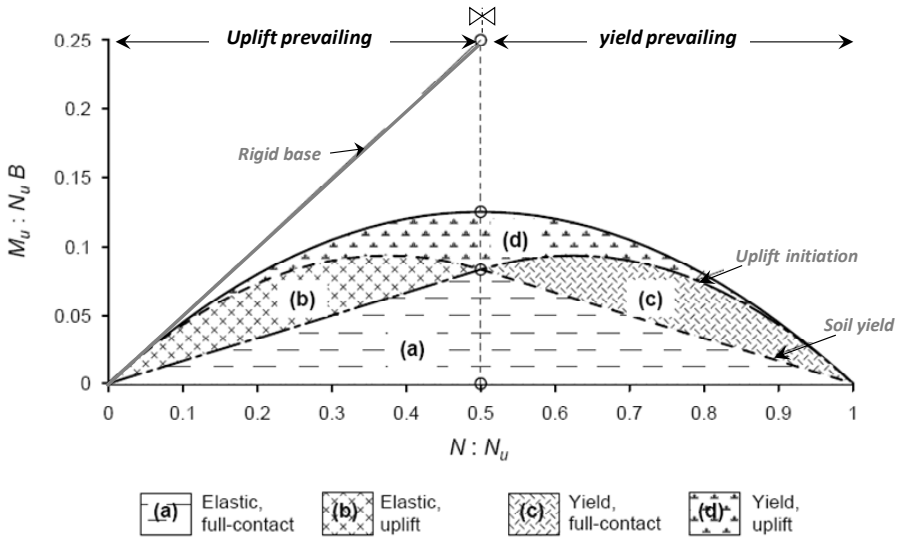

Figure 1.14. Interaction curves in the normalized N - M plane for bearing capacity failure on rigid or deformable soil. Decomposition of uplifting and soil - yielding mechanisms (Apostolou & Gazetas, 2007).

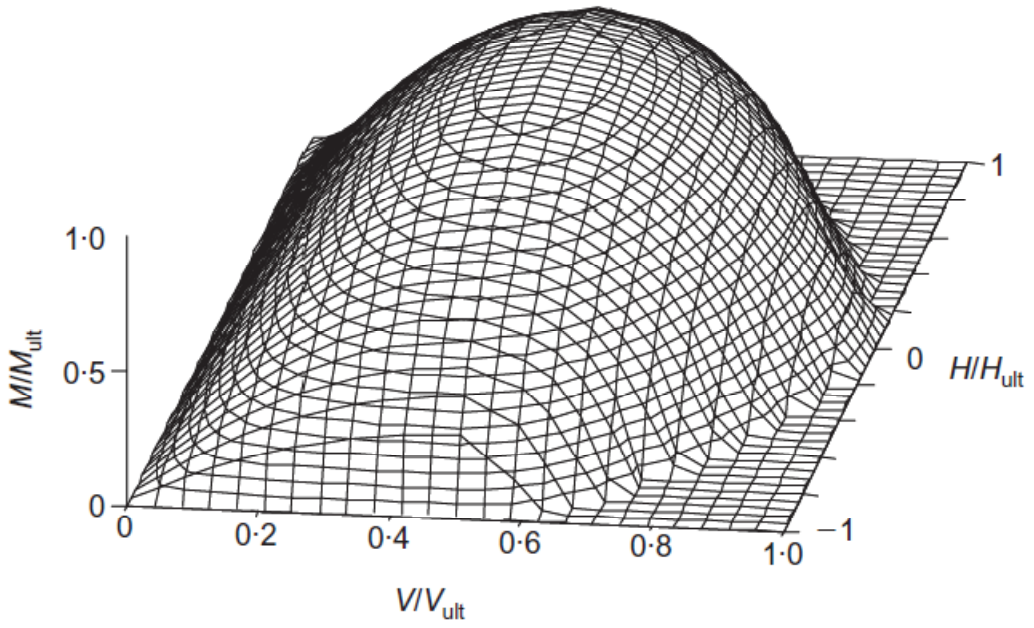

Figure 1.15. Three dimensional failure envelope for *VMH* loading for a zero tension interface [Gourvenec, 2007].

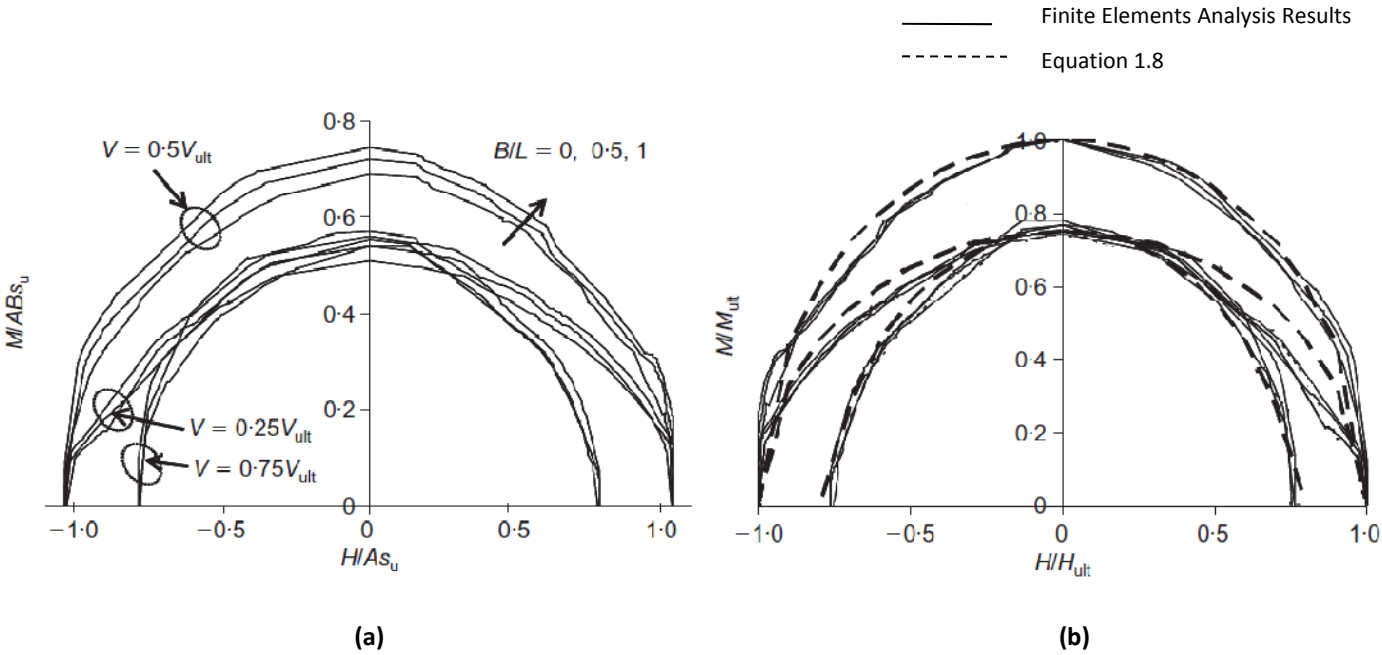

Figure 1.16. Failure envelopes for VMH loading for zero-tension interface **(a)** dimensionless load space **(b)** normalized load space [Gourvenec, 2007].

Methodology

3.1 PROBLEM STATEMENT

Tall structures such as bridge piers undergo combined loading (horizontal, vertical, moment) during an earthquake event. The response of such tall slender structures is governed by moment loading and is significantly modified when the structure enters the rocking mode and uplifting from the supporting soil occurs. As already mentioned, many researchers have noticed the beneficial effect of foundation uplift and mobilization of soil bearing capacity to the overall response of slender structures under dynamic loading.

According to *Priestley (1996)* the transverse dynamic behavior of bridges of regular shape can be as a first approximation modeled by only one pier. This diploma thesis will investigate the rocking response of a bridge pier, idealized as rigid or flexible 1-dof oscillator with shallow foundation supported on deformable soil medium and subjected to bi-directional loading. The bridge considered is of moderate height (H=20m) and is resting on a quite stiff homogenous clay stratum (Su=150 kPa), competent enough to justify the selection of shallow foundation. The system is allowed to uplift and due to the soil compliance possesses additional variables are introduced:

- The horizontal displacement of the footing along the x axis δ_1.
- The horizontal displacement along y axis δ_2.
- The vertical displacement of the footing measured at its center w.
- The rocking rotation of the footing about y axis ϑ_2.
- The rocking rotation of the footing about x axis ϑ_1.

3.2 ANALYSIS METHODOLOGY

3.2.1 FINITE ELEMENT MODELING

Non-linear analysis of rocking and uplift response under static and dynamic loading is implemented utilizing the *ABAQUS-3D F.E.* code. A lumped mass structure with a square footing represents the bridge-pier-foundation system. Elastic linear beam elements of circular section are utilized to model the superstructure whilst a massless rigid foundation is obtained by a combination of solid and rigid beam elements. The structural weight is concentrated at a mass element which represents the bridge deck. Foundation is modeled with elastic 8nodal hexahedral continuum elements. Soil is a homogeneous clay stratum modeled with non-linear 8nodal hexahedral continuum elements.

The foundation is connected to the soil with special contact elements allowing for realistic simulation of uplifting of the foundation and zero tensile capacity. The coefficient of friction is large enough so that sliding at the soil-footing interface is prevented. In each case material nonlinearity, emerging from the soil non-linear behavior, and geometrical non-linearities (*P-δ* effects and *uplifting*) are taken into account through appropriate large deformation formulation. A static step preceding any static or dynamic analysis establishes geostatic conditions within.

The 3-dimensional finite element mesh is a square footing of width B=10 m and equal length L. The mesh extends 3B from the edges of the footing and 2.5B beneath the footing. This is mainly because the rocking response of the footing is of interest. Zero-displacement boundary conditions prevent out-of- plane displacements of the vertical boundaries, and the base of the mesh is fixed in all three coordinate directions. Several finite element models, varying the mesh density – a sensitivity analysis to make a trade-off between accuracy and computing time requirements.

For the analysis of earthquake response seismic excitation is imposed to the soil medium through underlying rigid bedrock.

An implicit direct integration algorithm, incorporated in the ABAQUS code , is utilized to compute the non-linear dynamic response of the system. With this

technique the global equations of motion are integrated though time using the implicit Hilbert-Hughes –Taylor operator. Equilibrium solutions within each time increment are obtained by an iterative process applying Newton method. An automatic incrementation scheme is also used with the general implicit dynamic integration method. The scheme uses a a half-step residual control to ensure an accurate dynamic solution which is the basis of the adaptive time incrementation scheme. If the half-step residual is small the time step can be increased safely; conversely, if the half step is large the time step is reduced. This automatic incrementation scheme is crucial in cases when a sudden event is introduced to the dynamic problem e.g. the foundation impacts the soil during cyclic rocking motion.

3.2.2 SOIL BEHAVIOR

The elasto-plastic soil behavior is described with Von-Mises yield criterion with non-linear kinematic hardening and associated plastic flow rule. This constituitive model is based on the simulation of nonlinear cyclic behavior of cohesive soils under un-drained conditions with the behavior of ductile metals and can capture effectively the ductile-post yield behavior of the clay studied herein.

According to the Von Mises failure criterion, the evolution of stresses is described by the following relation:

$$\sigma = \sigma_0 + \alpha \qquad [3.2.1]$$

where σ_0 is the value of stress at zero plastic strain, assumed to remain constant. The parameter α is the “backstress” which defines the kinematic evolution of the yield surface in the stress space.

The function F defines the pressure independent yield surface:

$$F = f(\sigma - \alpha) - \sigma_0 \qquad [3.2.2]$$

The evolution law of the model consists of two components: a non linear kinematic hardening component, which describes the translation of the yield surface

in the stress space (defined through the back-stress α), and an isotropic hardening component, which describes the change of the equivalent stress defining the size of the yield surface σ_0 as a function of plastic deformation. The kinematic hardening component is defined as an additive combination of a purely kinematic term (linear *Ziegler* hardening law) and a relaxation term (the *recall* term), which introduces the nonlinearity. The evolution of the kinematic component of the yield stress is described as follows:

$$\dot{\alpha} = C\frac{1}{\sigma_0}(\sigma - \alpha)\dot{\bar{\varepsilon}}^{\mathrm{pl}} - \gamma\alpha\dot{\bar{\varepsilon}}^{\mathrm{pl}} \qquad [3.2.3]$$

where, $\dot{\bar{\varepsilon}}^{\mathrm{pl}}$ is the equivalent plastic strain rate, C is the initial kinematic hardening modulus ($C = \frac{\sigma_{\mathrm{y}}}{\varepsilon_{\mathrm{y}}} = E$) and γ determines the rate at which the kinematic hardening decreases with increasing plastic deformation.

In other words an initial pressure independent yield surface is inflated and translated in the stress space through the development of plastic strains. The evolution of the kinematic and the isotropic hardening components is illustrated in figures for unidirectional and multi-axial loading respectively. The evolution law for the kinematic hardening component implies that the backstress is contained within a cylinder of radius:

$$\sqrt{\frac{2}{3}\alpha^s} = \sqrt{\frac{2}{3}}\frac{C}{\gamma} \qquad [3.2.4]$$

where, α^s is the magnitude of α at saturation. Since the yield surface remains bounded, this implies that any stress point must lie within a cylinder of radius $\sqrt{2/3}\sigma_y$.

At large plastic strains, any stress point is contained within a cylinder of radius $\sqrt{2/3}(\alpha^s + \sigma^s)$ where σ^s is the equivalent stress defining the size of the yield surface at large plastic strain.

The maximum yield stress at saturation is:

$$\sigma_y = \frac{C}{\gamma} + \sigma_0 \qquad [3.2.5\ ]$$

According to the Von Mises yield criterion this ultimate stress is:

$$\sigma_y = \sqrt{3} S_u \qquad [3.2.6]$$

From equations 3.2.5. and 3.2.6 we have:

$$\gamma = \frac{C}{\sqrt{3} S_u - \sigma_0} \qquad [3.2.6]$$

3.2.3 PIER AND FOOTING DESIGN

The pier and footing behavior is considered elastic and is described by the modulus of elasticity *E*. With respect to the pier flexibility, the modulus of elasticity is properly adjusted in order to achieve a rigid structure or a structure with a fixed-base natural period .

The initial step in foundations design is to supply adequate bearing capacity to sustain static vertical loading. The minimum vertical safety for solely vertical loading of shallow foundation bridges of moderate height and regular type is FSv=2.5.

The ultimate bearing capacity of the footing for solely vertical loading is calculated according EC-7:

$$s_c = 1 + 0.2\frac{B}{L} = 1.2$$

$$q_u = (\pi + 2) \times S_u \times s_c = 925.5\ \text{kPa}$$

$$Q_{ult} = q_u \times B^2 = 92.550\ \text{kPa}$$

3.2.4 STATIC AND CYCLIC LOADING

Displacement control vertical and horizontal push-over loading is applied at the mass center of the superstructure so that vertical and moment capacity of the soil-foundation system are calculated.

The ultimate vertical capacity of the foundation was derived through pushover displacement control vertical loading tests and is 91.570 kPa. The vertical load-settlement curve is illustrated and there is a good agreement between the code provisions and the actual case.

In order to investigate the overall rocking response of the system and achieve different factors of safety the mass varies accordingly. A set of static analyses applying 1-directional monotonic pushover loading is employed to evaluate the proposed model. Subsequently the system is subjected to bi-directional monotonic pushover loadings and is observed how the ultimate moment capacity of the system varies when the horizontal force is applied to the mass with an incidence angle relative to the major axes. Interaction diagrams for two-dimensional loading are produced for various factors of safety and incidence angles.

Afterward, cyclic analyses subject the foundation to gradually increasing bi-directional loading, in order to assess the effect of the second load component on the accumulation of settlement and to examine the overall behavior of lightly and heavily loaded footings (pressure distributions, mobilization of bearing capacity mechanisms).

3.2.5 DYNAMIC LOADING

The examined system is subjected to different sequences of idealized pulse excitations (*Ricker*, *Harmonic, Tsang* [IXA] wavelets). By altering the phase between the two components of the excitations, the effect of asynchronous bi-directional seismic loading has been parametrically investigated, emphasizing on the influence of the frequency content.

Real earthquake records have been employed to investigate the seismic performance of the proposed system. In each case, the seismic excitation is applied at the bedrock level.

RICKER WAVELETS

Ricker wavelets have a distinct advantage over cycloidal pulses in simulating near-fault ground motion as demonstrated by *Anooshehpoor et al(1999), Makris et al (1998,1999), Mavroeidis & Papageorgiou (2003).* This is attributed to the fact that asymmetric pulses represented by Ricker wavelets can that can capture forward directivity phenomena or contain long duration pulses (flings). Ricker pulses possess the inherent asymmetry which is the main characteristic of most near-fault excitations.

In this study a considerably wide range of excitation frequencies was employed. (The high frequency Ricker-2 with an effective period of 0.3 sec and Ricker-1 representing excitations of moderate frequency)

Pulses of higher frequency band, tend to leave rocking and overturning response of slender blocks unaffected whereas excitations with very large dominant periods (quite larger than the natural period of the system) practically resemble static loading and therefore have been excluded.

REAL EARTHQUAKE RECORDS

Real earthquake accelerograms are clearly a viable option for providing input to dynamic analysis of structures, being more realistic than spectrum-compatible artificial records and easier to obtain than synthetic accelerograms generated from seismological source models. The increasing availability of strong-motion accelerograms , makes the use of real records an ever more attractive option for defining the input to dynamic analyses in geotechnical engineering.

However guidelines on procedures for the selection of appropriate suites of acceleration time-series for this purpose are lacking, and seismic design codes are particularly poor in this respect. Discussing the selection criteria (matching code

design spectrum or seismological characteristics such as source, path, site effects etc) for real earthquake records deviates from the scope of this study and the a selection of accelerogramms has been made purely to address the significance of the second-horizontal component. The set of records utilized in the study comprises of moderate and low intensity earthquakes.

PRESENTATION OF RESULTS

The results of the dynamic analyses for each case are presented in terms of acceleration, velocity, horizontal displacement , rotation as well as in terms of response loops in the moment-rotation, moment-settlement and rotation-settlement plane. Since analyses contain bi-axial excitation components results are arranged in two sets a, b referring to X,Y axes respectively.

The acceleration time history at bedrock (excitation) is compared with the time history at free field which is affected by the non-linear response of the soil stratum and the acceleration time history generated at the lumped mass (deck level) of the proposed system.

The amplitude of horizontal displacement at the deck level is a matter of great importance for the response of bridges. The total horizontal component is composed of a rotational and a structural bending component. The first is the product of the rotation of the footing whereas the latter is the result of the flexural bending of the pier. The time histories of the drift at the deck level are presented in terms of total the dominant mode (rotational/ translational) of motion in the response.

Total horizontal displacement (drift), vertical settlements, rotation and effective footing contact area time histories as well as under the foundation press distribution diagrams for selected time increments are compared with single axial loading cases to illustrate the effect of the second component of excitation in the systems response.

Static Pushover

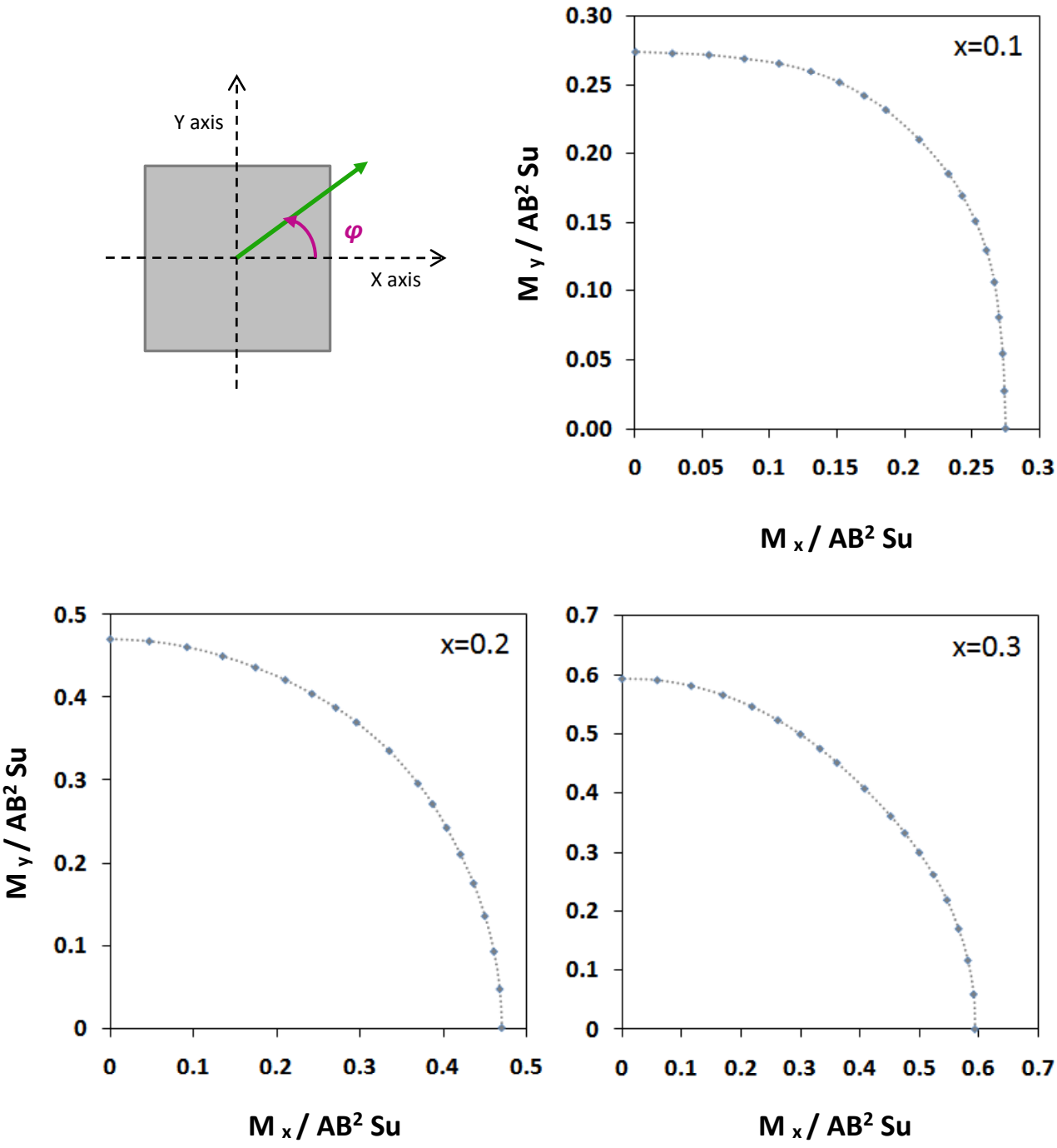

Figure 3.1 . Moment interaction diagrams for inverse factors of safety x=0.1, 0.2, 0.3. Static pushover in two directions ϕ=45°

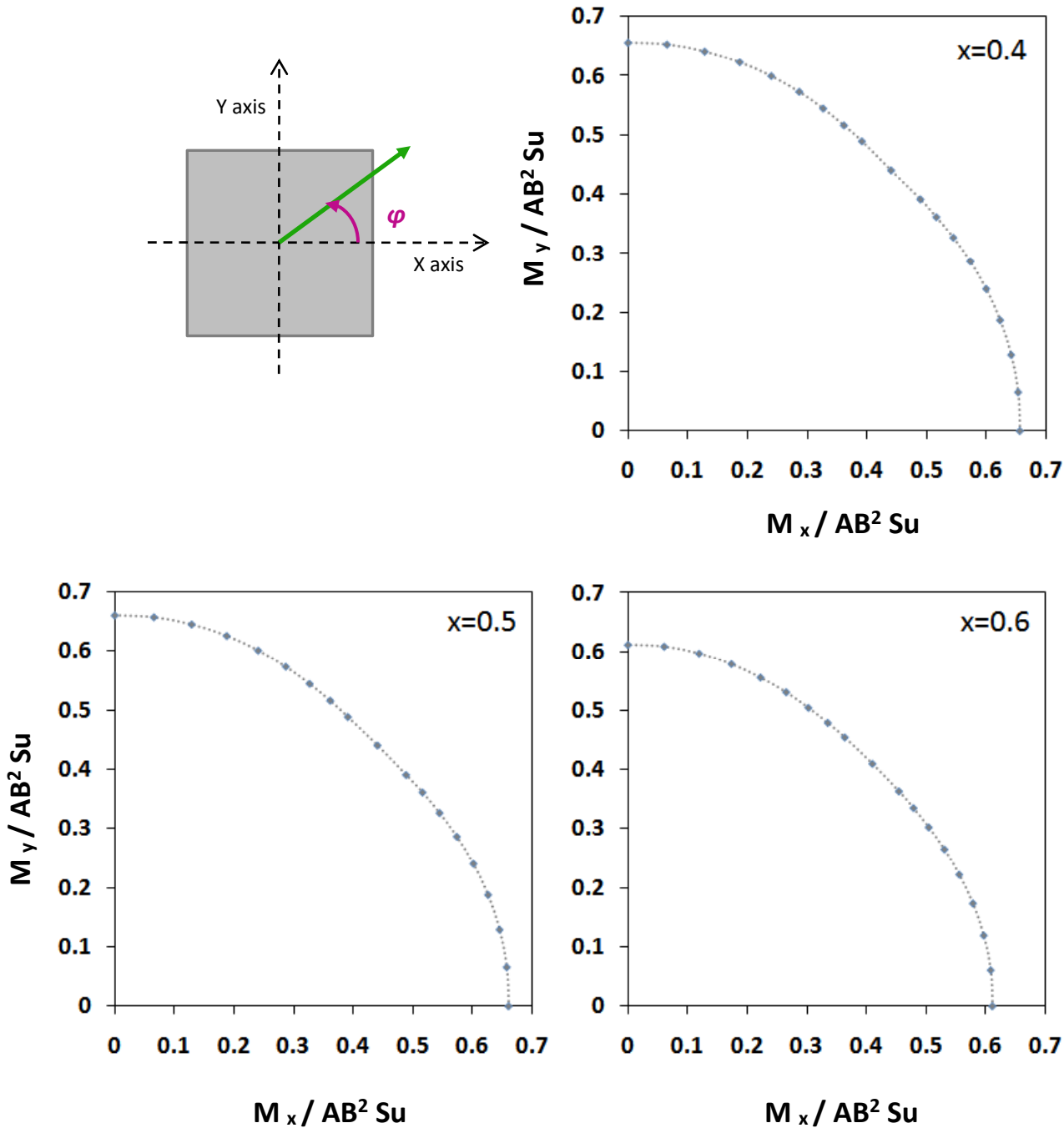

Figure 3.2. Moment interaction diagrams for inverse factors of safety x=0.4, 0.5, 0.6. Static pushover in two directions ϕ=45^{o}

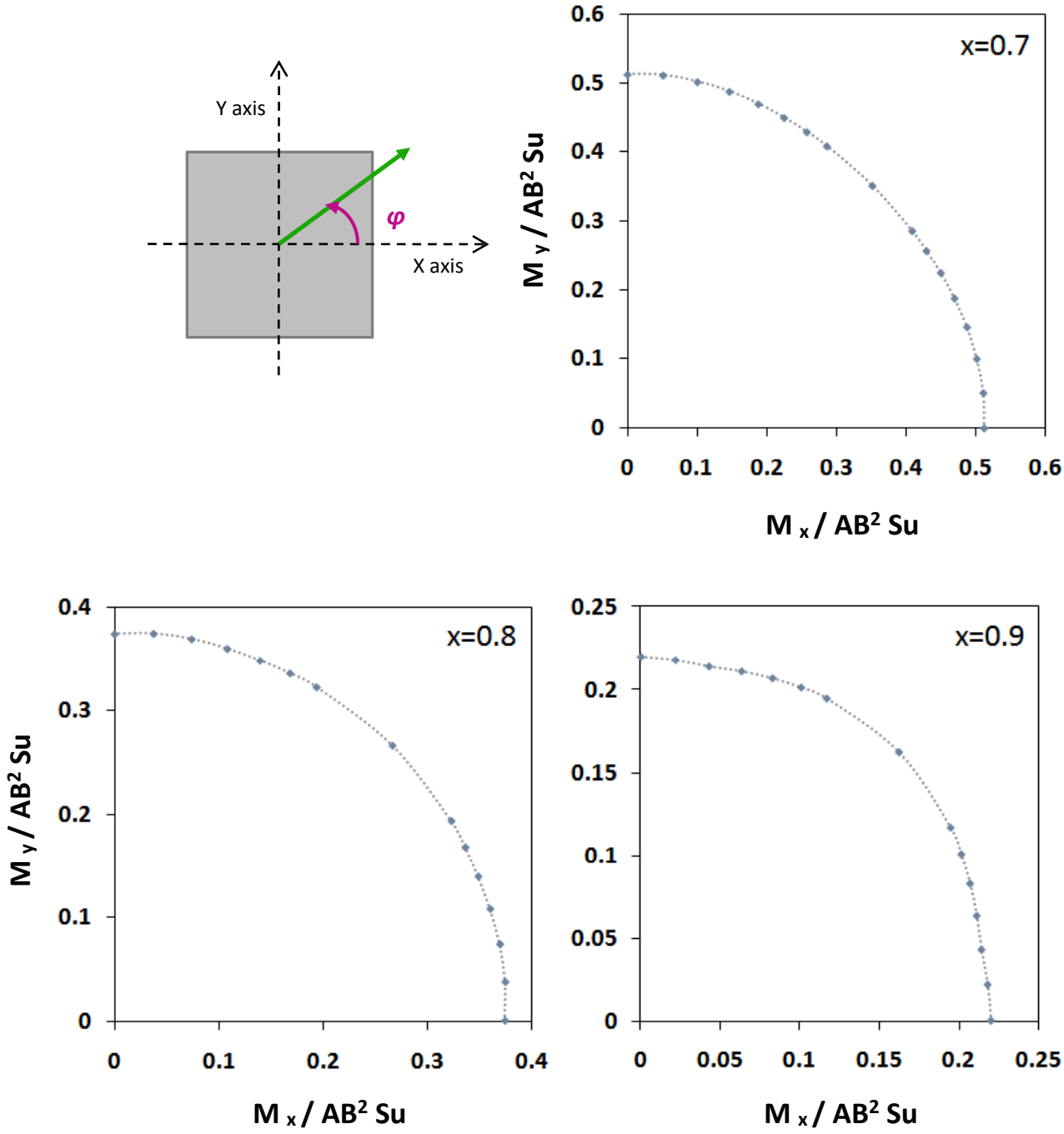

Figure 3.3 . Moment interaction diagrams for inverse factors of safety x=0.7, 0.8, 0.9. Static pushover in two directions ϕ=45°

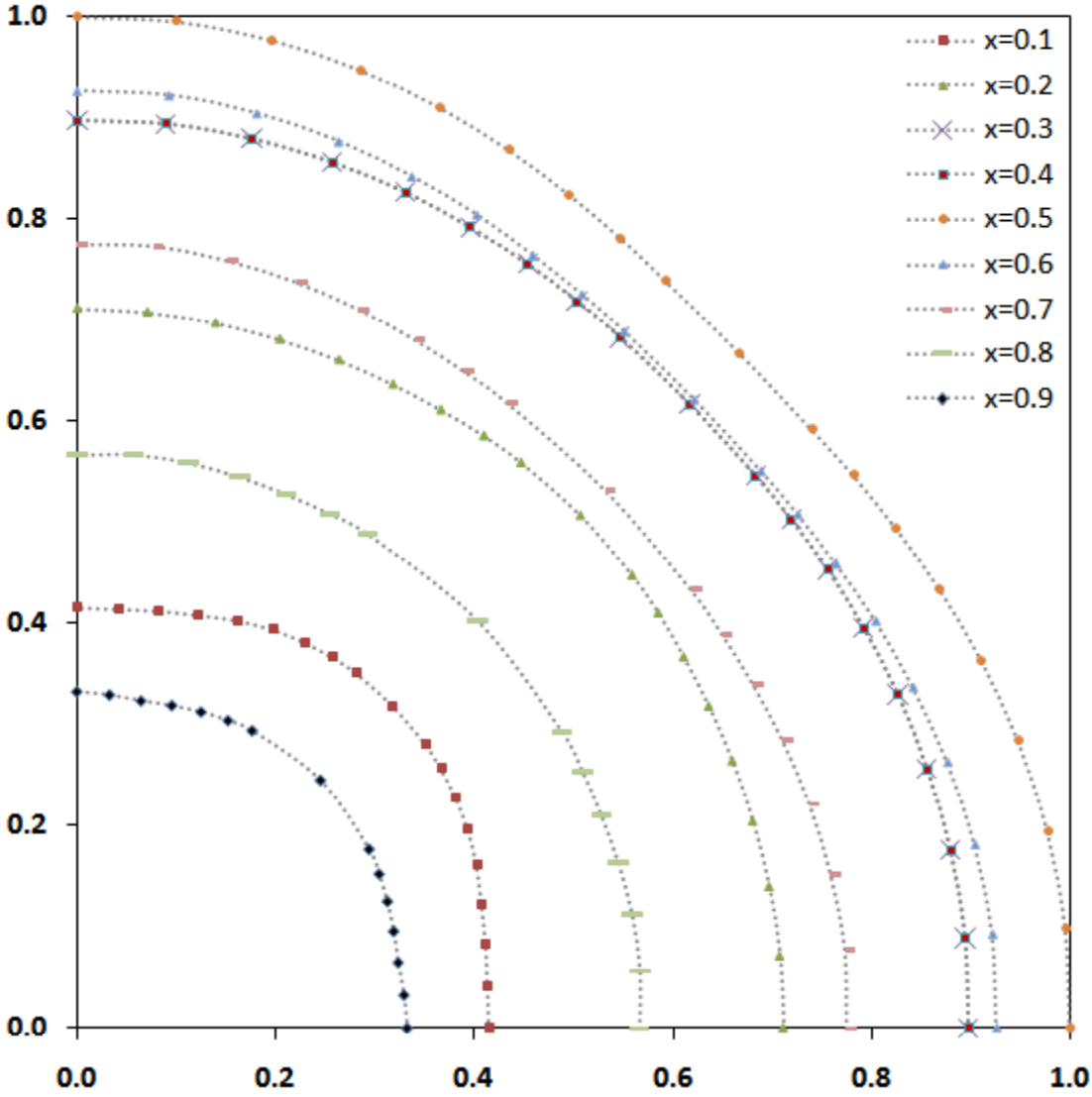

Figure 3.4 . Nomalized Moment interaction diagrams for different inverse factors of safety . Static pushover in two directions .

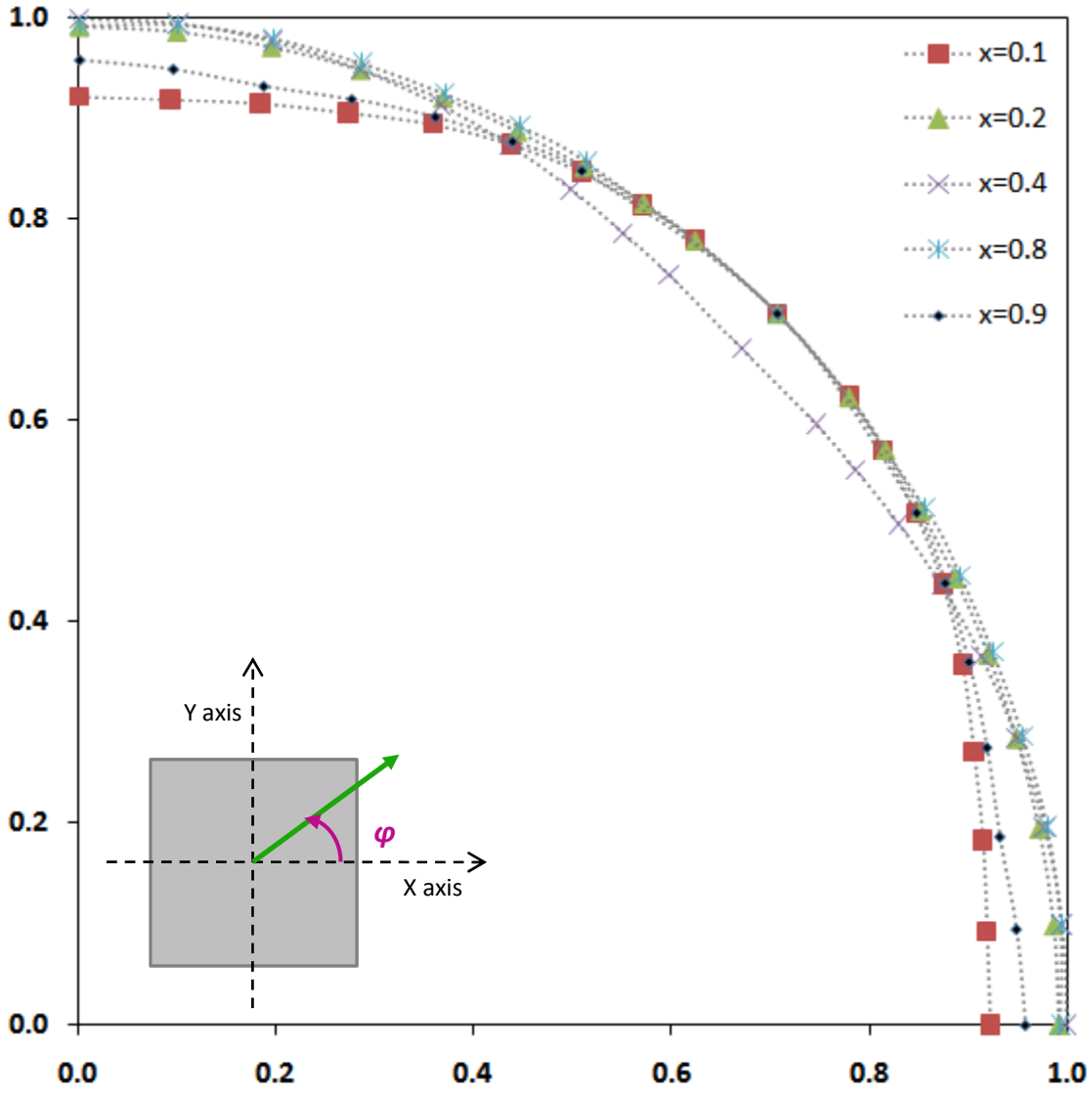

Figure 3.5 . Moment interaction diagrams for different inverse factors of safety . Static pushover in two directions . Normalized to M_{max} for ech case.

Ricker pulses Loading

5. PRESENTATION – DISCUSSION OF RICKER LOADING RESULTS

5.1 CODE PROVISIONS

Tall structures like bridge piers are particularly vulnerable to large moments at their base during horizontal-earthquake loading. Consequently, moment loading capacity is the decisive parameter in their design. Seismic design codes introduce strict limitations at the rocking response of foundations and only a small part of the footing is allowed to uplift.

According to the Greek Aseismic Code (EAK-2000) maximum accepted eccentricity equals to 1/3 of the footing width. Figure 5. 125 illustrates the design spectrum after Greek Aseismic Code for the 4 site categories and highlights the spectrum that corresponds to the studied soil profile.

For structural systems with at least the 50% of their mass concentrated to the upper 1/3 of their height the coefficient of behavior q equals 2. The system is designed for design peak ground acceleration A= 0.24 g, which refers to Seismic loading zone III.

The single-degree-of-freedom model of the bridge-pier-foundation is used to calculate the seismic excitation applied at the level of the deck. This is a rational approach since the mass and the stiffness of the pier are significantly lower of the deck. The equivalent fixed base oscillator has the following characteristics:

- **H** = 20.0 m
- d = 3.0 m (circular section)
- **I** = (*pi**d^4)/64 = 63.62 m^4
- **E** = 30*10^6 kPa
- **K** =3EI/H^3 = 71.5695 kN/m
- $\mathbf{T_N}$ = 2*pi**(**K**/**M**)^0.5

For the cases of earthquake loading a safety factor of SFv=5 is selected so the mass is :

M = 1.870 Mgr

$\mathbf{T_N}$ **= 0.32** sec

5.2 THE EFFECT OF EXCITATION FREQUENCY

It is well renowned that the response of an oscillator subjected to dynamic loading is determined by the relation between the excitation frequency and its natural frequency. However, due to the non-linear nature of the problem the effective period of the system is related to imposed deformations. As a result, the loading applied to the system depends on its effective period but at the same time the effective period of the system depends on the amplitude of distress deformation.

In the framework of purely elastic conditions, we would contend that an excitation has a more catastrophic impact the closer its dominant frequency approaches the systems natural frequency irrespectively of excitation intensity. However this is not the case when the non-linear nature of the problem is accounted, as the T_E/T_N ratio alters with increasing excitation intensity and the resonance of the system moves towards higher period bands. To explore this complex behavior the proposed system is subjected to different excitation frequencies of varying excitation intensity (low, moderate, high).

5.3 RICKER -2 (T_E = 0.3 sec)

The response of the system is illustrated for maximum accelerations amplitudes $\mathbf{a}_E$ (g) = 0.2 ,0.5, 0.8 in figures 5.1-5.66. T he secondary excitation component is another pulse (in the y axis) of the same frequency but combined with the primary (x axis) under the following rules:

(A) Coinciding peak acceleration with intensity up to 30% of the peak acceleration of the primary pulse.

(B) Coinciding peak acceleration with intensity up to 40% of the peak acceleration of the primary pulse.

(C) Same peak acceleration but peak maxima out of phase. The secondary pulse (y axis component) is time lagged to attain a value of 30% of the primary acceleration when the latter reaches its peak value.

(D) In phase pulses with the same peak acceleration. A rather non-realistic combination for the case of real earthquake loading but under performance demands perspective the worst case scenario.

- **a_g = 0.2 g (roughly elastic response)**

Figures 5.1-5.24 illustrate the systems response. Moment-rotation curves show a rather elastic behavior. The system responds faintly and remains in the linear-elastic area as the maximum moment loading does not exceed the ultimate capacity of the system. This is mainly attributed to the low amplitude and high frequency excitation input.

It is to be noted that we have an amplification of the peak acceleration in the free field. The pulse applied at the bedrock level has a peak acceleration of 0.2 g whereas in the free field it's value reaches 0.5 g. As far as the lumped mass is concerned, due to the rocking response of the pier it experiences significantly lower levels of acceleration (0.1 g).

- **Ax= 0.2g , Ay =30% x 0.2 g (in phase)**

In terms of accumulated vertical settlements, rotation and total drift the second component seems to have practically no effect on the response.

	Ax=0.2g	Ay=30%Ax	
w/B	0.00052	0.00055	5.77%
δ /H	0.0013	0.0013	0.00%
A eff	66.53	66.53	0.00%
ϑ (rad)	0.00084	0.0008	-4.76%

At the time increment when maximum uplift occurs the effective contact area is 66.5% of the total practically coinciding with the single direction excitation case. However the distribution of contact presses (figure 5.4) shows an accumulation of stresses at the corner area whereas for the single direction excitation case the pressure diagram is symmetrical to the y axis.

The orbit- time history (figure 5.5) illustrates that the motion of the center of mass is along the a straight line with tanϕ=0.3 which is expected as long as the excitation components are in phase and the ratio Ay/Ax=0.3 is constant.

- **Ax= 0.2g , Ay =40% x 0.2 g (in phase)**

In terms of accumulated vertical settlement , rotation and total drift (figure 5.6) there is a small amplification according to the following chart:

	Ax=0.2g	Ay=40%Ax	
w/B	0.00052	0.000623	19.81%
δ	0.0013	0.0015	15.38%
A eff	66.53	59.09	-11.18%
ϑ (rad)	0.00084	0.001	19.05%

At the time increment when maximum uplift occurs the effective contact area is 59% of the total practically coinciding with the single direction excitation case. However the distribution of contact presses (figure 5.10) shows an accumulation of stresses at the corner area whereas for the single direction excitation case the pressure diagram is symmetrical to the y axis.

The orbit- time history (figure 5.11) illustrates that the motion of the center of mass is along the a straight line with tanϕ=0.4 which is expected as long as the excitation components are in phase and the ratio Ay/Ax=0.4 is constant.

- **Ax= 0.2g , Ay = 0.2 g (out of phase)**

Figure 5.18 and the following chart show the deterioration in terms of vertical settlement and effective contact area when the peak acceleration of the x-axis component is followed by a peak of the same intensity along the y-axis compared to the single direction excitation scenario:

	Ax=0.2g	Ay=0.2g asynchronous	
w/B	0.00052	0.000832	60.00%
δ /H	0.0013	0.0012	-7.69%
A eff	66.53	48.35	-27.33%
ϑ (rad)	0.00084	0.0009	7.14%

The orbit- time history (figure 5.11) illustrates that the motion of the center of mass follows no certain pattern and the vector of the resultant force is constantly changing which is expected as long as the excitation components are out of phase and ratio Ay/Ax is not constant in time.

- **Ax= 0.2g , Ay = 0.2 g (in phase)**

Figure 5.24 illustrates the effect of the concurring pulse of the same maximum along the y-axis. Counter institutively the systems performance in terms of total drift, rotation and effective contact area has slightly deteriorated in comparison with the previous case.

	Ax=0.2g	Ay=0.2g in phase	
w/B	0.00052	0.00073	40.38%
δ /H	0.0013	0.0013	0.00%
A eff	66.53	69.01	3.73%
ϑ (rad)	0.00084	0.00086	2.38%

The orbit- time history (figure 5.23) illustrates that the motion of the center of mass is along the a straight line with tanϕ=1 which is expected as long as the excitation components are in phase and the ratio Ay/Ax=1 is constant.

- **a_E = 0.5 g (moderate amplitude)**

In general upon unloading, after a small excursion in the descending branch of the monotonic curve, the path follows with small deviations the original monotonic curve in the moment-rotation plane. This is evidence of reversible behavior the result of nonlinearly elastic uplift response.

There is a significant amplification of the peak acceleration in the free field. The pulse applied at the bedrock level has a peak acceleration of 0.5 g whereas in the free field it's value reaches 0.8 g. As far as the lumped mass is concerned, due to the rocking response of the pier it experiences significantly lower levels of acceleration (0.18 g) .

- **Ax= 0.5g , Ay =30% x 0.5 g (in phase)**

In terms of accumulated vertical settlements, rotation and effective contact area the second component seems to have a small effect on the response about 10% deterioration (figure 5.30). However in terms of total drift there is no change compared to the single component case.

	Ax=0.5g	Ay=30%Ax	
w/B	0.00101	0.00112	10.89%
δ /H	0.00218	0.0022	0.92%
A eff	59.09	53.31	-9.78%
ϑ (rad)	0.0022	0.002	-9.09%

In the distribution of contact presses (figure 5.28) there is a more intense accumulation of stresses at the corner with the contact pressures reaching the value of 500 k Pa when maximum uplift occurs.

The orbit- time history (figure 5.29) illustrates that the motion of the center of mass is along the a straight line with tanϕ=0.3 which is expected as long as the excitation components are in phase and the ratio Ay/Ax=0.3 is constant.

- **Ax= 0.5g , Ay =40% x 0.5 g (in phase)**

Figure 5.36 and the following chart illustrate the effect of the this second horizontal component:

	Ax=0.5g	Ay=40%Ax	
w/B	0.00101	0.00118	16.83%
δ	0.00218	0.0019	-12.84%
A eff	59.09	45.87	-22.37%
ϑ (rad)	0.0022	0.0025	13.64%

The vertical settlement and the rotation are amplified about 15% as well as the effective contact area that is reduced up to 22% compared to the single direction case.

- **Ax= 0.5g , Ay = 0.5 g (in phase)**

According to figure 5.48 and the following chart the same intensity synchronous pulse greatly increases the permanent vertical settlement up to 30% compared to the single direction case. On the other hand it seems to reduce the demand in term of total drift.

	Ax=0.5g	Ay=0.5g in phase	
w/B	0.00101	0.0013	28.71%
δ /H	0.00218	0.0011	-49.54%
A eff	59.09	45.04	-23.78%
ϑ (rad)	0.0022	0.0022	0.00%

- **Ax= 0.5g , Ay = 0.5 g (out of phase)**

Figure 5.42 reveals that this scenario is vividly the most detrimental in terms of induced settlements since the vertical settlement w is amplified about 60% (single component case).

	Ax=0.5g	Ay=0.2g asynchronous	
w/B	0.00101	0.0016	58.42%
δ /H	0.00218	0.0011	-49.54%
A eff	59.09	52.48	-11.19%
ϑ (rad)	0.0022	0.0024	9.09%

In contrast, the existence of a same intensity pulse acting out of phase along the y-axis , seems to play a beneficial role in terms of effective contact area. According to figure 5.41 the orbit of the centre of mass follows a complex path with no certain pattern restituting contact with the supporting soil as suggested by the effective contact area value.

- **a_E = 0.8 g (high amplitude)**

Figures 5.43, 5.55 ,5.63 demonstrate a significant amplification of the peak acceleration in the free field. The pulse applied at the bedrock level has a peak acceleration of 0.8 g whereas in the free field it's value reaches 1.1 g. Whereas the lumped mass experiences significantly lower levels of acceleration (0.13 g) . This is attributed to the fact that the rocking response prevails acting as an isolation mechanism.

In the moment-rotation plane the path noticeably deviates from the monotonic curve, a symptom of inelastic behavior, but due to the symmetry of the applied pulse the systems ends with small permanent rotation.

- **Ax= 0.8g , Ay =30% x 0.8 g (in phase)**

Figure 5.54 shows that, in this case, the performance of the systems is slightly affected by the second horizontal component.

	Ax=0.8g	Ay=30%Ax	
w/B	0.0014	0.0015	7.14%
δ /H	0.0036	0.0038	5.56%
A eff	45.04	39.26	-12.83%
ϑ (rad)	0.0034	0.0038	11.76%

Worthy of note is that although the uplift of the foundation is more extended at certain increments overall the footing exhibits larger contact area than the single direction case.

- **Ax= 0.8g , Ay =40% x 0.8 g (in phase)**

According to data there is a small deterioration about 10% in terms of vertical settlement ,total drift and maximum rotation.

	Ax=0.8g	Ay=40%Ax	
w/B	0.0014	0.00155	10.71%
δ	0.0036	0.0039	8.33%
A eff	45.04	41.74	-7.33%
ϑ (rad)	0.0034	0.0037	8.82%

Again the existence of the second horizontal component seems to have a beneficial effect restoring contact with the supporting soil.

- **Ax= 0.8g , Ay =75% x 0.8 g (in phase)**

Figure 5.66 suggests that, although we have a case of moderately high levels of acceleration along both axes the effect is not as detrimental as expected.

	Ax=0.8g	Ay=75%Ax	
w/B	0.0014	0.00158	12.86%
δ /H	0.0036	0.0026	-27.78%
A eff	45.04	45.87	1.84%
ϑ (rad)	0.0034	0.0024	-29.41%

The maximum rotation and total drift (closely intertwined since the total drift is mainly attributed to the rotation of the pier) are reduced up to 30%. Whereas the effective contact area is at all time increments has larger values than the single direction case.

5.4 RICKER -1 (TE = 0.6 sec)

The response of the system for maximum accelerations amplitudes $\mathbf{a}_g$ (g) = 0.2 ,0.5 , 0.8 is illustrated in figures 5.67-5.124.

The frequency of this excitation is closer to the natural period of the system. Based to that concept it is expected that effect of Ricker 1 on the response of the system will be more intense.

- **$\mathbf{a}_g$ = 0.2 g (roughly elastic response)**

- **Ax = 0.2g , Ay =30% x 0.2 g (in phase)**

Figures 5.67 , 5.73 , 5.73 ,5.79 show that the lumped mass experiences higher levels of acceleration (0.19g) compared to Ricker2 loading cases. The response of the system is illustrated in figures 5.67-5.72.

	Ax=0.2g	Ay=30%Ax	
w/B	0.0008	0.0007	-12.50%
δ /H	0.0048	0.0049	2.08%
A eff	45.04	40.08	-11.01%
ϑ (rad)	0.0048	0.0047	-2.08%

The vertical settlement is reduced by 12% as well as the maximum total drift.
The orbit- time history (figure 5.76) illustrates that the motion of the center of mass is along the a straight line with tanϕ=0.3 which is expected as long as the excitation components are in phase and the ratio Ay/Ax=0.3 is constant.

- **Ax = 0.2g , Ay =40% x 0.2 g (in phase)**

The effect of the second excitation component proves to be beneficial since it reduces the vertical settlement, maximum drift and maximum rotation.

	Ax=0.2g	Ay=40%Ax	
w/B	0.0008	0.00078	-2.50%
δ	0.0048	0.0046	-4.17%
A eff	45.04	43.39	-3.66%
ϑ (rad)	0.0048	0.0045	-6.25%

- **Ax = 0.2g , Ay = 0.2 g (in phase)**

	Ax=0.2g	Ay=0.2g in phase	
w/B	0.0008	0.0011	37.50%
δ /H	0.0048	0.0045	-6.25%
A eff	45.04	40.08	-11.01%
ϑ (rad)	0.0048	0.0047	-2.08%

- **Ax = 0.2g , Ay = 0.2 g (out of phase)**

For the case of Ricker1 pulses the existence of an out of phase low amplitude pulse along the y-axis seems to greatly increase vertical settlement w.

	Ax=0.2g	Ay=0.2g asynchronous	
w/B	0.0008	0.0017	112.50%
δ /H	0.0048	0.0042	-12.50%
A eff	45.04	42.56	-5.51%
ϑ (rad)	0.0048	0.004	-16.67%

- **a_g = 0.5 g (moderate amplitude)**

· **Ax= 0.5g , Ay =30% x 0.5 g (in phase)**

There is no significant change. The systems performance in terms of vertical settlement, maximum rotation is about the same with the single direction case. See figure 5.94.

	Ax=0.5g	Ay=30%Ax	
w/B	0.00189	0.0019	0.53%
δ /H	0.0084	0.0083	-1.19%
A eff	37.6	38.43	2.21%
ϑ (rad)	0.0086	0.0085	-1.16%

· **Ax= 0.5g , Ay =40% x 0.5 g (in phase)**

Figure 5.100 shows that also in this case there is no significant change.

	Ax=0.5g	Ay=40%Ax	
w/B	0.00189	0.00172	-8.99%
δ	0.0084	0.0076	-9.52%
A eff	37.6	35.95	-4.39%
ϑ (rad)	0.0086	0.0078	-9.30%

· **Ax= 0.5g , Ay = 0.5 g (in phase)**

	Ax=0.5g	Ay=0.5g in phase	
w/B	0.00189	0.0019	0.53%
δ /H	0.0084	0.0084	0.00%
A eff	37.6	35.14	-6.54%
ϑ (rad)	0.0086	0.0086	0.00%

· **Ax= 0.5g , Ay = 0.5 g (out of phase)**

Figure 5.106 illustrates a significant deterioration in terms of vertical settlement. The effective contact area at the time when maximum uplift occurs is slightly reduced.

	Ax=0.5g	Ay=0.2g asynchronous	
w/B	0.00189	0.00248	31.22%
δ /H	0.0084	0.0074	-11.90%
A eff	37.6	35.12	-6.60%
ϑ (rad)	0.0086	0.008	-6.98%

Although maximum rotation and drift reach the values of single direction case overall during the excitation tend to hold much lower values.

5.6 OVERVIEW OF RESPONSE TO RICKER PULSES IN VIEW OF PERMANENT DEFORMATIONS.

Excitation with Ricker pulses triggers the rocking regime of the structure's response. As the footing is allowed to uplift only a small portion of it remains in contact with the resting soil. That results in a significant increase of pressures in the remaining contact area and leads to plastic soil deformations. So even when the direction of the horizontal acceleration is reversed and the footing rotates back to it's initial position the contact with the supporting soil is never fully restituted.

Another significant aspect of Ricker loading is the accumulation of settlements that is going to be thoroughly examined for all amplitudes hereafter.

Ricker 1 (T_E =0.6 sec)

- a_g = 0.2 g

	Ax=0.2g	Ay=30%Ax	Ay=40%Ax	Ay=0.2g in phase	Ay=0.2g asynchronous
w/B	0.0008	0.0007	0.00078	0.0011	0.0017

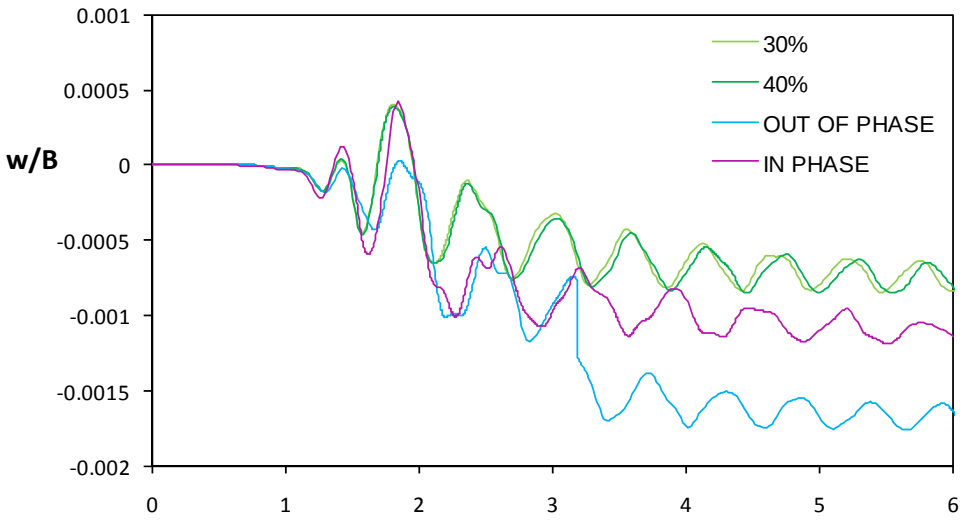

- a_g = 0.5 g

	Ax=0.5g	Ay=30%Ax	Ay=40%Ax	Ay=0.5g in phase	Ay=0.2g asynchronous
w/B	0.00189	0.0019	0.00172	0.0019	0.00248

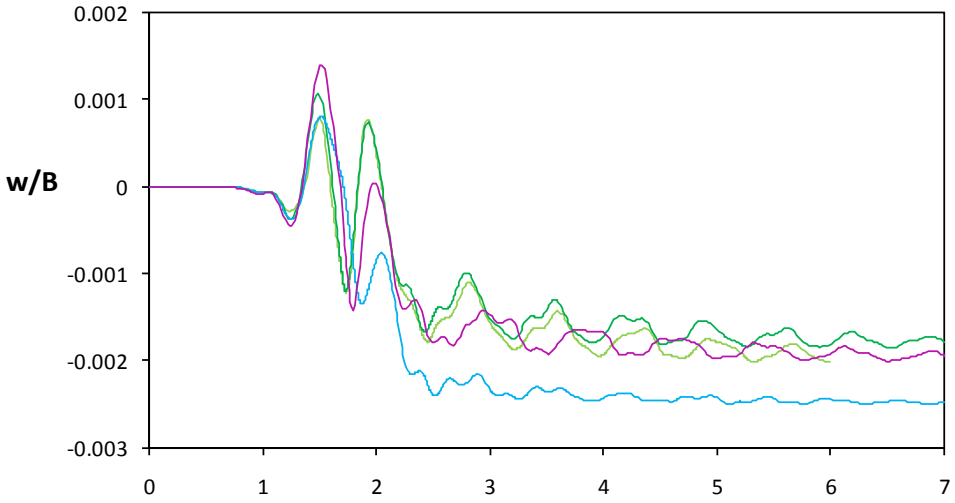

- a_g = 0.8 g

	Ax=0.8g	Ay=30%Ax	Ay=40%Ax
w/B	0.0027	0.0022	0.0022

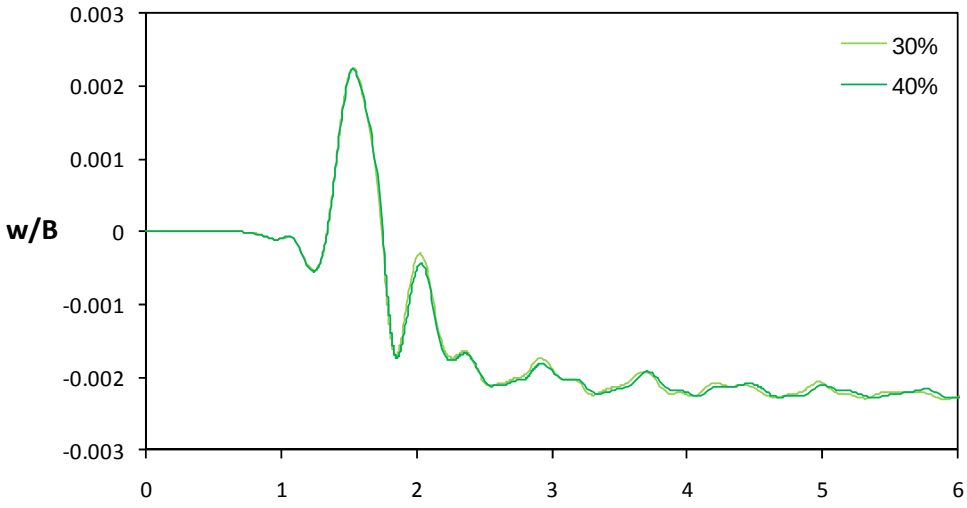

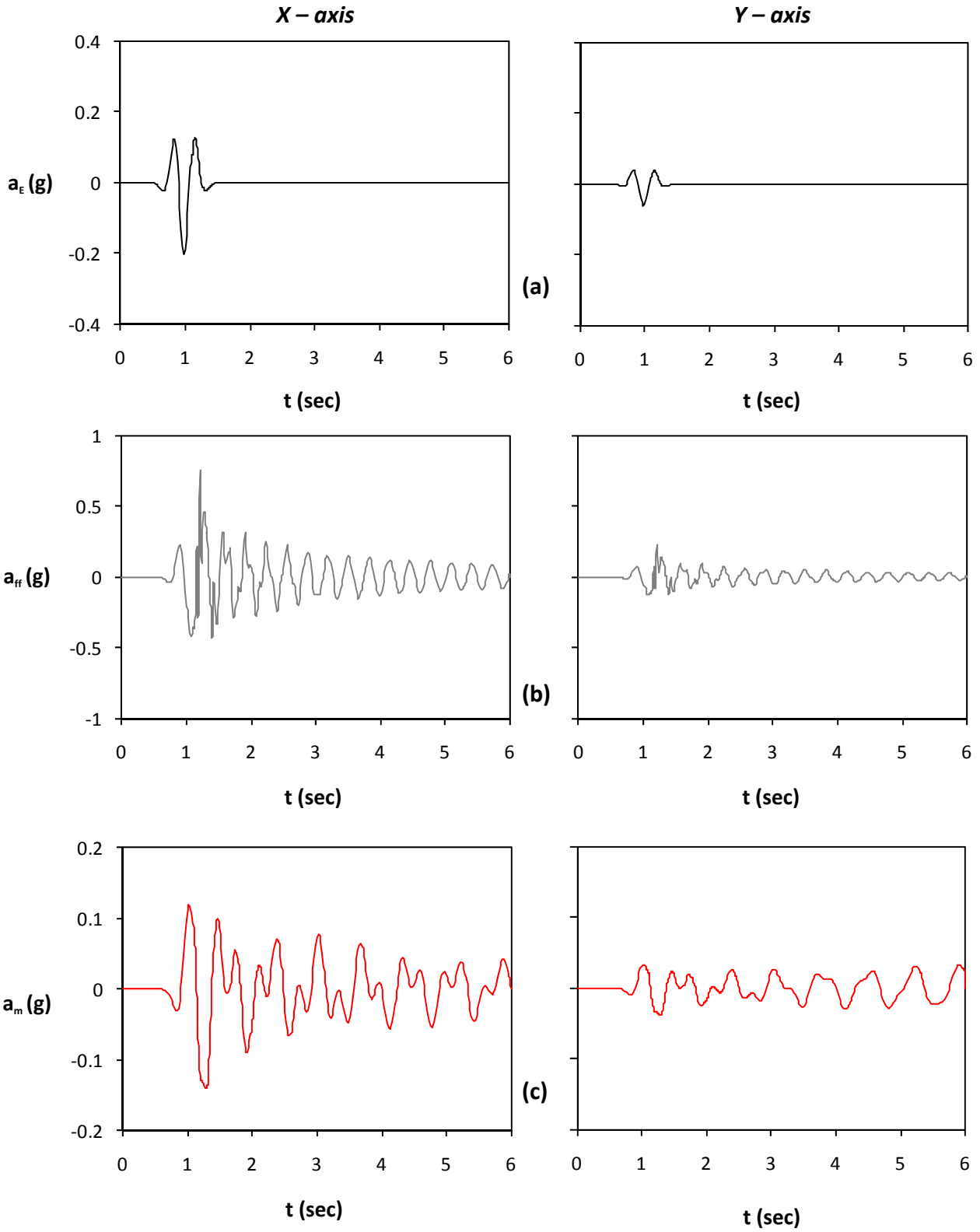

Figure 5.1. Seismic excitation in both directions, Ricker 2 A_x = 0.2 g and A_y =30% x 0.2 g : (a) acceleration time histories of bedrock excitation along the *x* axis (left) and the *y* axis (right) ; (b) acceleration time histories at the free field ; and (c) acceleration time histories of lumped mass.

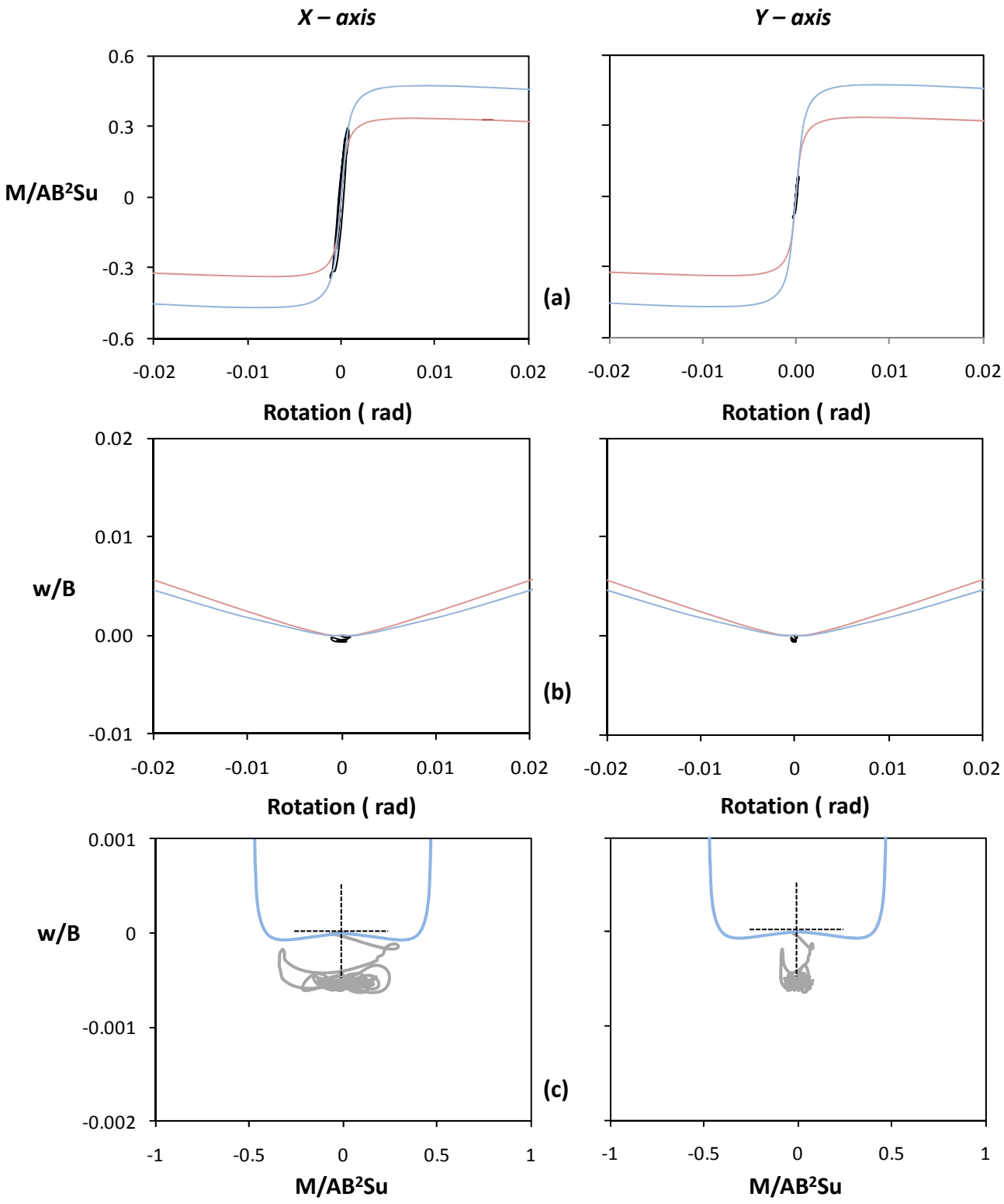

Figure 5.2. Seismic excitation in both directions, Ricker 2 A_x = 0.2 g and A_y =30% x 0.2 g :
(a) Normalized moment versus rotation along the *x* axis (left) and the *y* axis (right) ;
(b) Normalized to width vertical settlement versus rotation ; and
(c) Normalized vertical settlement to moment along the *x* axis (left) and the *y* axis (right) .

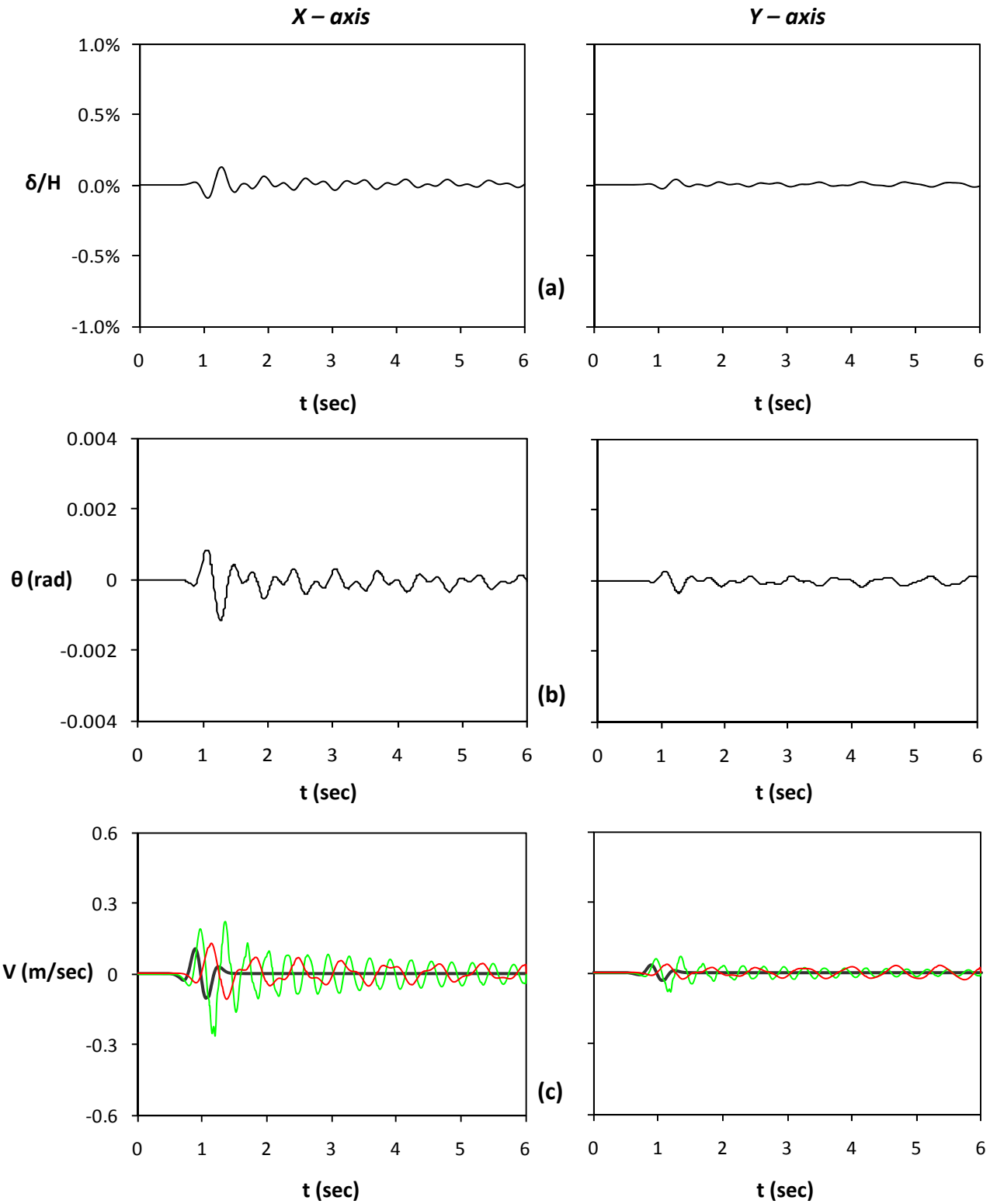

Figure 5.3. Seismic excitation in both directions, A_x = 0.2 g and A_y =30% x 0.2 g :
(a) Horizontal displacement normalized to height time histories along the *x* axis (left) and the *y* axis (right) ; (b) rotation time histories along the *x* axis (left) and the *y* axis (right) ; (c) velocity time histories (Green line stands for free field motion and red line for lumped mass)

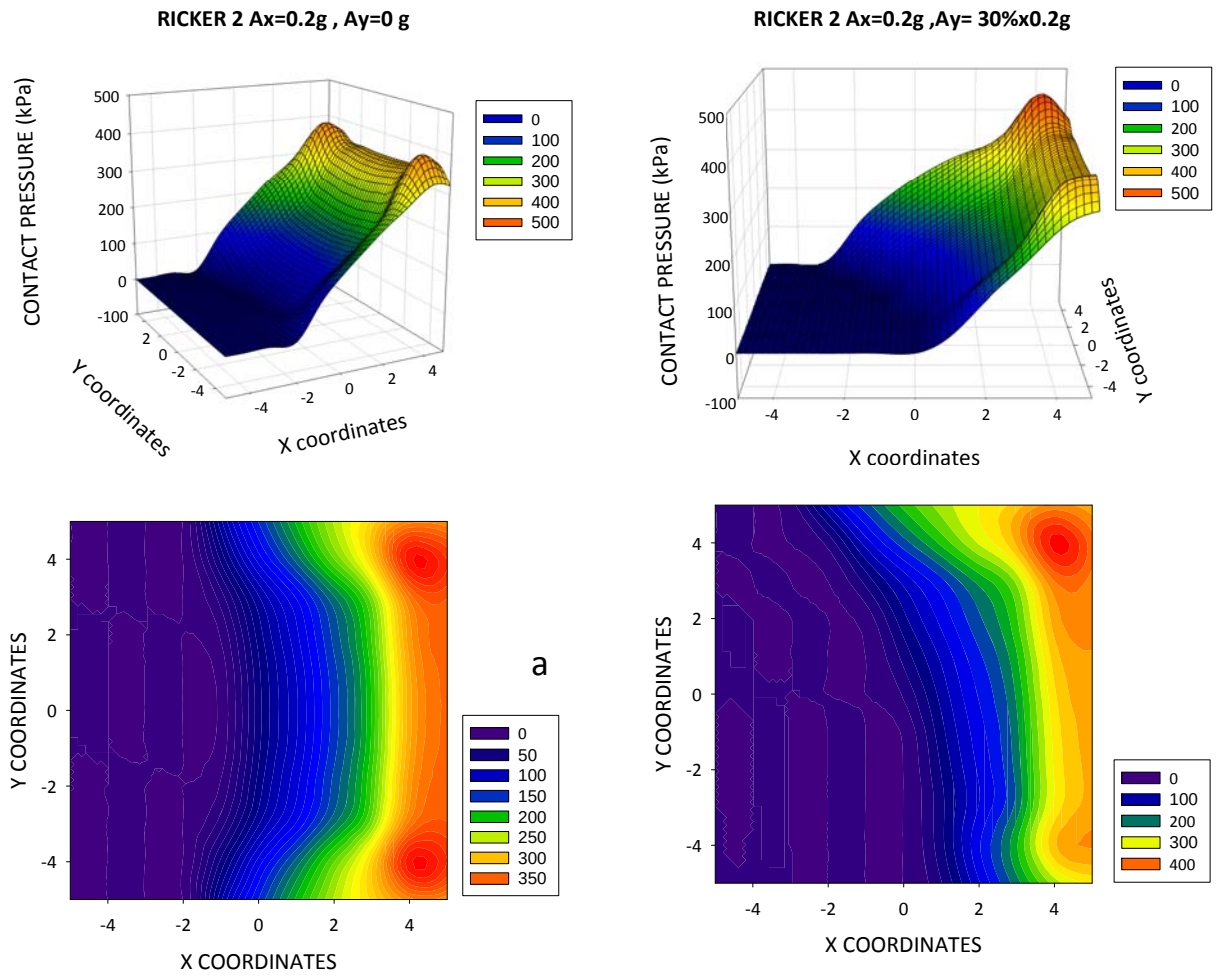

Figure 5.4. Seismic excitation in both directions, Ricker 2 A_x = 0.2 g and A_y = 30% x 0.2 g : Distribution of pressures under the footing at the time increment when the maximum uplift occurs for excitation in a) one direction (left) b) both directions (right) .

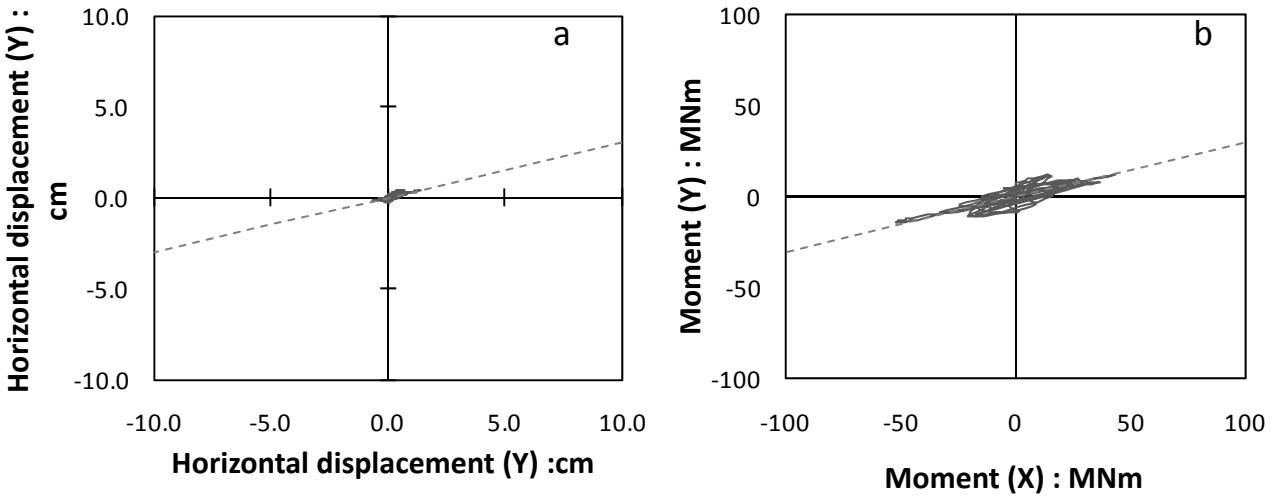

Figure 5.5 **a)** Orbit of center of mass in the X-Y plane.
b) Orbit in the M_X –M_Y plane.

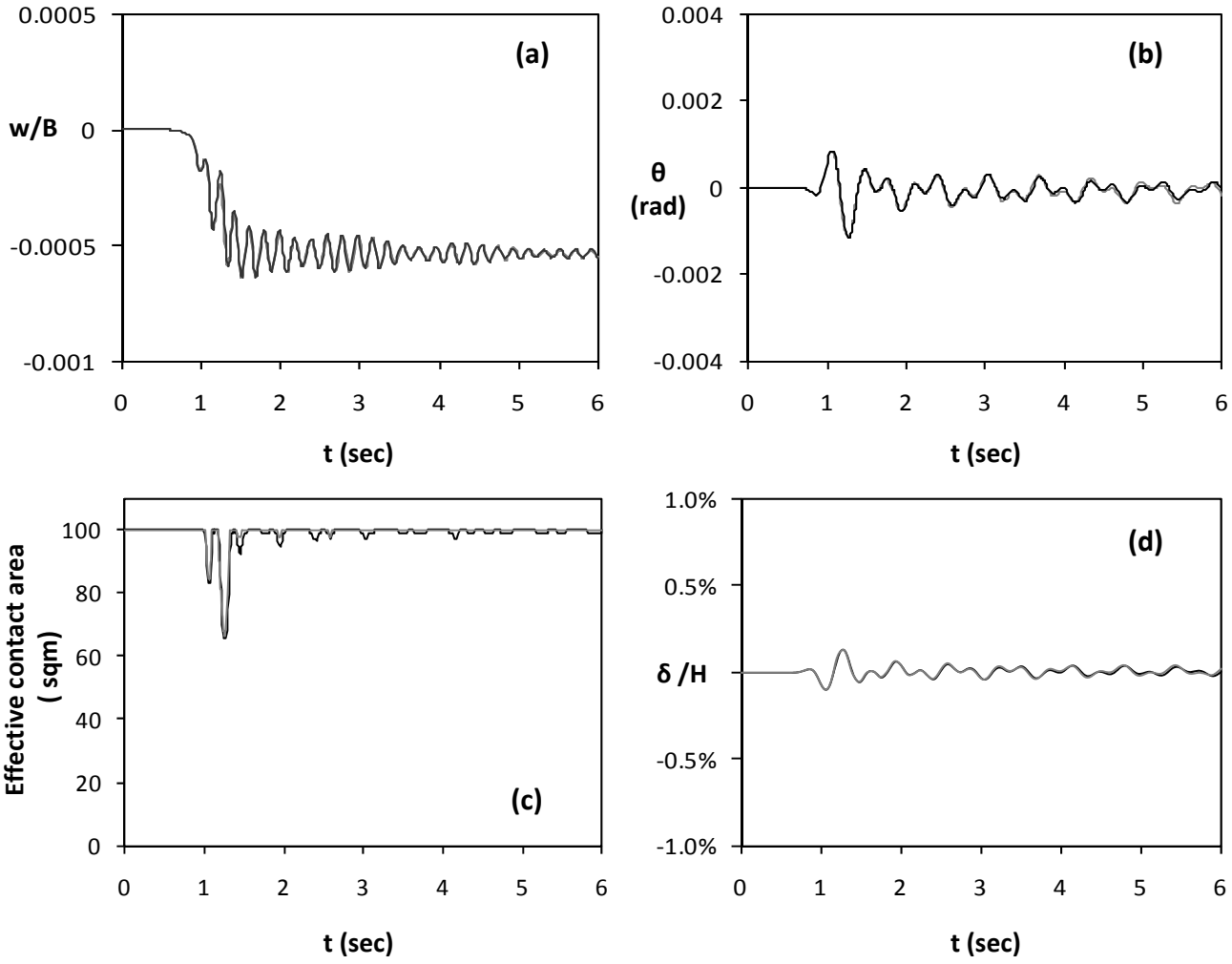

Figure 5.6. Seismic excitation in both directions, Ricker 2 A_x = 0.2 g and A_y =30% x 0.2 g and comparison with the single direction case.
Time histories of (a) Vertical settlement (b) Rotation ; (c) Effective contact area time ; (d) horizontal displacement normalized to height. (Black line represents excitation in both directions and grey line single direction excitation)

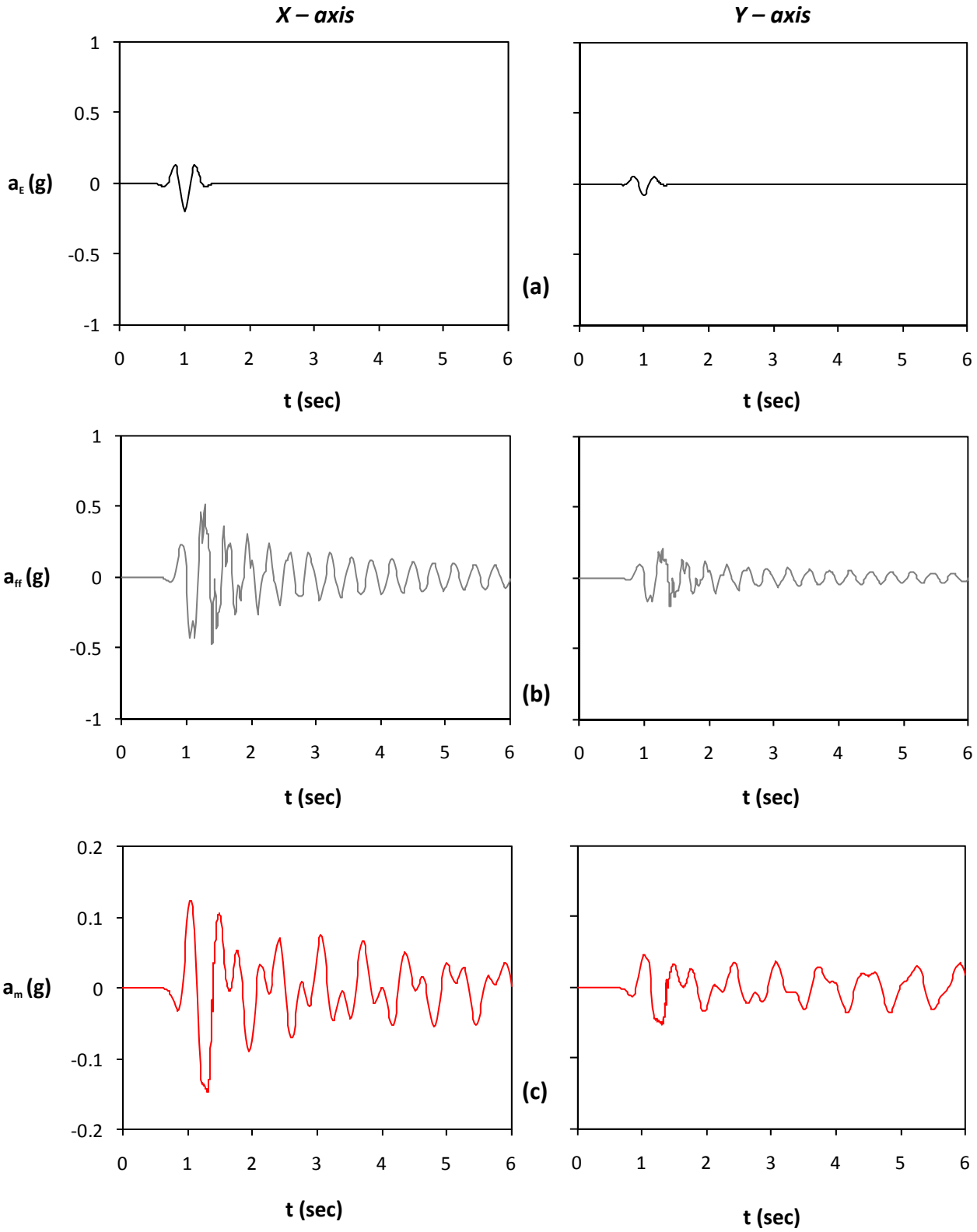

Figure 5.7. Seismic excitation in both directions, Ricker 2 A_x = 0.2 g and A_y =40% x 0.2 g: (a) acceleration time histories of bedrock excitation along the *x* axis (left) and the *y* axis (right) ; (b) acceleration time histories at the free field ; and (c) acceleration time histories of lumped mass.

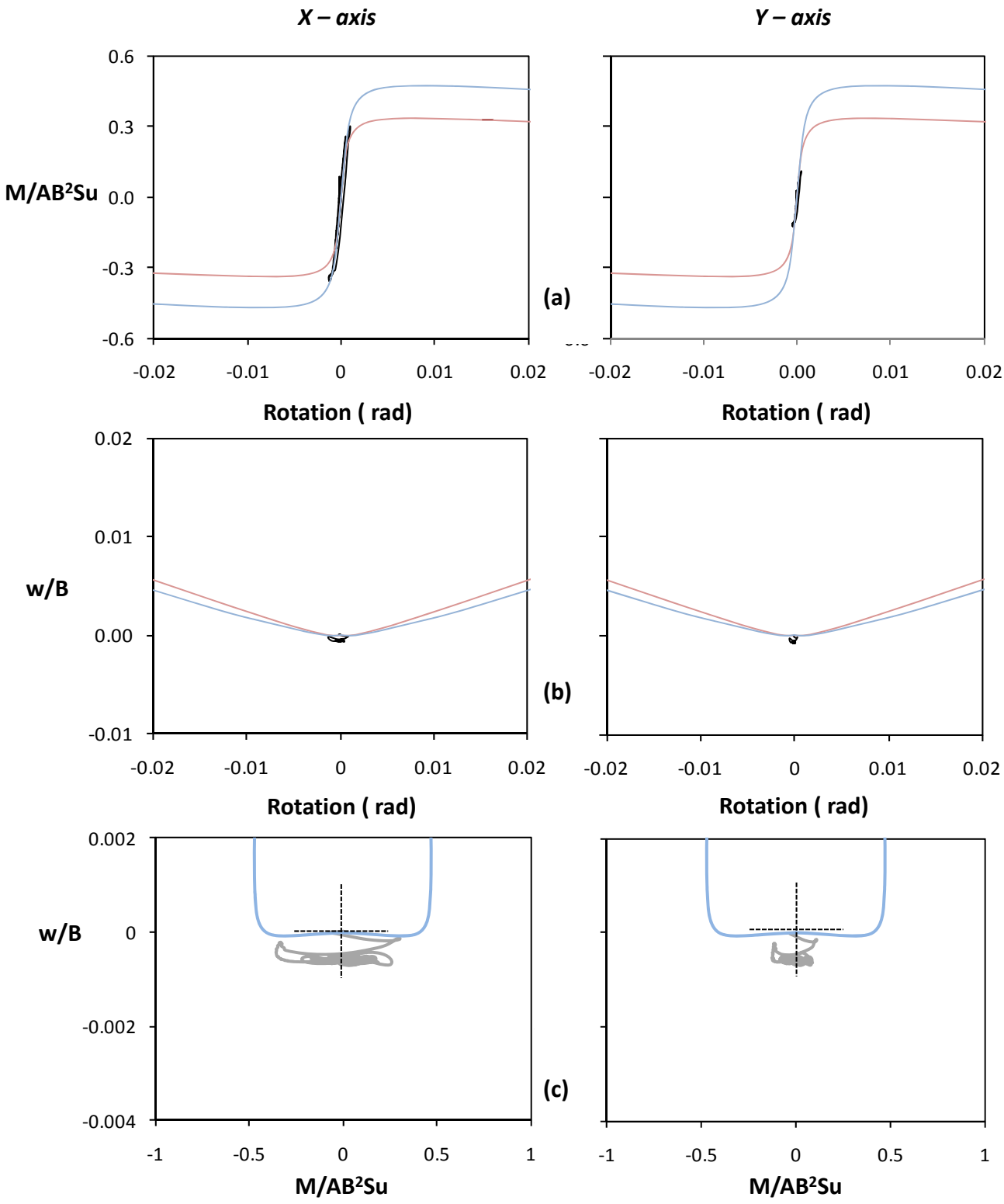

Figure 5.8. Seismic excitation in both directions, Ricker 2 A_x = 0.2 g and A_y = 0.2 g asynchronous peaks:
(a) Normalized moment versus rotation along the *x* axis (left) and the *y* axis (right) ;
(b) Normalized to width vertical settlement versus rotation ; and
(c) Normalized vertical settlement to moment along the *x* axis (left) and the *y* axis (right) .

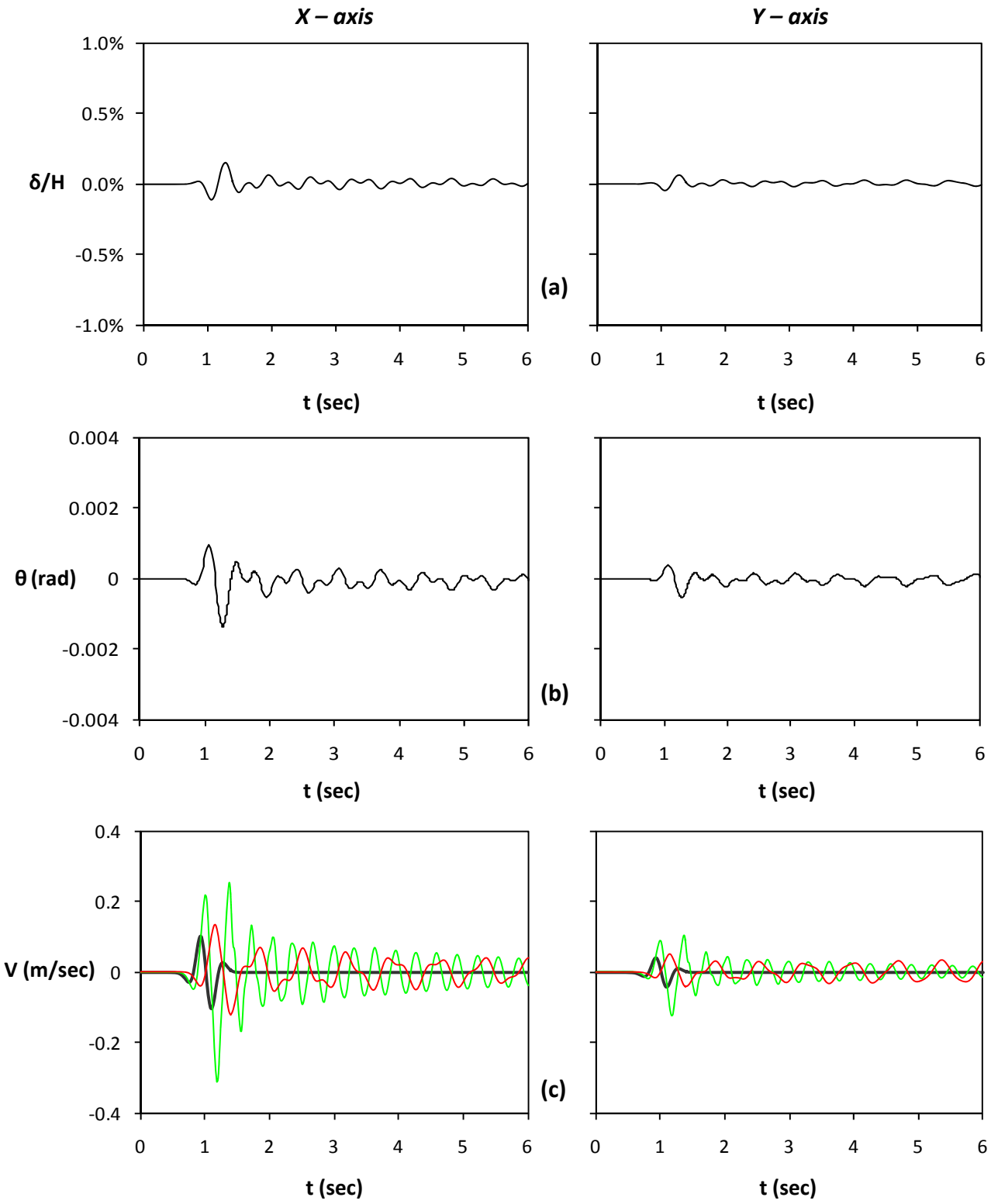

Figure 5.9. Seismic excitation in both directions, Ricker 2 A_x = 0.2 g and A_y =40% x 0.2 g : (a) Horizontal displacement normalized to height time histories along the *x* axis (left) and the *y* axis (right) ; (b) rotation time histories along the *x* axis (left) and the *y* axis (right) ; (c) velocity time histories (Green line stands for free field motion and red line for lumped mass)

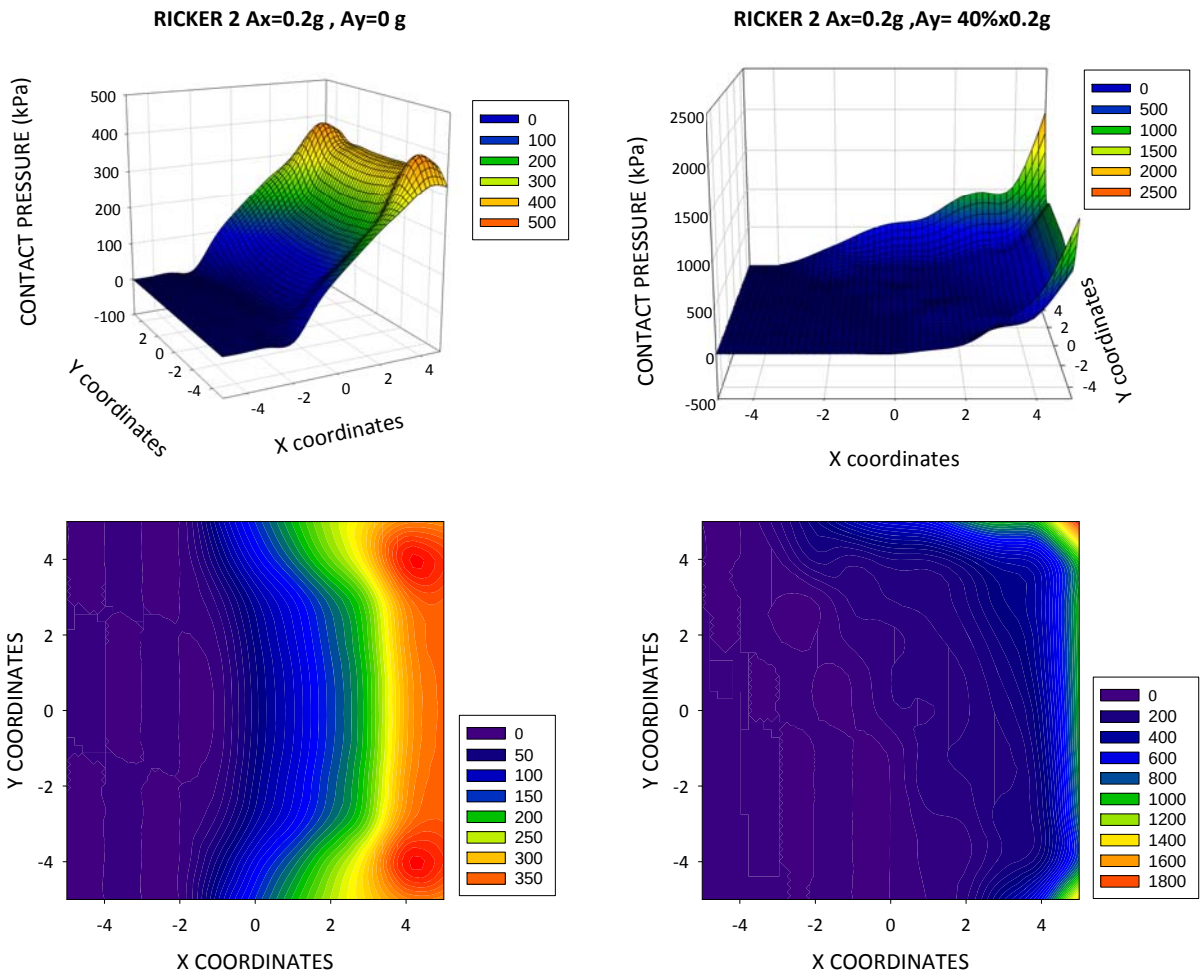

Figure 5.10. Seismic excitation in both directions, Ricker 2 A_x = 0.2 g and A_y =40% x 0.2 g : Distribution of pressures under the footing at the time increment when the maximum uplift occurs for excitation in a) one direction (left) b) both directions (right) .

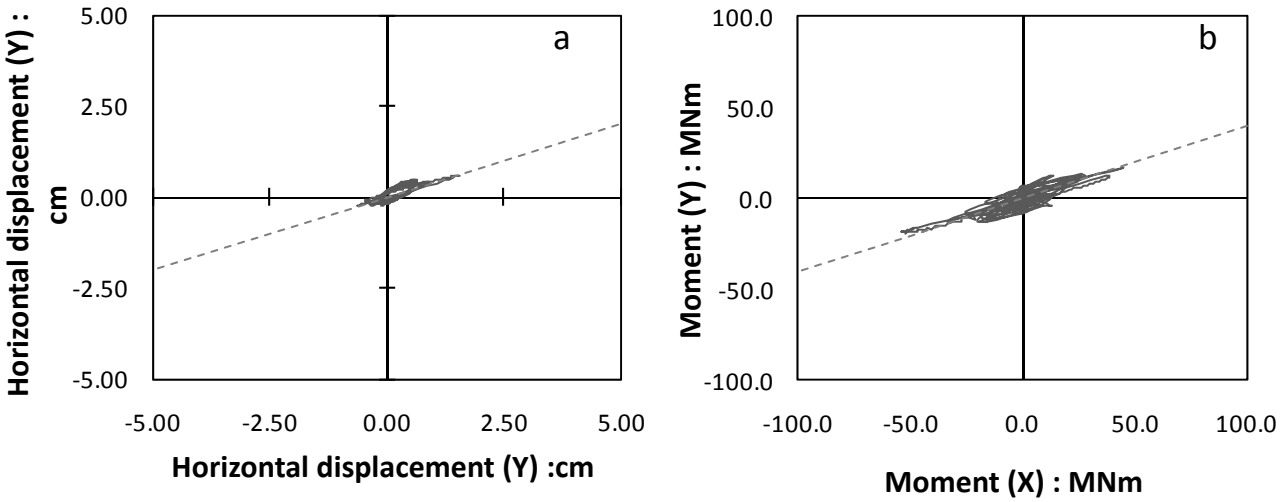

Figure 5.11. **a)** Orbit of center of mass in the X-Y plane.
b) Orbit in the M_X –M_Y plane.

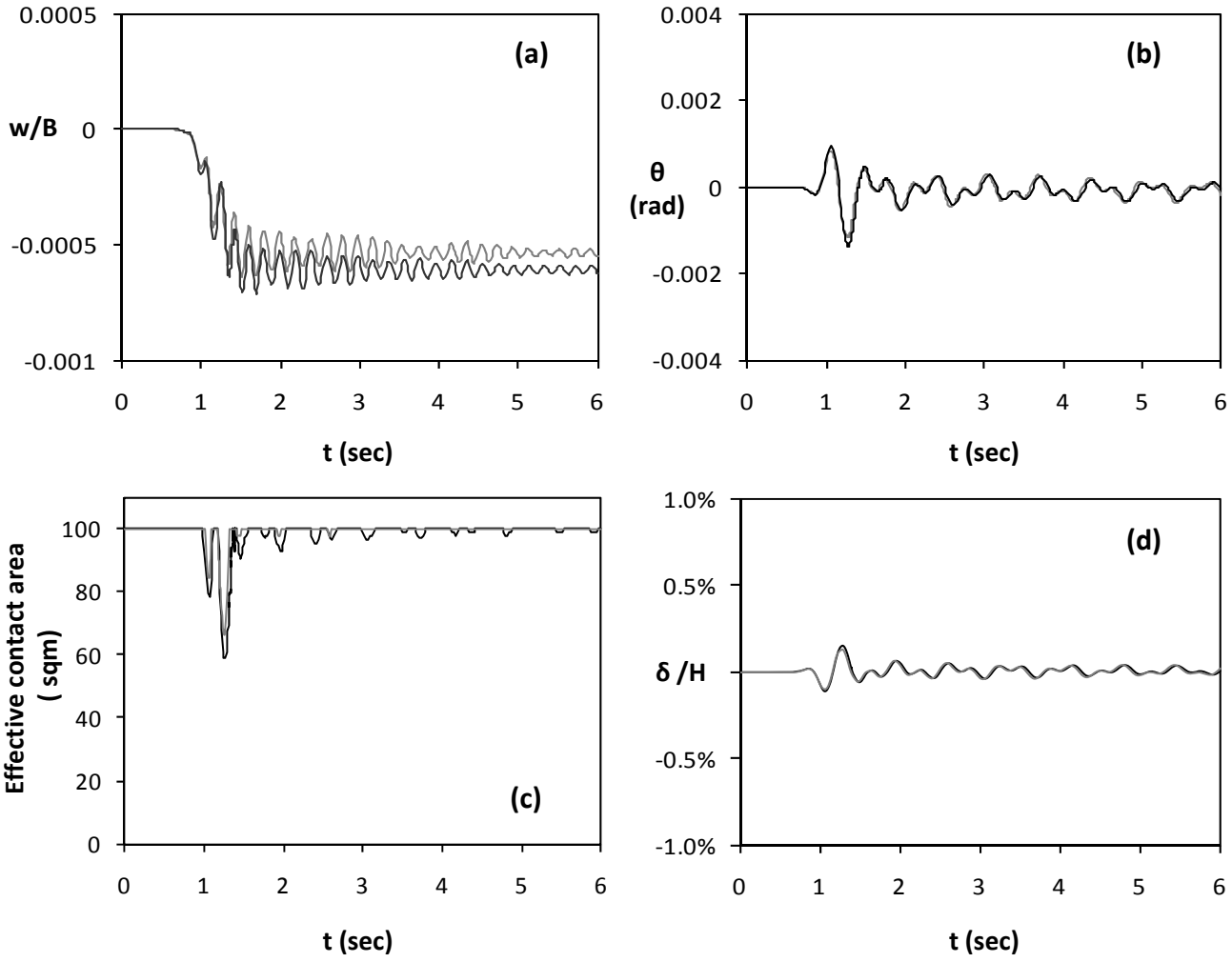

Figure 5.12. Seismic excitation in both directions, Ricker 2 A_x = 0.2 g and A_y =40% x 0.2 g and comparison with the single direction case.
Time histories of (a) Vertical settlement (b) Rotation ; (c) Effective contact area time ; (d) horizontal displacement normalized to height. (Black line represents excitation in both directions and grey line single direction excitation)

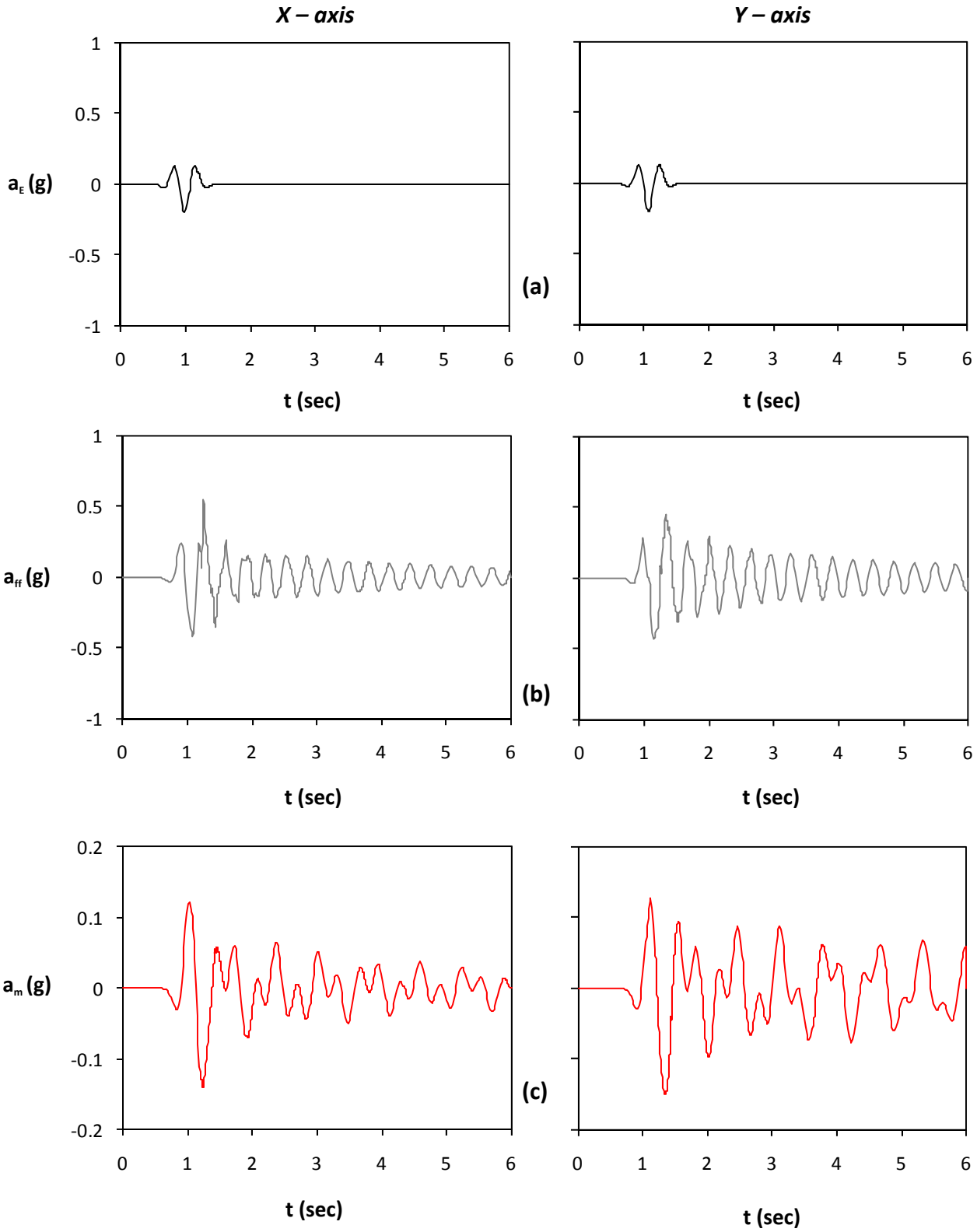

Figure 5.13. Seismic excitation in both directions, Ricker 2 A_x = 0.2 g and A_y = 0.2 g out of phase: (a) acceleration time histories of bedrock excitation along the *x* axis (left) and the *y* axis (right) ; (b) acceleration time histories at the free field ; and (c) acceleration time histories of lumped mass.

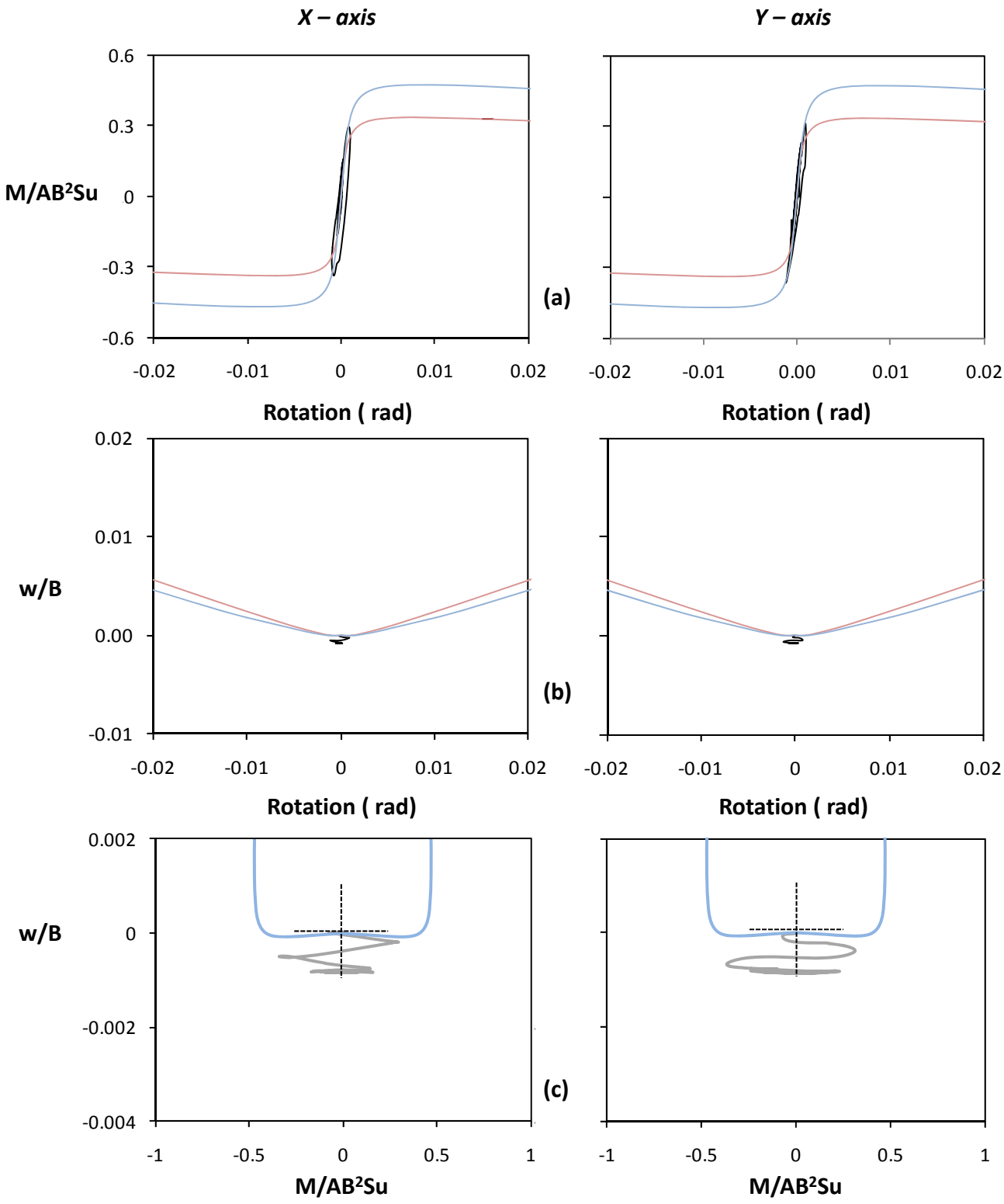

Figure 5.14. Seismic excitation in both directions, Ricker 2 A_x = 0.2 g and A_y = 0.2 g out of phase:
(a) Normalized moment versus rotation along the *x* axis (left) and the *y* axis (right) ;
(b) Normalized to width vertical settlement versus rotation ; and
(c) Normalized vertical settlement to moment along the *x* axis (left) and the *y* axis (right) .

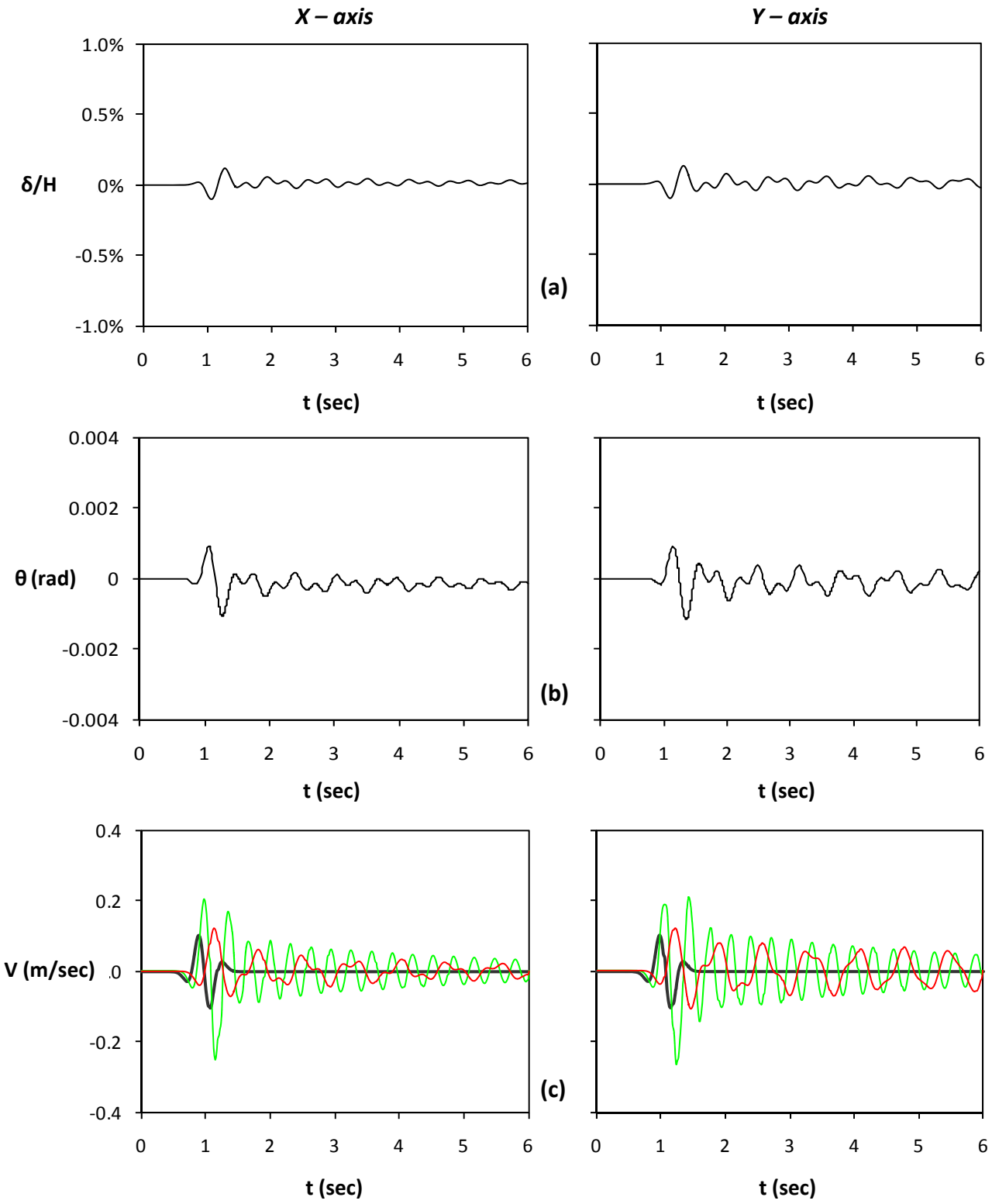

Figure 5.15. Seismic excitation in both directions, Ricker 2 A_x = 0.2 g and A_y = 0.2 g out of phase:
(a) Horizontal displacement normalized to height time histories along the *x* axis (left) and the *y* axis (right) ; (b) rotation time histories along the *x* axis (left) and the *y* axis (right) ; (c) velocity time histories (Green line stands for free field motion and red line for lumped mass)

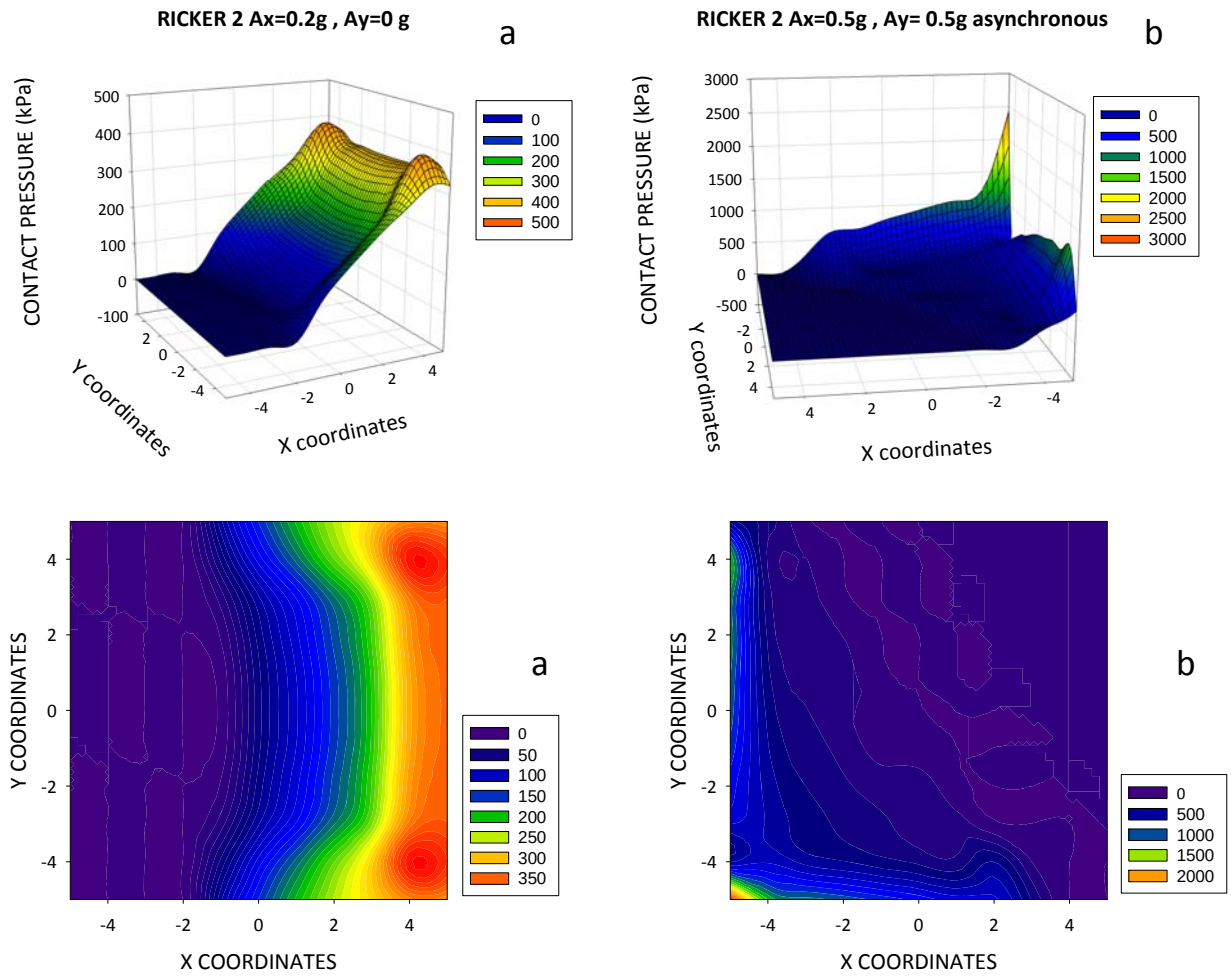

Figure 5.16. Seismic excitation in both directions, Ricker 2 A_x = 0.2 g and A_y = 0.2 g out of phase : Distribution of pressures under the footing at the time increment when the maximum uplift occurs for exitation in a) one direction (left) b) both directions (right) .

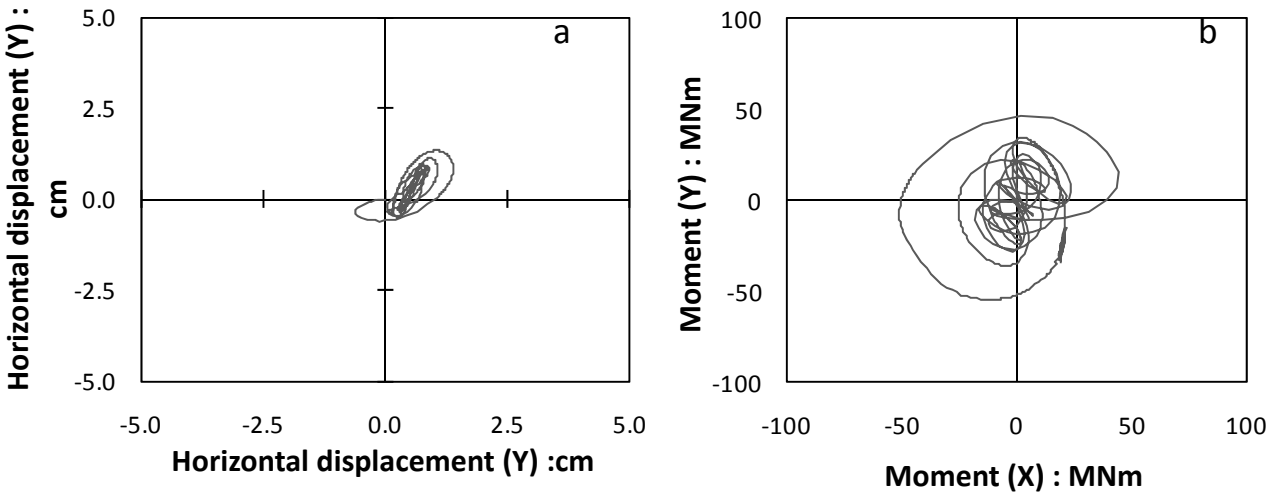

Figure 5.17. **a)** Orbit of center of mass in the X-Y plane.
b) Orbit in the M_X –M_Y plane.

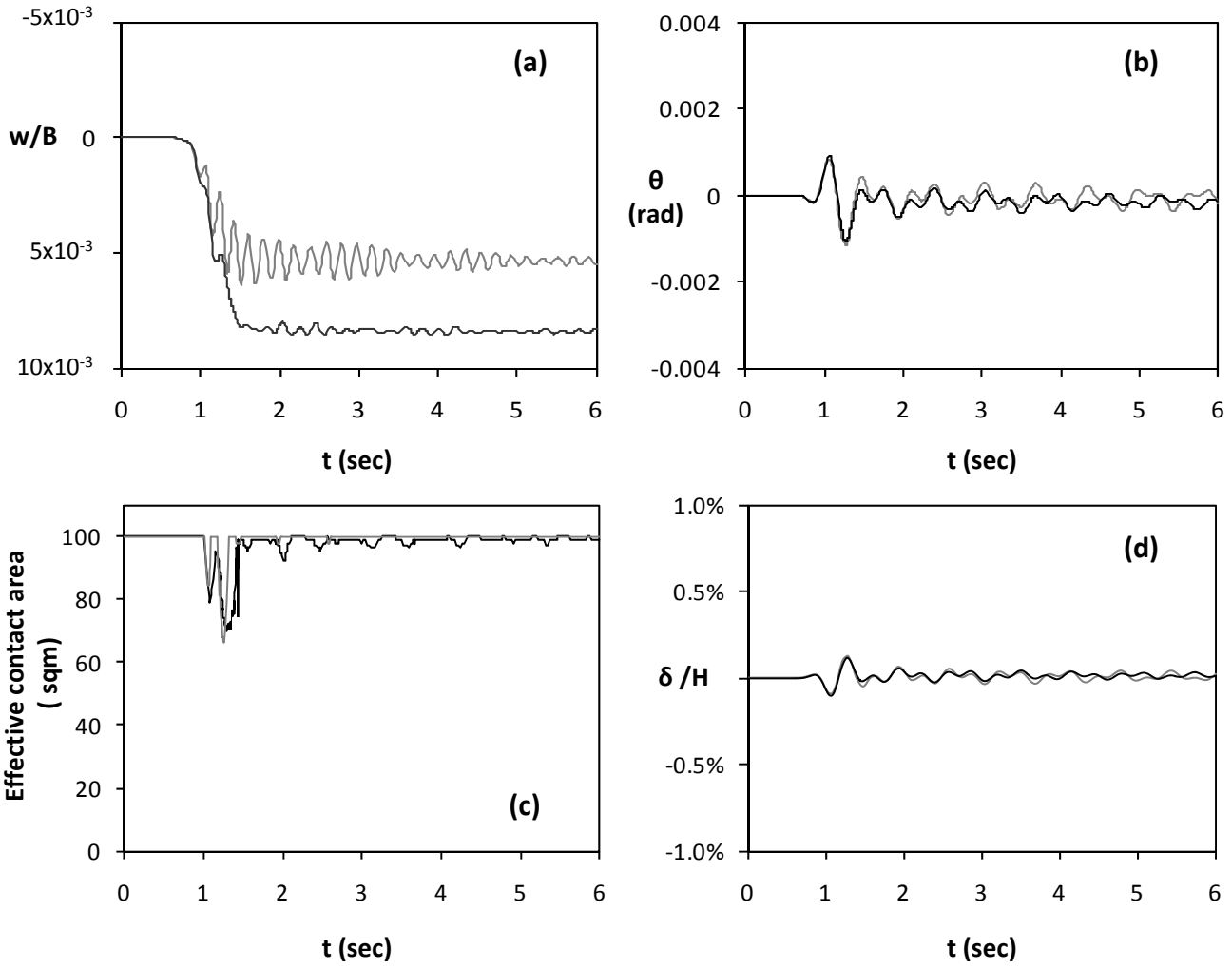

Figure 5.18. Seismic excitation in both directions, Ricker 2 A_x = 0.2 g and A_y = 0.2 g out of phase and comparison with the single direction case.
Time histories of (a) Vertical settlement (b) Rotation ; (c) Effective contact area time ; (d) horizontal displacement normalized to height. (Black line represents excitation in both directions and grey line single direction excitation)

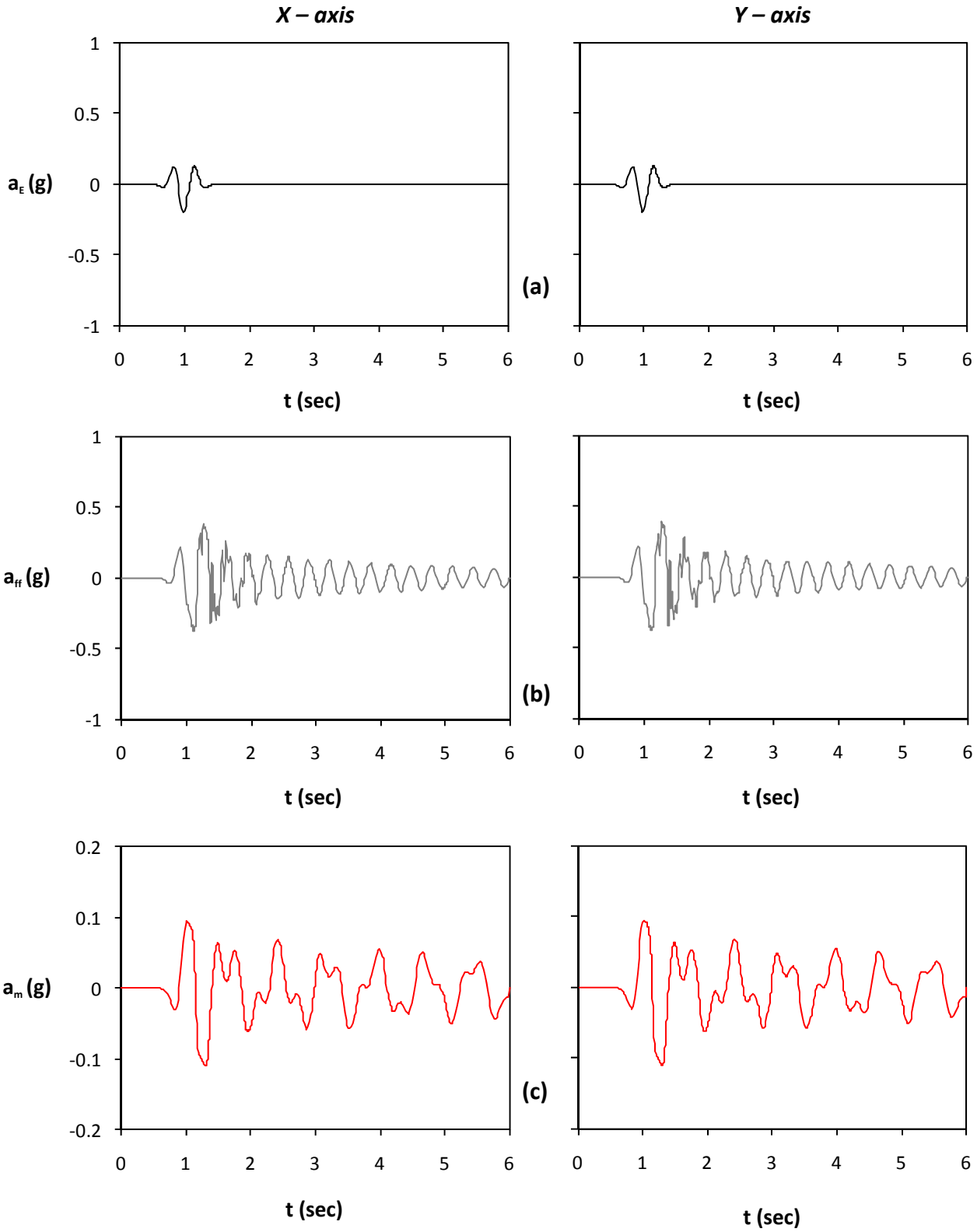

Figure 5.19. Seismic excitation in both directions, Ricker 2 A_x = 0.2 g and A_y = 0.2 g in phase: (a) acceleration time histories of bedrock excitation along the *x* axis (left) and the *y* axis (right) ; (b) acceleration time histories at the free field ; and (c) acceleration time histories of lumped mass.

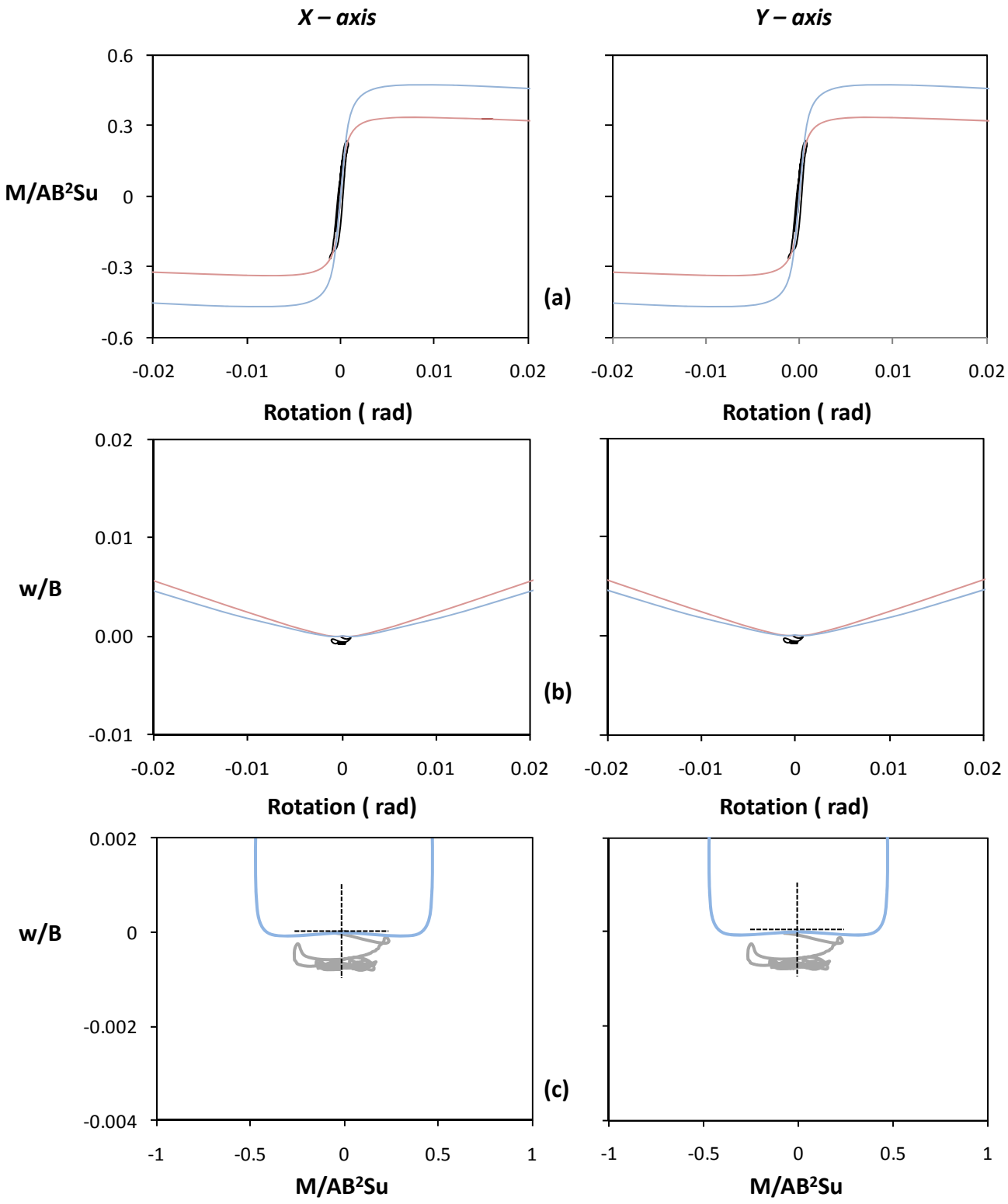

Figure 5.20. Seismic excitation in both directions, Ricker 2 A_x = 0.2 g and A_y = 0.2 g in phase:
(a) Normalized moment versus rotation along the *x* axis (left) and the *y* axis (right) ;
(b) Normalized to width vertical settlement versus rotation ; and
(c) Normalized vertical settlement to moment along the *x* axis (left) and the *y* axis (right) .

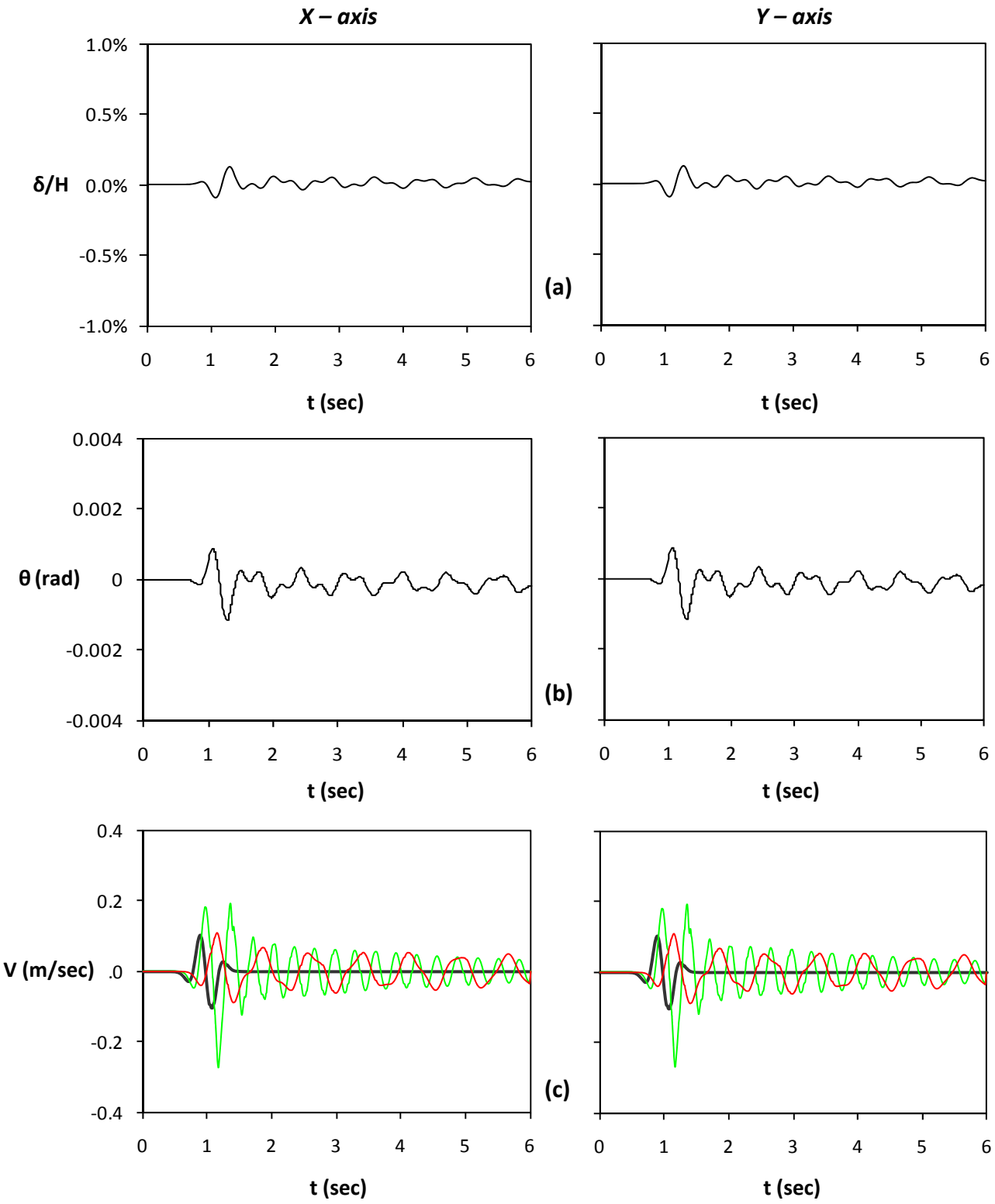

Figure 5.21. Seismic excitation in both directions, Ricker 2 A_x = 0.2 g and A_y = 0.2 g in phase: (a)Horizontal displacement normalized to height time histories along the *x* axis (left) and the *y* axis (right) ; (b) rotation time histories along the *x* axis (left) and the *y* axis (right) ; (c) velocity time histories (Green line stands for free field motion and red line for lumped mass)

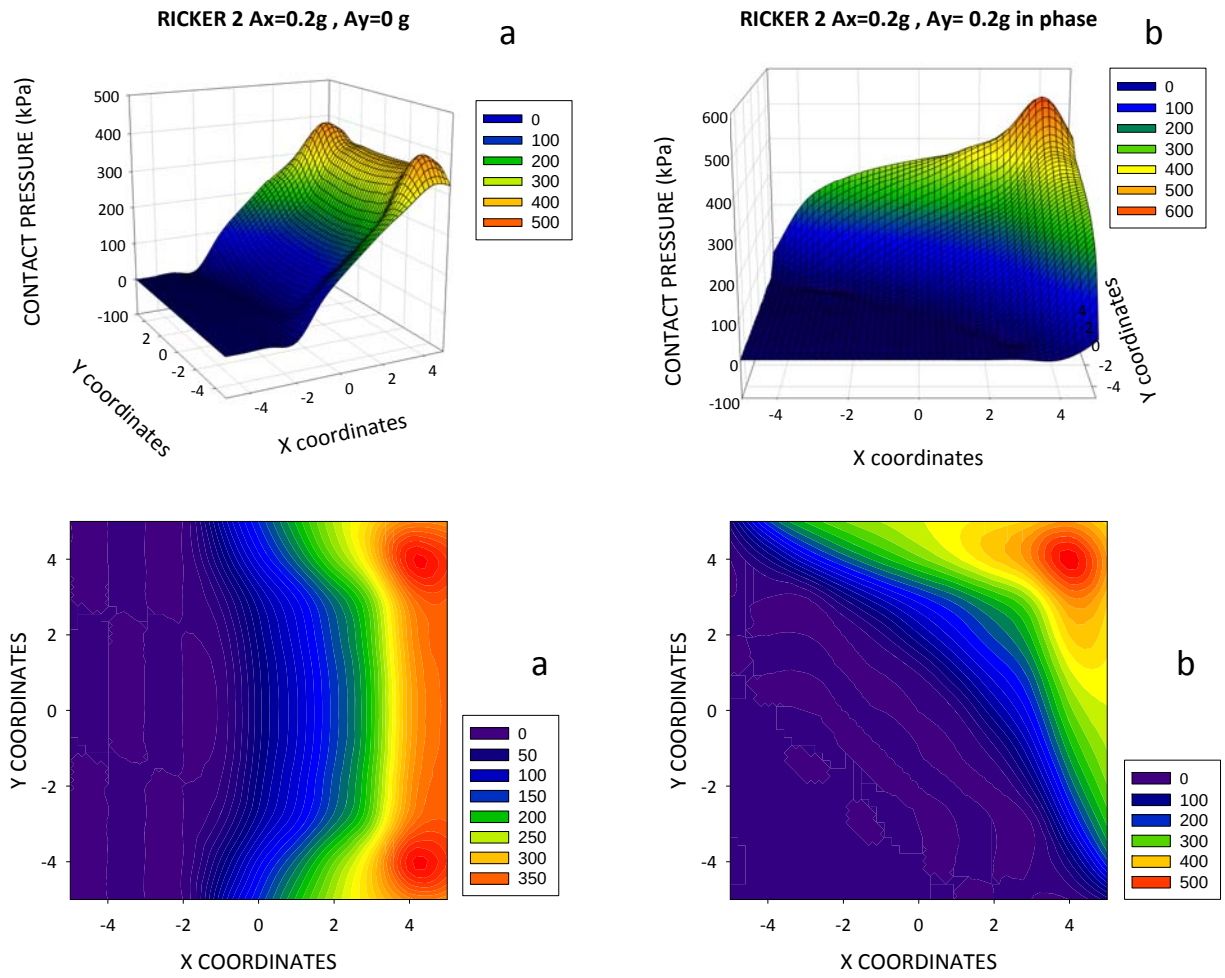

Figure 5.22. Seismic excitation in both directions, Ricker 2 A_x = 0.2 g and A_y = 0.2 g in phase : Distribution of pressures under the footing at the time increment when the maximum uplift occurs for excitation in a) one direction (left) b) both directions (right) .

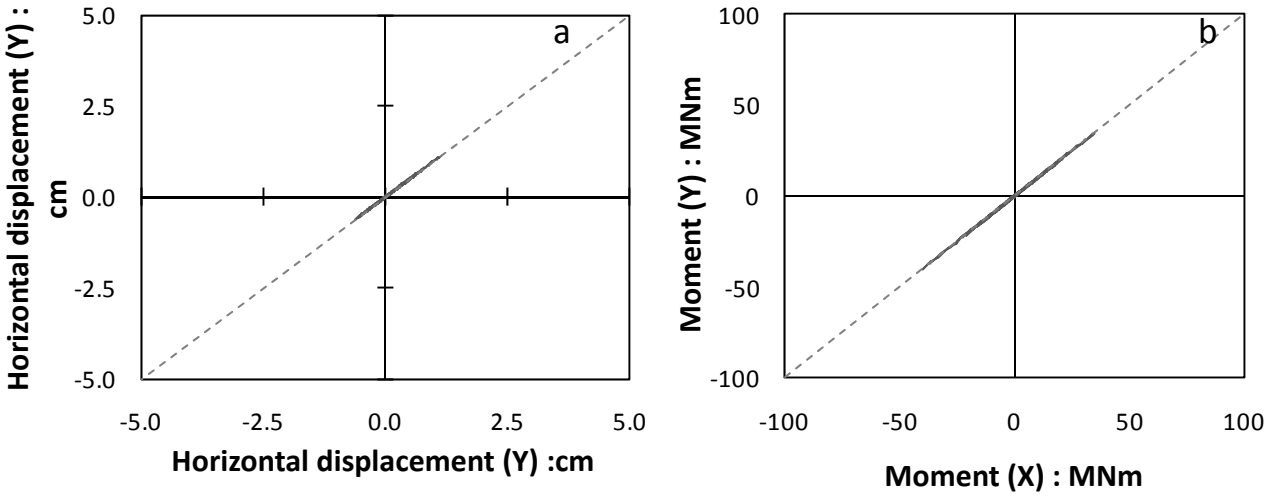

Figure 5.23. **a)** Orbit of center of mass in the X-Y plane.
b) Orbit in the M_X –M_Y plane.

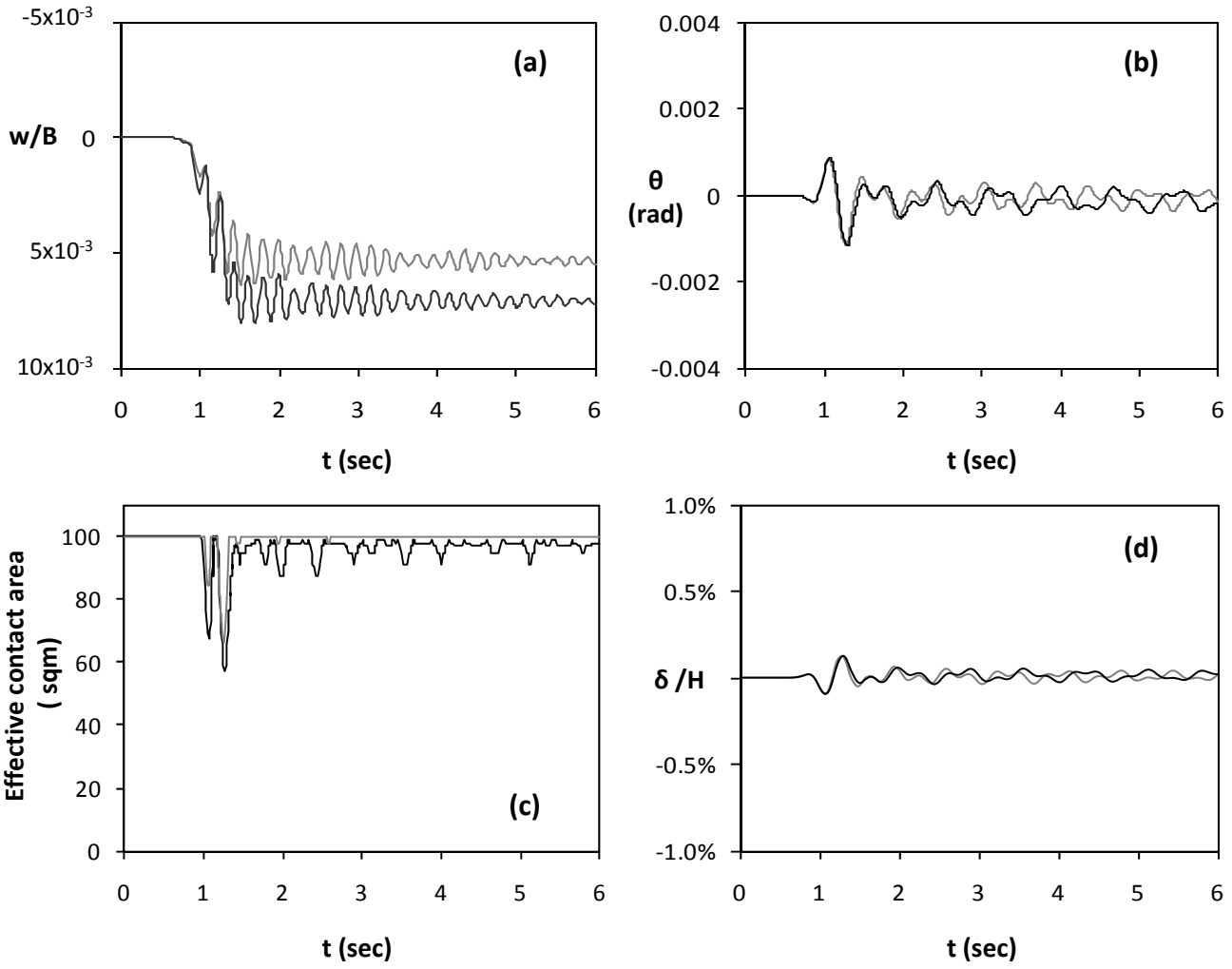

Figure 5.24. Seismic excitation in both directions, Ricker 2 A_x = 0.2 g and A_y = 0.2 g in phase and comparison with the single direction case.
Time histories of (a) Vertical settlement (b) Rotation ; (c) Effective contact area time ; (d) horizontal displacement normalized to height. (Black line represents excitation in both directions and grey line single direction excitation)

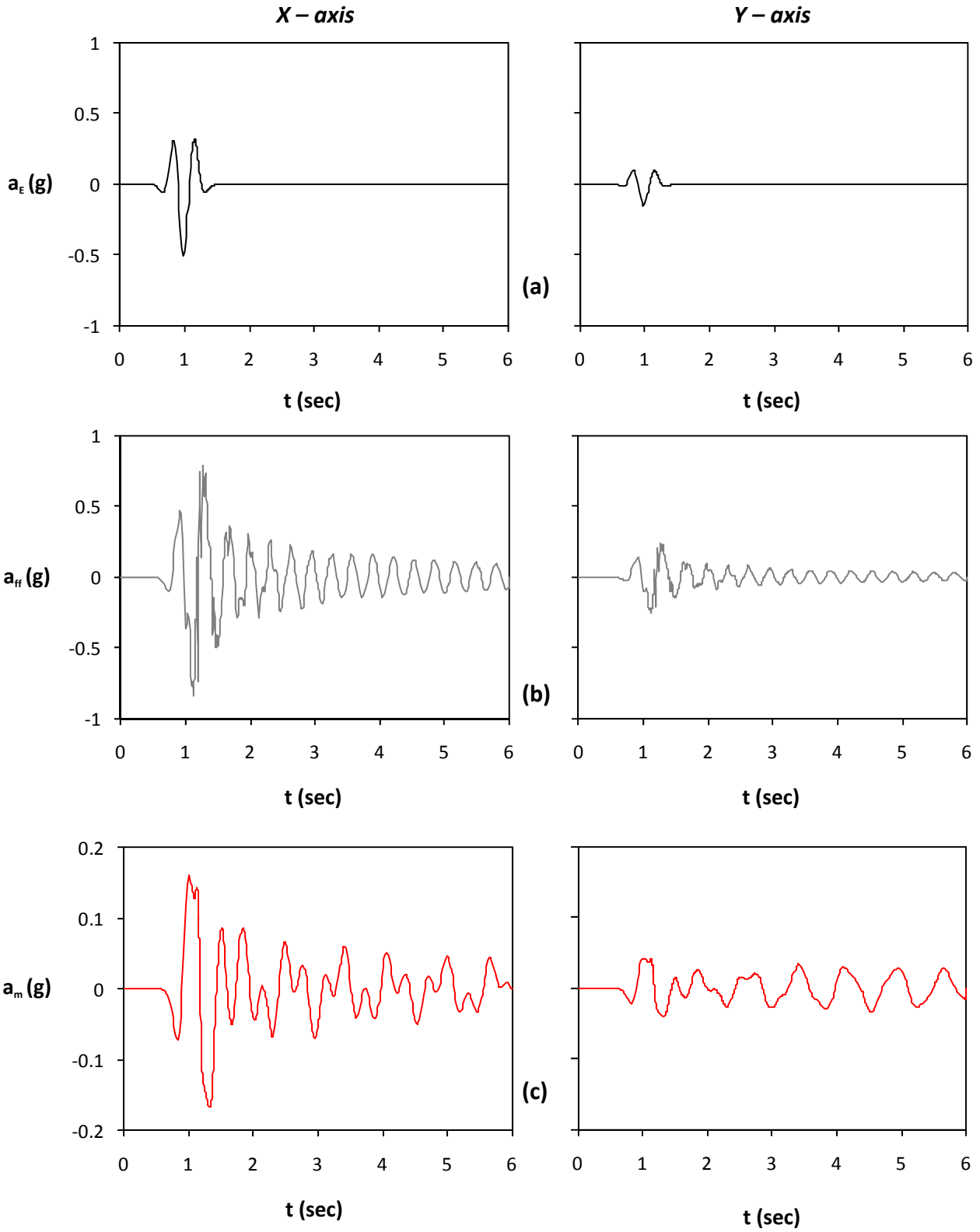

Figure 5.25. Seismic excitation in both directions, Ricker 2 A_x = 0.5 g and A_y =30% x 0.5 g : (a) acceleration time histories of bedrock excitation along the *x* axis (left) and the *y* axis (right) ; (b) acceleration time histories at the free field ; and (c) acceleration time histories of lumped mass.

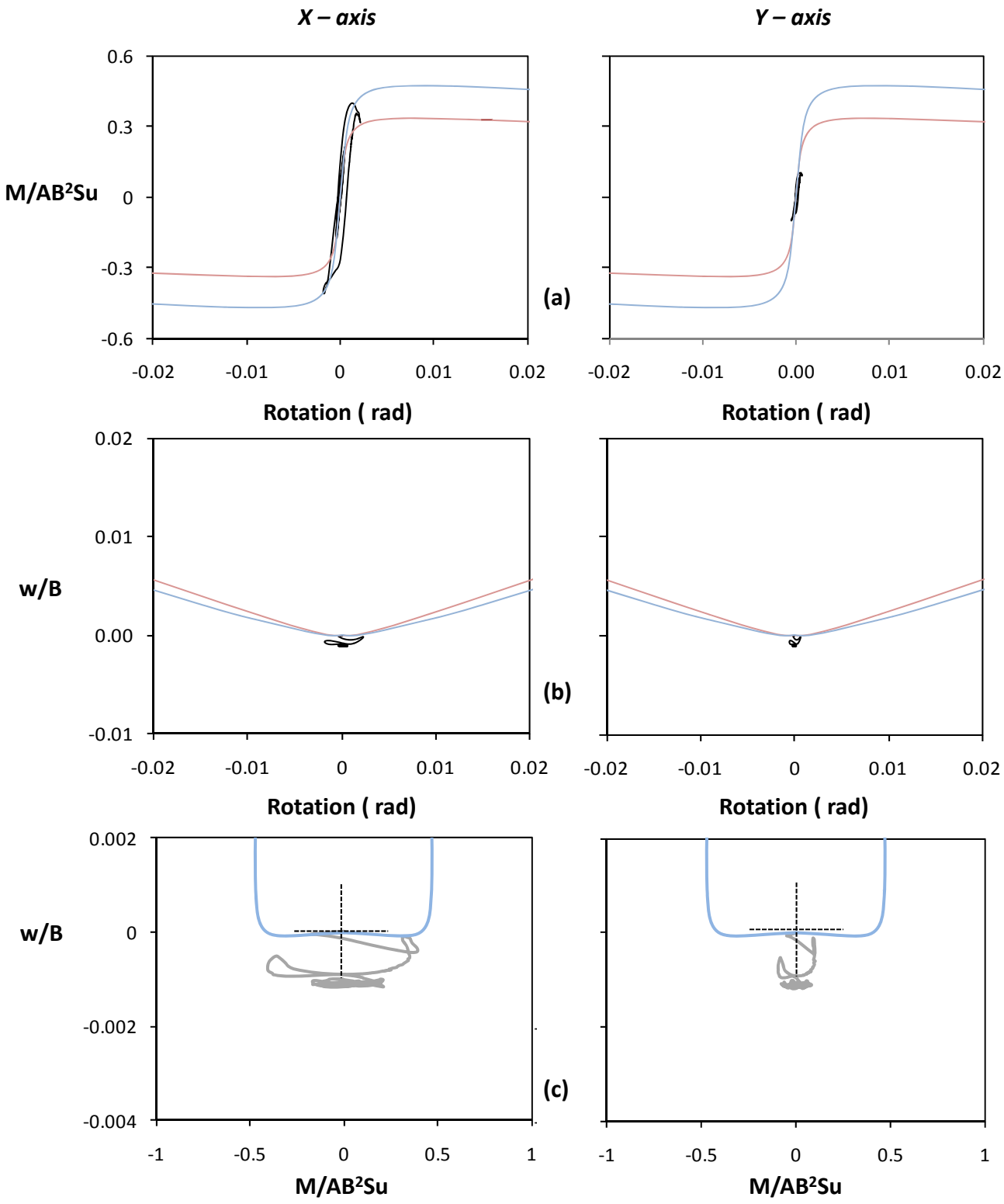

Figure 5.26. Seismic excitation in both directions, Ricker 2 A_x = 0.5 g and A_y =30% x 0.5 g :
(a) Normalized moment versus rotation along the *x* axis (left) and the *y* axis (right) ;
(b) Normalized to width vertical settlement versus rotation ; and
(c) Normalized vertical settlement to moment along the *x* axis (left) and the *y* axis (right) .

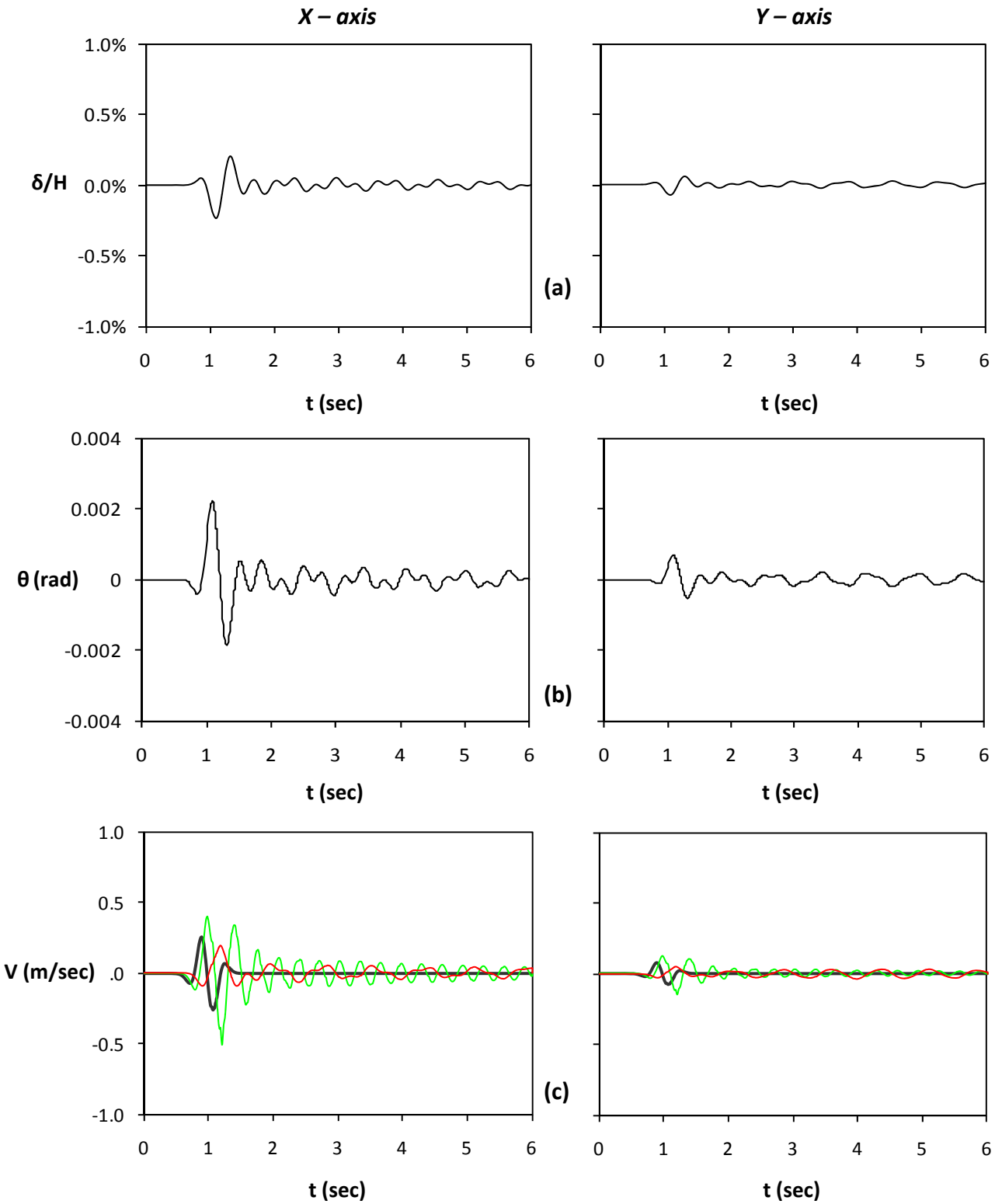

Figure 5.27. Seismic excitation in both directions, Ricker 2 A_x = 0.5 g and A_y = 30 x 0.5 g : (a) Horizontal displacement normalized to height time histories along the *x* axis (left) and the *y* axis (right) ; (b) rotation time histories along the *x* axis (left) and the *y* axis (right) ; (c) velocity time histories (Green line stands for free field motion and red line for lumped mass)

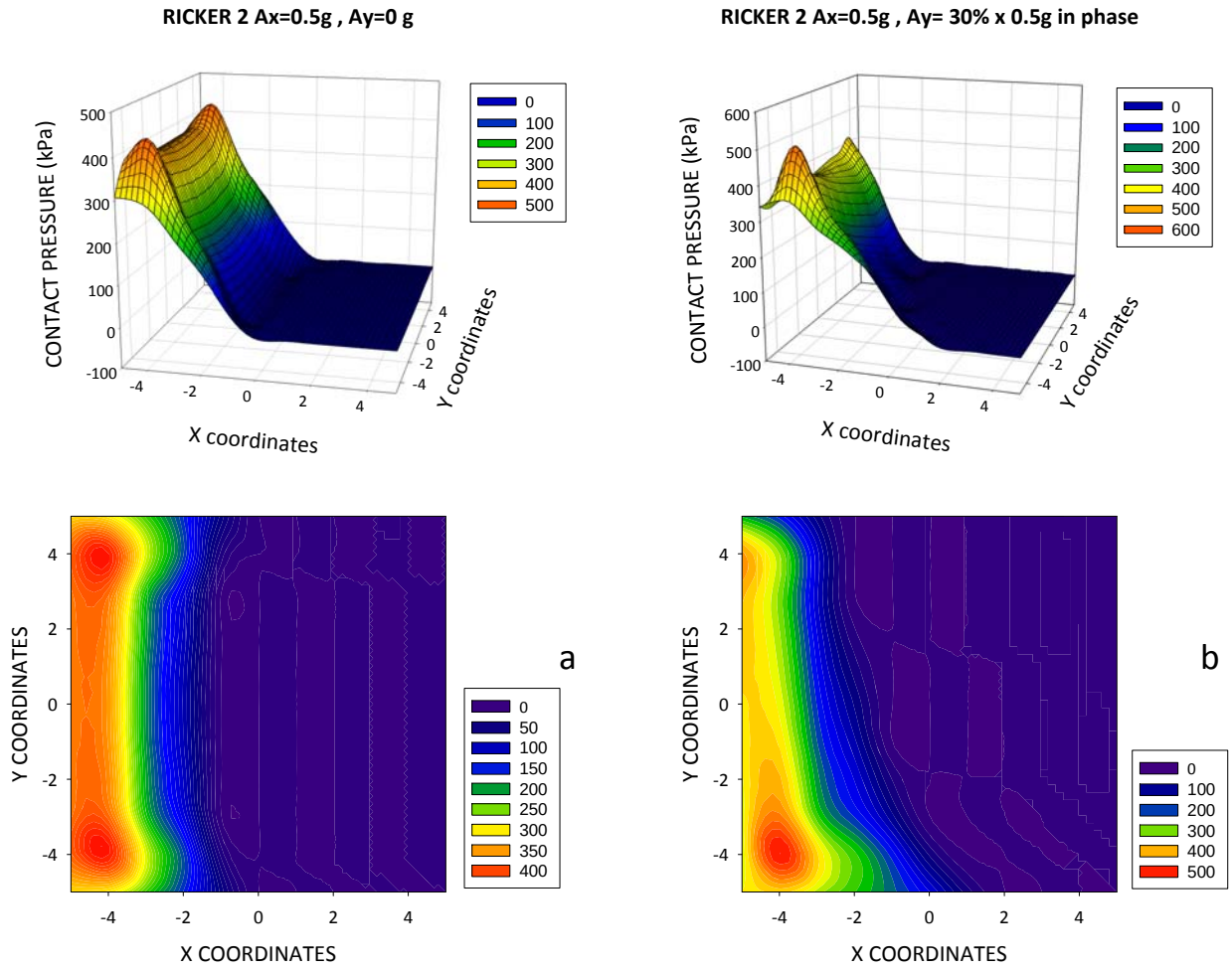

Figure 5.28. Seismic excitation in both directions, Ricker 2 A_x = 0.5 g and A_y =30% x 0.5 g: Distribution of pressures under the footing at the time increment when the maximum uplift occurs for excitation in a) one direction (left) b) both directions (right) .

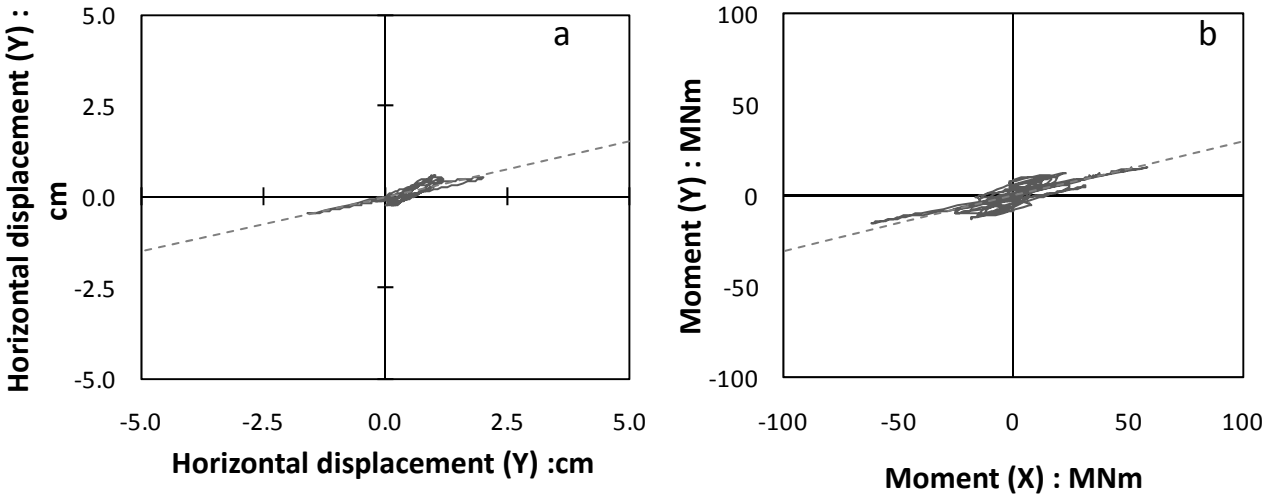

Figure 5.29. **a)** Orbit of center of mass in the X-Y plane.
b) Orbit in the M_X –M_Y plane.

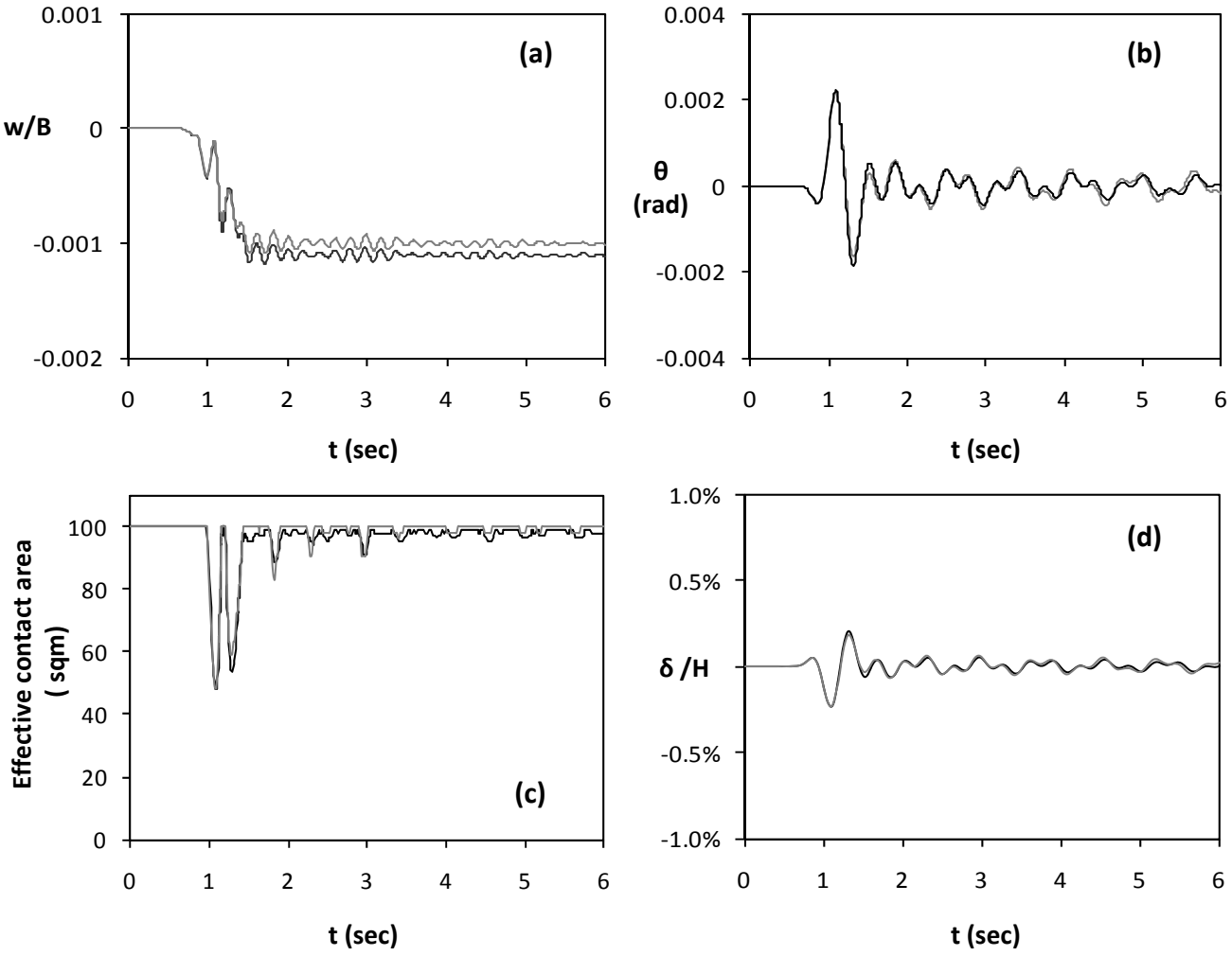

Figure 5.30. Seismic excitation in both directions, Ricker 2 A_x = 0.5 g and A_y = 30% x 0.5 g and comparison with the single direction case.
Time histories of (a) Vertical settlement (b) Rotation ; (c) Effective contact area time ; (d) horizontal displacement normalized to height. (Black line represents excitation in both directions and grey line single direction excitation)

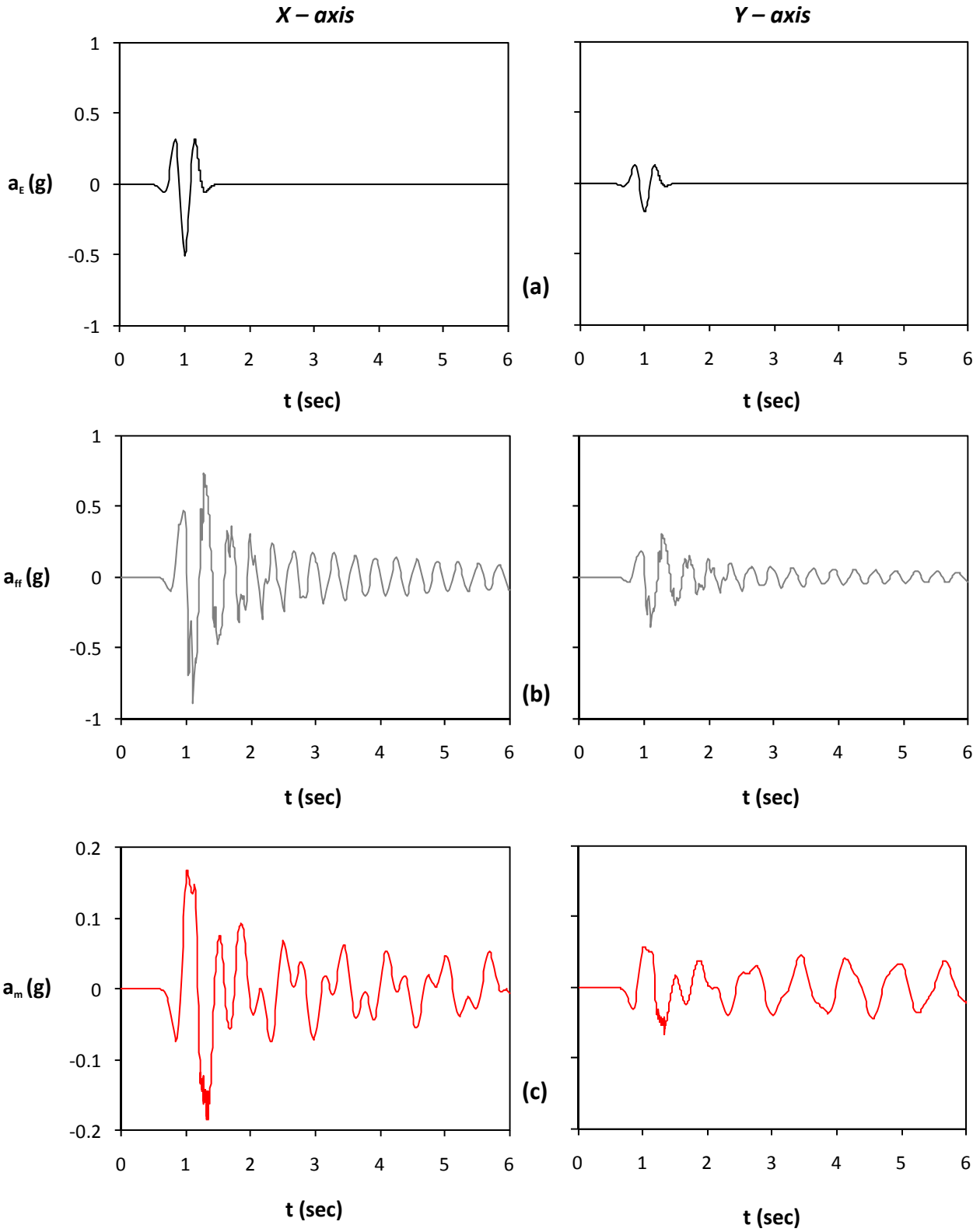

Figure 5.31. Seismic excitation in both directions, Ricker 2 A_x = 0.5 g and A_y = 40% x 0.5 g : (a) acceleration time histories of bedrock excitation along the *x* axis (left) and the *y* axis (right) ; (b) acceleration time histories at the free field ; and (c) acceleration time histories of lumped mass.

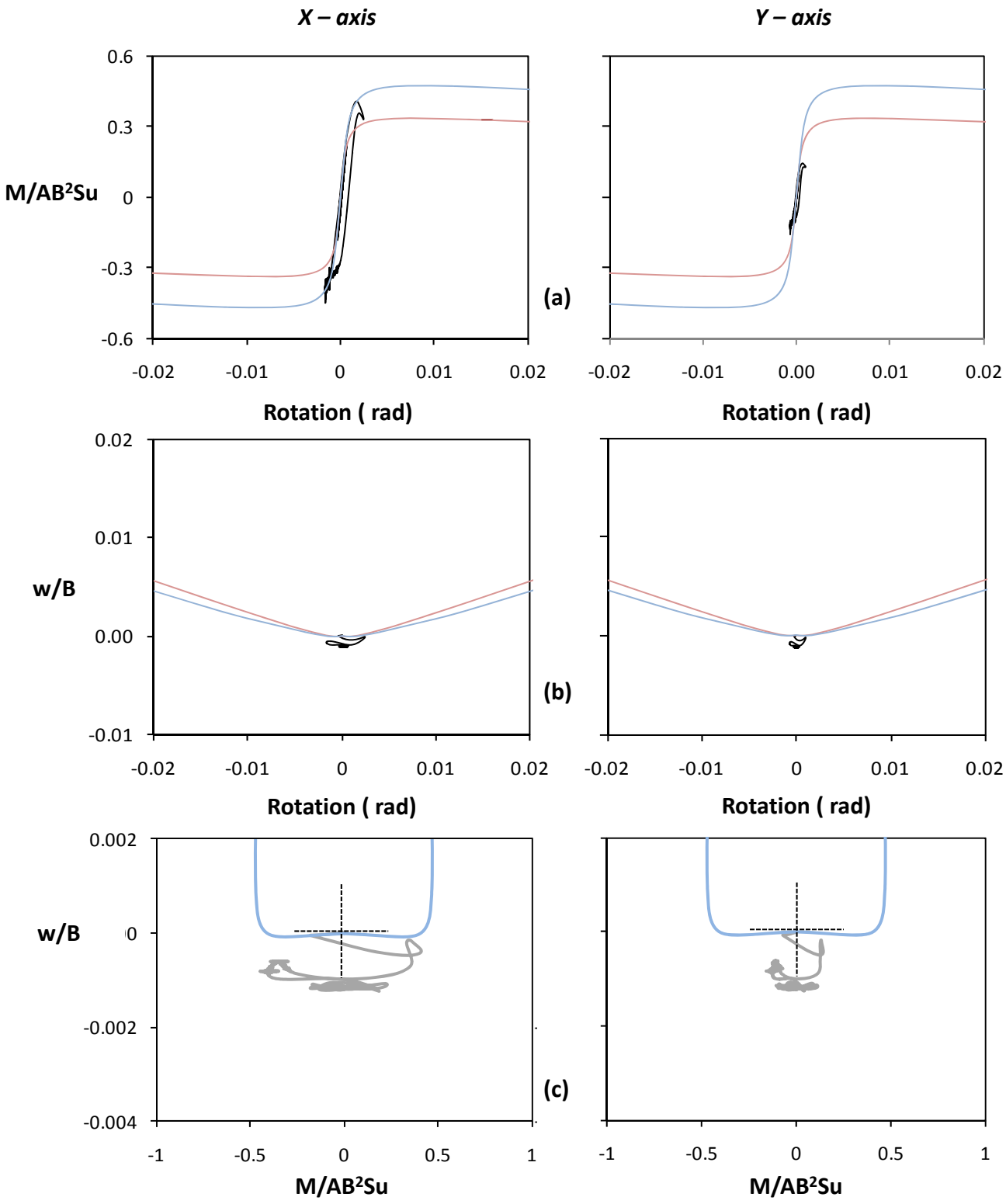

Figure 5.32. Seismic excitation in both directions, Ricker 2 A_x = 0.5 g and A_y = 40% x 0.5 g :
(a) Normalized moment versus rotation along the *x* axis (left) and the *y* axis (right) ;
(b) Normalized to width vertical settlement versus rotation ; and
(c) Normalized vertical settlement to moment along the *x* axis (left) and the *y* axis (right) .

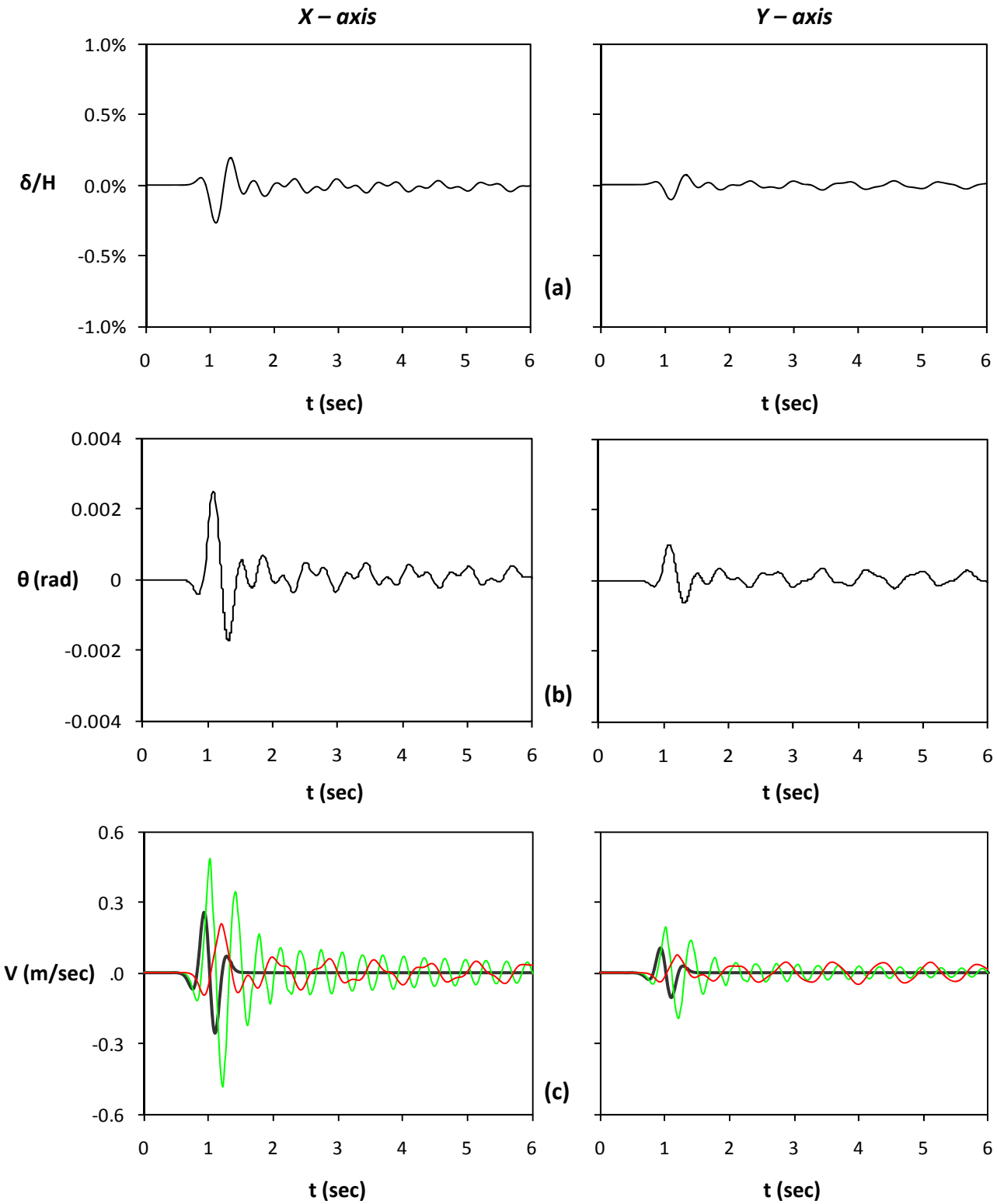

Figure 5.33. Seismic excitation in both directions, Ricker 2 A_x = 0.5 g and A_y = 40% x 0.5 g : (a) Horizontal displacement normalized to height time histories along the *x* axis (left) and the *y* axis (right) ; (b) rotation time histories along the *x* axis (left) and the *y* axis (right) ; (c) velocity time histories (Green line stands for free field motion and red line for lumped mass)

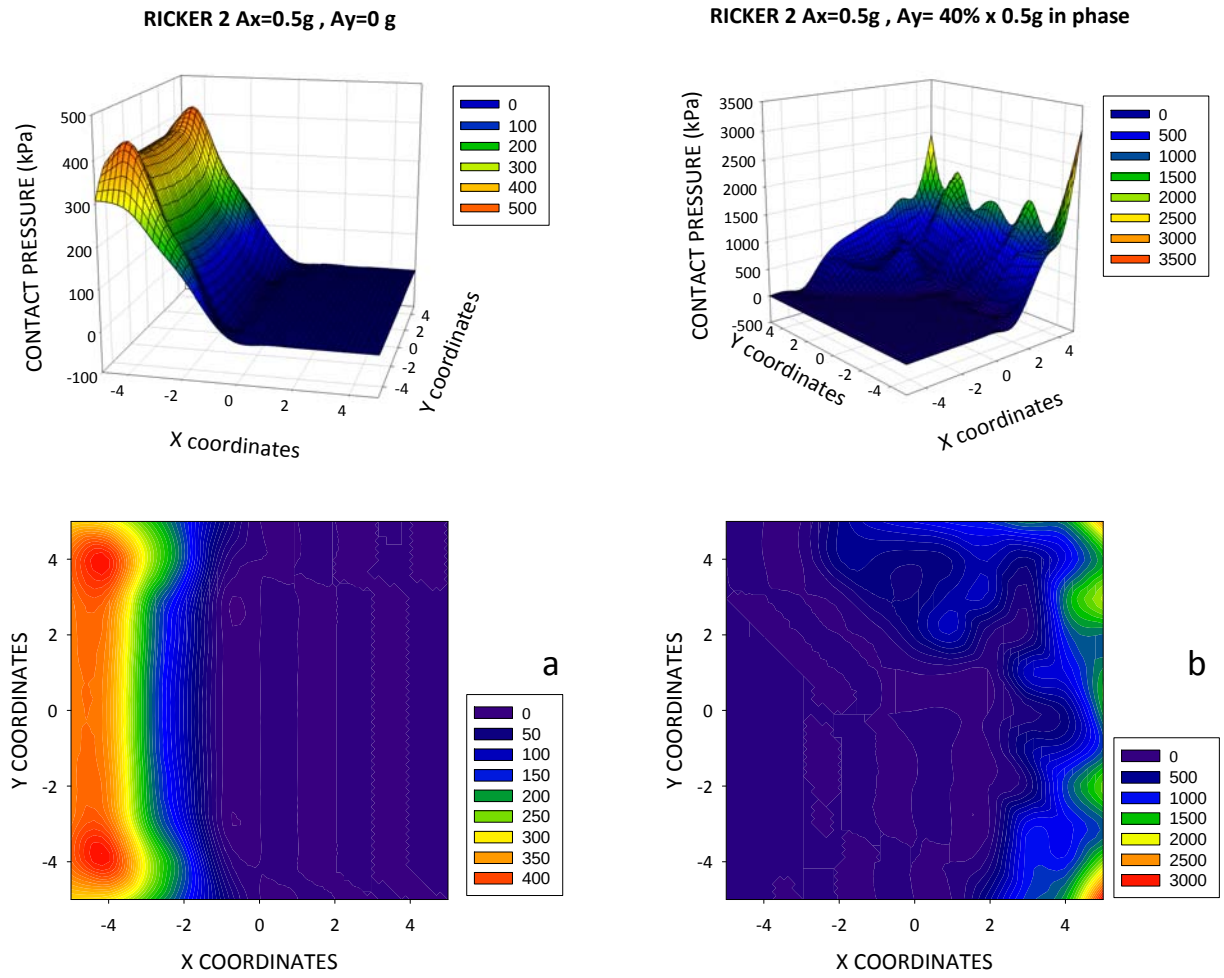

Figure 5.34. Seismic excitation in both directions, Ricker 2 A_x = 0.5 g and A_y =40% x 0.5 g : Distribution of pressures under the footing at the time increment when the maximum uplift occurs for excitation in a) one direction (left) b) both directions (right) .

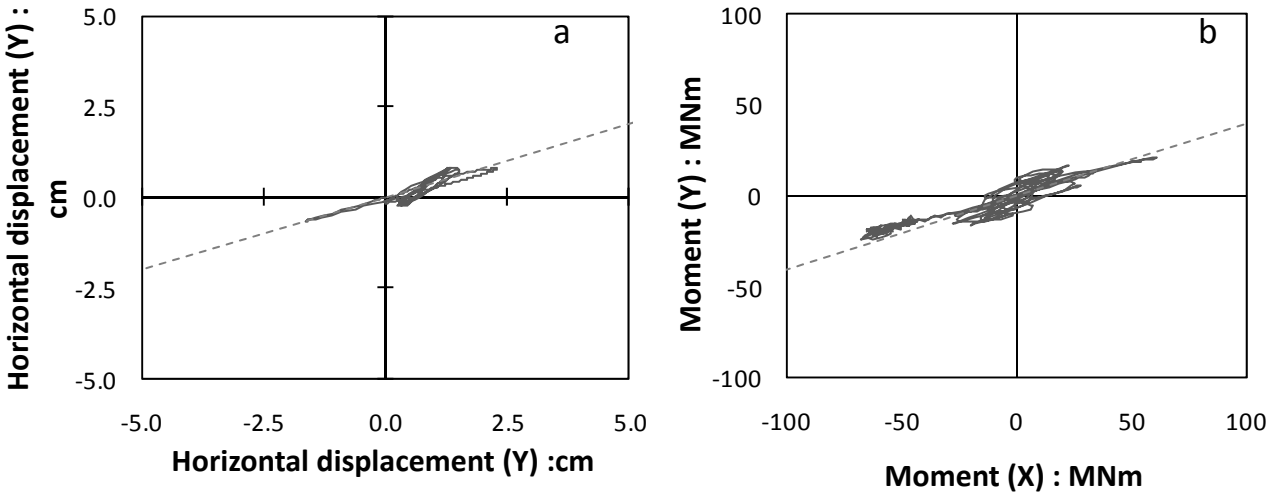

Figure 5.35. **a)** Orbit of center of mass in the X-Y plane.
b) Orbit in the M_X –M_Y plane.

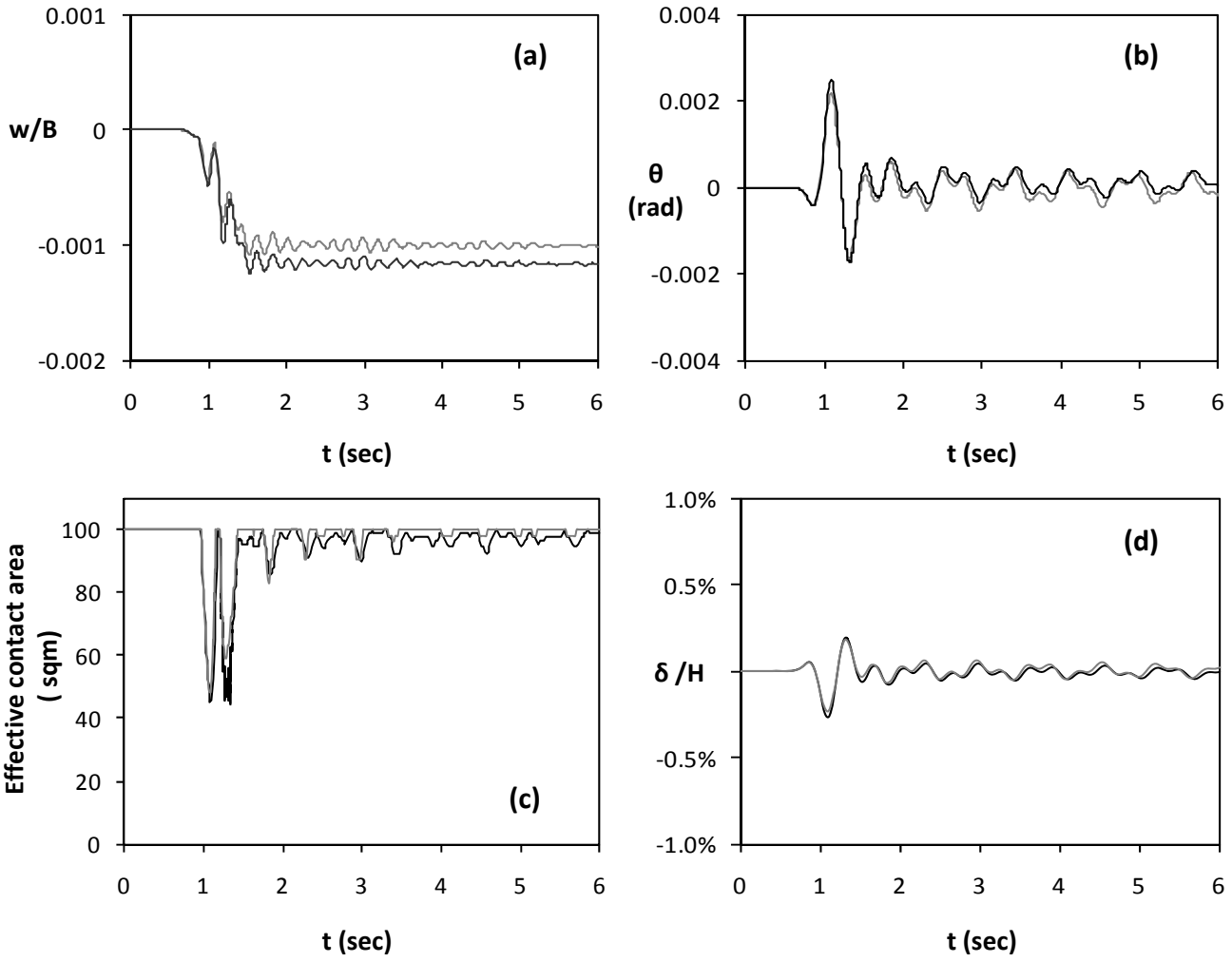

Figure 5.36. Seismic excitation in both directions, Ricker 2 A_x = 0.5 g and A_y =40% x 0.5 g and comparison with the single direction case.
Time histories of (a) Vertical settlement (b) Rotation ; (c) Effective contact area time ; (d) horizontal displacement normalized to height. (Black line represents excitation in both directions and grey line single direction excitation)

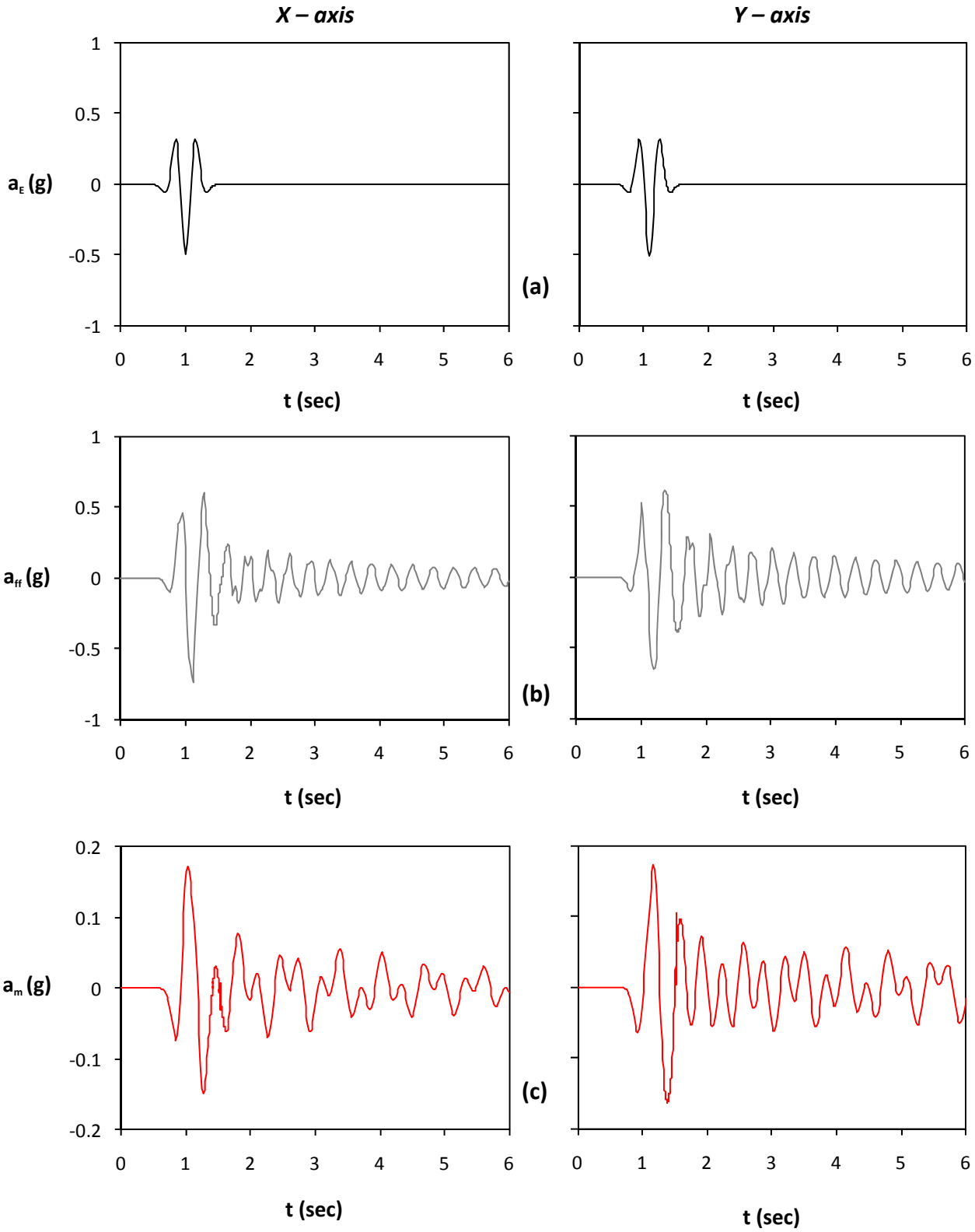

Figure 5.37. Seismic excitation in both directions, Ricker 2 A_x = 0.5 g and A_y = 0.5 g out of phase : (a) acceleration time histories of bedrock excitation along the *x* axis (left) and the *y* axis (right) ; (b) acceleration time histories at the free field ; and (c) acceleration time histories of lumped mass.

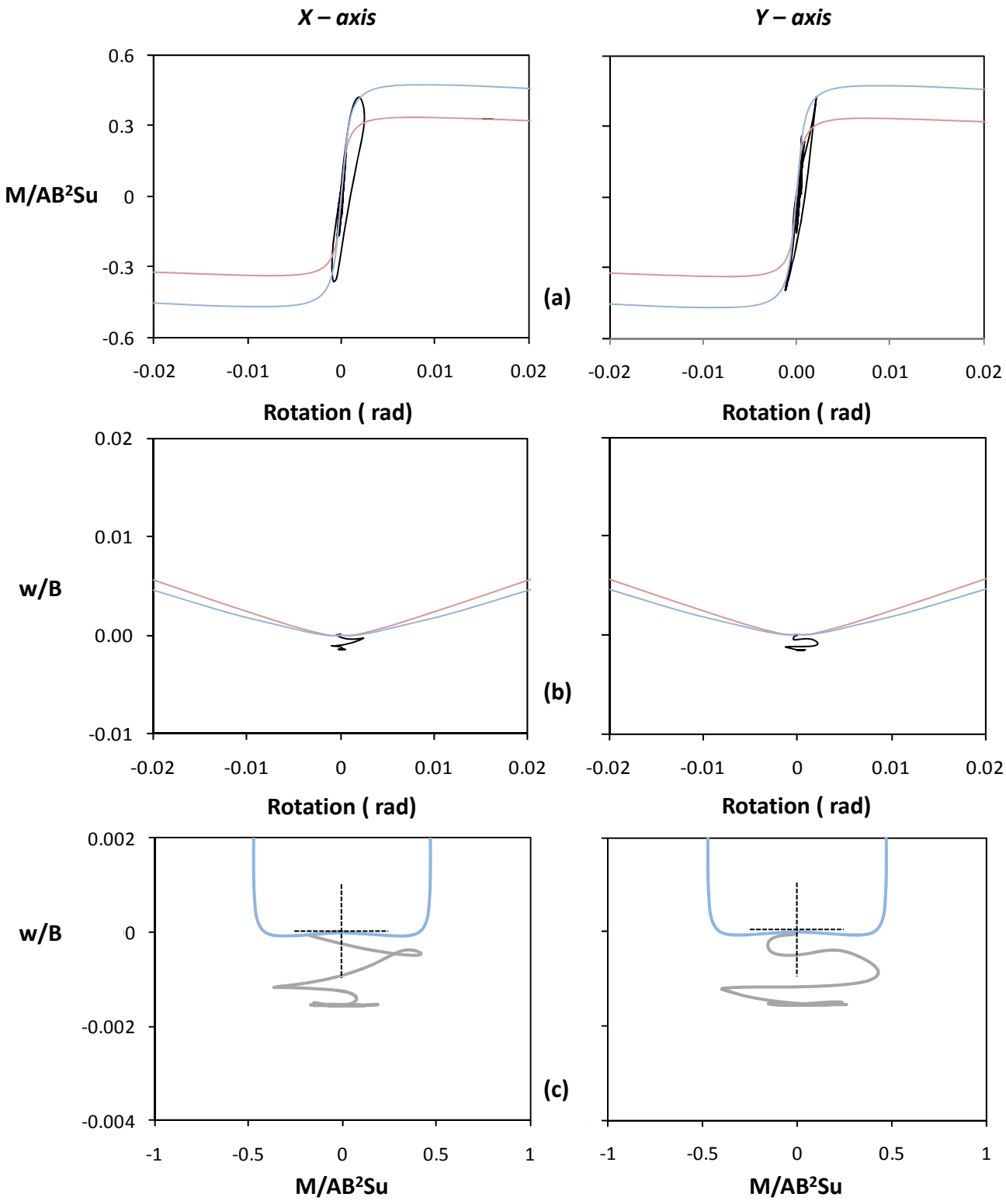

Figure 5.38. Seismic excitation in both directions, Ricker 2 A_x = 0.2 g and A_y = 0.2 g out of phase :

(a) Normalized moment versus rotation along the *x* axis (left) and the *y* axis (right) ;

(b) Normalized to width vertical settlement versus rotation ; and

(c) Normalized vertical settlement to moment along the *x* axis (left) and the *y* axis (right) .

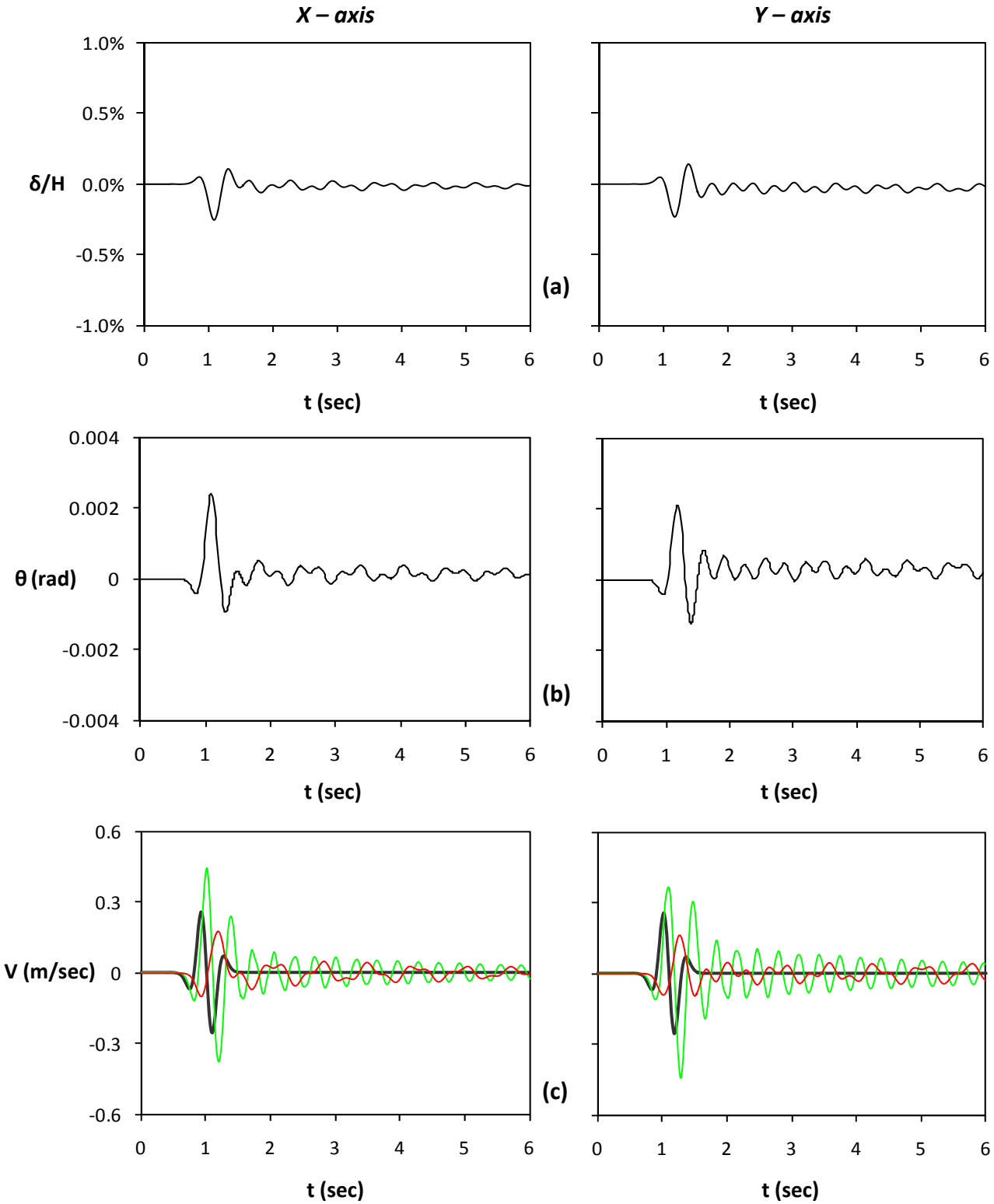

Figure 5.39. Seismic excitation in both directions, Ricker 2 A_x = 0.5 g and A_y = 0.5 g out of phase:
(a) Horizontal displacement normalized to height time histories along the *x* axis (left) and the *y* axis (right) ; (b) rotation time histories along the *x* axis (left) and the *y* axis (right) ; (c) velocity time histories (Green line stands for free field motion and red line for lumped mass)

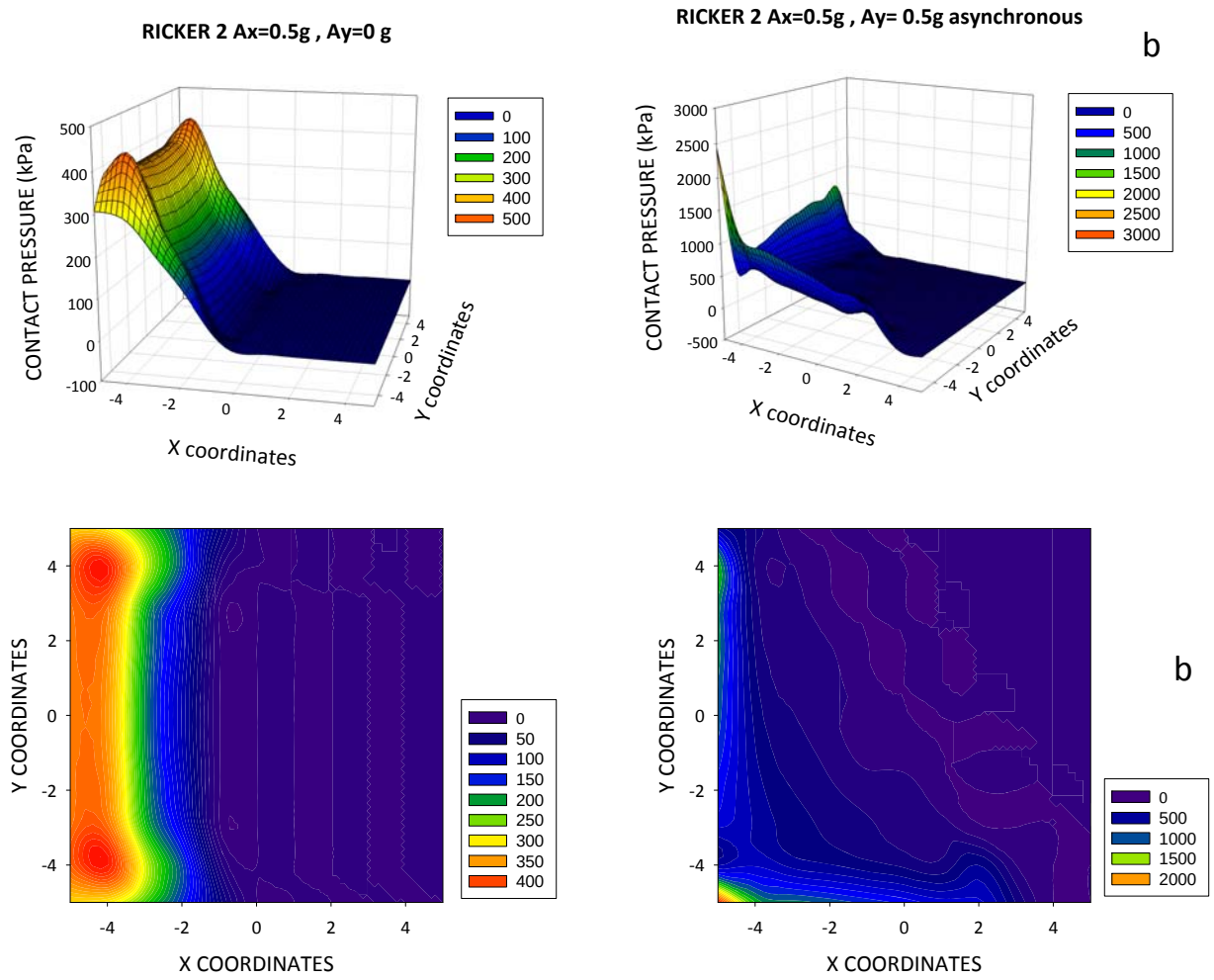

Figure 5.40. Seismic excitation in both directions, Ricker 2 A_x = 0.5 g and A_y = 0.5 g out of phase: Distribution of pressures under the footing at the time increment when the maximum uplift occurs for excitation in a) one direction (left) b) both directions (right) .

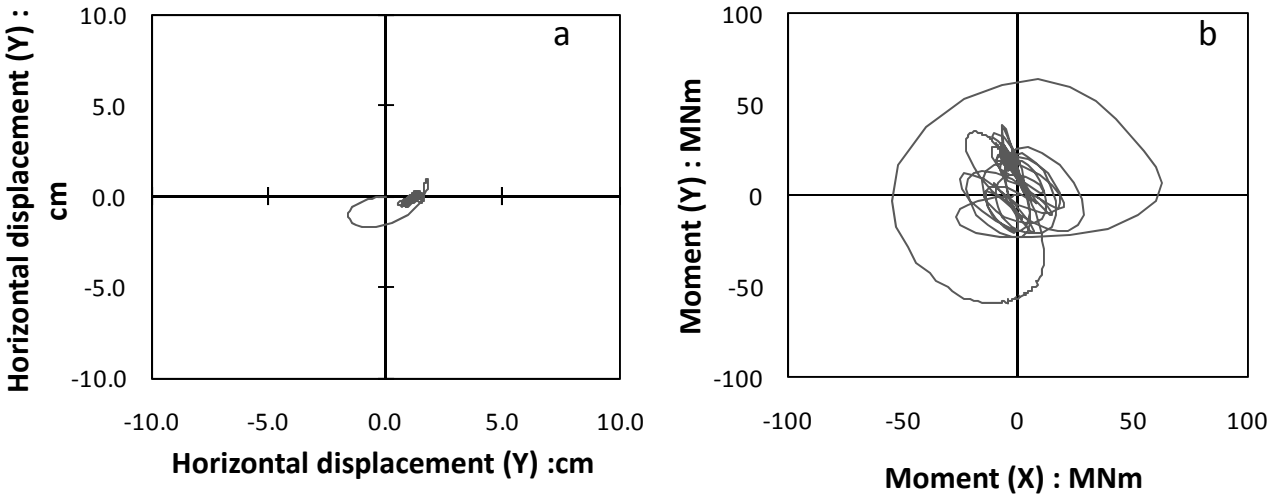

Figure 5.41. **a)** Orbit of center of mass in the X-Y plane.
b) Orbit in the M_X –M_Y plane.

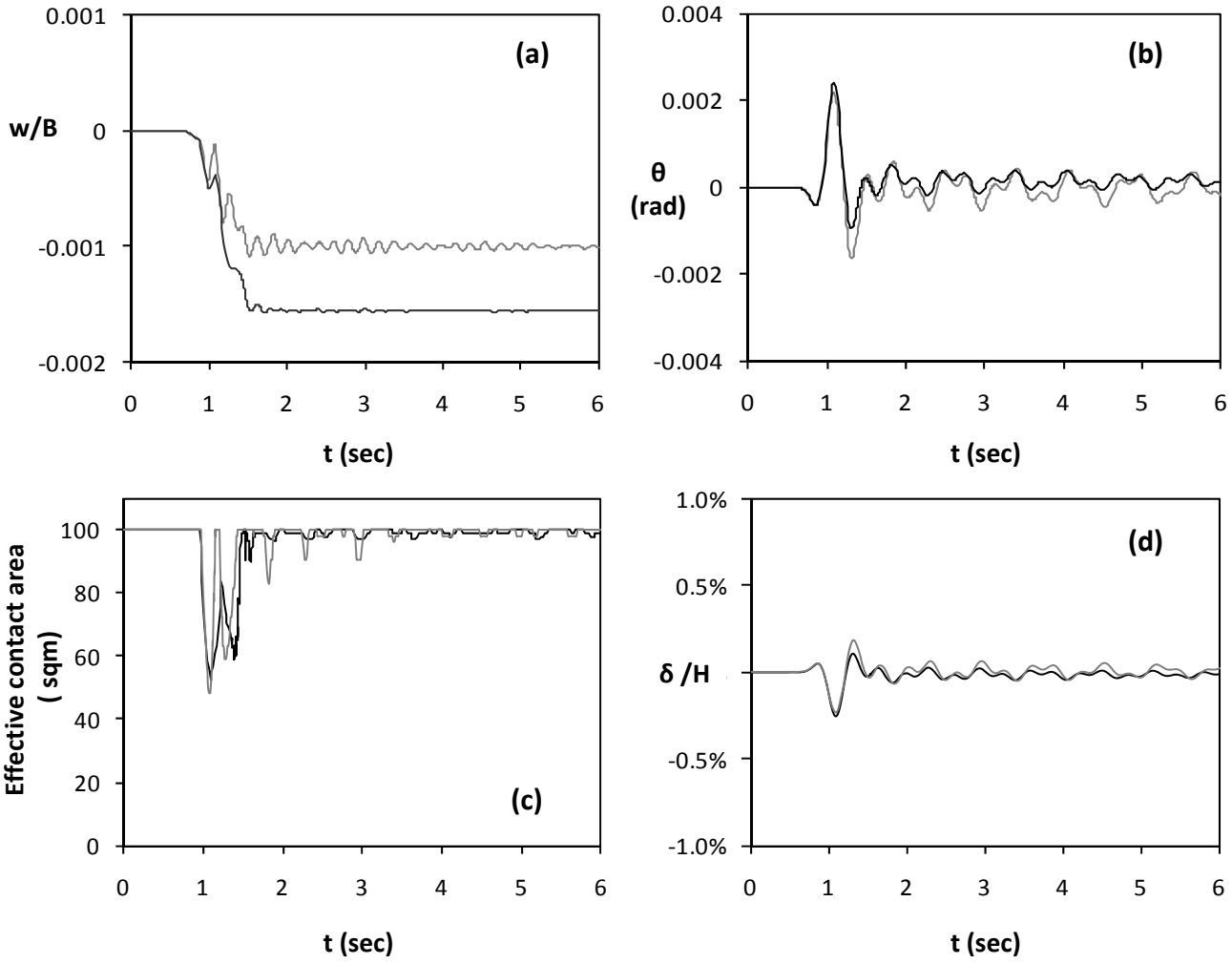

Figure 5.42. Seismic excitation in both directions, Ricker 2 A_x = 0.5 g and A_y = 0.5 g out of phase and comparison with the single direction case.
Time histories of (a) Vertical settlement (b) Rotation ; (c) Effective contact area time ; (d) horizontal displacement normalized to height. (Black line represents excitation in both directions and grey line single direction excitation)

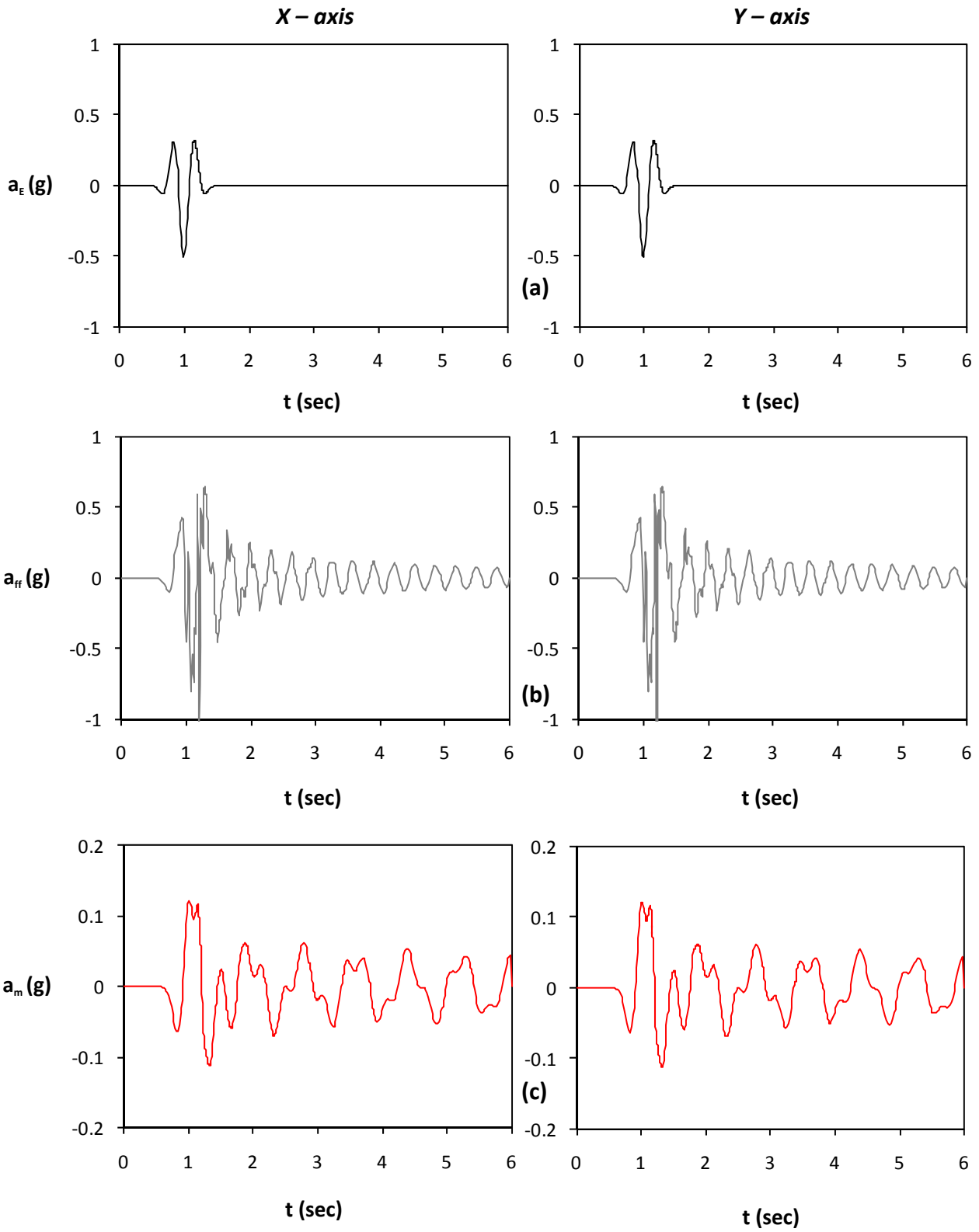

Figure 5.43. Seismic excitation in both directions, Ricker 2 A_x = 0.5 g and A_y = 0.5 g in phase: (a) acceleration time histories of bedrock excitation along the *x* axis (left) and the *y* axis (right) ; (b) acceleration time histories at the free field ; and (c) acceleration time histories of lumped mass.

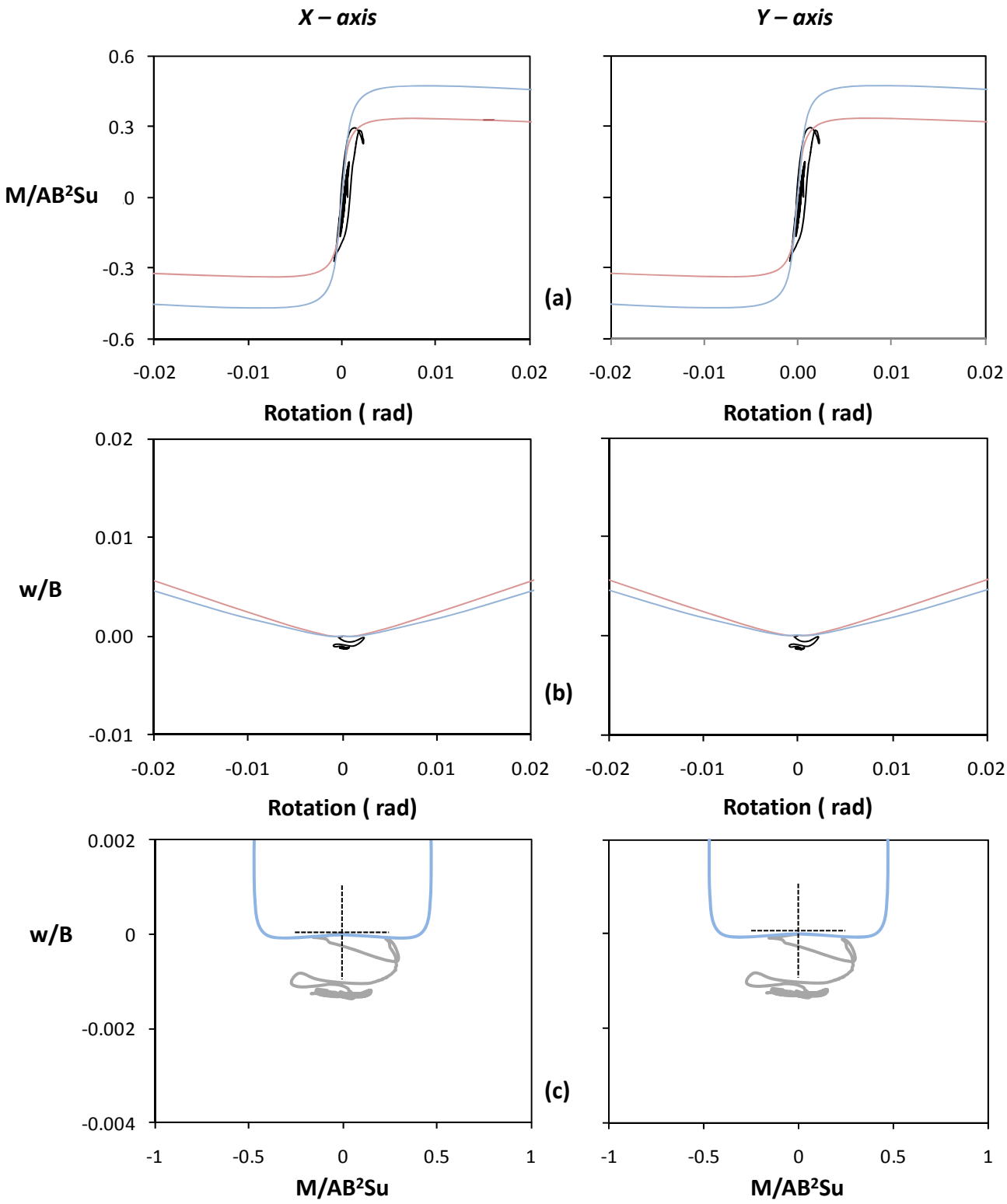

Figure 5.44. Seismic excitation in both directions, Ricker 2 A_x = 0.5 g and A_y = 0.5 g in phase:
(a) Normalized moment versus rotation along the *x* axis (left) and the *y* axis (right) ;
(b) Normalized to width vertical settlement versus rotation ; and
(c) Normalized vertical settlement to moment along the *x* axis (left) and the *y* axis (right) .

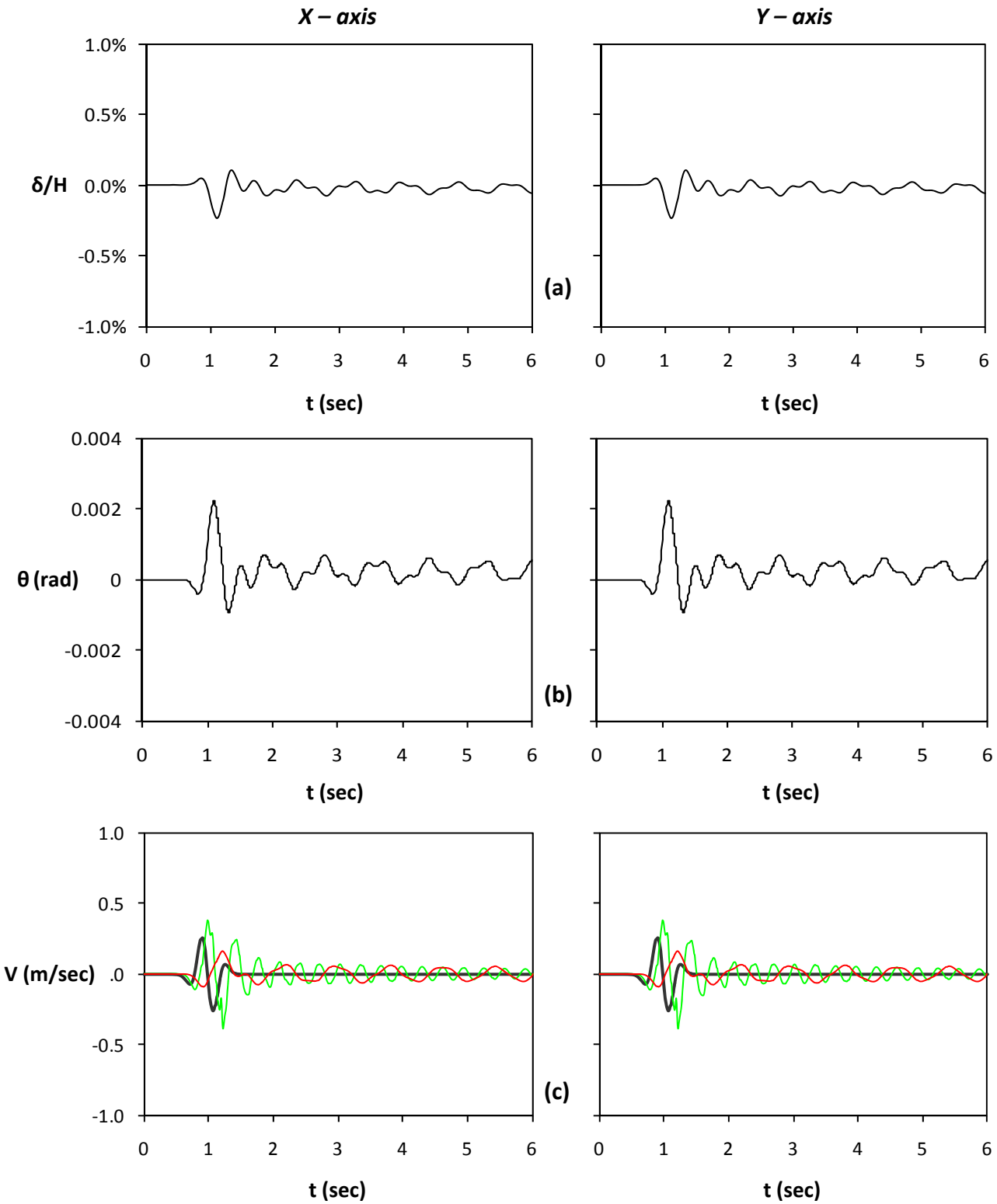

Figure 5.45. Seismic excitation in both directions, Ricker 2 A_x = 0.5g and A_y = 0.5 g in phase: (a) Horizontal displacement normalized to height time histories along the *x* axis (left) and the *y* axis (right) ; (b) rotation time histories along the *x* axis (left) and the *y* axis (right) ; (c) velocity time histories (Green line stands for free field motion and red line for lumped mass)

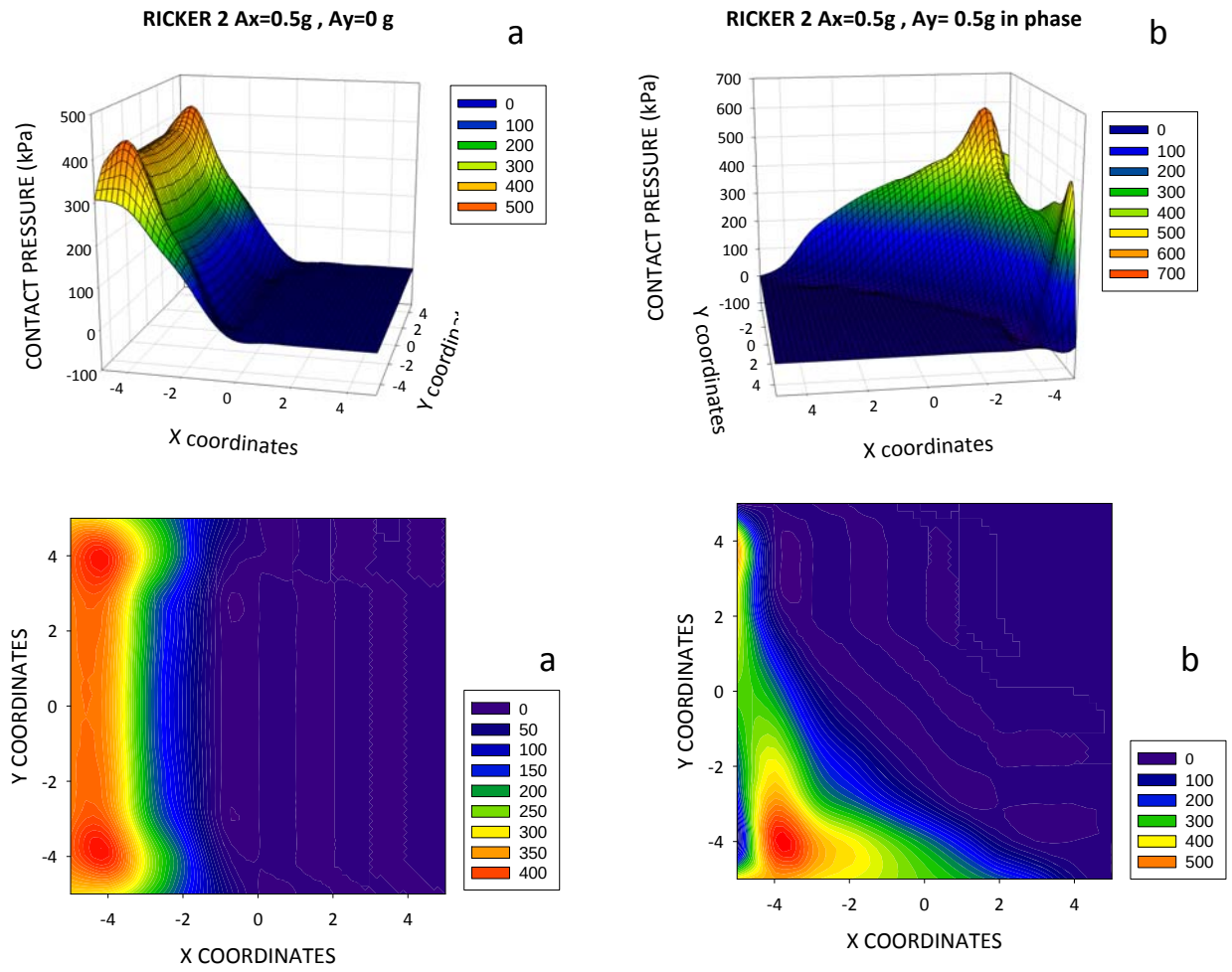

Figure 5.46. Seismic excitation in both directions, Ricker 1 A_x = 0.5 g and A_y = 0.5 g in phase : Distribution of pressures under the footing at the time increment when the maximum uplift occurs for excitation in a) one direction (left) b) both directions (right) .

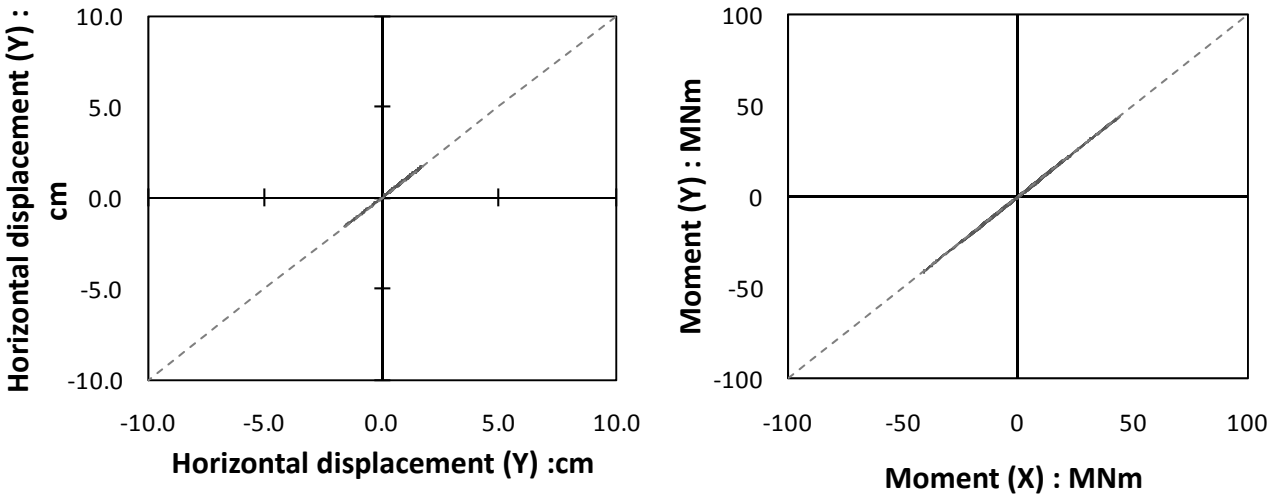

Figure 5.47. **a)** Orbit of center of mass in the X-Y plane.
b) Orbit in the M_X –M_Y plane.

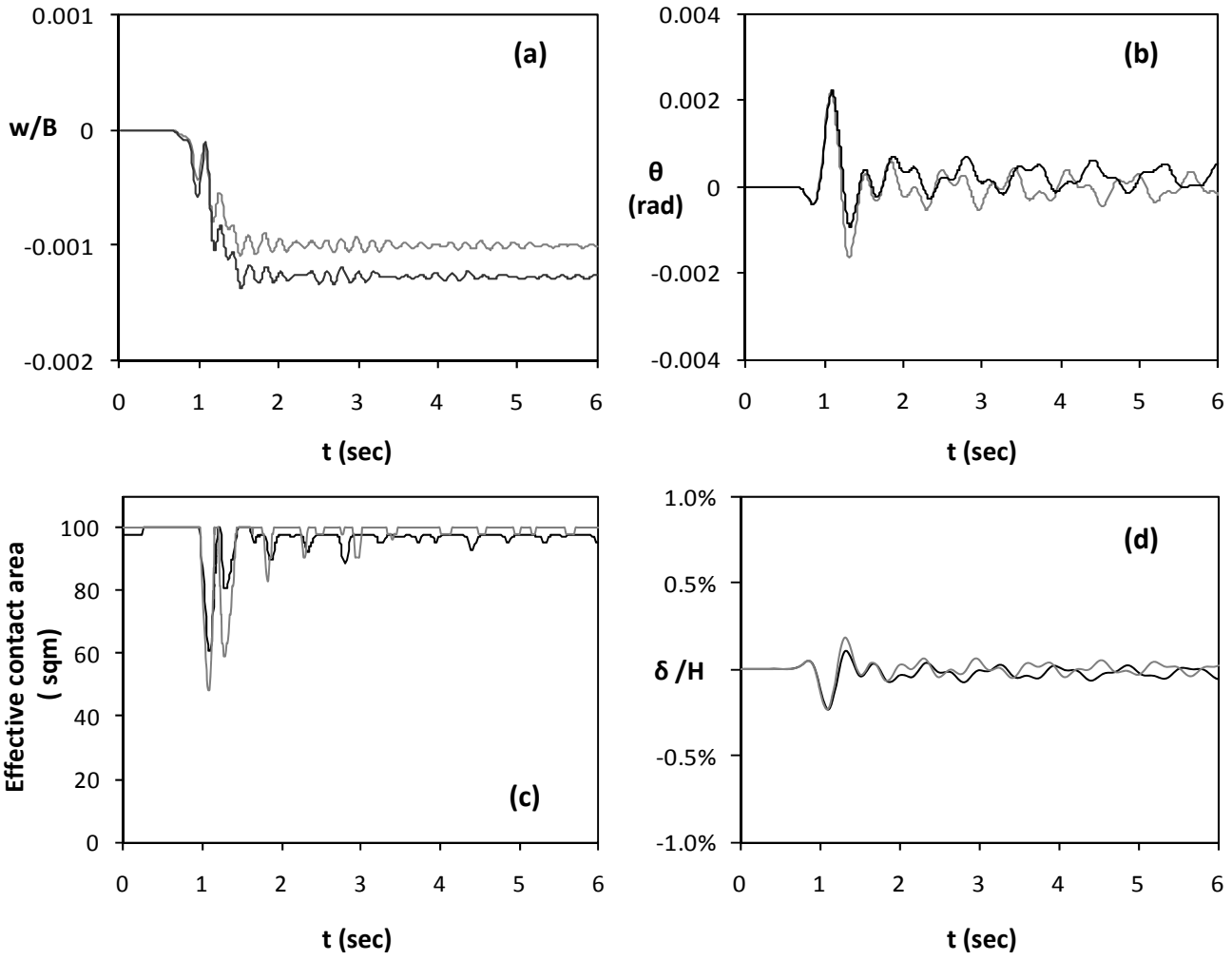

Figure 5.48. Seismic excitation in both directions, Ricker 2 A_x = 0.5 g and A_y = 0.5 g in phase and comparison with the single direction case.
Time histories of (a) Vertical settlement (b) Rotation ; (c) Effective contact area time ; (d) horizontal displacement normalized to height. (Black line represents excitation in both directions and grey line single direction excitation)

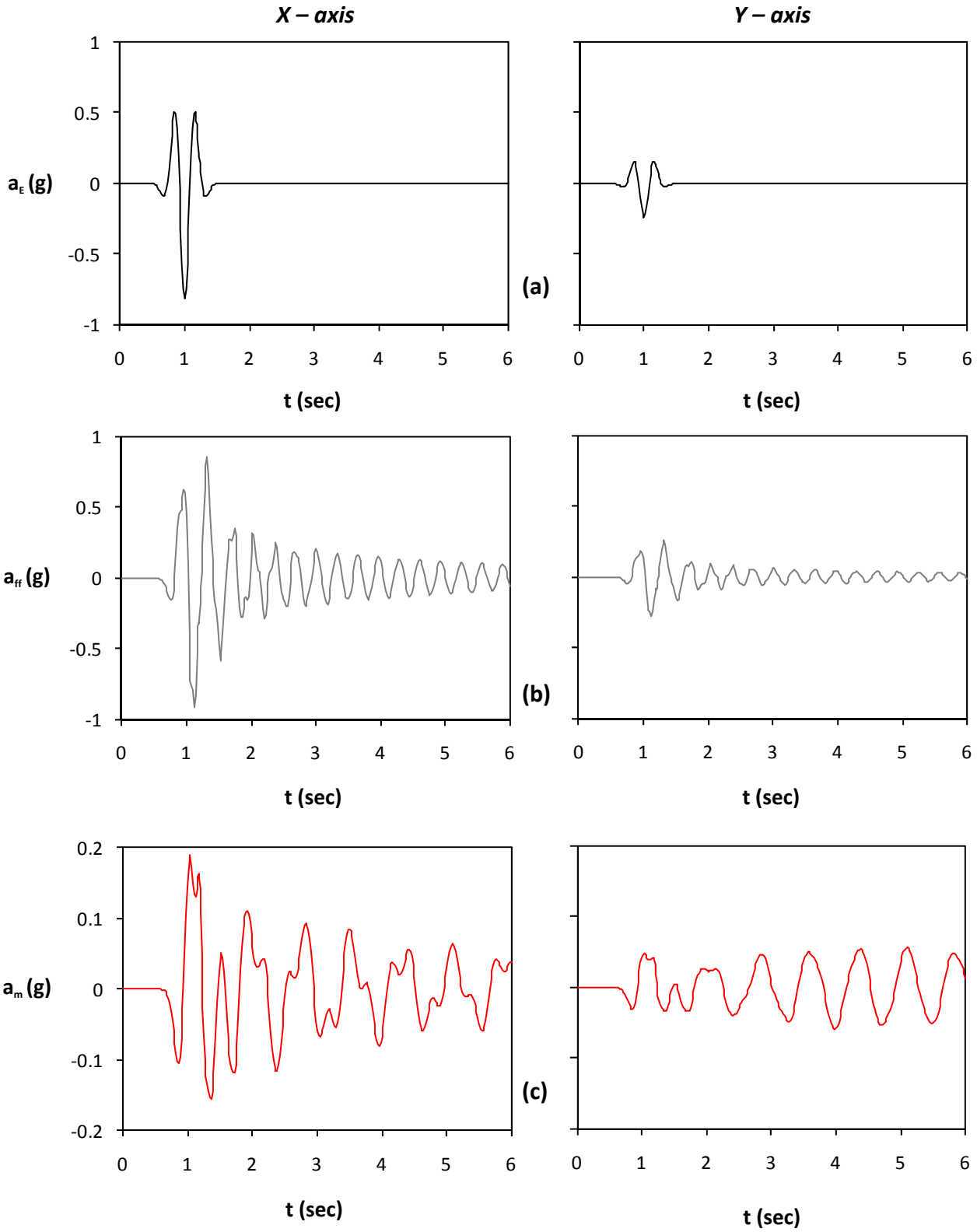

Figure 5.49. Seismic excitation in both directions, Ricker 2 A_x = 0.8 g and A_y = 30% x 0.8 g : (a) acceleration time histories of bedrock excitation along the *x* axis (left) and the *y* axis (right) ; (b) acceleration time histories at the free field ; and (c) acceleration time histories of lumped mass.

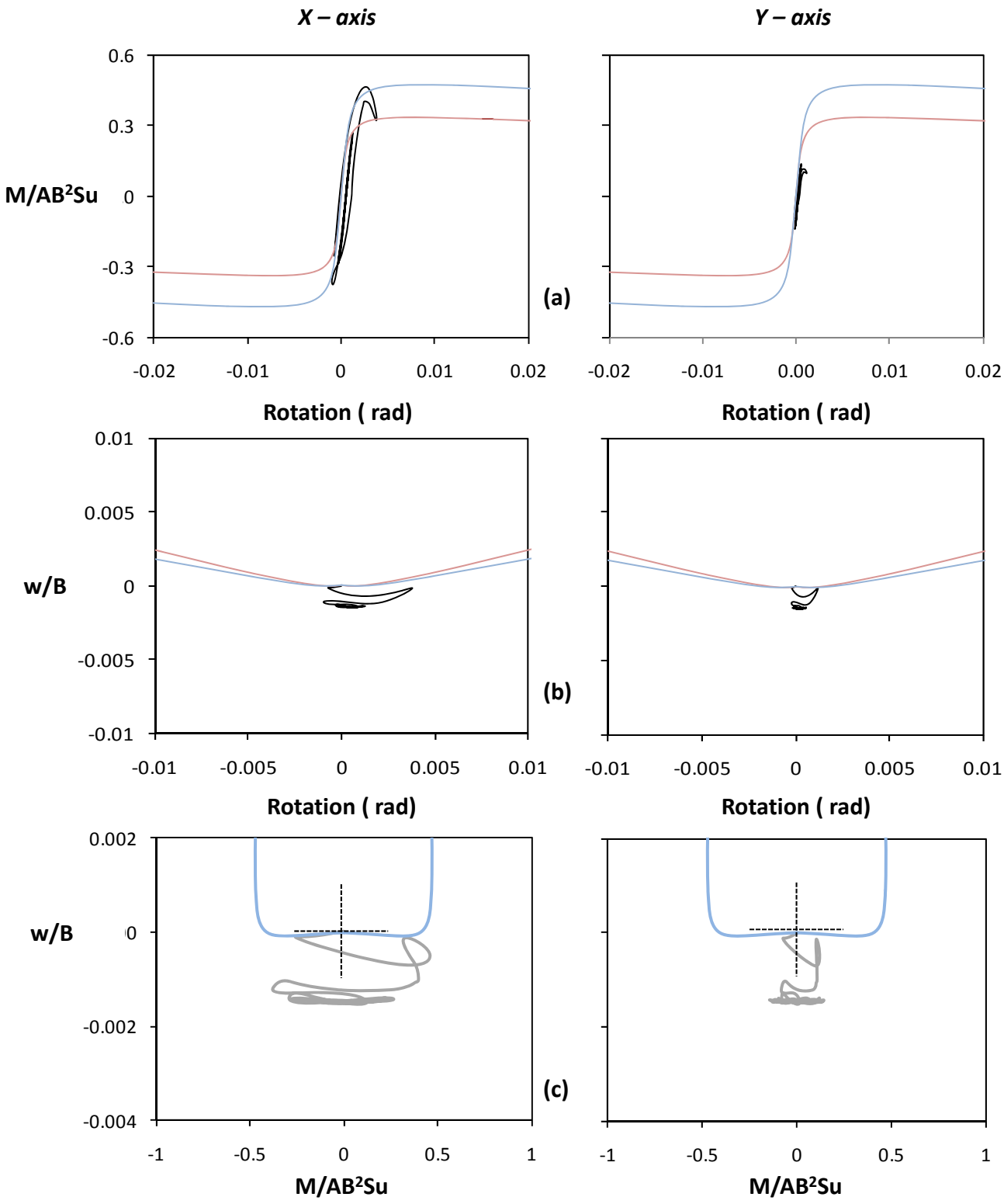

Figure 5.50. Seismic excitation in both directions, Ricker 2 A_x = 0.8 g and A_y =30% x 0.8 g :
(a) Normalized moment versus rotation along the *x* axis (left) and the *y* axis (right) ;
(b) Normalized to width vertical settlement versus rotation ; and
(c) Normalized vertical settlement to moment along the *x* axis (left) and the *y* axis (right) .

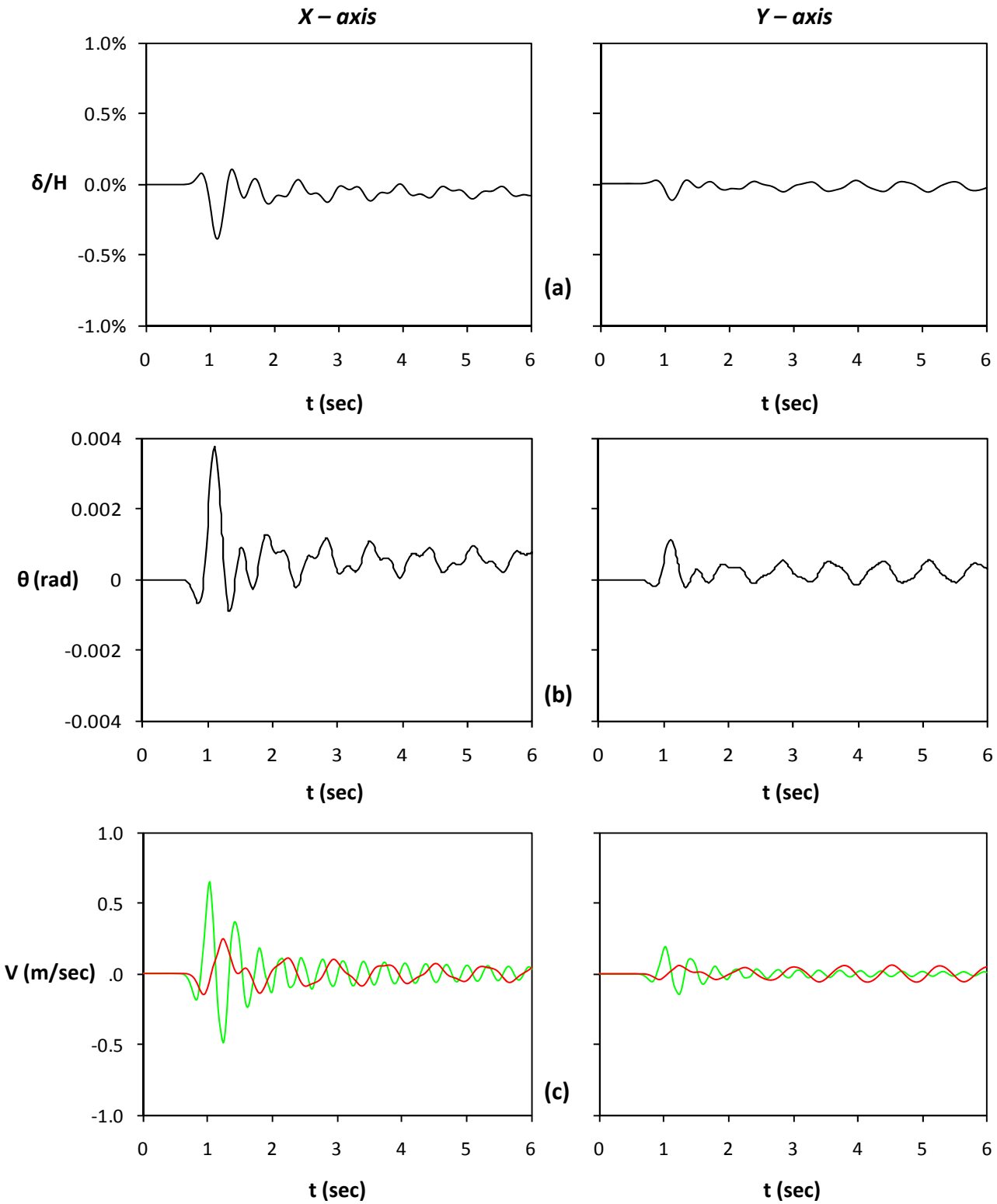

Figure 5.51. Seismic excitation in both directions, Ricker 2 A_x = 0.8 g and A_y =30% x 0.8 g : (a) Horizontal displacement normalized to height time histories along the *x* axis (left) and the *y* axis (right) ; (b) rotation time histories along the *x* axis (left) and the *y* axis (right) ; (c) velocity time histories (Green line stands for free field motion and red line for lumped mass)

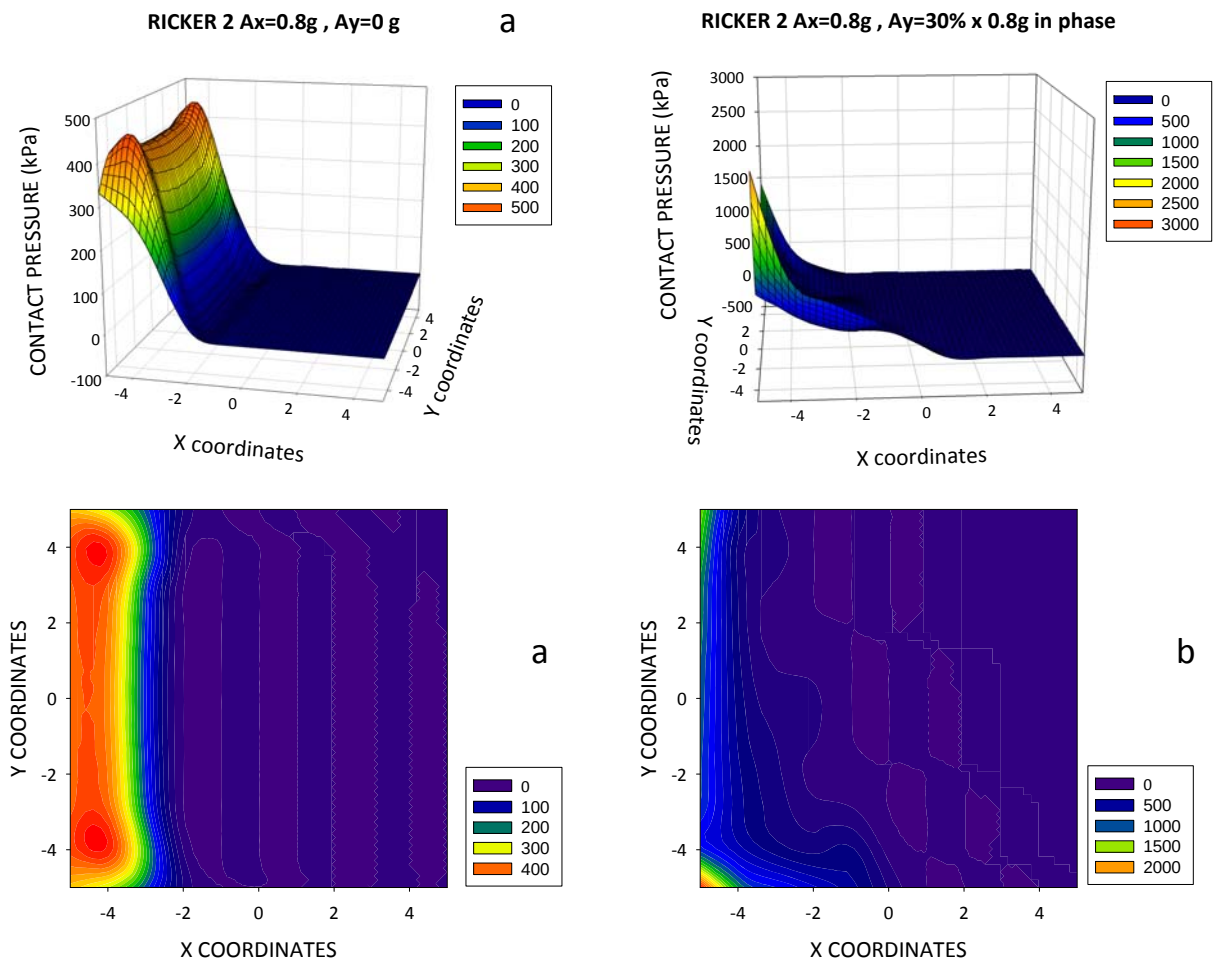

Figure 5.52. Seismic excitation in both directions, Ricker 2 A_x = 0.8 g and A_y =30% x 0.8 g : Distribution of pressures under the footing at the time increment when the maximum uplift occurs for exitation in a) one direction (left) b) both directions (right) .

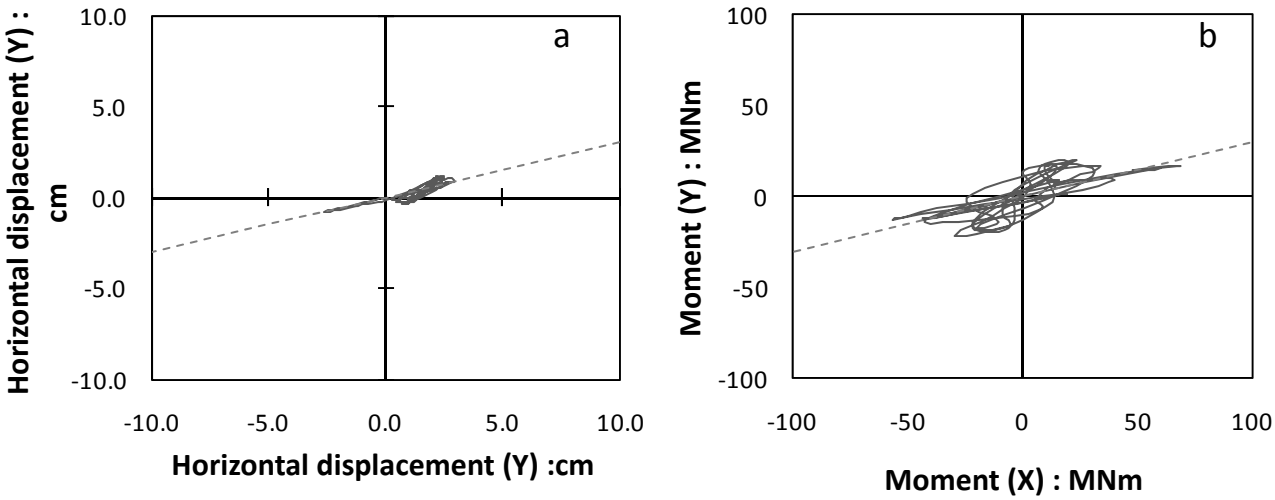

Figure 5.53. **a)** Orbit of center of mass in the X-Y plane.
b) Orbit in the M_X –M_Y plane.

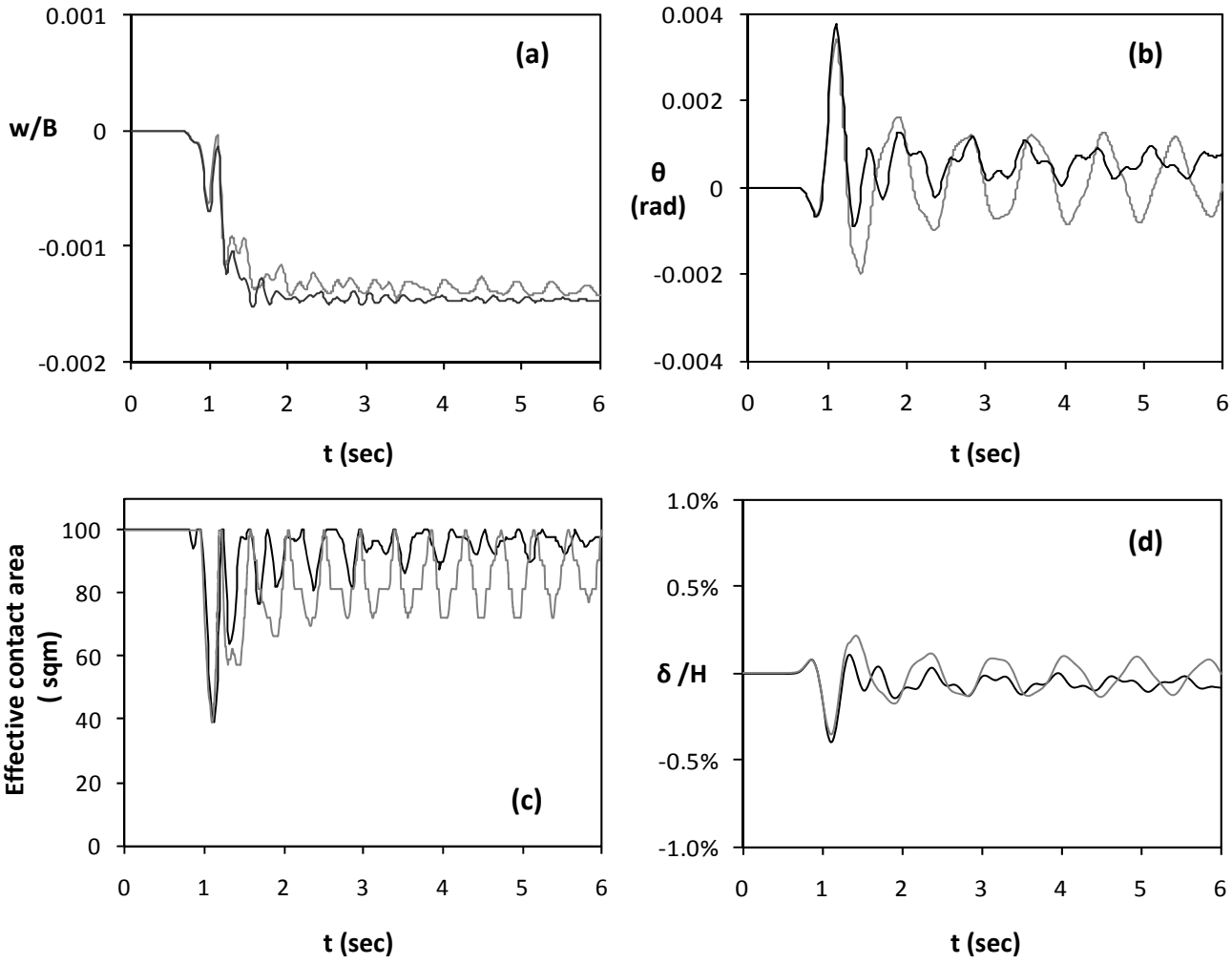

Figure 5.54. Seismic excitation in both directions, Ricker 2 A_x = 0.8 g and A_y =30% x 0.8 g and comparison with the single direction case.
Time histories of (a) Vertical settlement (b) Rotation ; (c) Effective contact area time ; (d) horizontal displacement normalized to height. (Black line represents excitation in both directions and grey line single direction excitation)

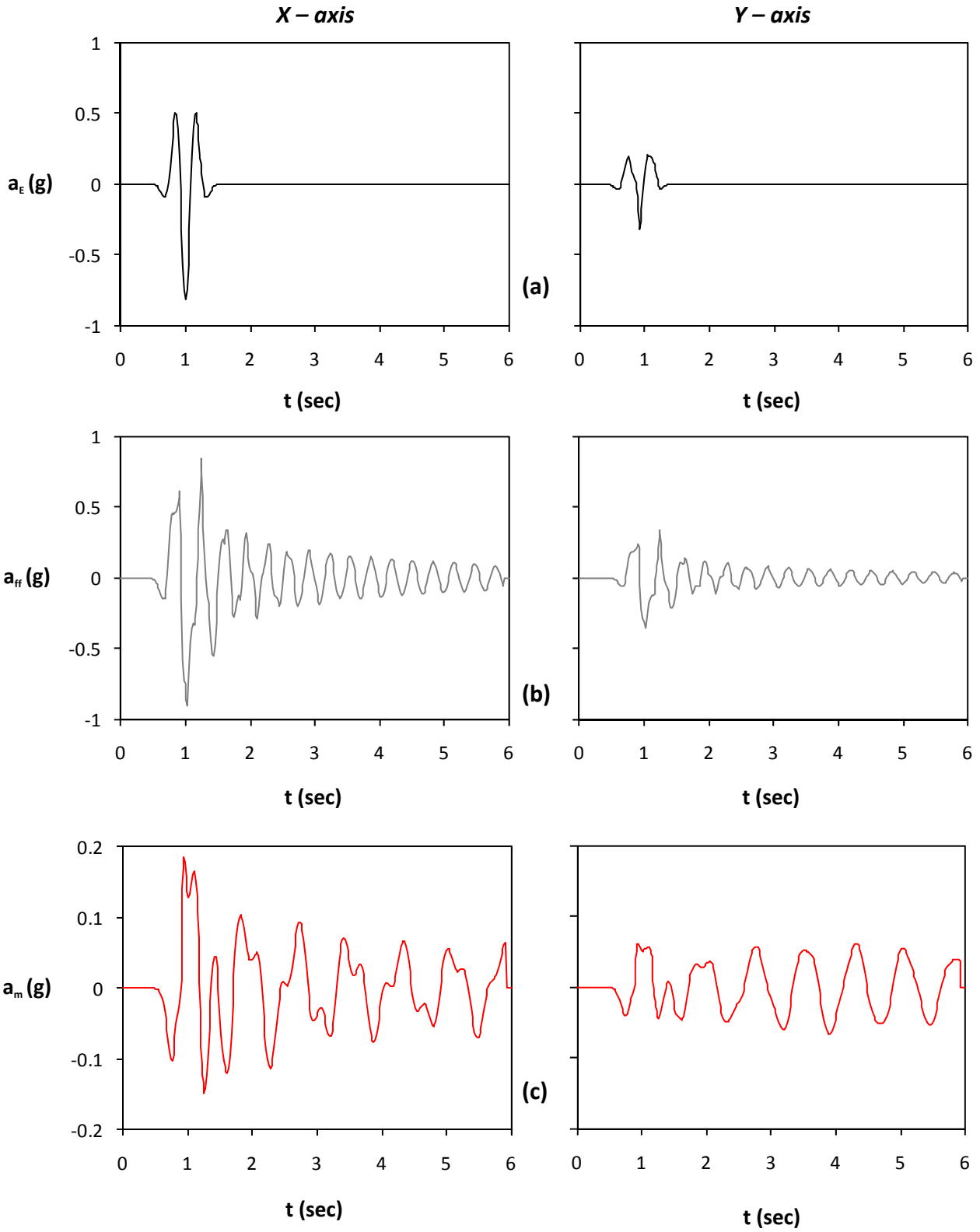

Figure 5.55. Seismic excitation in both directions, Ricker 2 A_x = 0.8 g and A_y = 40% x 0.8 g : (a) acceleration time histories of bedrock excitation along the *x* axis (left) and the *y* axis (right) ; (b) acceleration time histories at the free field ; and (c) acceleration time histories of lumped mass.

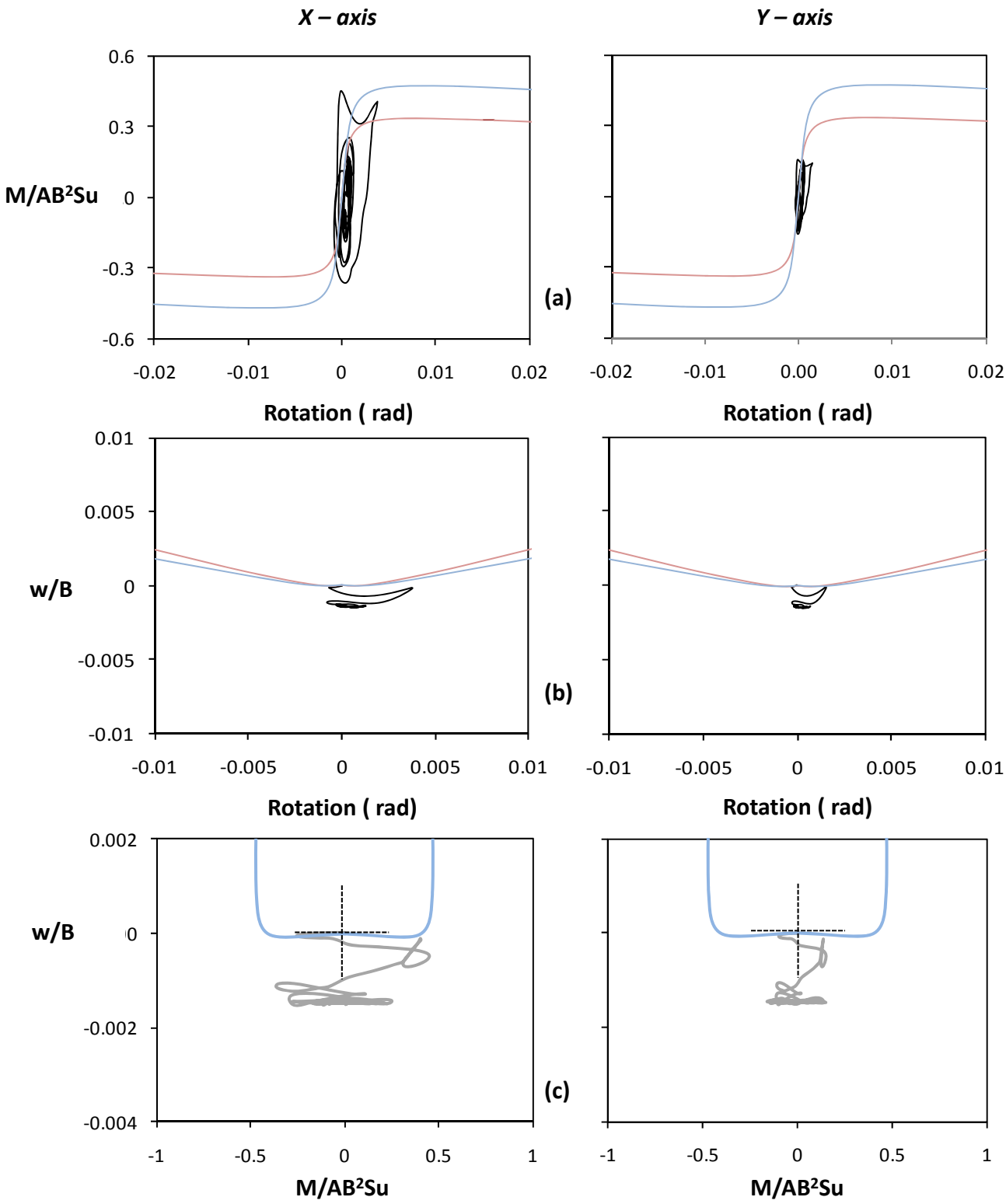

Figure 5.56. Seismic excitation in both directions, Ricker 2 A_x = 0.8 g and A_y = 40% x 0.8 g :
(a) Normalized moment versus rotation along the *x* axis (left) and the *y* axis (right) ;
(b) Normalized to width vertical settlement versus rotation ; and
(c) Normalized vertical settlement to moment along the *x* axis (left) and the *y* axis (right) .

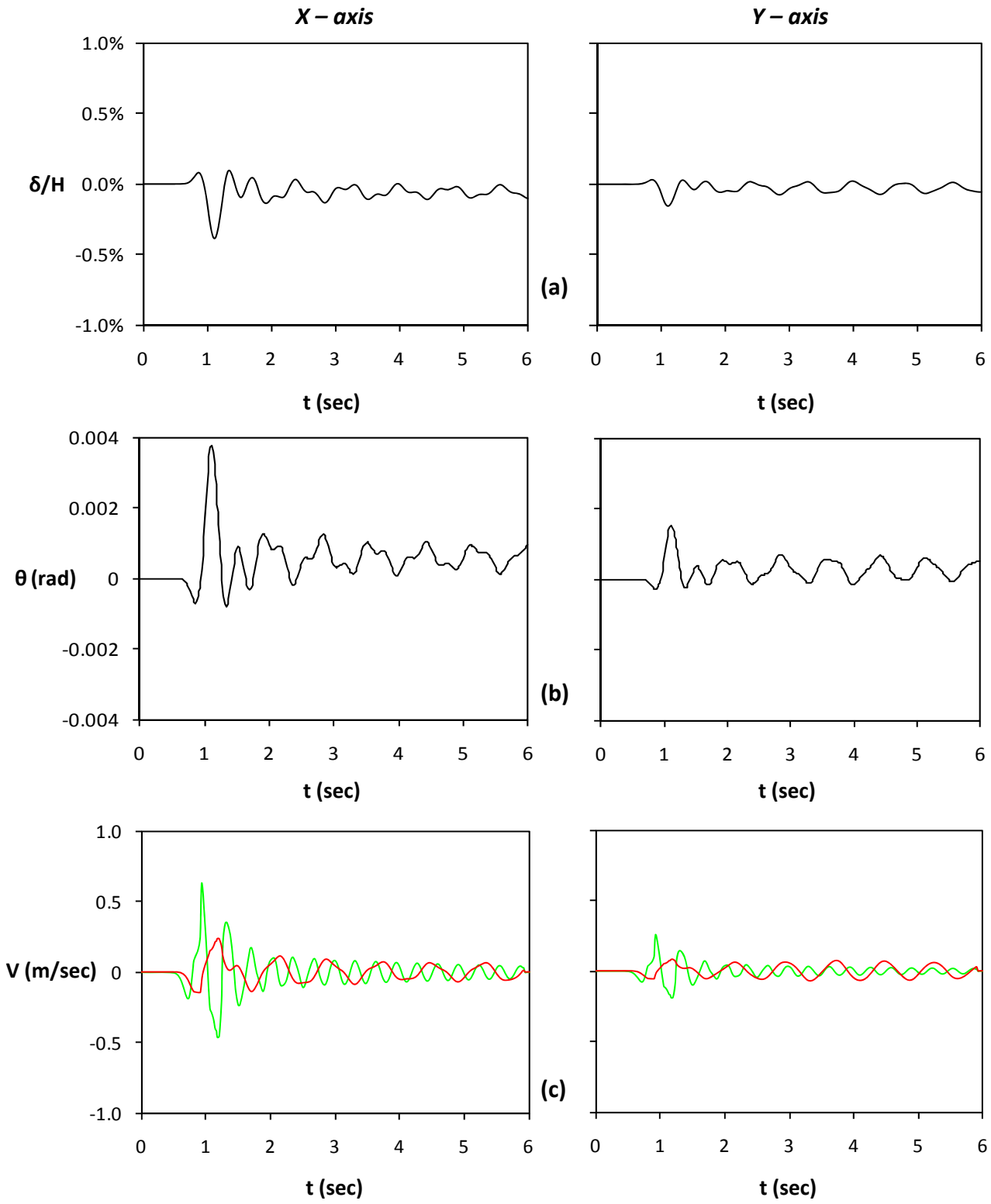

Figure 5.57. Seismic excitation in both directions, Ricker 2 A_x = 0.8 g and A_y = 40% x 0.8 g : (a) Horizontal displacement normalized to height time histories along the *x* axis (left) and the *y* axis (right) ; (b) rotation time histories along the *x* axis (left) and the *y* axis (right) ; (c) velocity time histories (Green line stands for free field motion and red line for lumped mass)

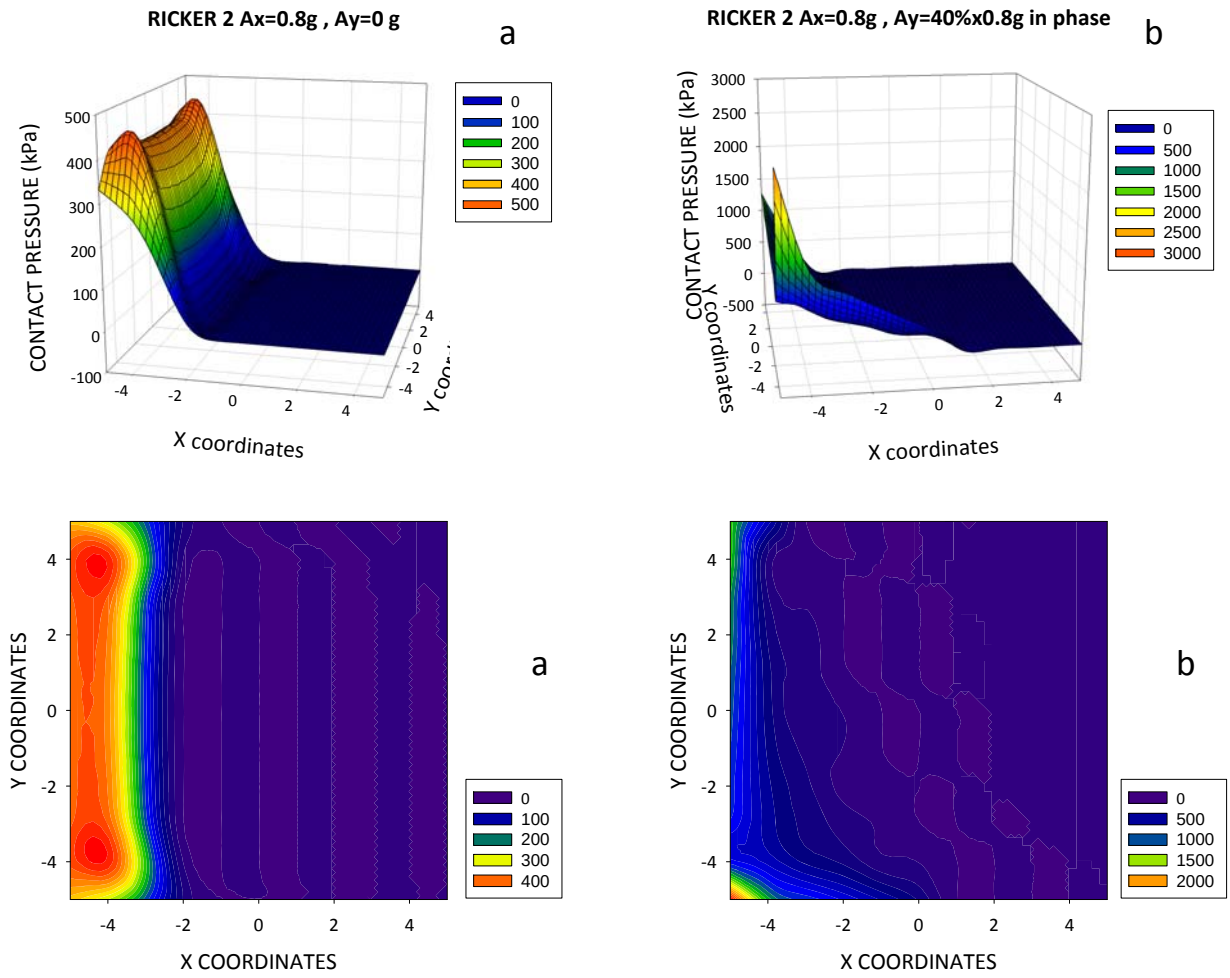

Figure 5.58. Seismic excitation in both directions, Ricker 2 A_x = 0.8 g and A_y = 40% x 0.8 g : Distribution of pressures under the footing at the time increment when the maximum uplift occurs for excitation in a) one direction (left) b) both directions (right) .

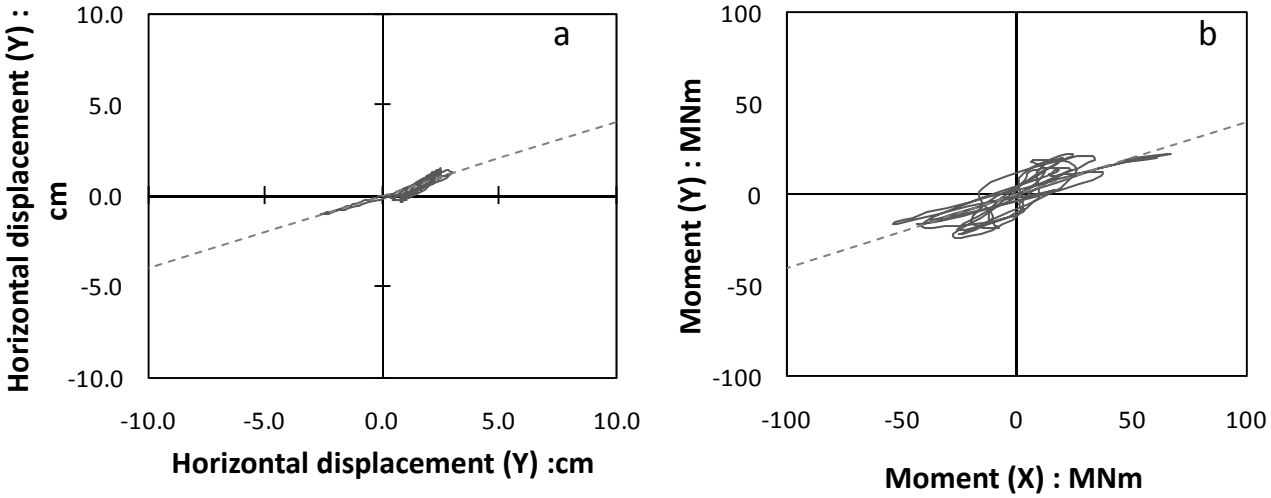

Figure 5.59. a) Orbit of center of mass in the X-Y plane.
b) Orbit in the M_X –M_Y plane.

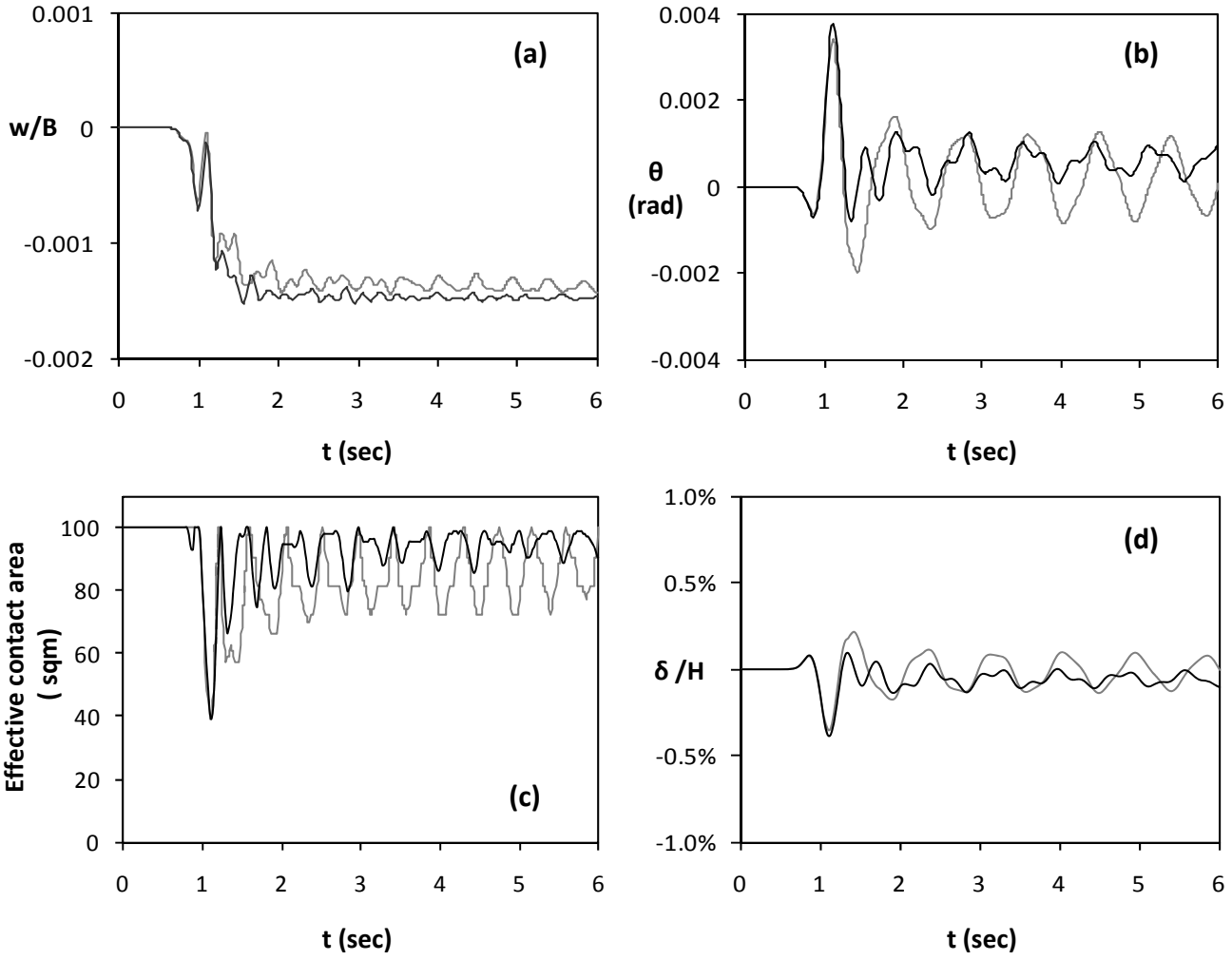

Figure 5.60. Seismic excitation in both directions, Ricker 2 A_x = 0.8 g and A_y = 40% x 0.8 g and comparison with the single direction case.
Time histories of (a) Vertical settlement (b) Rotation ; (c) Effective contact area time ; (d) horizontal displacement normalized to height. (Black line represents excitation in both directions and grey line single direction excitation)

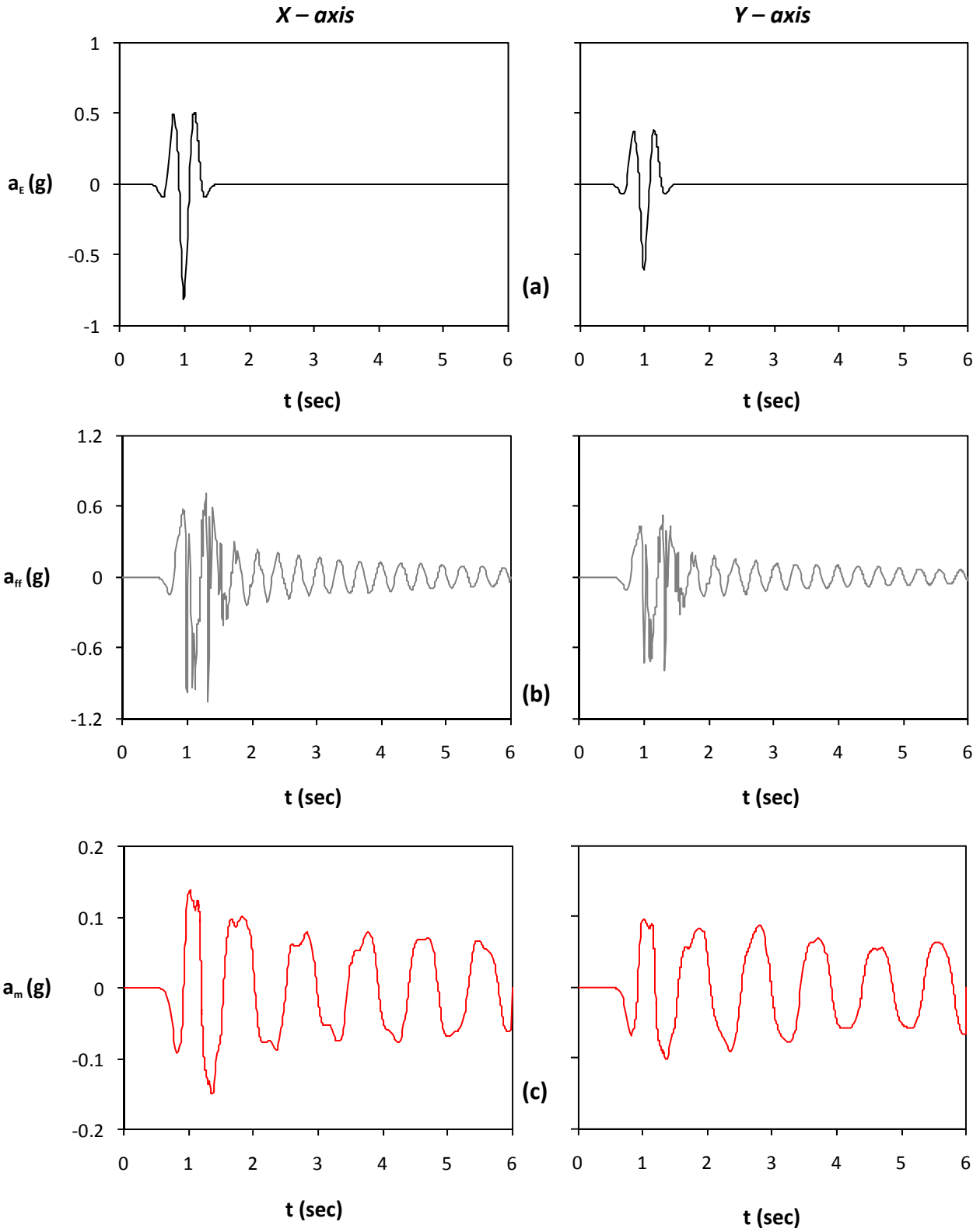

Figure 5.61. Seismic excitation in both directions, Ricker 2 A_x = 0.8 g and A_y = 75% x 0.8 g : (a) acceleration time histories of bedrock excitation along the *x* axis (left) and the *y* axis (right) ; (b) acceleration time histories at the free field ; and (c) acceleration time histories of lumped mass.

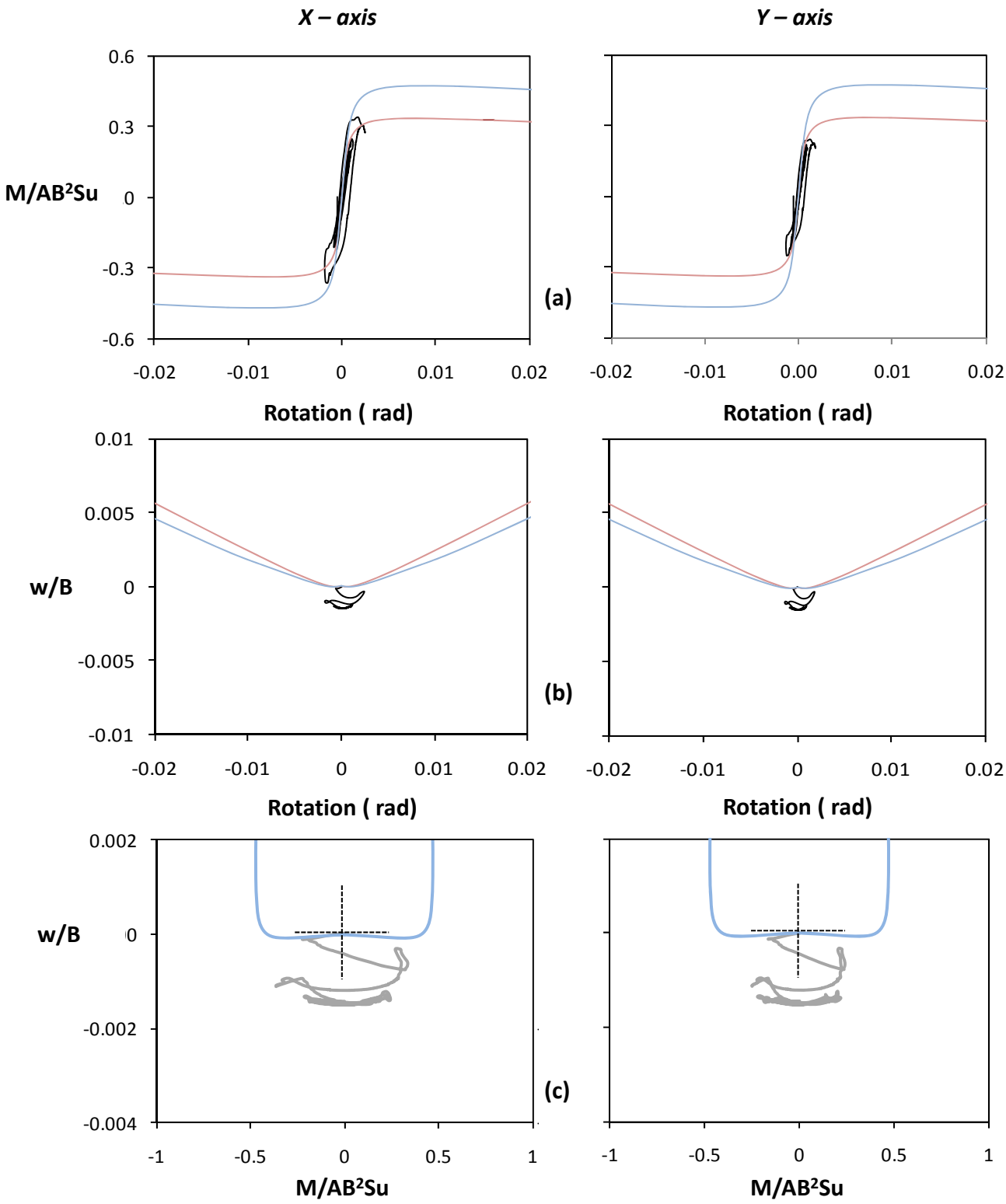

Figure 5.62. Seismic excitation in both directions, Ricker 2 A_x = 0.8 g and A_y = 75% x 0.8 g :
(a) Normalized moment versus rotation along the *x* axis (left) and the *y* axis (right) ;
(b) Normalized to width vertical settlement versus rotation ; and
(c) Normalized vertical settlement to moment along the *x* axis (left) and the *y* axis (right) .

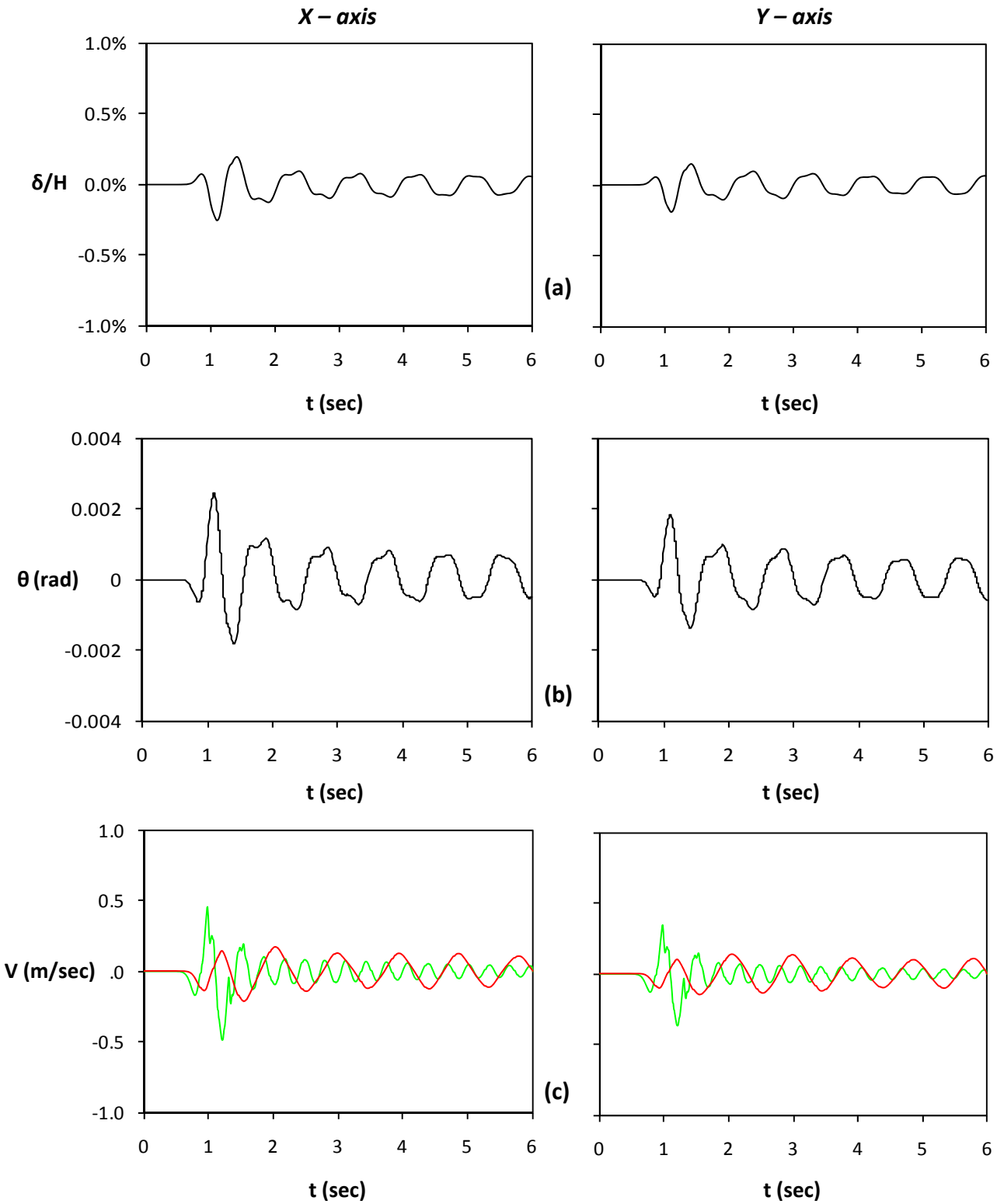

Figure 5.63. Seismic excitation in both directions, Ricker 2 A_x = 0.8 g and A_y = 75% x 0.8 g : (a) Horizontal displacement normalized to height time histories along the *x* axis (left) and the *y* axis (right) ; (b) rotation time histories along the *x* axis (left) and the *y* axis (right) ; (c) velocity time histories (Green line stands for free field motion and red line for lumped mass)

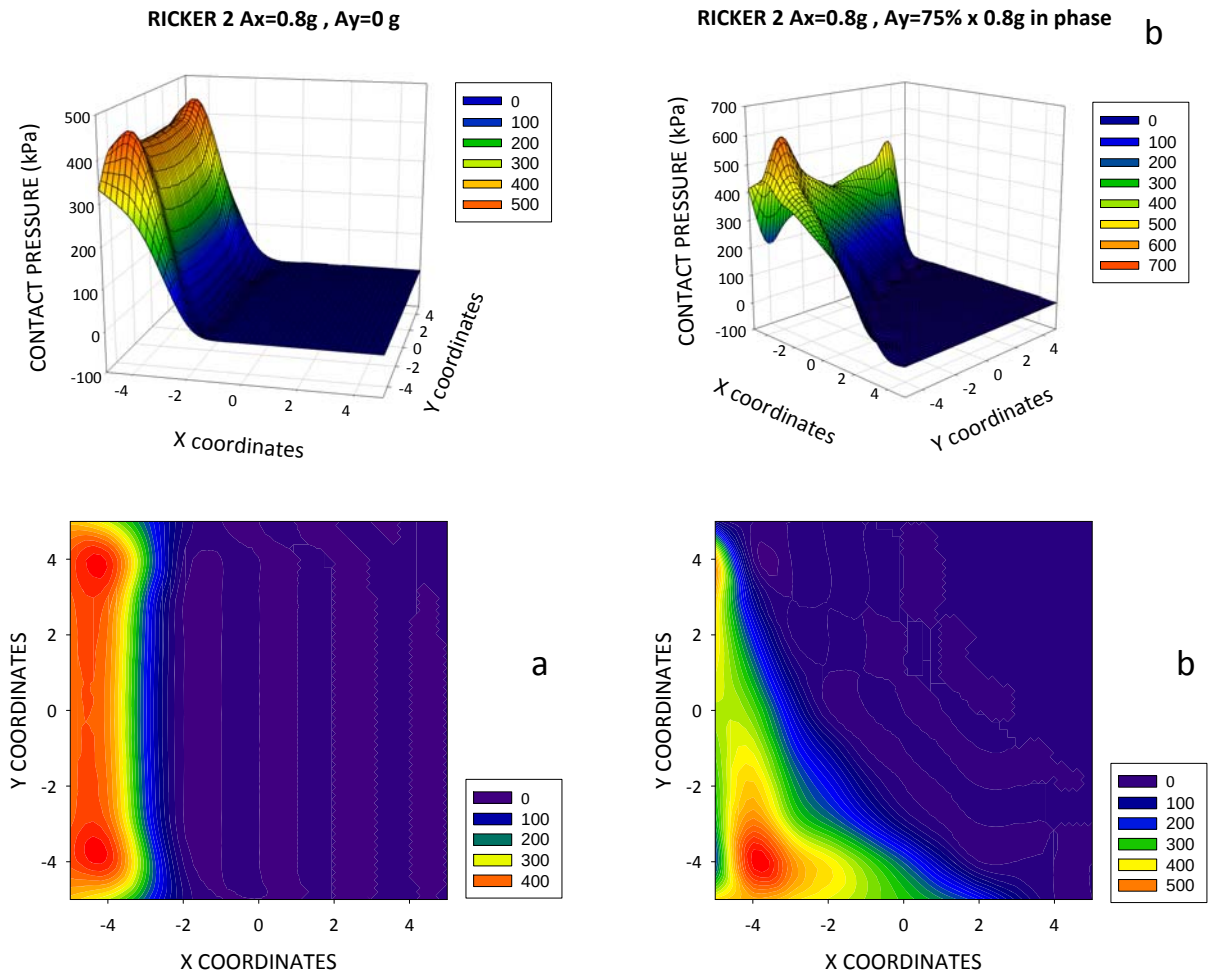

Figure 5.64. Seismic excitation in both directions, Ricker 2 A_x = 0.8 g and A_y =75% x 0.8 g : Distribution of pressures under the footing at the time increment when the maximum uplift occurs for excitation in a) one direction (left) b) both directions (right) .

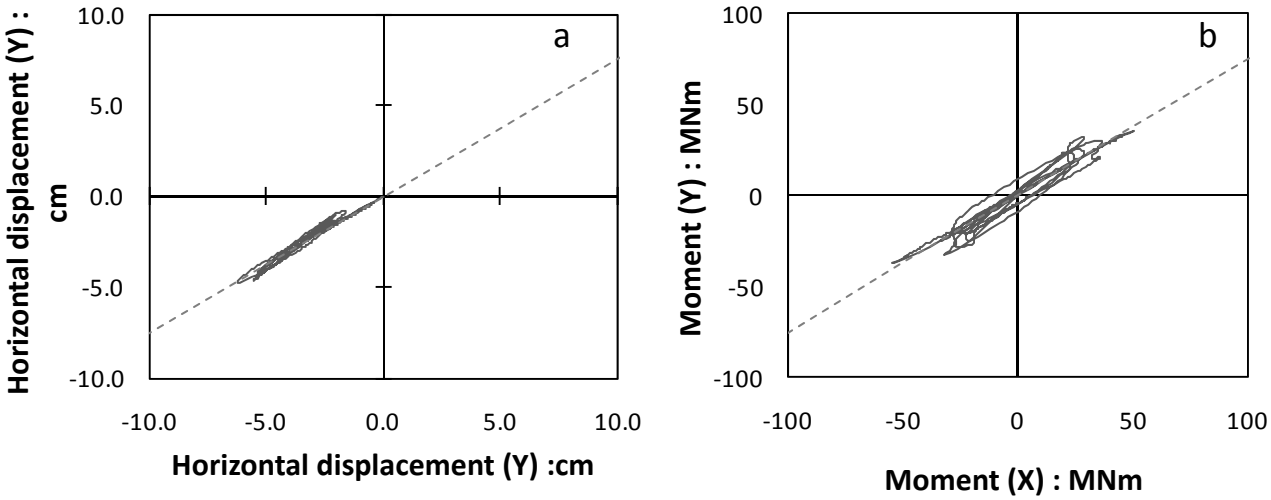

Figure 5.65. **a)** Orbit of center of mass in the X-Y plane.
b) Orbit in the M_X –M_Y plane.

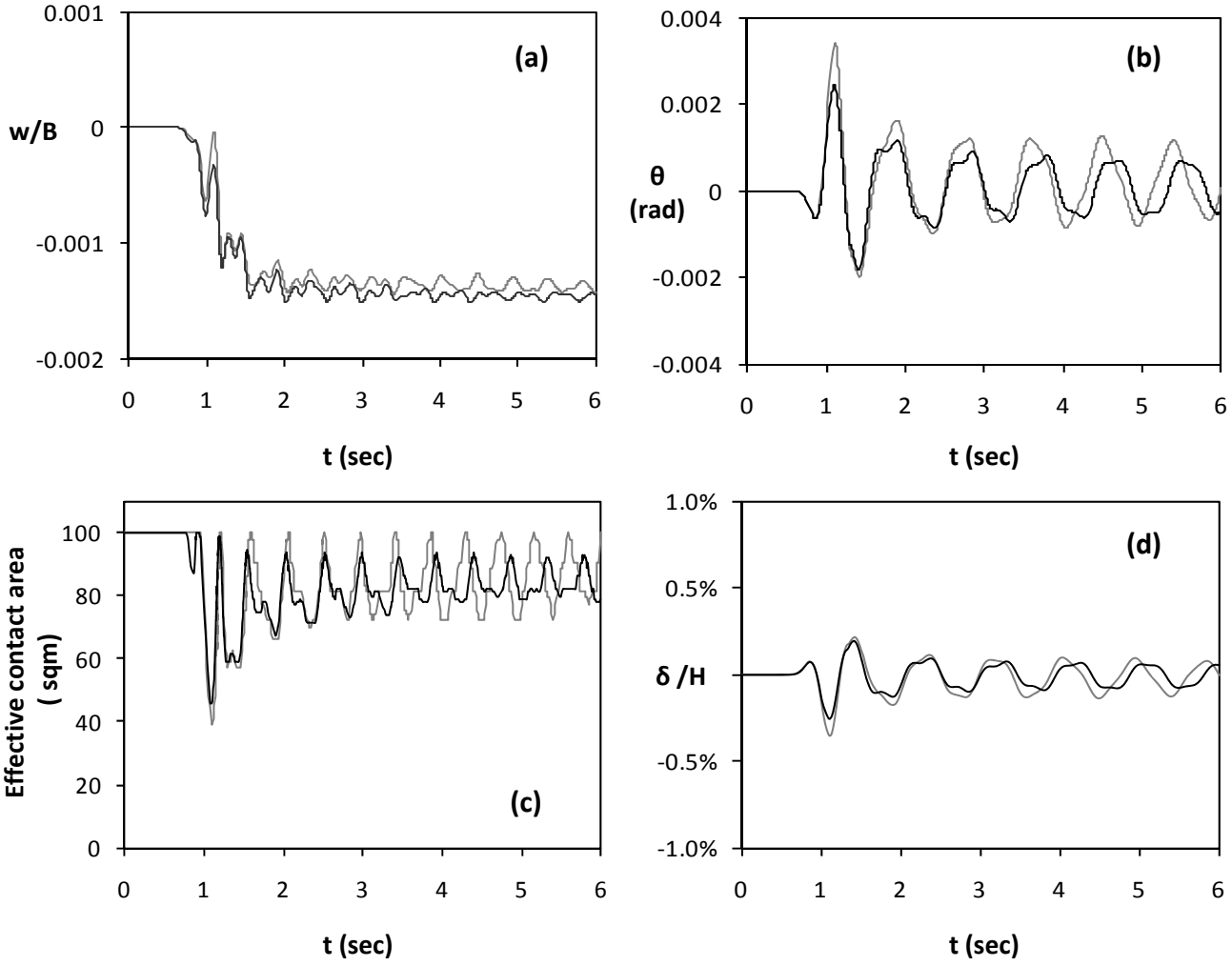

Figure 5.66. Seismic excitation in both directions, Ricker 2 A_x = 0.8 g and A_y =75% x 0.8 g and comparison with the single direction case.
Time histories of (a) Vertical settlement (b) Rotation ; (c) Effective contact area time ; (d) horizontal displacement normalized to height. (Black line represents excitation in both directions and grey line single direction excitation)

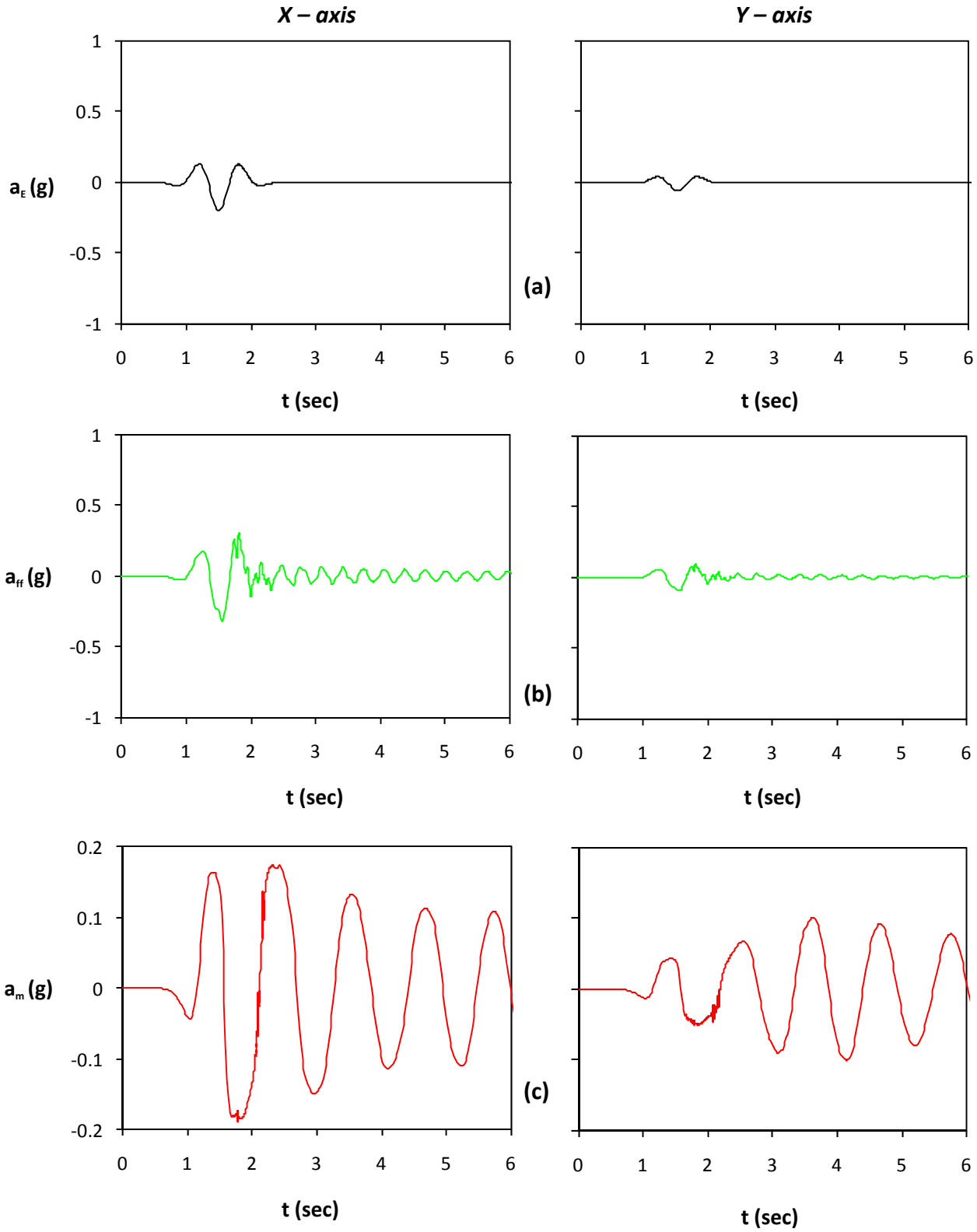

Figure 5.67. Seismic excitation in both directions, Ricker 1 A_x = 0.2 g and A_y = 30% x 0.2 g: (a) acceleration time histories of bedrock excitation along the *x* axis (left) and the *y* axis (right) ; (b) acceleration time histories at the free field ; and (c) acceleration time histories of lumped mass.

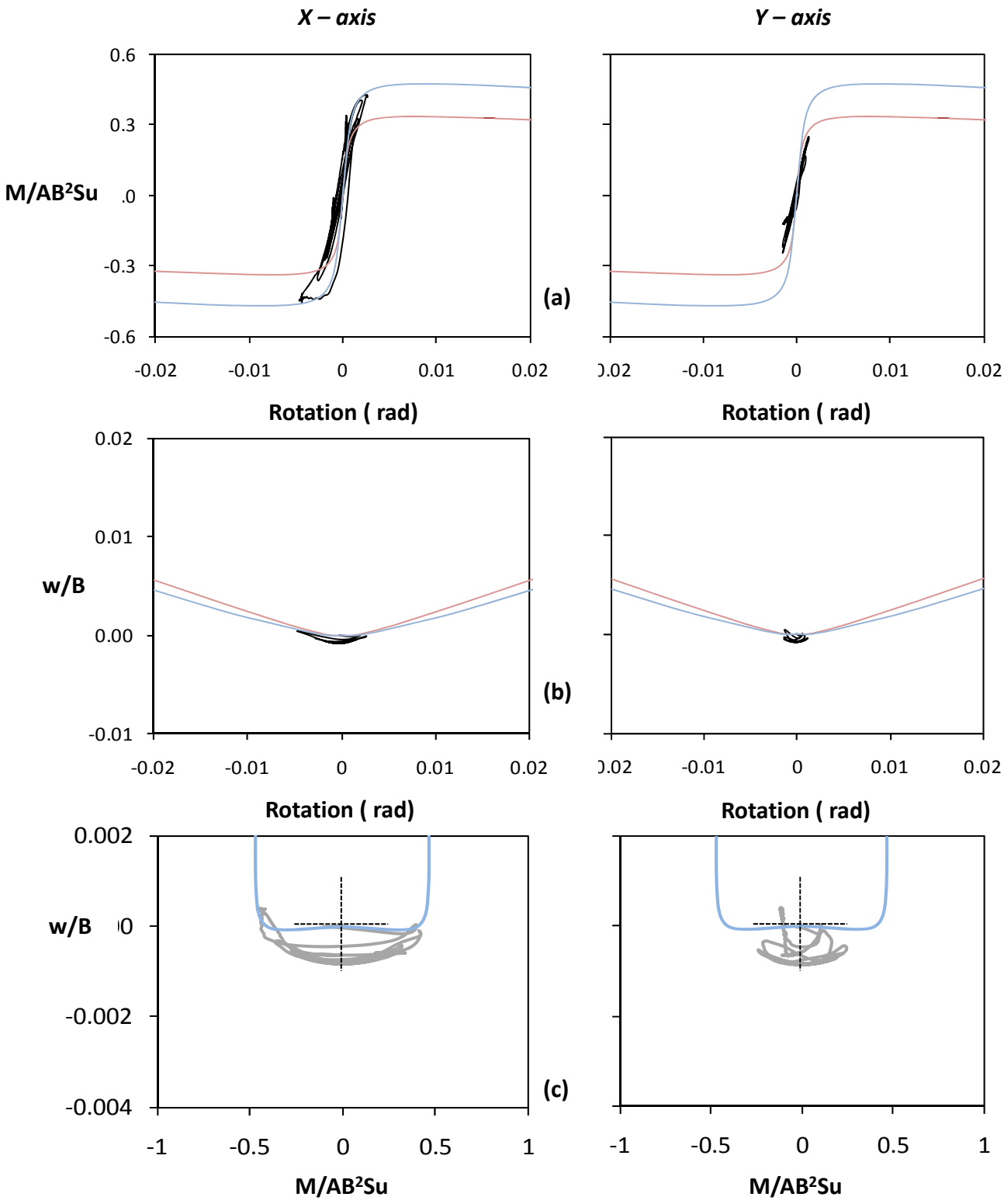

Figure 5.68. Seismic excitation in both directions, Ricker 1 A_x = 0.2 g and A_y = 30% x 0.2 g:
(a) Normalized moment versus rotation along the *x* axis (left) and the *y* axis (right) ;
(b) Normalized to width vertical settlement versus rotation ; and
(c) Normalized vertical settlement to moment along the *x* axis (left) and the *y* axis (right) .

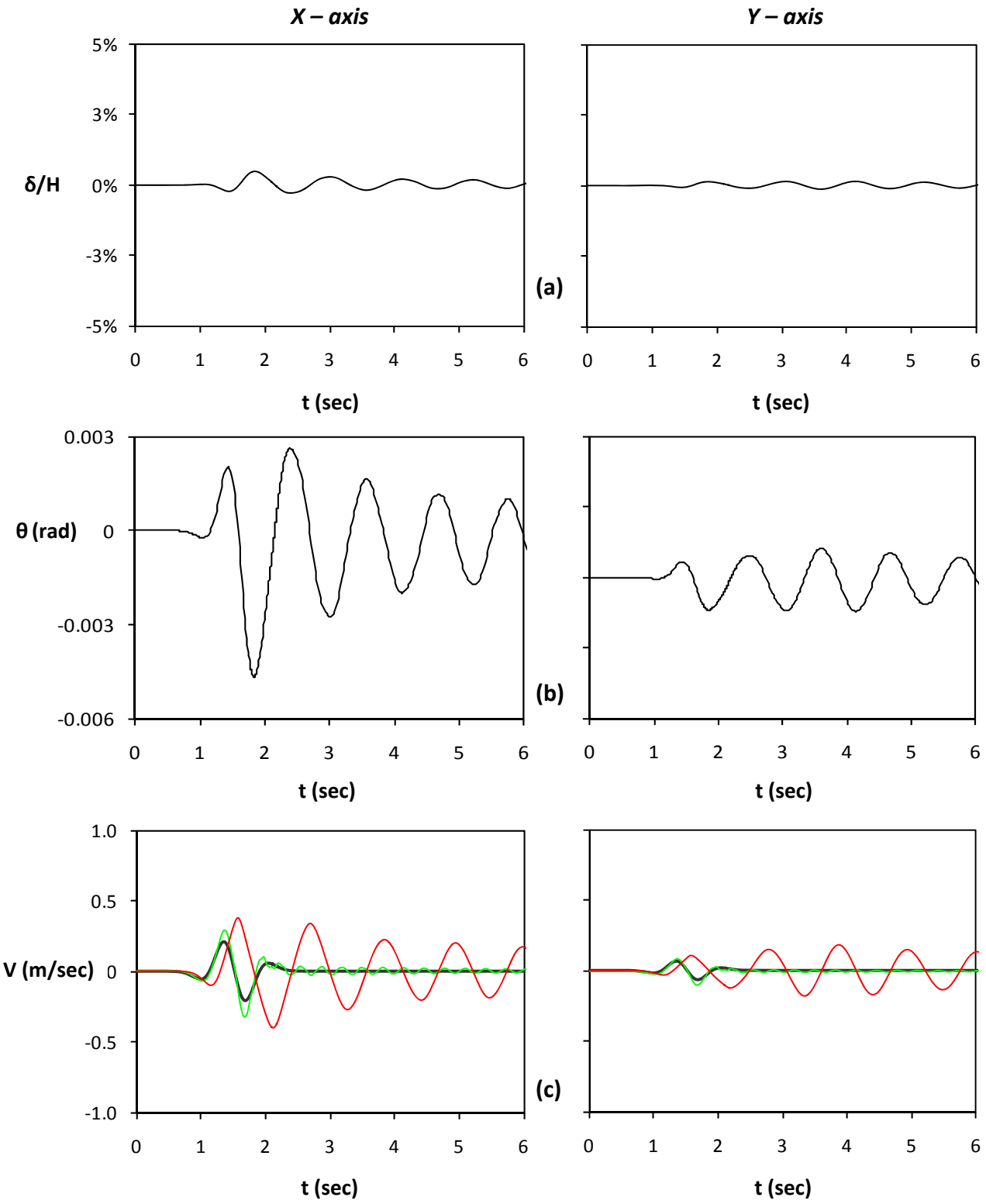

Figure 5.69. Seismic excitation in both directions, Ricker 1 A_x = 0.2 g and A_y = 30% x 0.2 g: (a) Horizontal displacement normalized to height time histories along the *x* axis (left) and the *y* axis (right) ; (b) rotation time histories along the *x* axis (left) and the *y* axis (right) ; (c) velocity time histories (Green line stands for free field motion and red line for lumped mass)

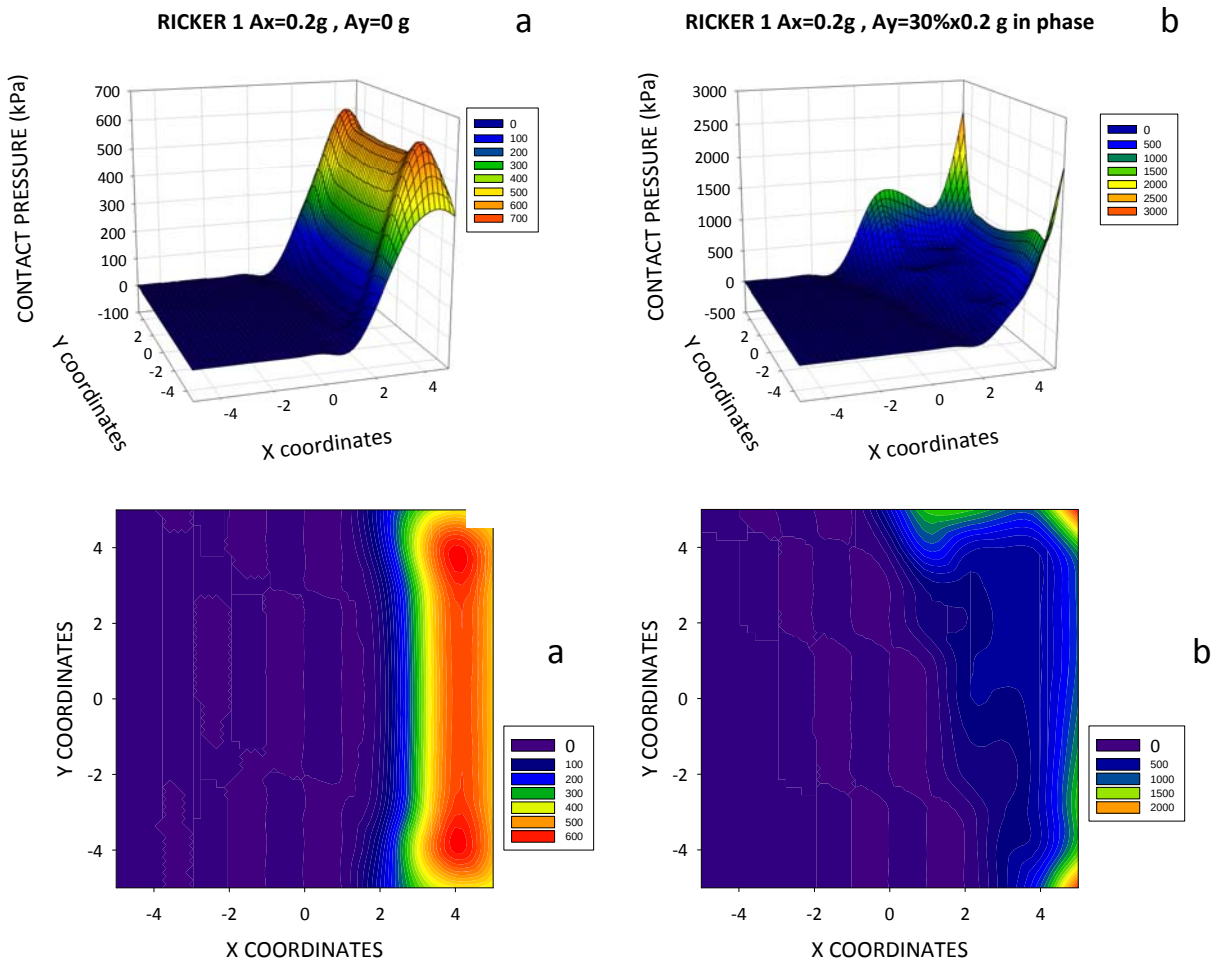

Figure 5.70. Seismic excitation in both directions, Ricker 1 A_x = 0.2 g and A_y = 30% x 0.2 g: Distribution of pressures under the footing at the time increment when the maximum uplift occurs for excitation in a) one direction (left) b) both directions (right) .

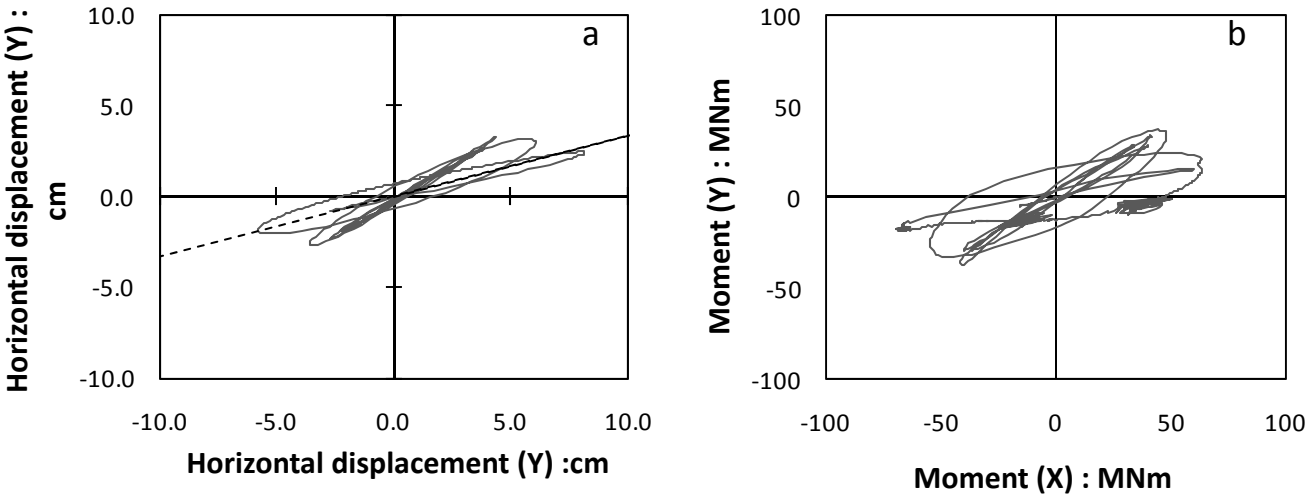

Figure 5.71. a) Orbit of center of mass in the X-Y plane.
b) Orbit in the M_X –M_Y plane.

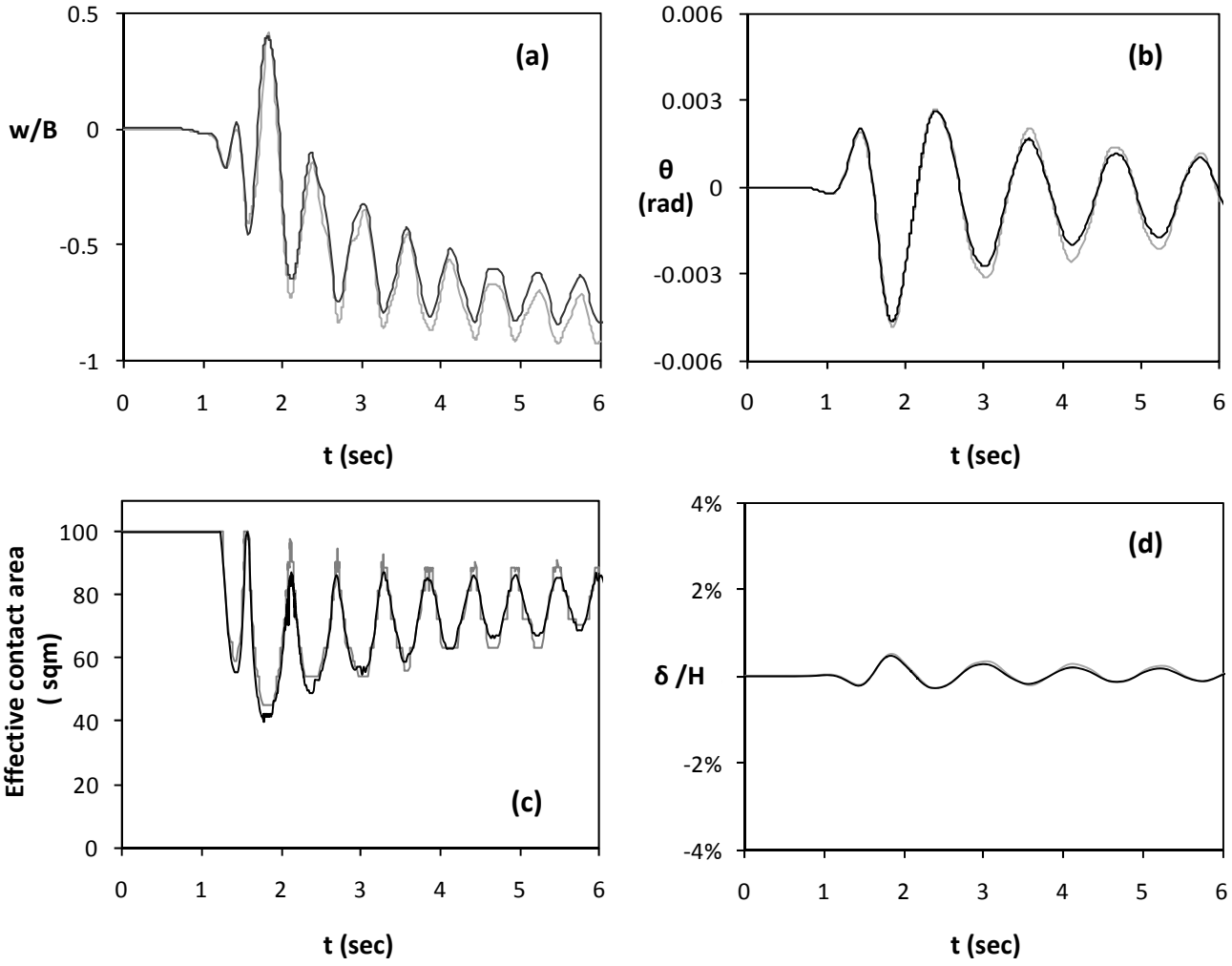

Figure 5.72. Seismic excitation in both directions, Ricker 1 A_x = 0.2 g and A_y = 30% x 0.2 g and comparison with the single direction case.
Time histories of (a) Vertical settlement (b) Rotation ; (c) Effective contact area time ; (d) horizontal displacement normalized to height. (Black line represents excitation in both directions and grey line single direction excitation)

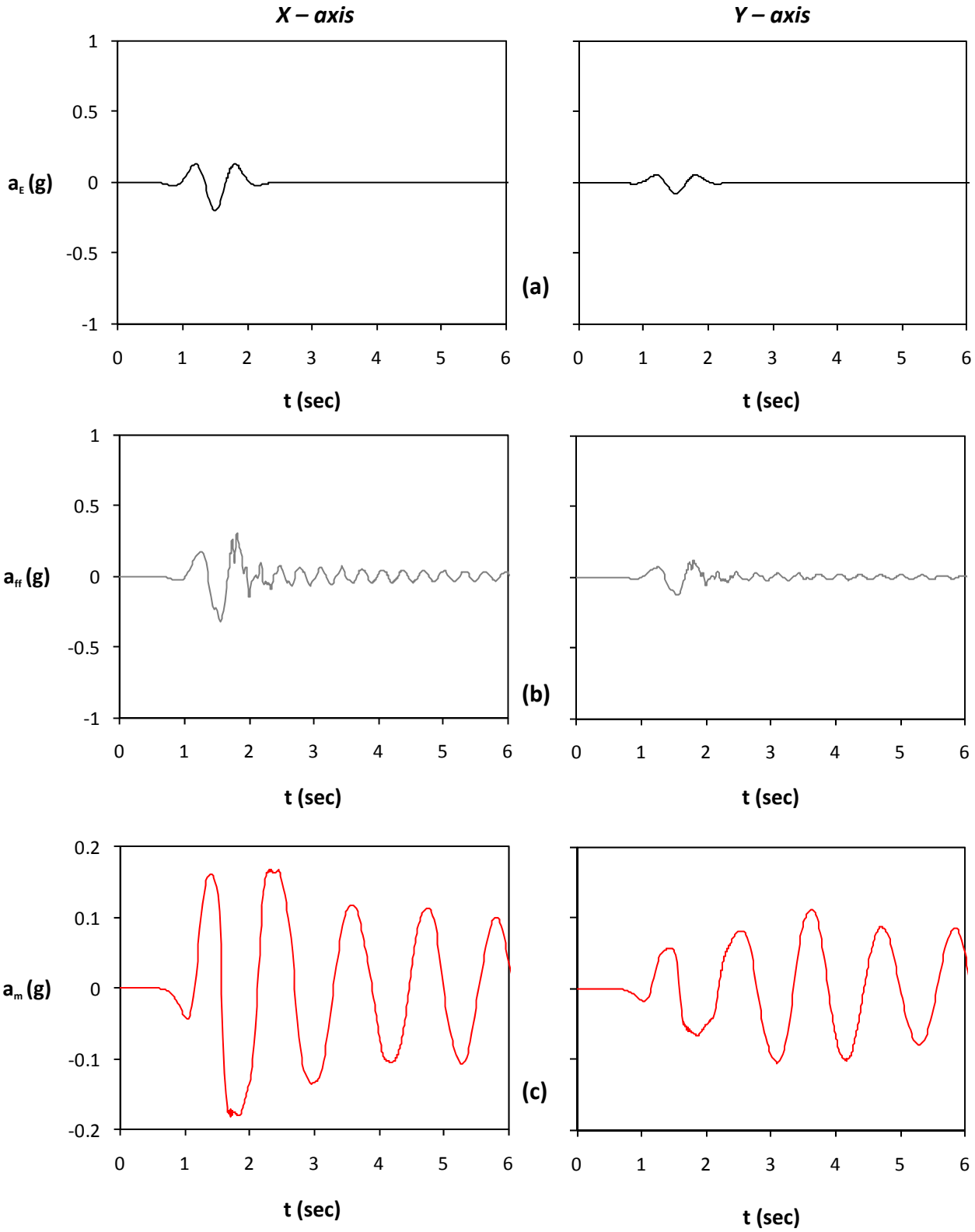

Figure 5.73. Seismic excitation in both directions, A_x = 0.2 g and A_y = 40% x 0.2 g: (a) acceleration time histories of bedrock excitation along the *x* axis (left) and the *y* axis (right) ; (b) acceleration time histories at the free field ; and (c) acceleration time histories of lumped mass.

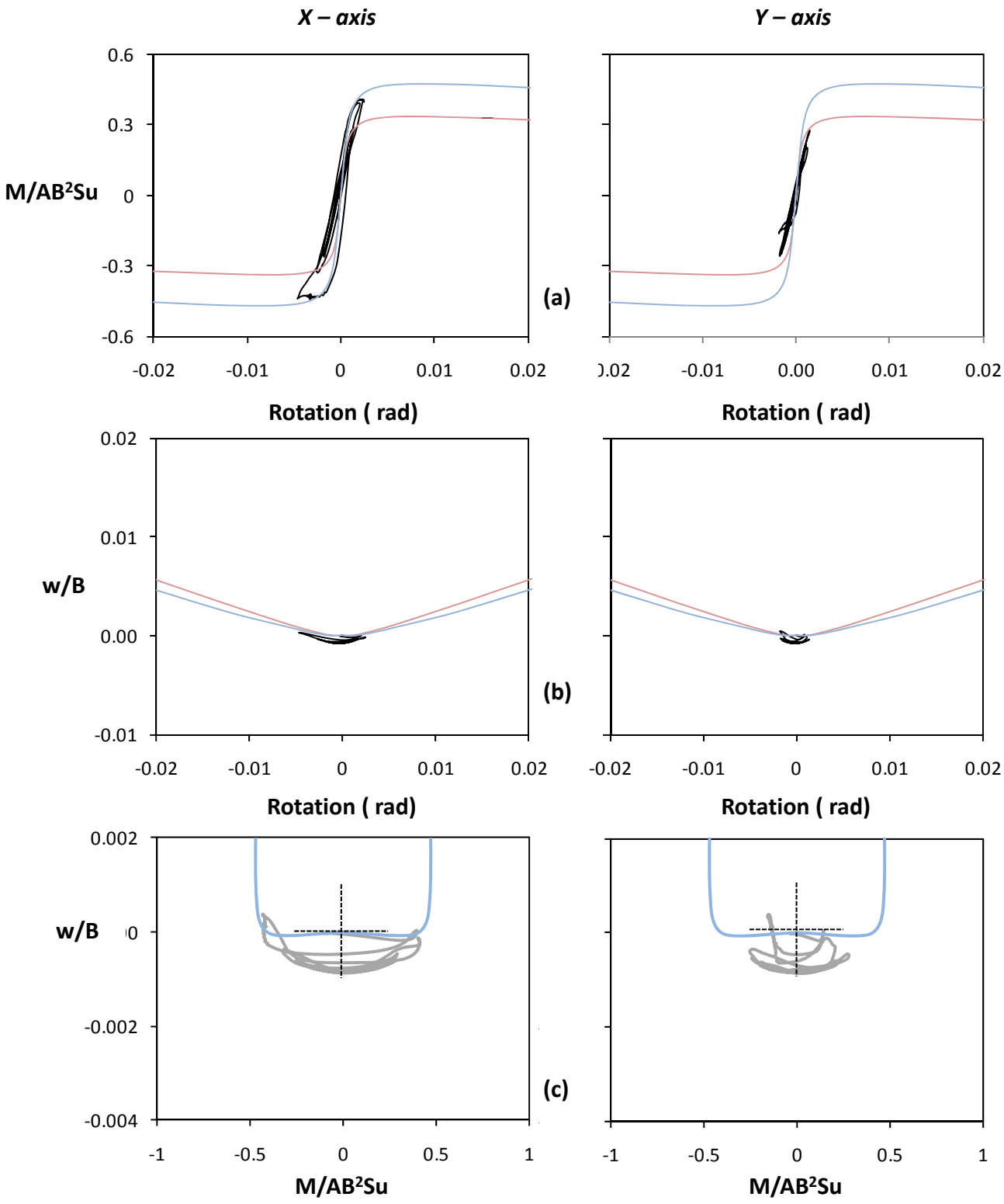

Figure 5.74. Seismic excitation in both directions, A_x = 0.2 g and A_y = 40% x 0.2 g:
(a) Normalized moment versus rotation along the *x* axis (left) and the *y* axis (right) ;
(b) Normalized to width vertical settlement versus rotation ; and
(c) Normalized vertical settlement to moment along the *x* axis (left) and the *y* axis (right) .

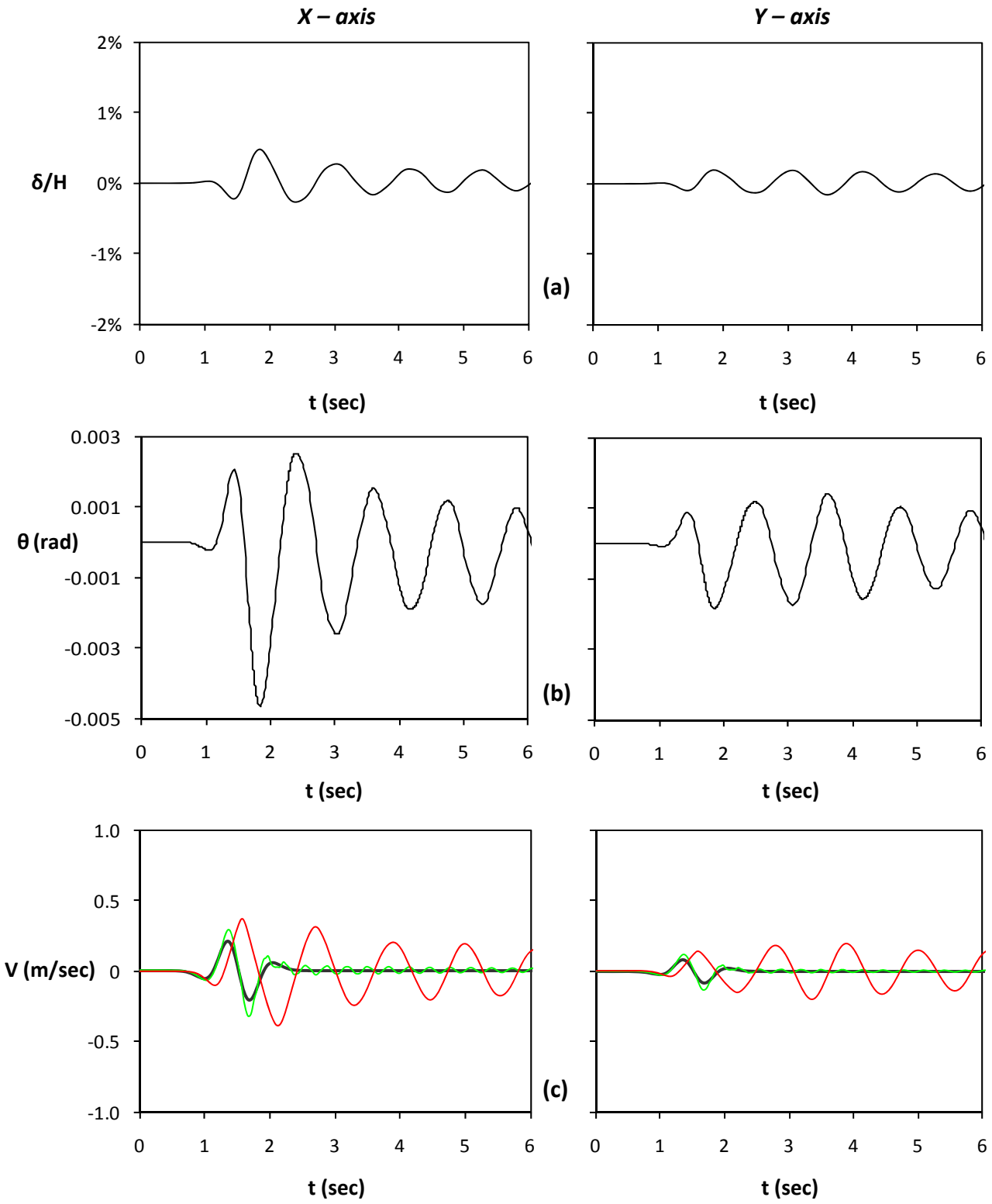

Figure 5.75. Seismic excitation in both directions, A_x = 0.2 g and A_y = 40% x 0.2 g:
(a) Horizontal displacement normalized to height time histories along the *x* axis (left) and the *y* axis (right) ; (b) rotation time histories along the *x* axis (left) and the *y* axis (right) ; (c) velocity time histories (Green line stands for free field motion and red line for lumped mass)

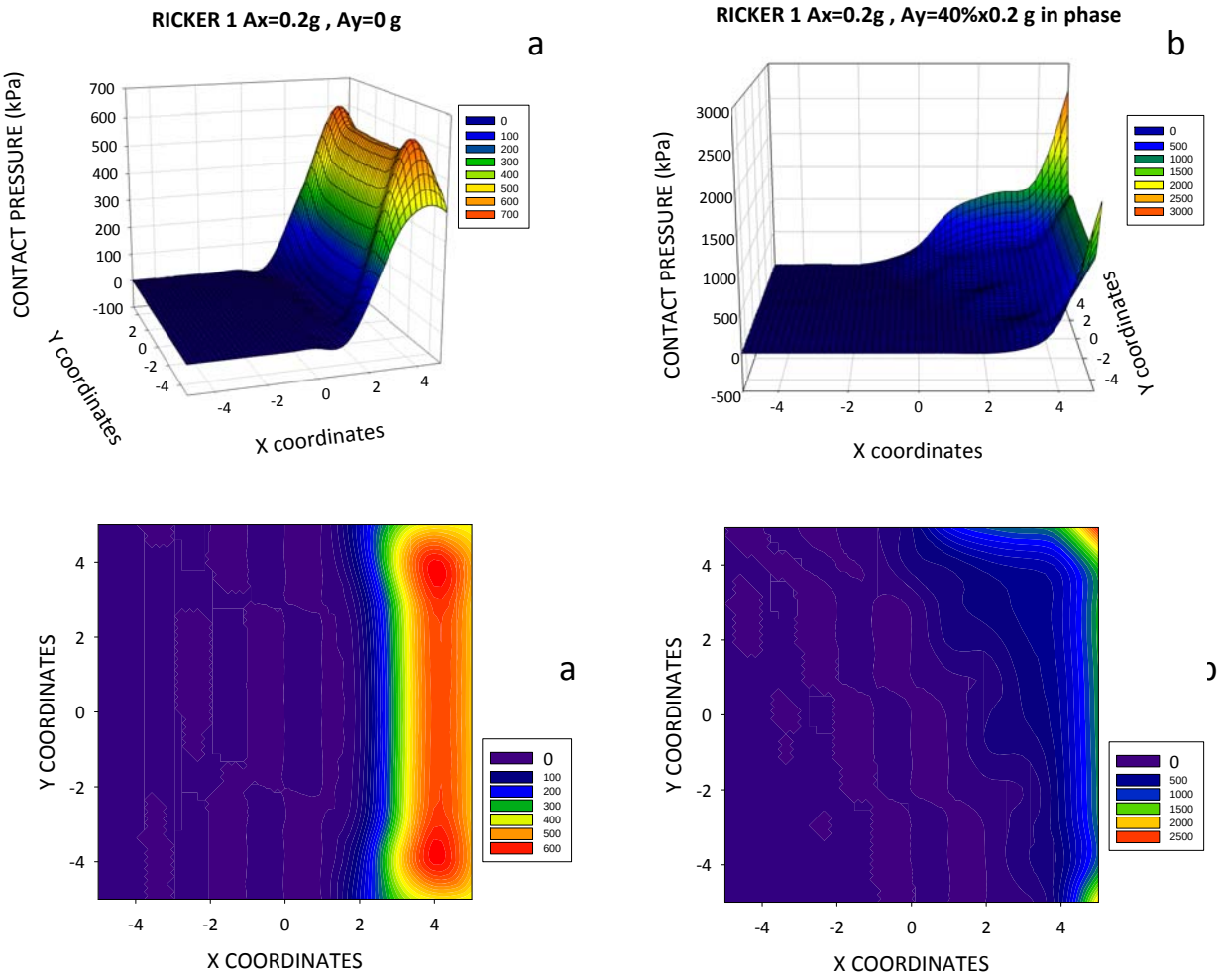

Figure 5.76. Seismic excitation in both directions, Ricker 1 A_x = 0.2 g and A_y = 30% x 0.2 g: Distribution of pressures under the footing at the time increment when the maximum uplift occurs for excitation in a) one direction (left) b) both directions (right) .

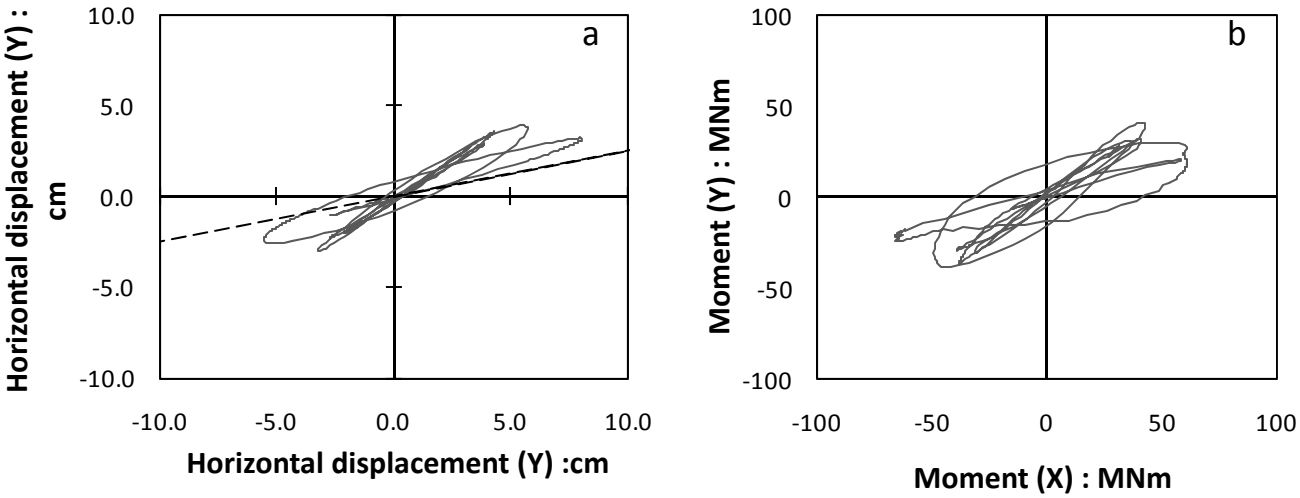

Figure 5.77. a) Orbit of center of mass in the X-Y plane.
b) Orbit in the M_X –M_Y plane.

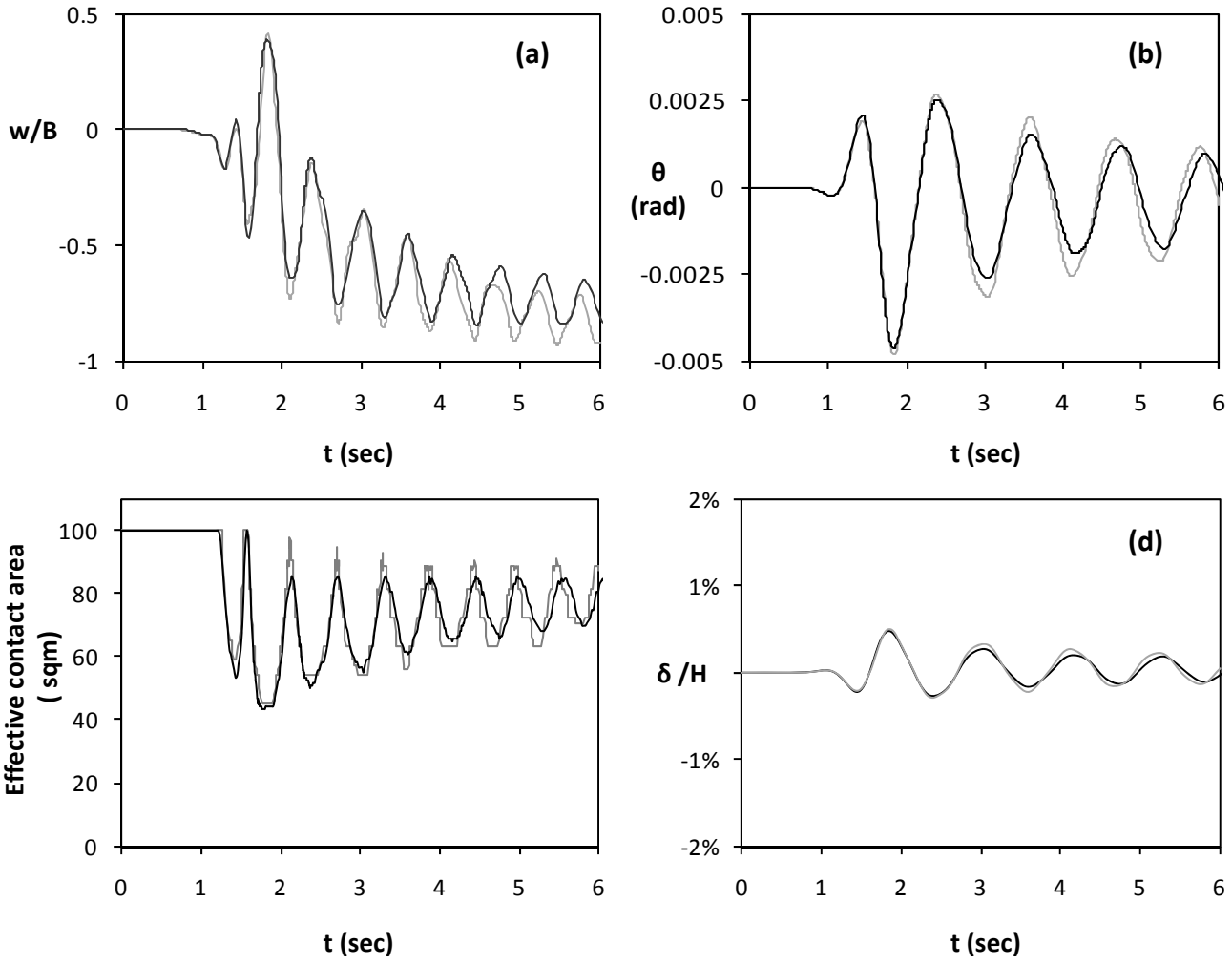

Figure 5.78. Seismic excitation in both directions, A_x = 0.2 g and A_y = 40% x 0.2 g and comparison with the single direction case.
Time histories of (a) Vertical settlement (b) Rotation ; (c) Effective contact area time ; (d) horizontal displacement normalized to height. (Black line represents excitation in both directions and grey line single direction excitation)

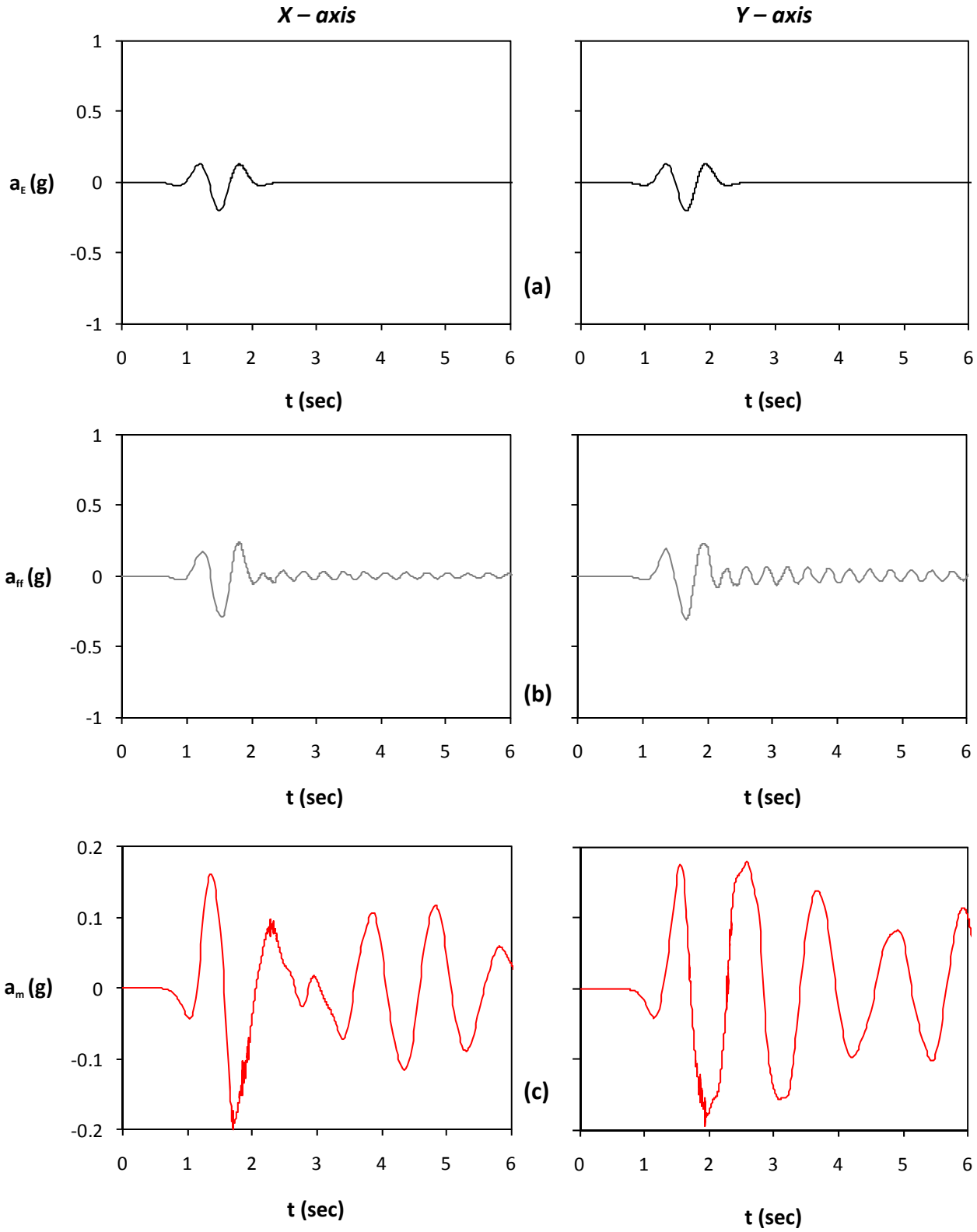

Figure 5.79. Seismic excitation in both directions, Ricker 1 A_x = 0.2 g and A_y = 0.2 g asynchronous : (a) acceleration time histories of bedrock excitation along the *x* axis (left) and the *y* axis (right) ; (b) acceleration time histories at the free field ; and (c) acceleration time histories of lumped mass.

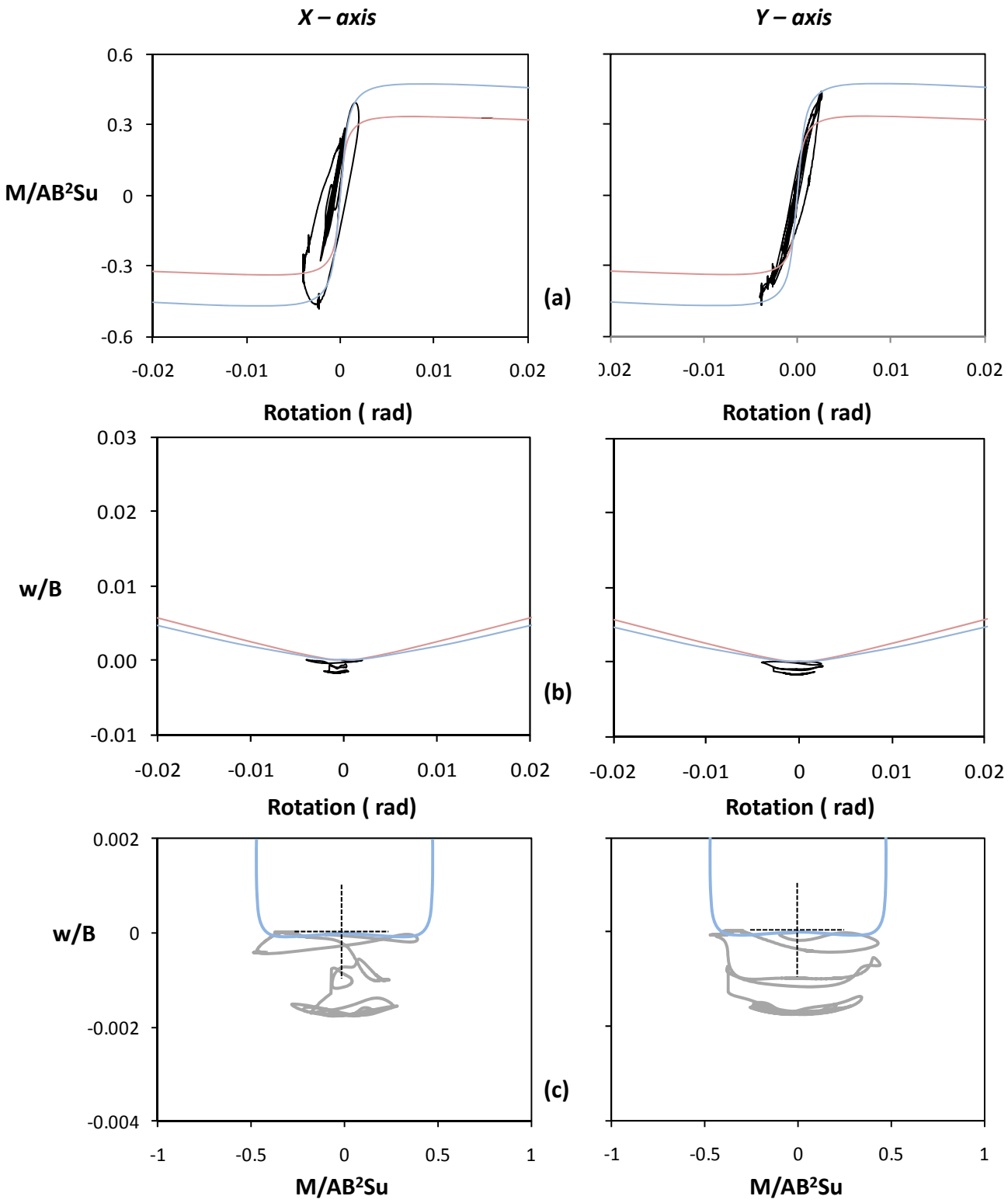

Figure 5.80. Seismic excitation in both directions, A_x = 0.2 g and A_y = 0.2 g asynchronous :
(a) Normalized moment versus rotation along the *x* axis (left) and the *y* axis (right) ;
(b) Normalized to width vertical settlement versus rotation ; and
(c) Normalized vertical settlement to moment along the *x* axis (left) and the *y* axis (right) .

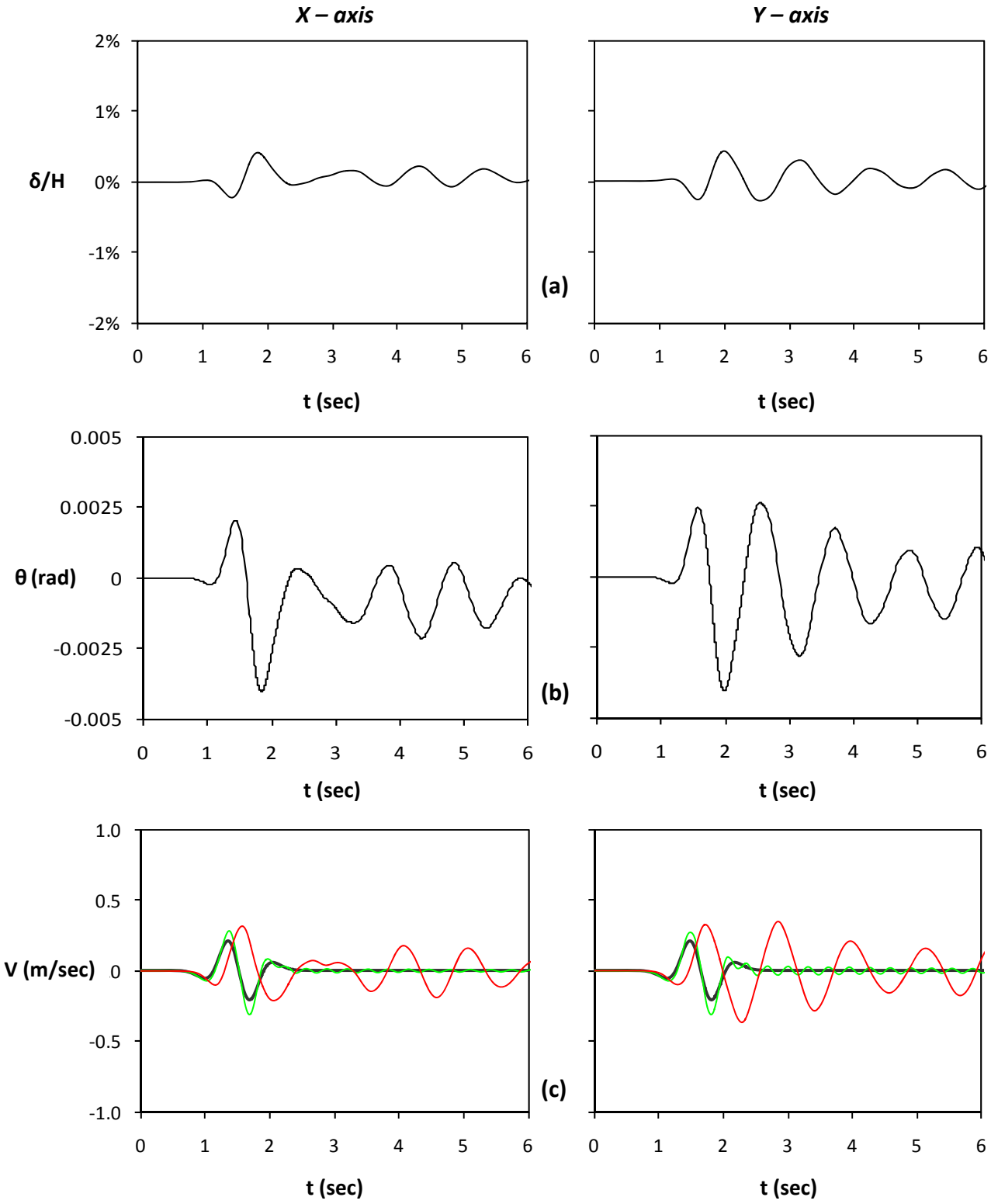

Figure 5.81. Seismic excitation in both directions, A_x = 0.2 g and A_y = 0.2 g asynchronous : (a) Horizontal displacement normalized to height time histories along the *x* axis (left) and the *y* axis (right) ; (b) rotation time histories along the *x* axis (left) and the *y* axis (right) ; (c) velocity time histories (Green line stands for free field motion and red line for lumped mass)

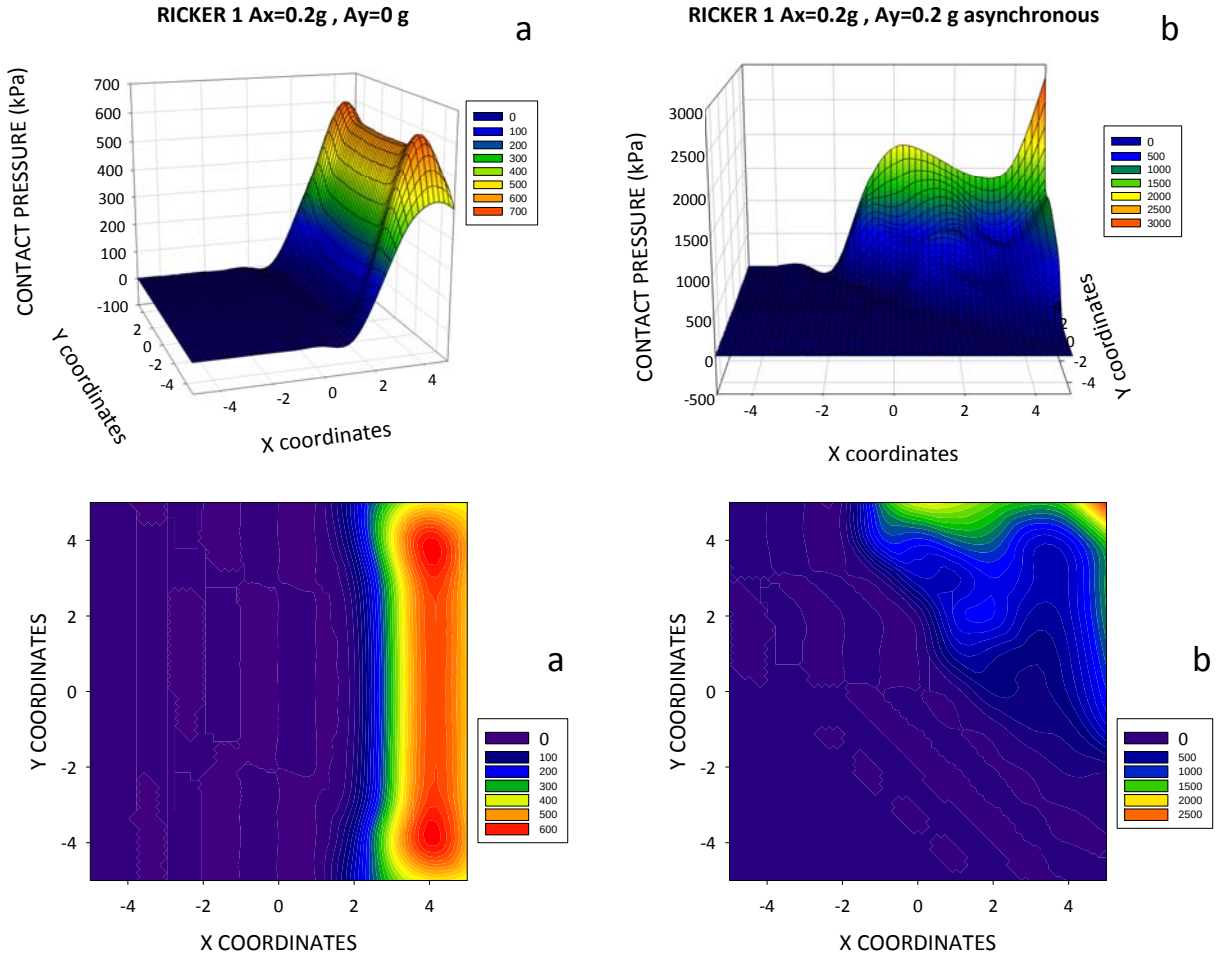

Figure 5.16. Seismic excitation in both directions, Ricker 1 A_x = 0.2 g and A_y = 0.2 g asynchronous : Distribution of pressures under the footing at the time increment when the maximum uplift occurs for excitation in a) one direction (left) b) both directions (right) .

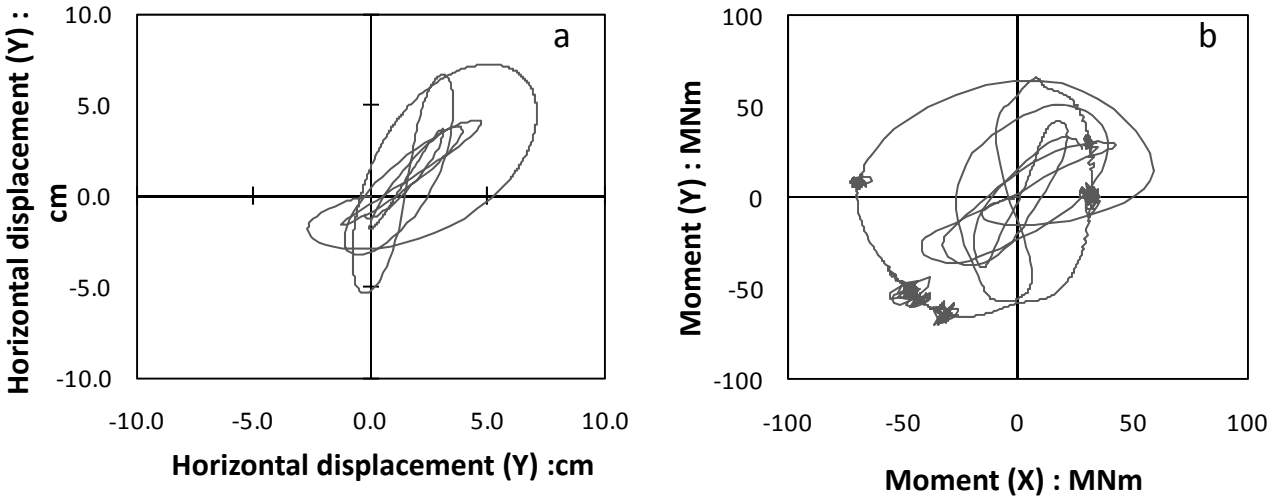

Figure 5.17. **a)** Orbit of center of mass in the X-Y plane.
b) Orbit in the M_X –M_Y plane.

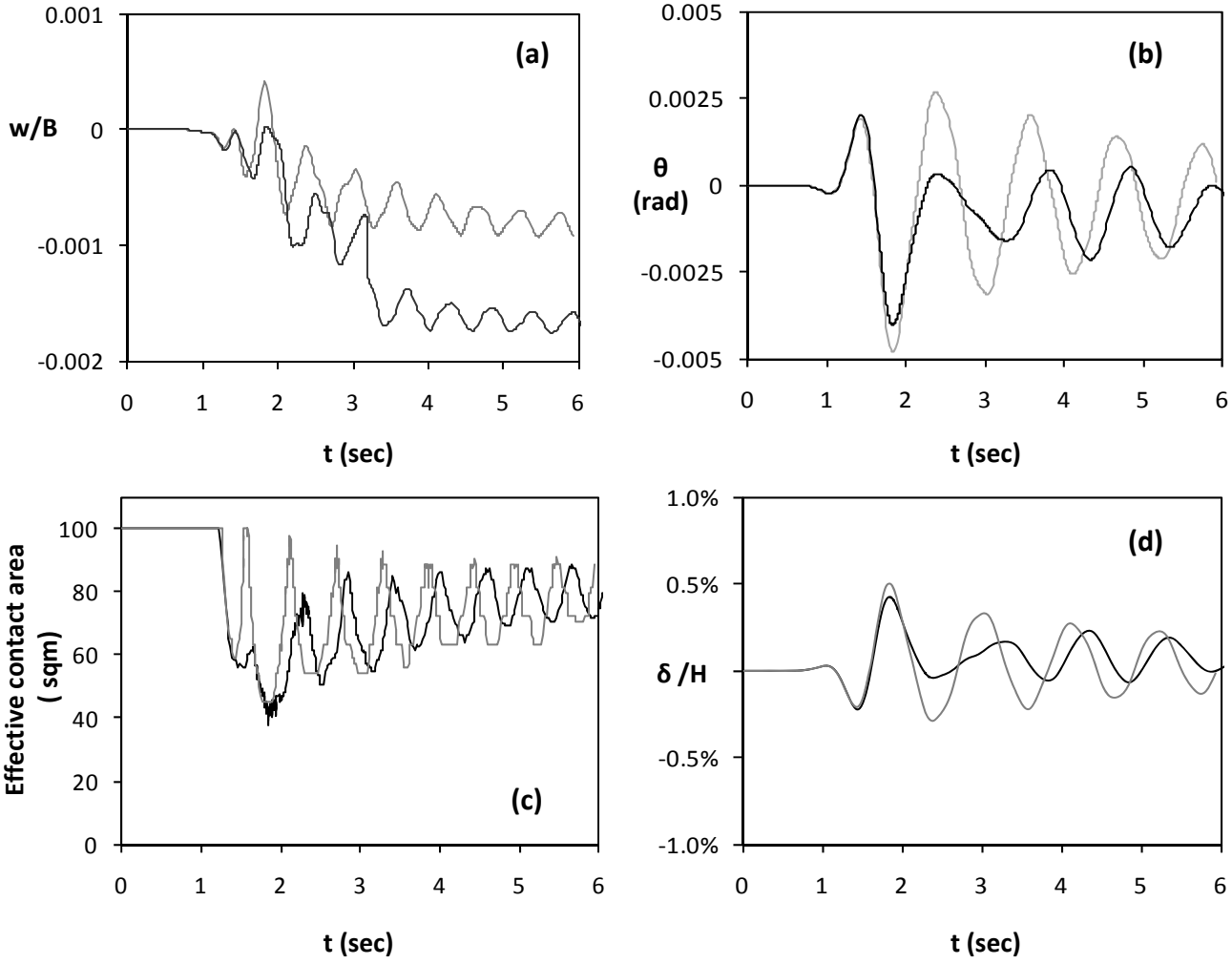

Figure 5.82. Seismic excitation in both directions, A_x = 0.2 g and A_y = 0.2 g and comparison with the single direction case.
Time histories of (a) Vertical settlement (b) Rotation ; (c) Effective contact area time ; (d) horizontal displacement normalized to height. (Black line represents excitation in both directions and grey line single direction excitation)

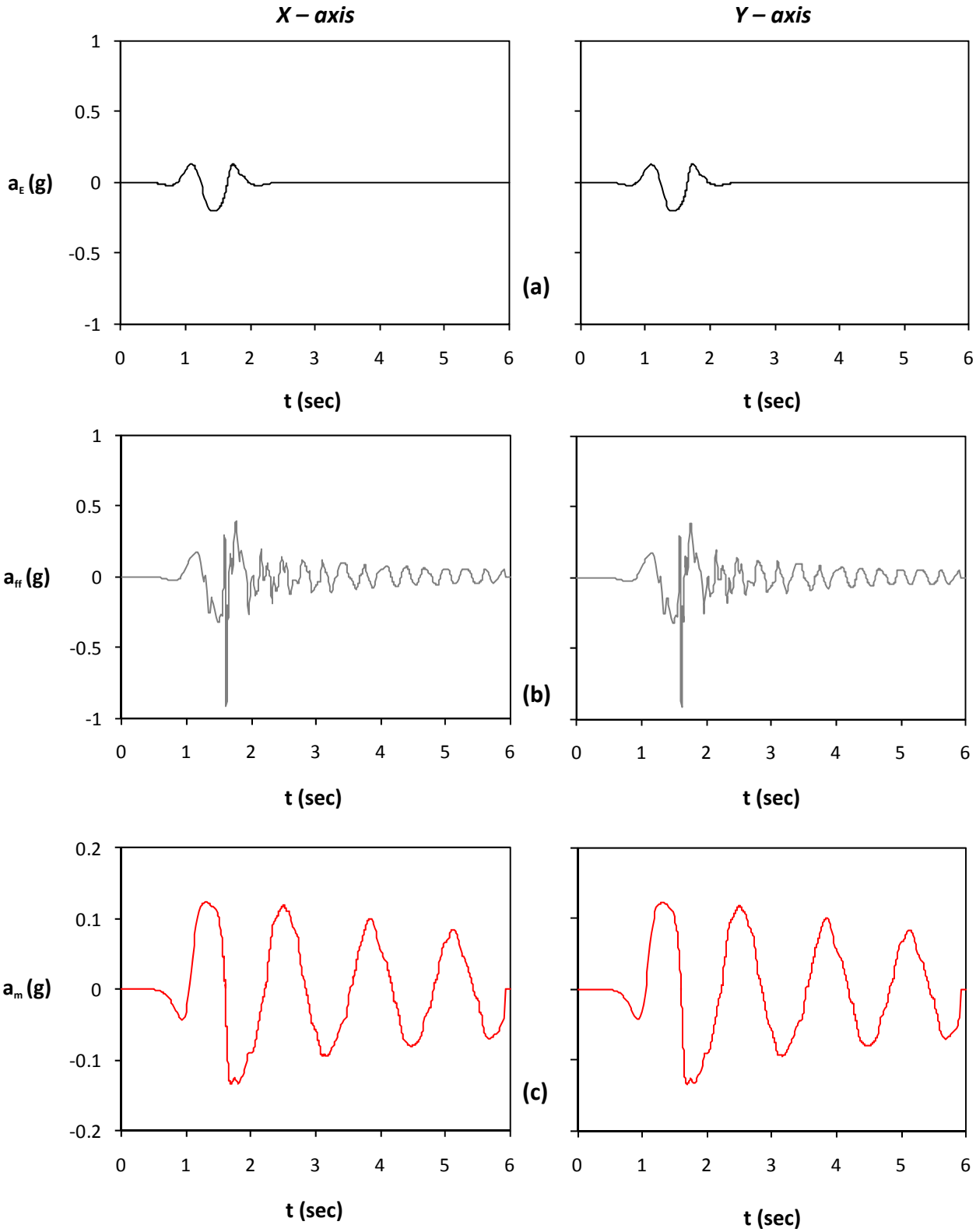

Figure 5.83. Seismic excitation in both directions, Ricker 1 A_x = 0.2 g and A_y = 0.2 g synchronous peaks: (a) acceleration time histories of bedrock excitation along the *x* axis (left) and the *y* axis (right) ; (b) acceleration time histories at the free field ; and (c) acceleration time histories of lumped mass.

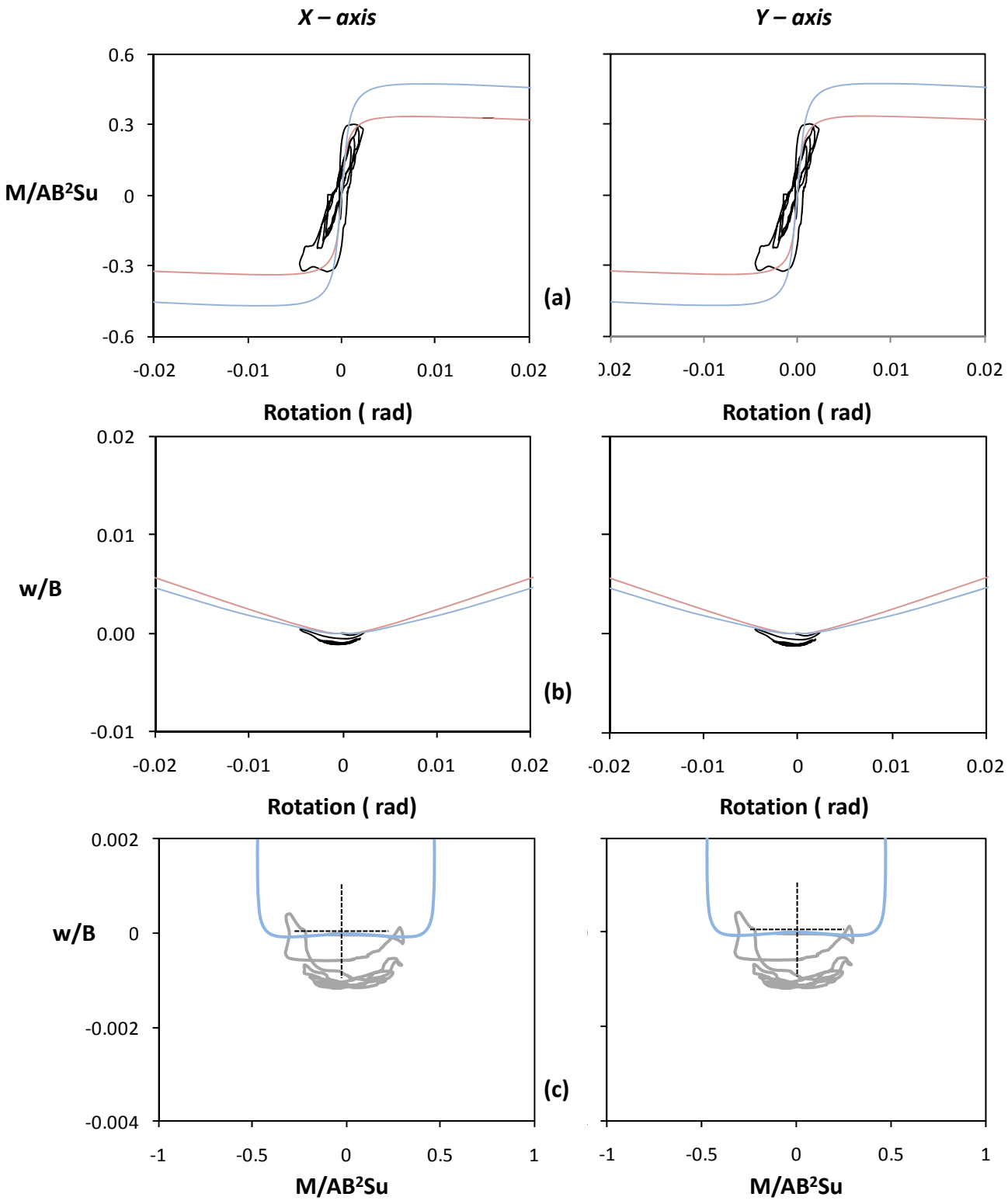

Figure 5.84. Seismic excitation in both directions, A_x = 0.2 g and A_y = 0.2 g synchronous peaks :
(a) Normalized moment versus rotation along the *x* axis (left) and the *y* axis (right) ;
(b) Normalized to width vertical settlement versus rotation ; and
(c) Normalized vertical settlement to moment along the *x* axis (left) and the *y* axis (right) .

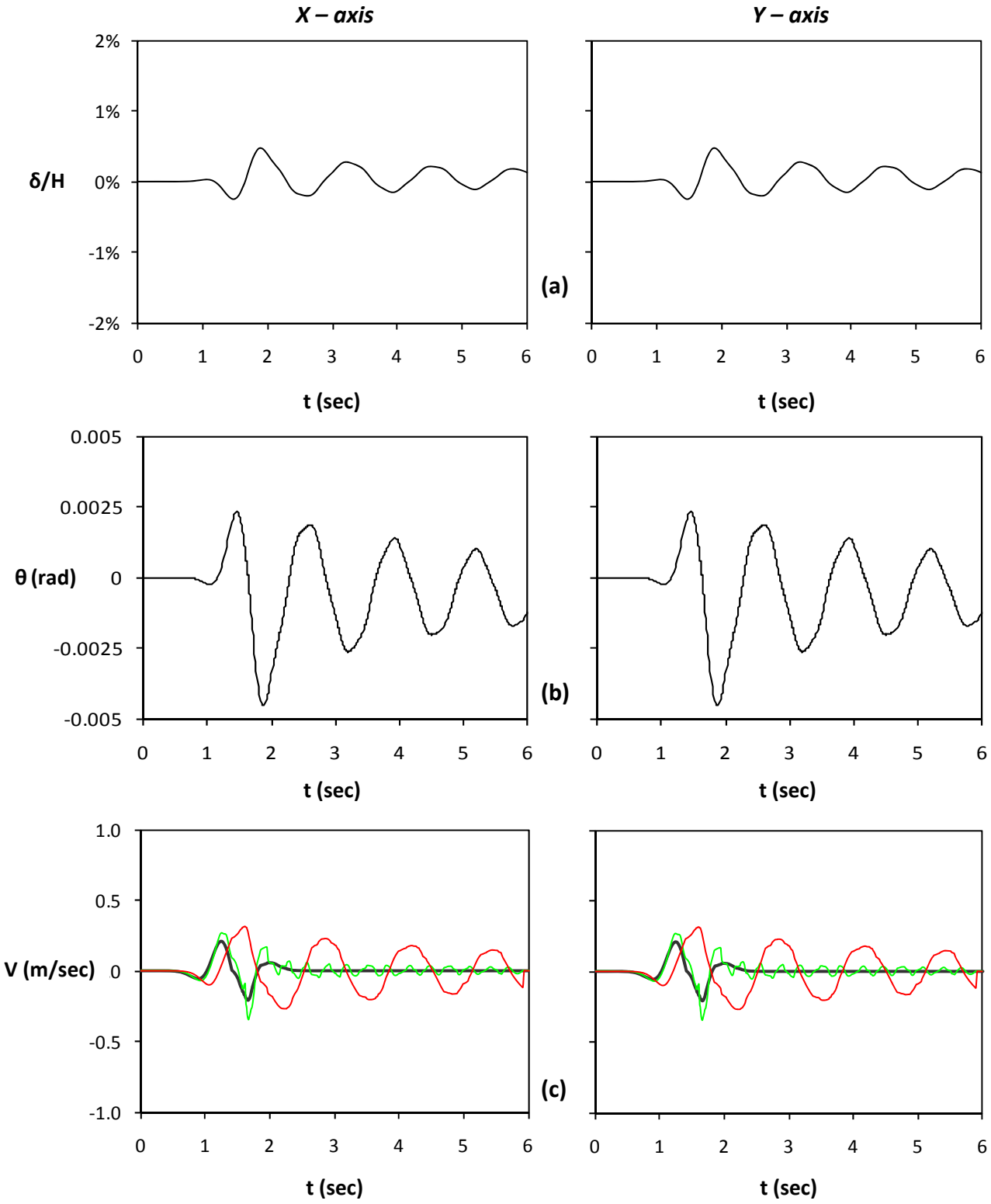

Figure 5.85. Seismic excitation in both directions, A_x = 0.2 g and A_y = 0.2 g synchronous : (a) Horizontal displacement normalized to height time histories along the *x* axis (left) and the *y* axis (right) ; (b) rotation time histories along the *x* axis (left) and the *y* axis (right) ; (c) velocity time histories (Green line stands for free field motion and red line for lumped mass)

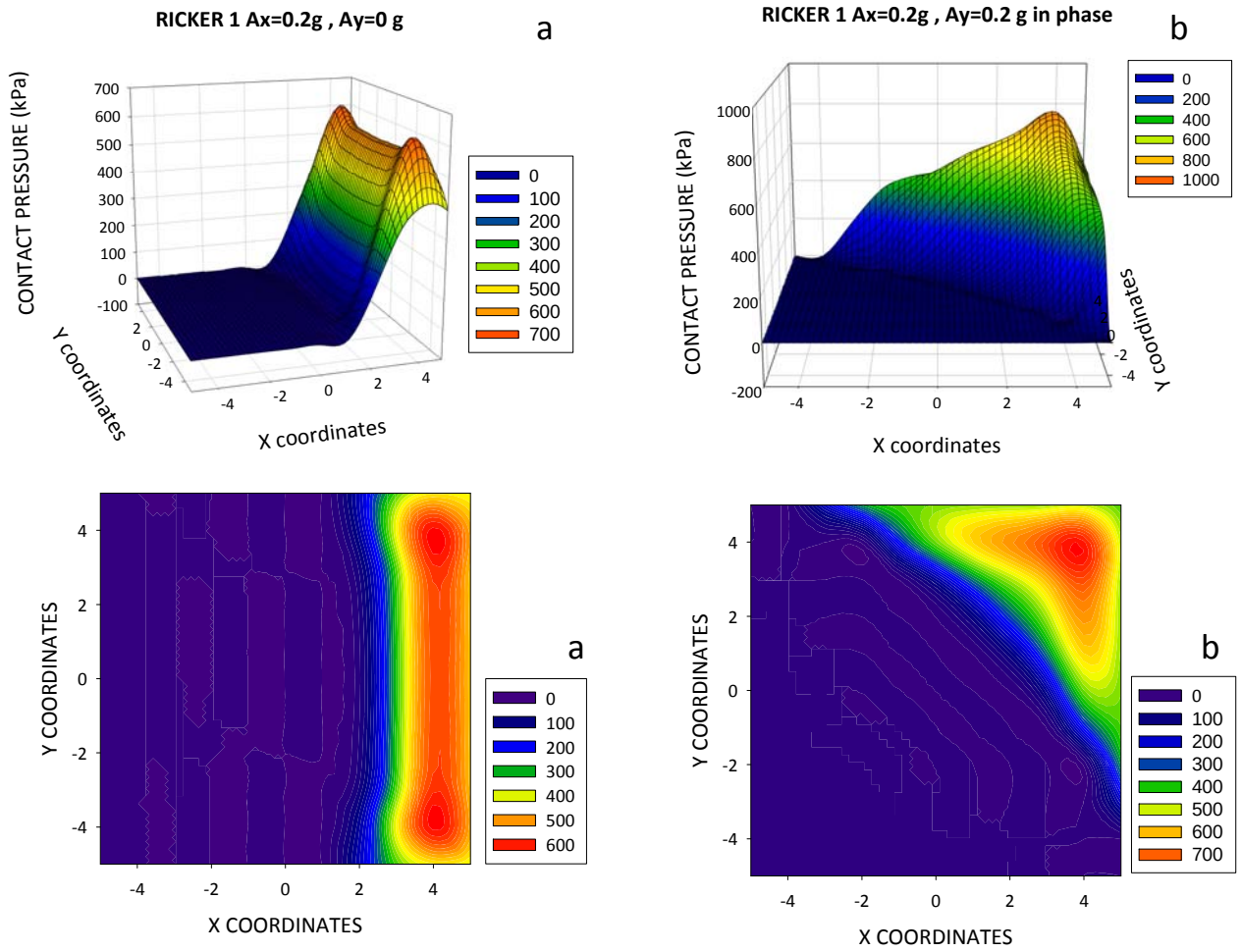

Figure 5.86. Seismic excitation in both directions, Ricker 1 A_x = 0.2 g and A_y = 0.2 g synchronous : Distribution of pressures under the footing at the time increment when the maximum uplift occurs for excitation in a) one direction (left) b) both directions (right) .

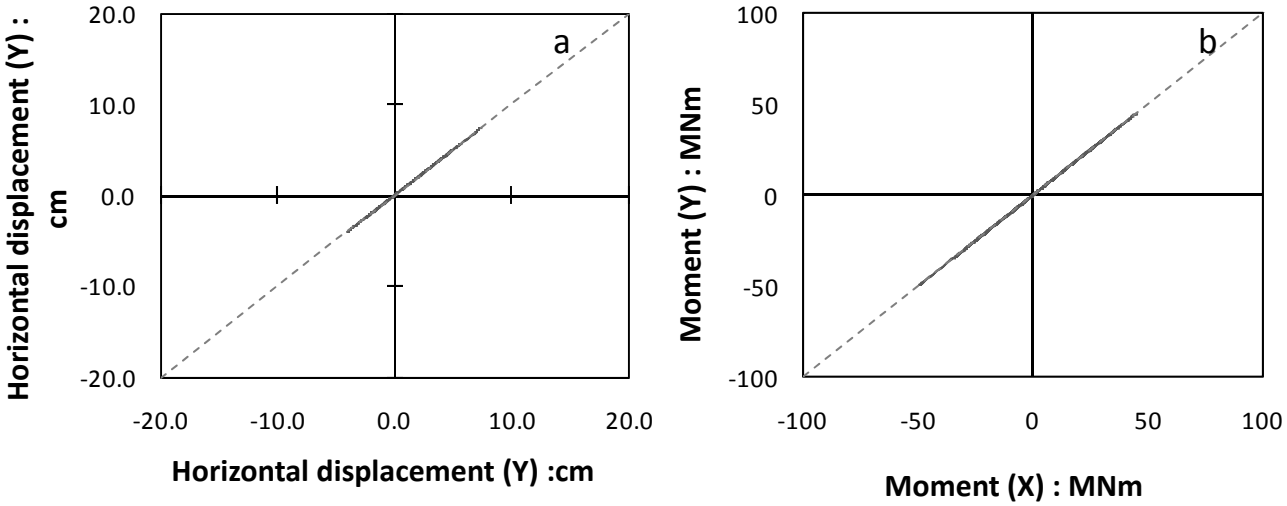

Figure 5.87. **a)** Orbit of center of mass in the X-Y plane.
b) Orbit in the M_X –M_Y plane.

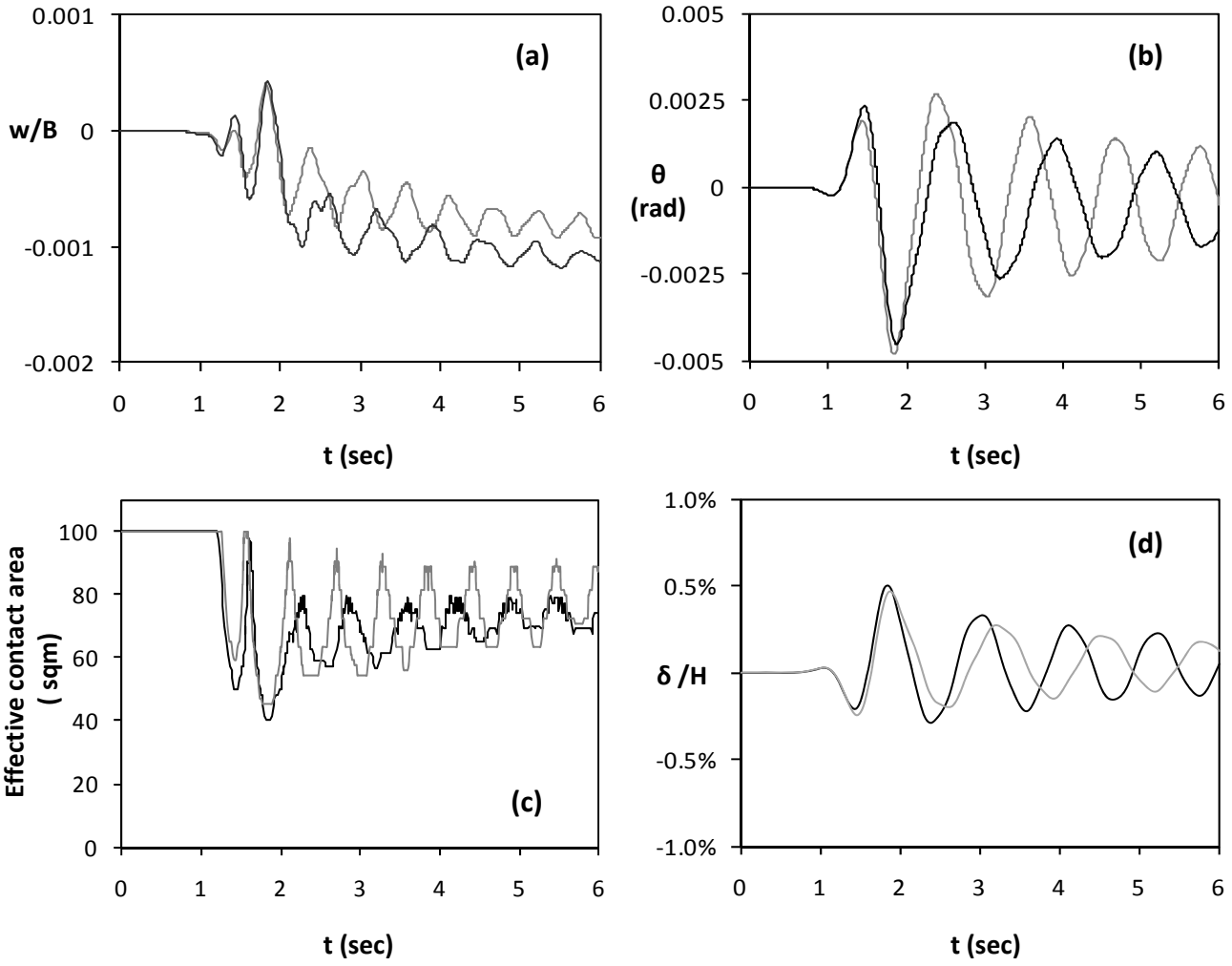

Figure 5.88. Seismic excitation in both directions, A_x = 0.2 g and A_y = 0.2 g synchronous peaks and comparison with the single direction case.
Time histories of (a) Vertical settlement (b) Rotation ; (c) Effective contact area time ; (d) horizontal displacement normalized to height. (Black line represents excitation in both directions and grey line single direction excitation)

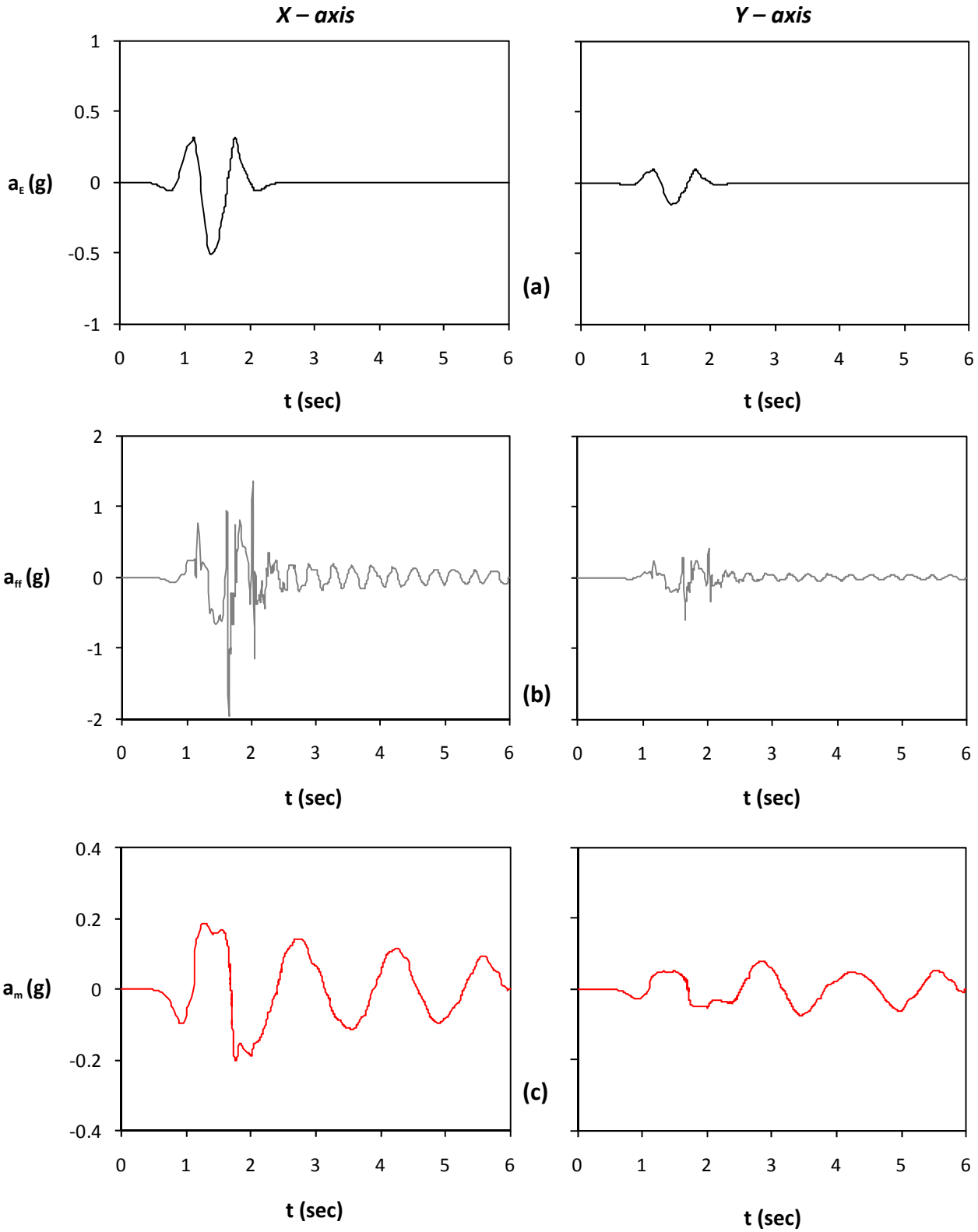

Figure 5.89. Seismic excitation in both directions, Ricker 1 A_x = 0.5 g and A_y = 30%x 0.5 g: (a) acceleration time histories of bedrock excitation along the *x* axis (left) and the *y* axis (right) ; (b) acceleration time histories at the free field ; and (c) acceleration time histories of lumped mass.

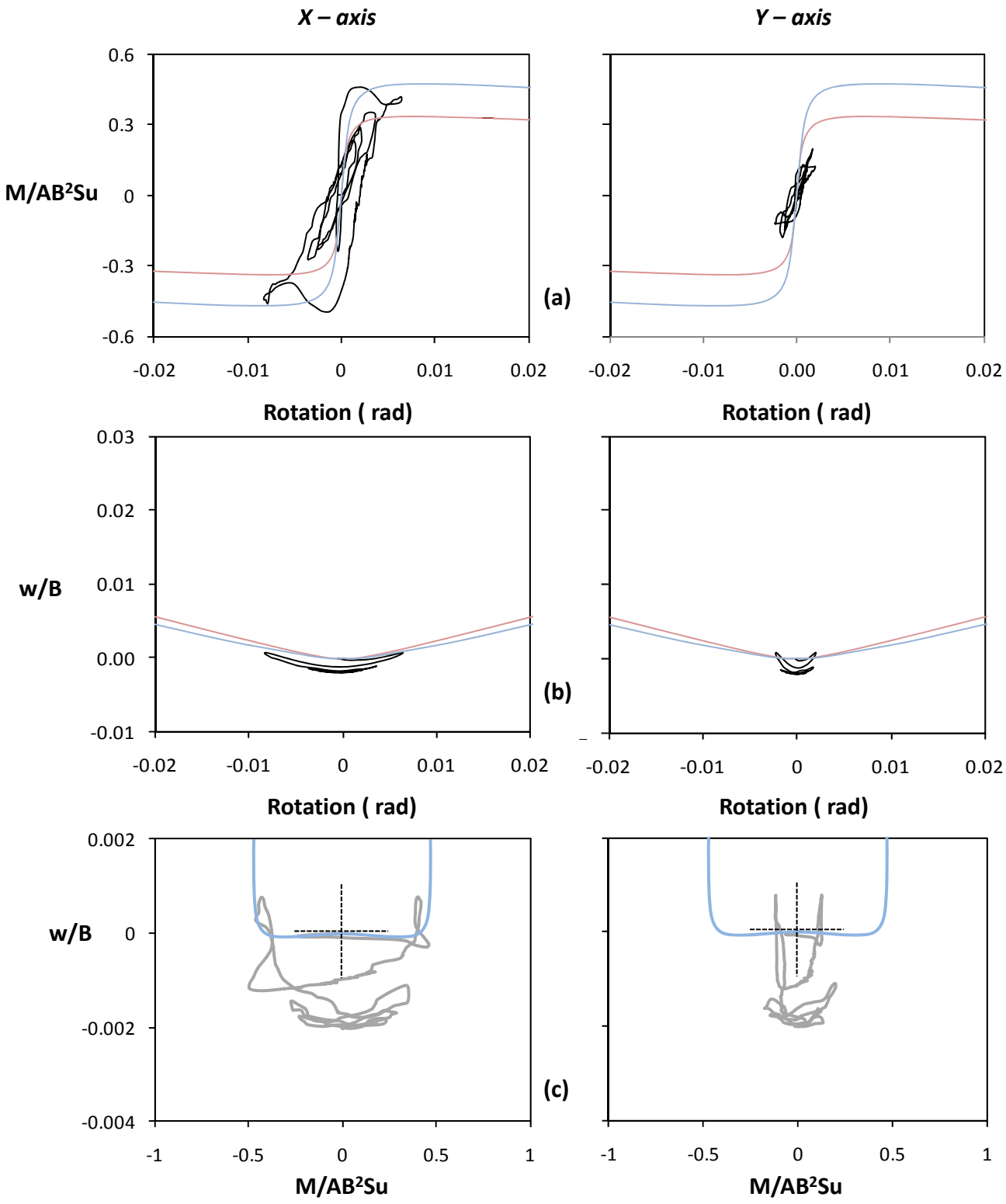

Figure 5.90. Seismic excitation in both directions, A_x = 0.5 g and A_y =30%x 0.5 g :
(a) Normalized moment versus rotation along the *x* axis (left) and the *y* axis (right) ;
(b) Normalized to width vertical settlement versus rotation ; and
(c) Normalized vertical settlement to moment along the *x* axis (left) and the *y* axis (right) .

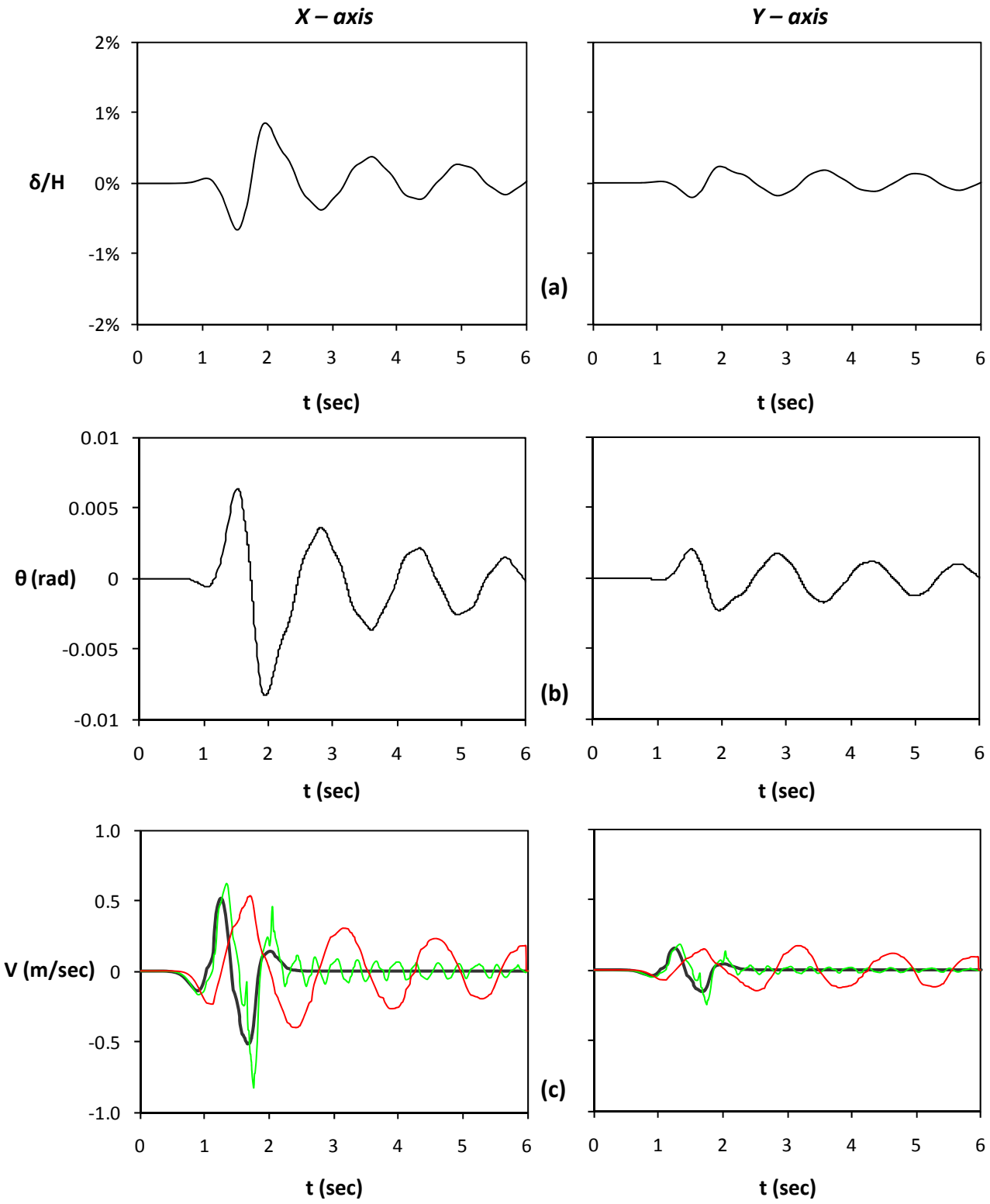

Figure 5.91. Seismic excitation in both directions, A_x = 0.5 g and A_y =30%x 0.5 g:
(a) Horizontal displacement normalized to height time histories along the *x* axis (left) and the *y* axis (right) ; (b) rotation time histories along the *x* axis (left) and the *y* axis (right) ; (c) velocity time histories (Green line stands for free field motion and red line for lumped mass)

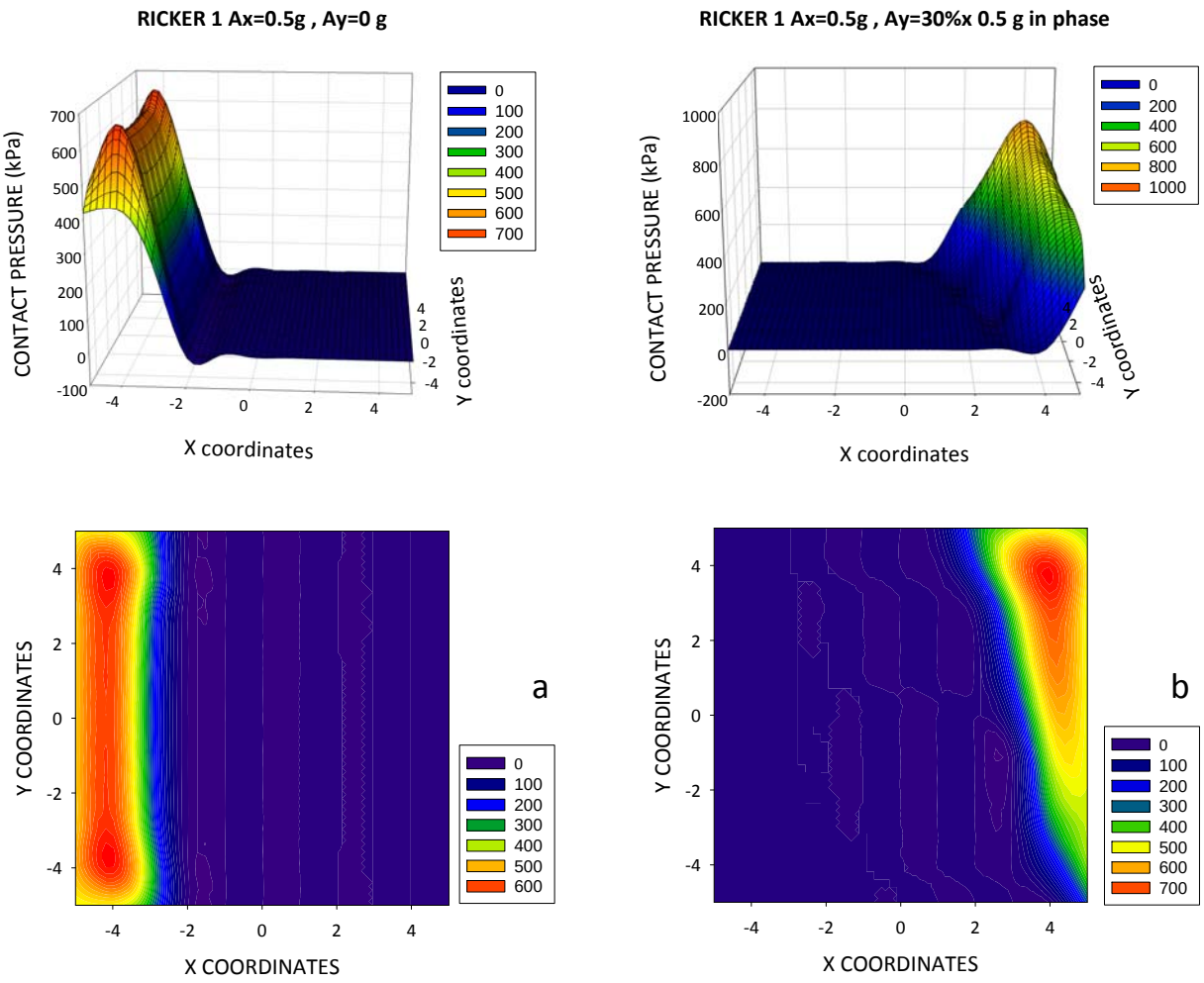

Figure 5.92. Seismic excitation in both directions, Ricker 1 A_x = 0.5 g and A_y =30%x 0.5 g : Distribution of pressures under the footing at the time increment when the maximum uplift occurs for excitation in a) one direction (left) b) both directions (right) .

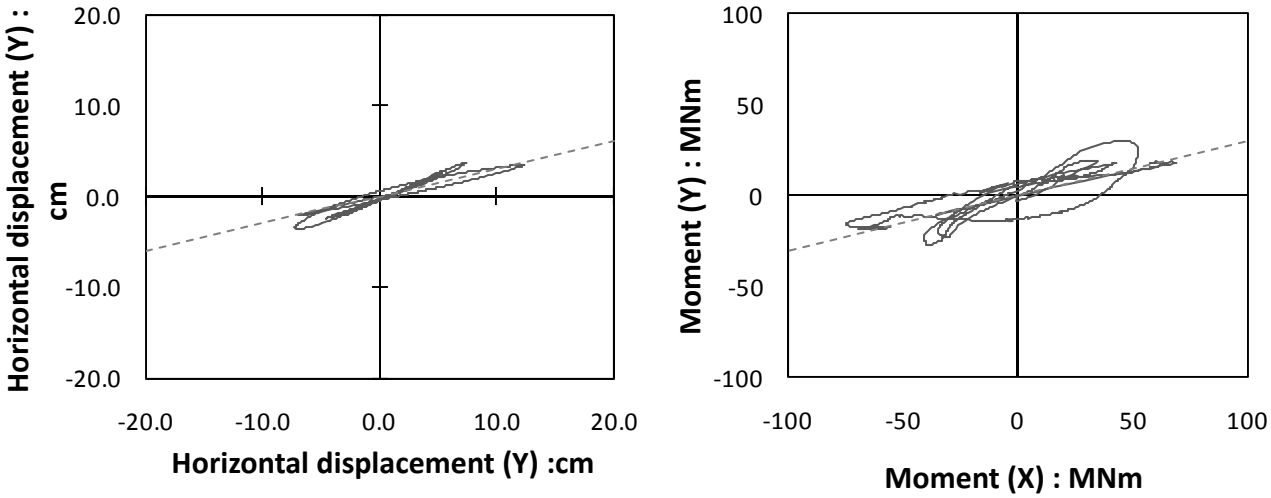

Figure 5.93. **a)** Orbit of center of mass in the X-Y plane.
b) Orbit in the M_X –M_Y plane.

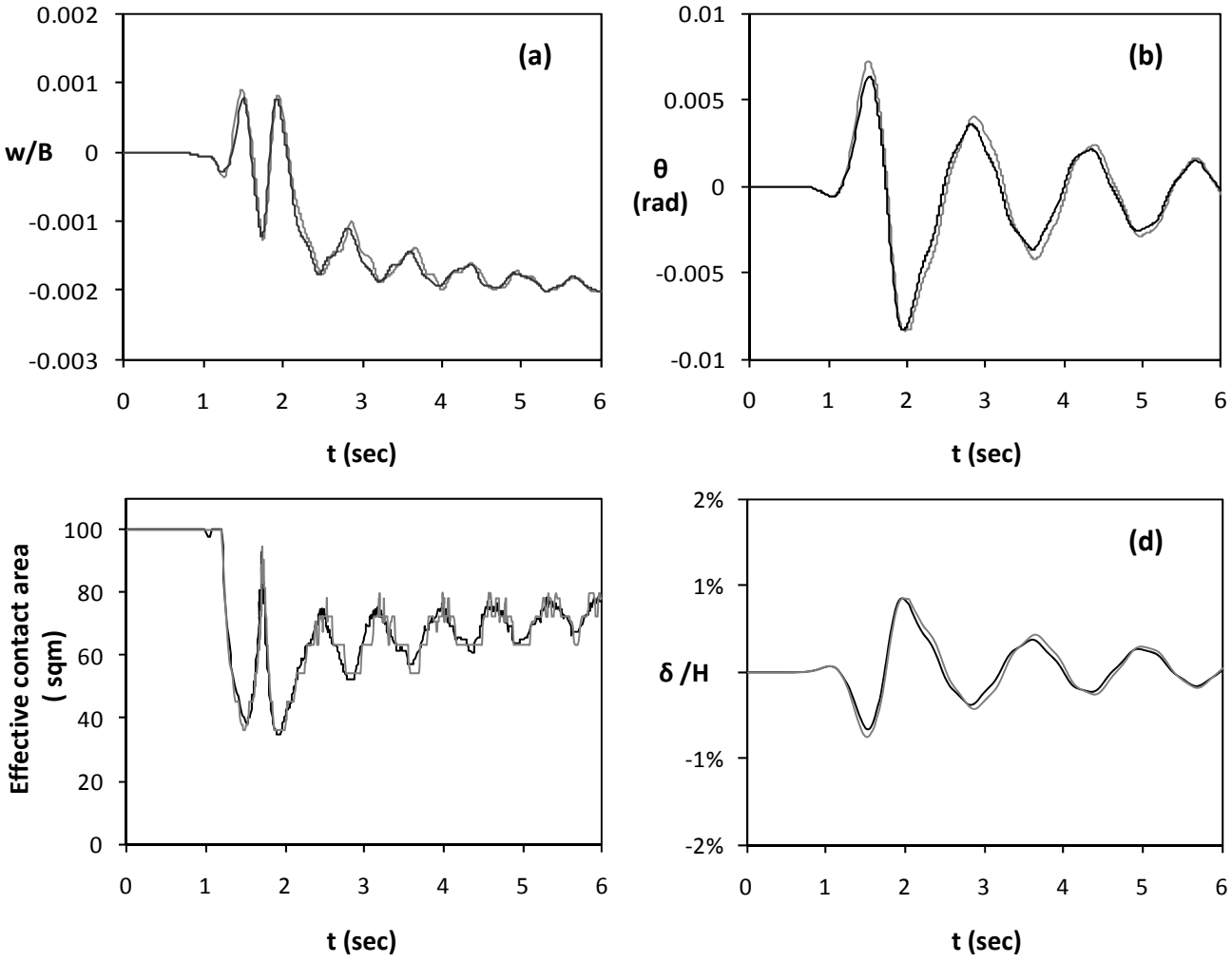

Figure 5.94. Seismic excitation in both directions, Ricker 1 A_x = 0.5 g and A_y = 30% x 0.5 g and comparison with the single direction case.
Time histories of (a) Vertical settlement (b) Rotation ; (c) Effective contact area time ; (d) horizontal displacement normalized to height. (Black line represents excitation in both directions and grey line single direction excitation)

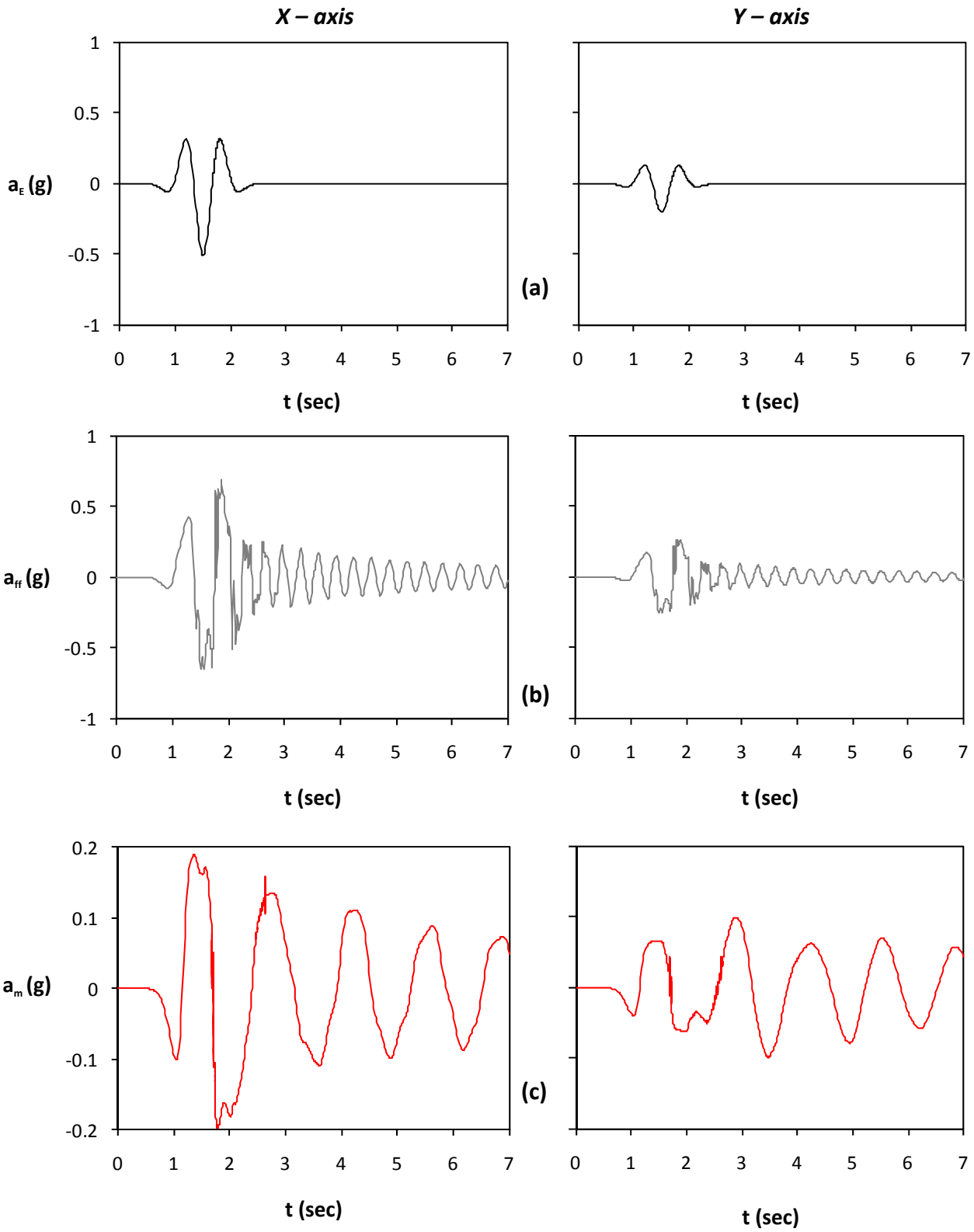

Figure 5.95. Seismic excitation in both directions, Ricker 1 A_x = 0.5 g and A_y =40%x 0.5 g : (a) acceleration time histories of bedrock excitation along the *x* axis (left) and the *y* axis (right) ; (b) acceleration time histories at the free field ; and (c) acceleration time histories of lumped mass.

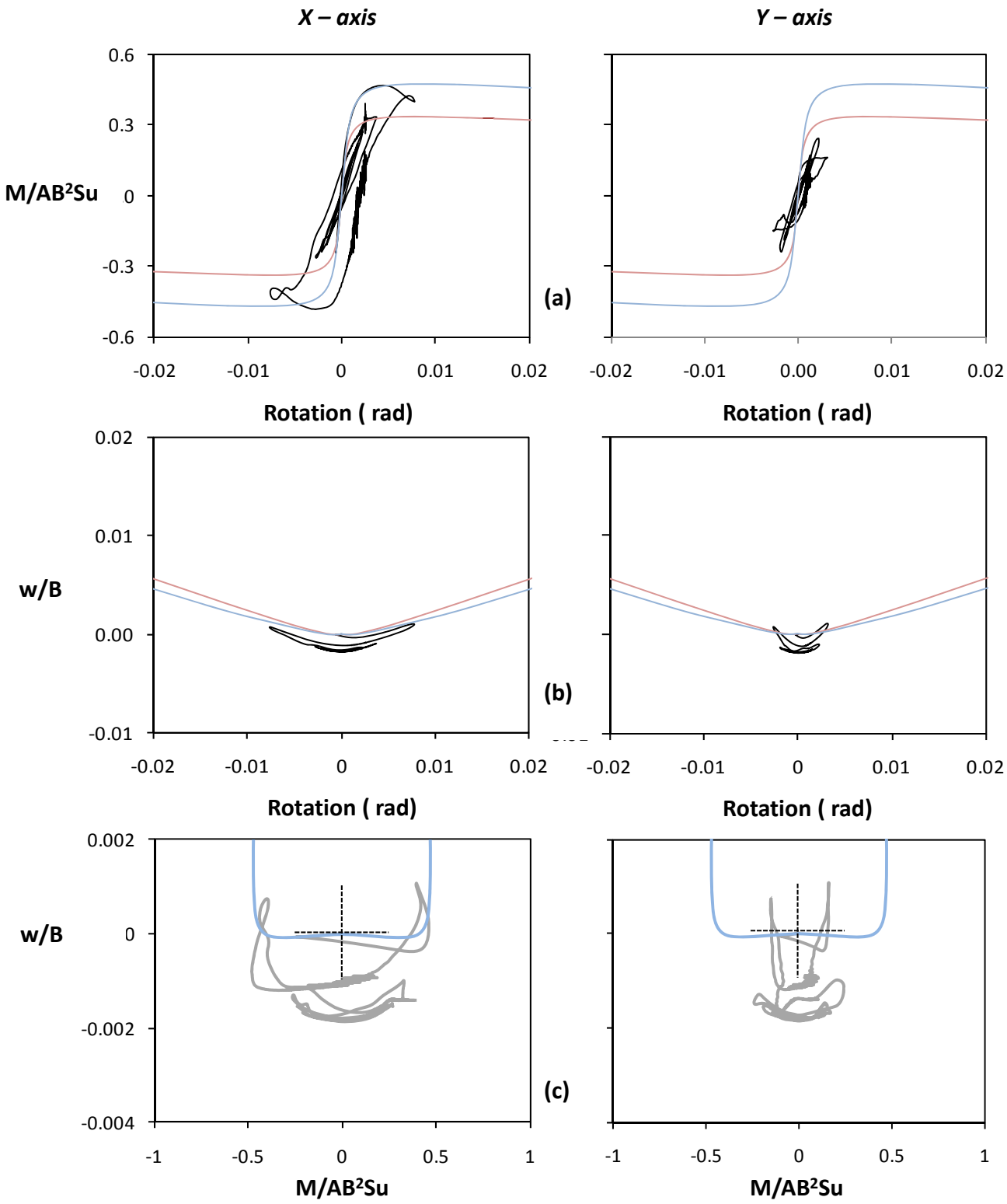

Figure 5.96. Seismic excitation in both directions, A_x = 0.5 g and A_y =40% x 0.5 g :
(a) Normalized moment versus rotation along the *x* axis (left) and the *y* axis (right) ;
(b) Normalized to width vertical settlement versus rotation ; and
(c) Normalized vertical settlement to moment along the *x* axis (left) and the *y* axis (right) .

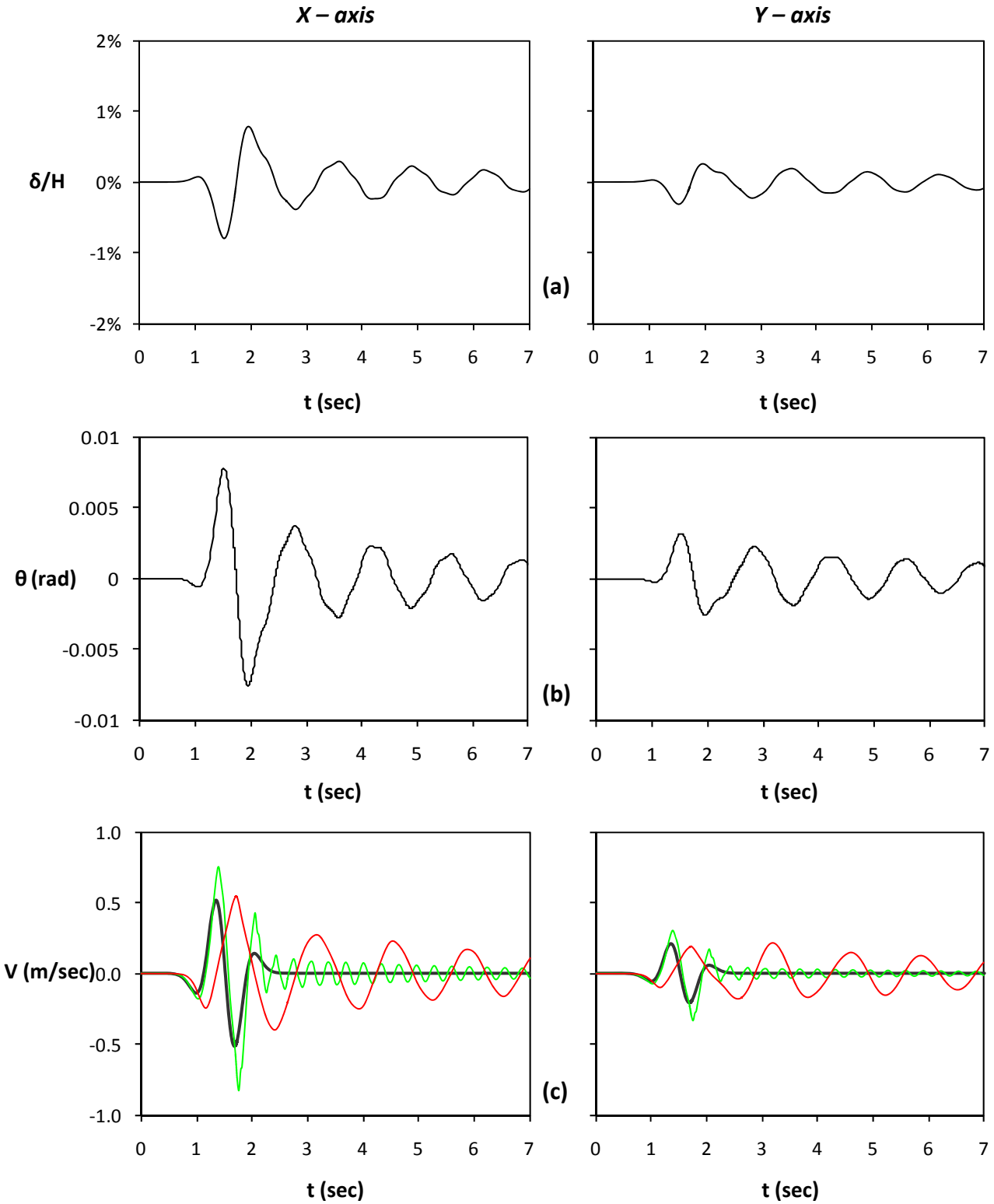

Figure 5.97. Seismic excitation in both directions, A_x = 0.5 g and A_y = 40% x 0.5 g:
(a) Horizontal displacement normalized to height time histories along the *x* axis (left) and the *y* axis (right) ; (b) rotation time histories along the *x* axis (left) and the *y* axis (right) ; (c) velocity time histories (Green line stands for free field motion and red line for lumped mass)

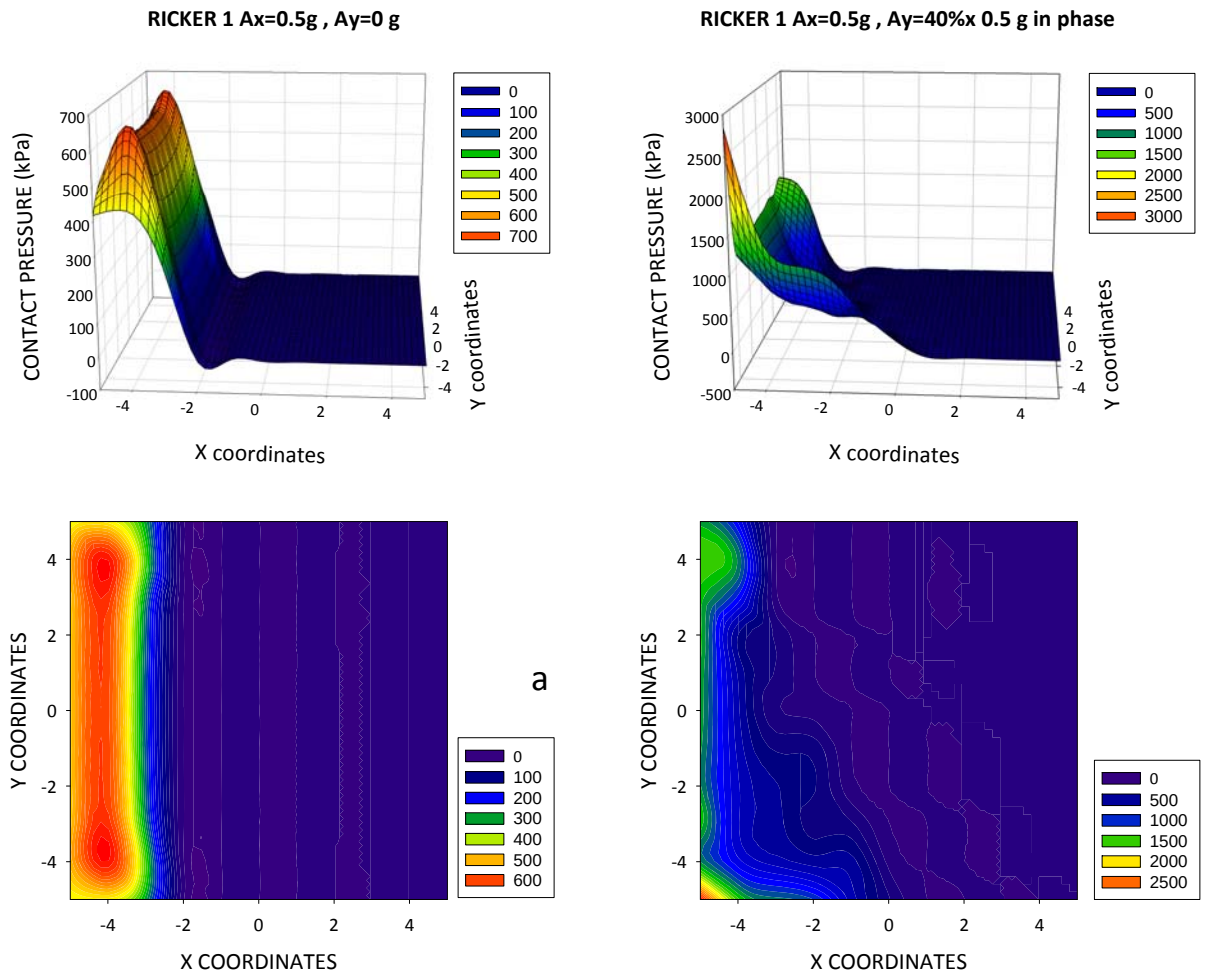

Figure 5.98. Seismic excitation in both directions, Ricker 1 A_x = 0.5 g and A_y =40% x 0.5 g : Distribution of pressures under the footing at the time increment when the maximum uplift occurs for excitation in a) one direction (left) b) both directions (right) .

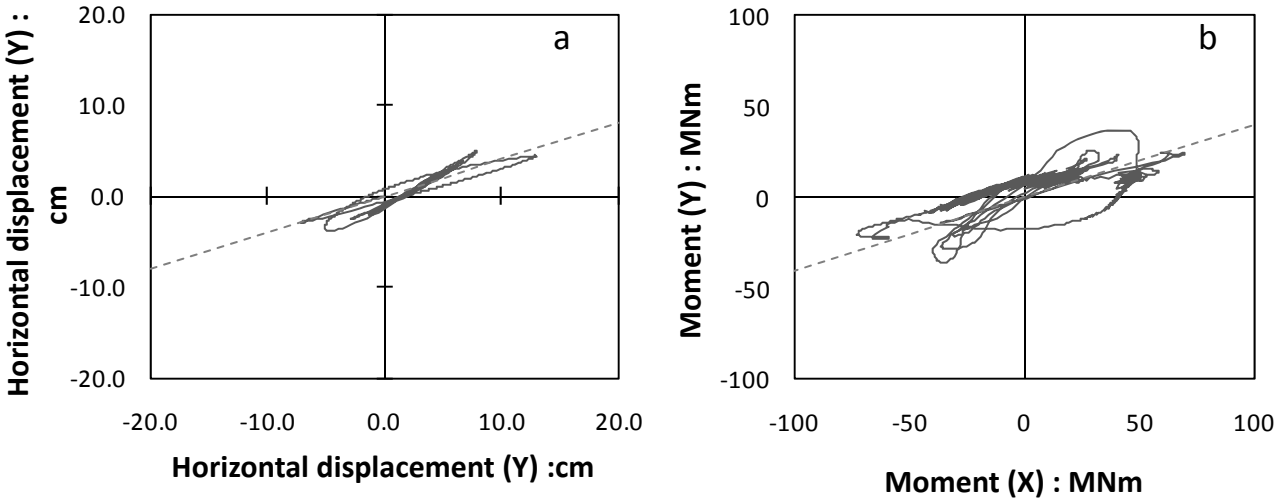

Figure 5.99. **a)** Orbit of center of mass in the X-Y plane.
b) Orbit in the M_X –M_Y plane.

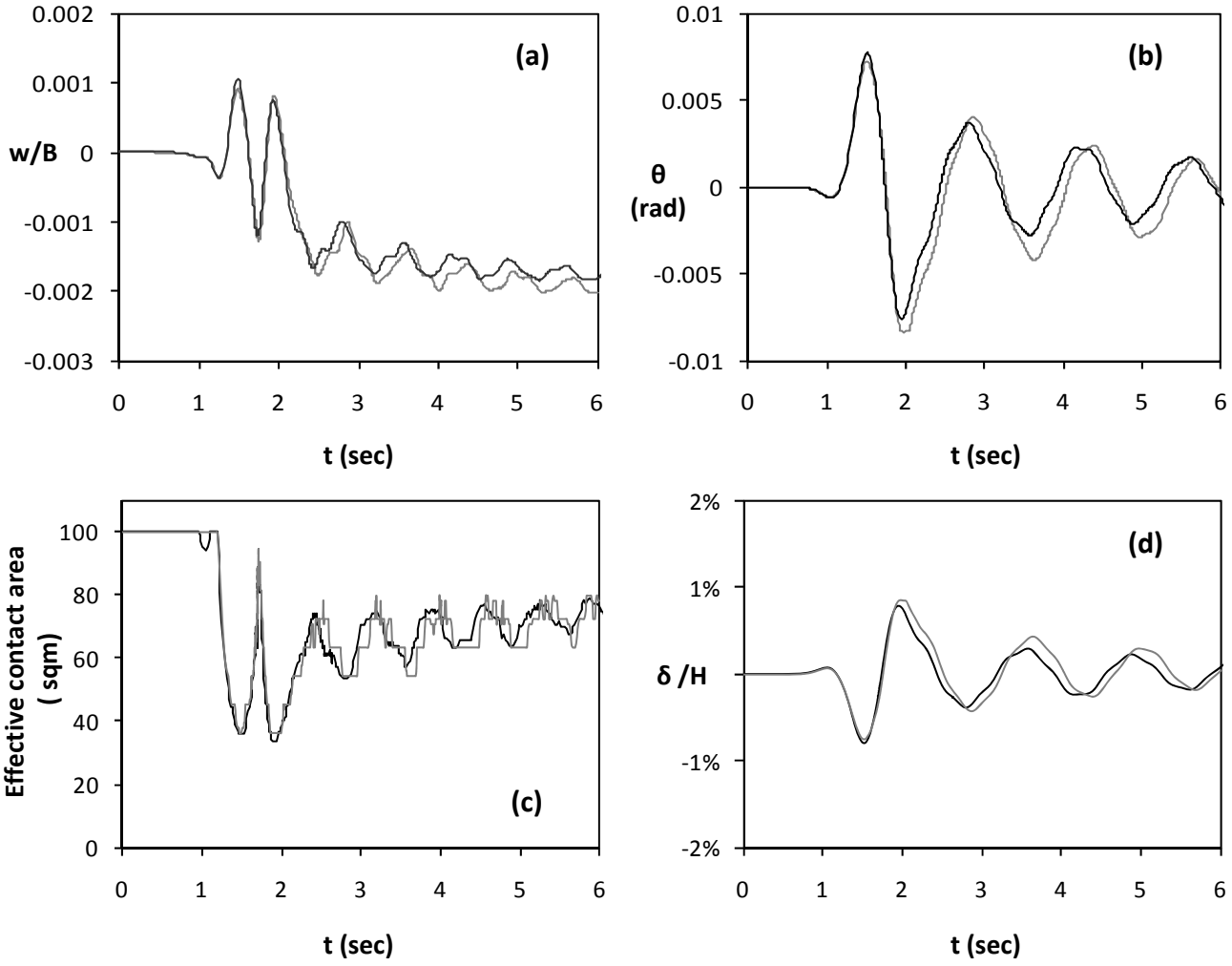

Figure 5.100. Seismic excitation in both directions, Ricker 1 A_x = 0.5 g and A_y = 40% x 0.5 g and comparison with the single direction case.
Time histories of (a) Vertical settlement (b) Rotation ; (c) Effective contact area time ; (d) horizontal displacement normalized to height. (Black line represents excitation in both directions and grey line single direction excitation)

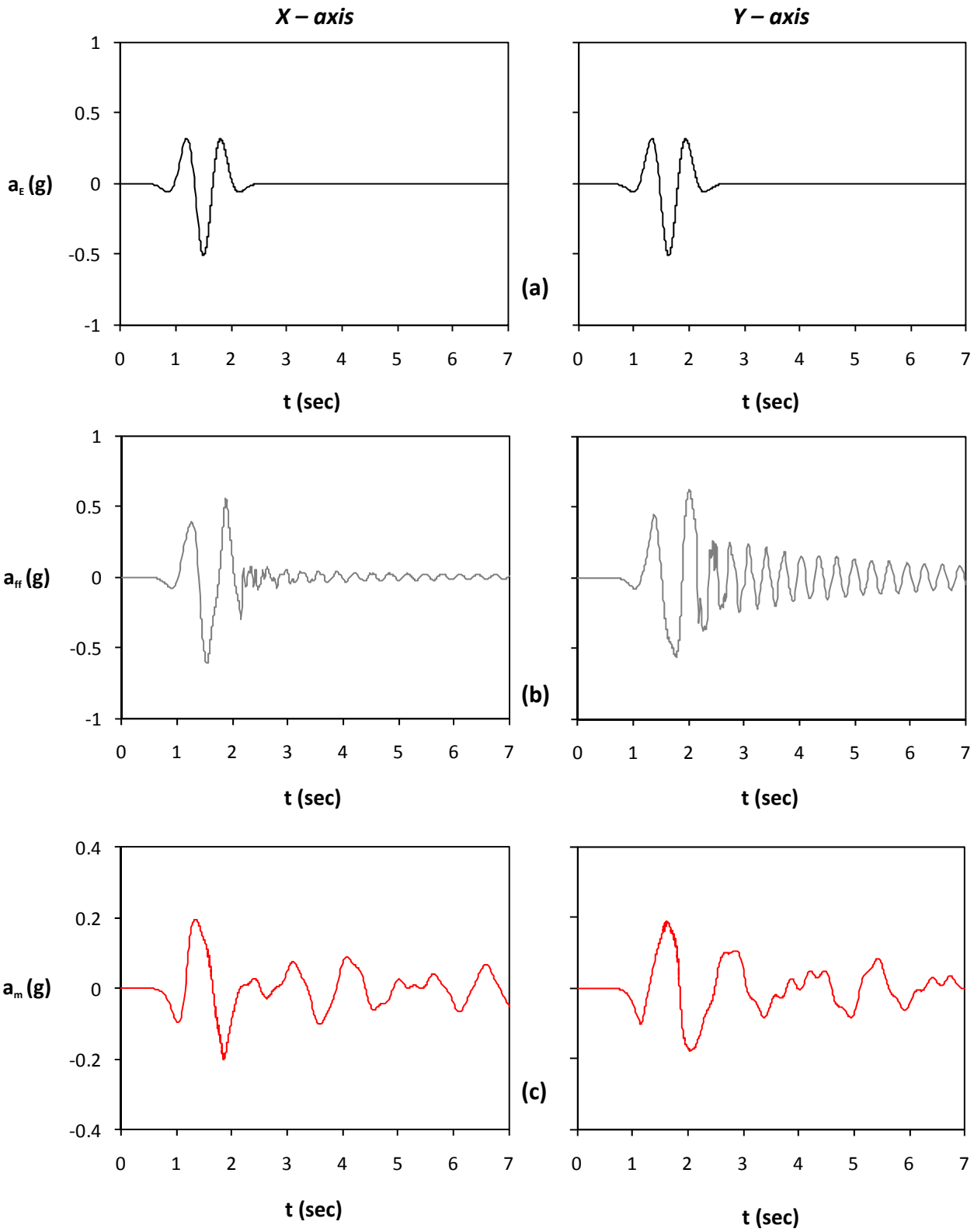

Figure 5.101. Seismic excitation in both directions, Ricker 1 A_x = 0.5 g and A_y = 0.5 g asynchronous : (a) acceleration time histories of bedrock excitation along the *x* axis (left) and the *y* axis (right) ; (b) acceleration time histories at the free field ; and (c) acceleration time histories of lumped mass.

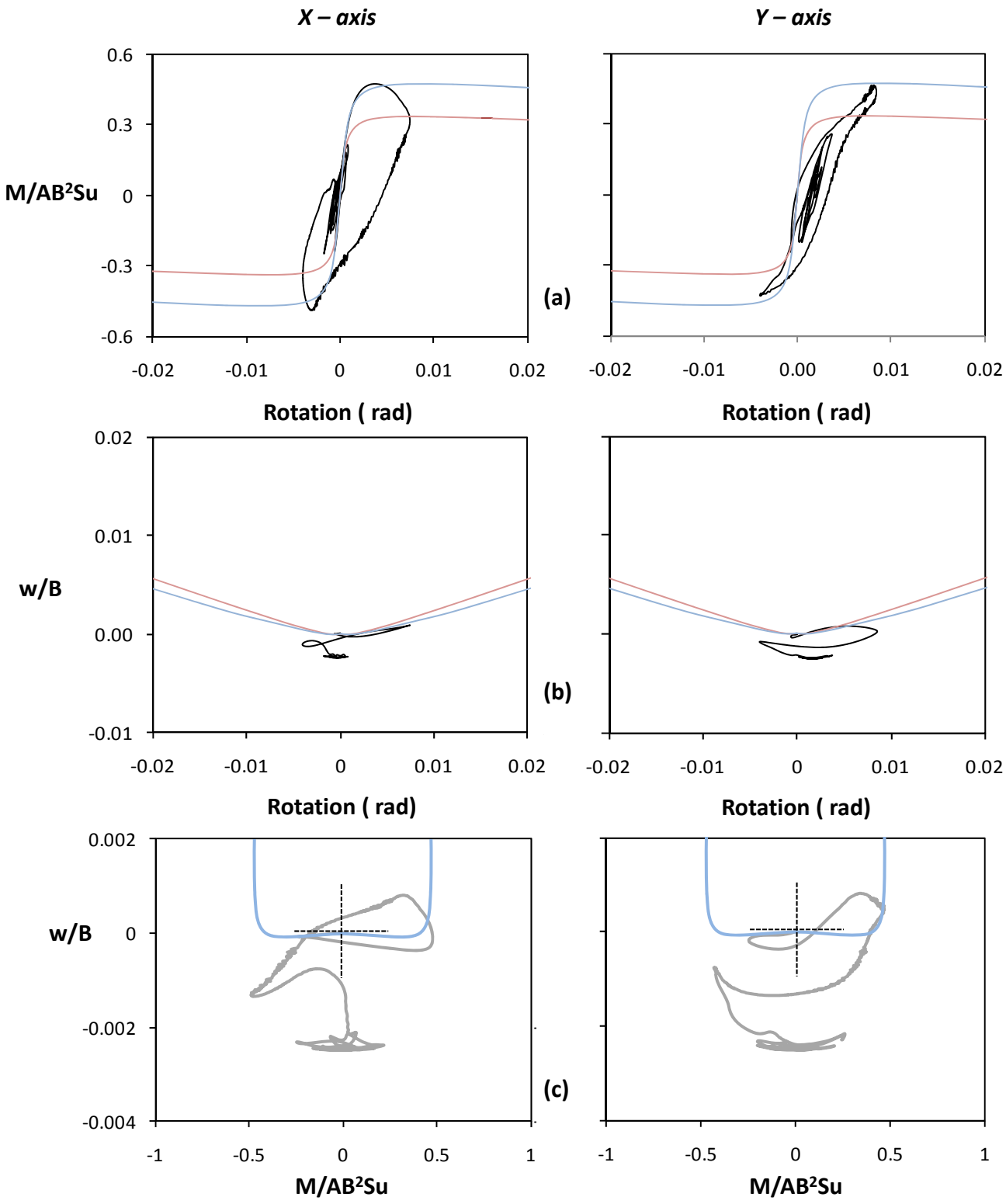

Figure 5.102. Seismic excitation in both directions, A_x = 0.5 g and A_y = 0.5 g asynchronous :
(a) Normalized moment versus rotation along the *x* axis (left) and the *y* axis (right) ;
(b) Normalized to width vertical settlement versus rotation ; and
(c) Normalized vertical settlement to moment along the *x* axis (left) and the *y* axis (right) .

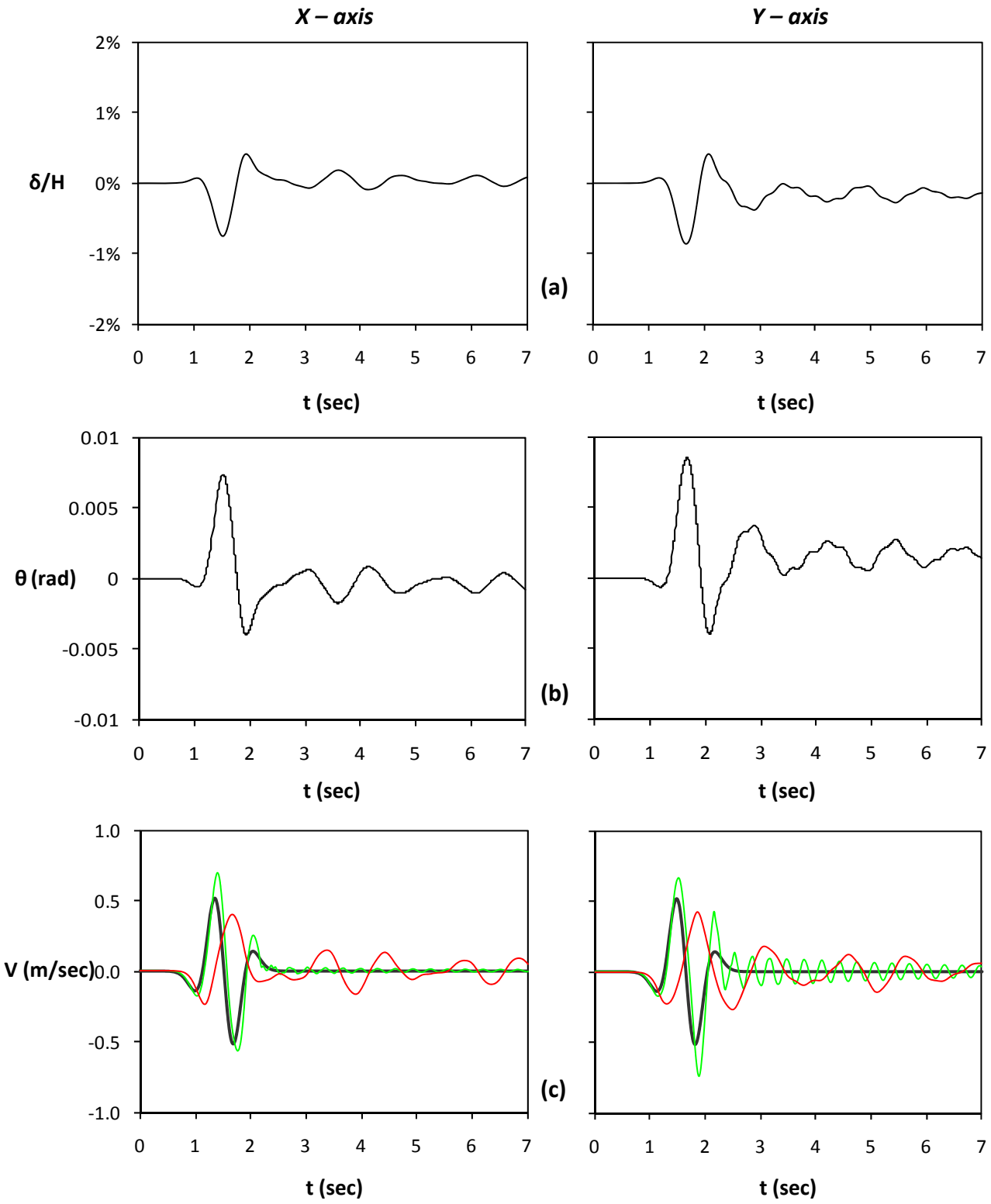

Figure 5.103. Seismic excitation in both directions, A_x = 0.5 g and A_y = 0.5 g asynchronous : (a)Horizontal displacement normalized to height time histories along the *x* axis (left) and the *y* axis (right) ; (b) rotation time histories along the *x* axis (left) and the *y* axis (right) ; (c) velocity time histories (Green line stands for free field motion and red line for lumped mass)

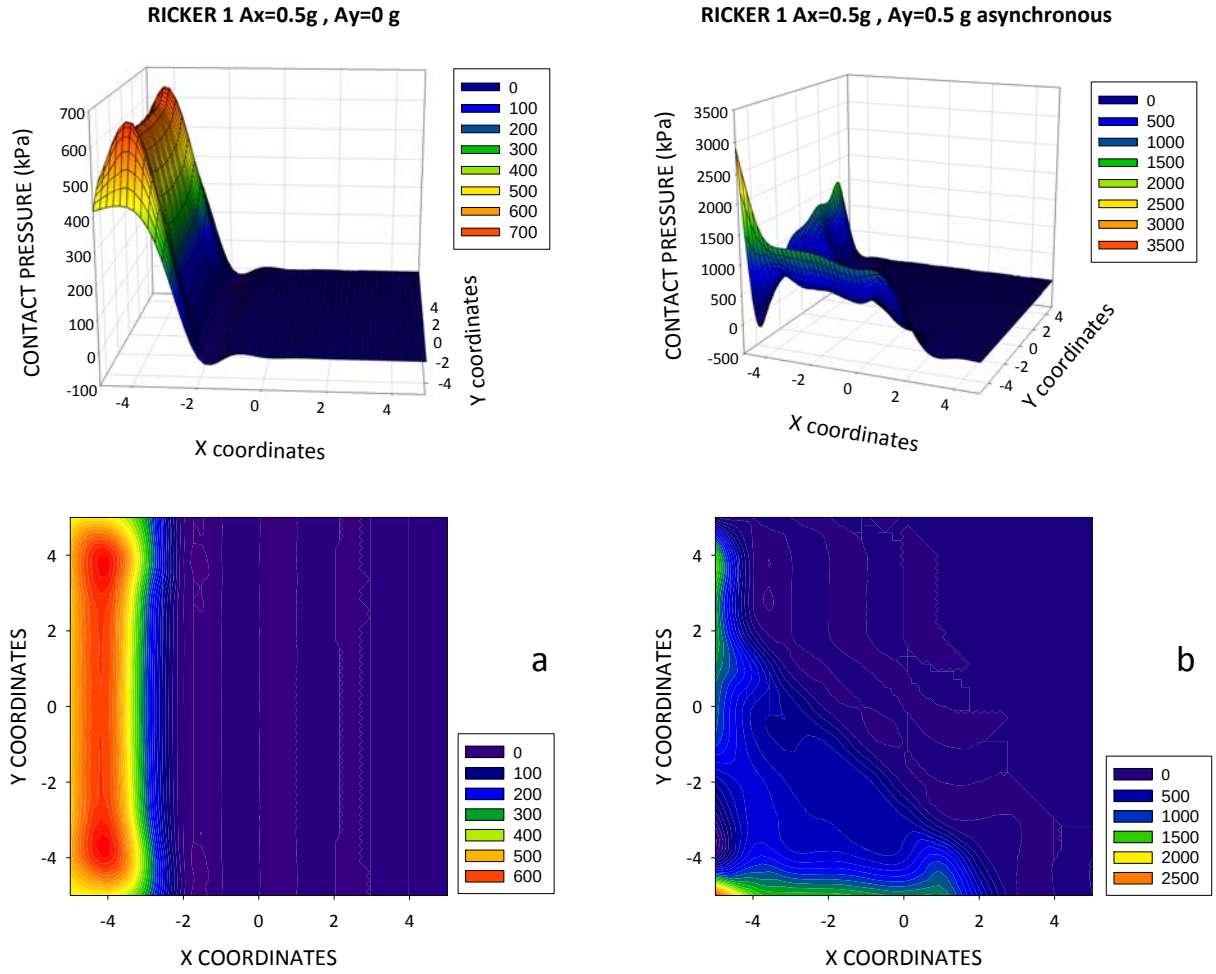

Figure 5.104. Seismic excitation in both directions, Ricker 1 A_x = 0.5 g and A_y = 0.5 g asynchronous : Distribution of pressures under the footing at the time increment when the maximum uplift occurs for excitation in a) one direction (left) b) both directions (right) .

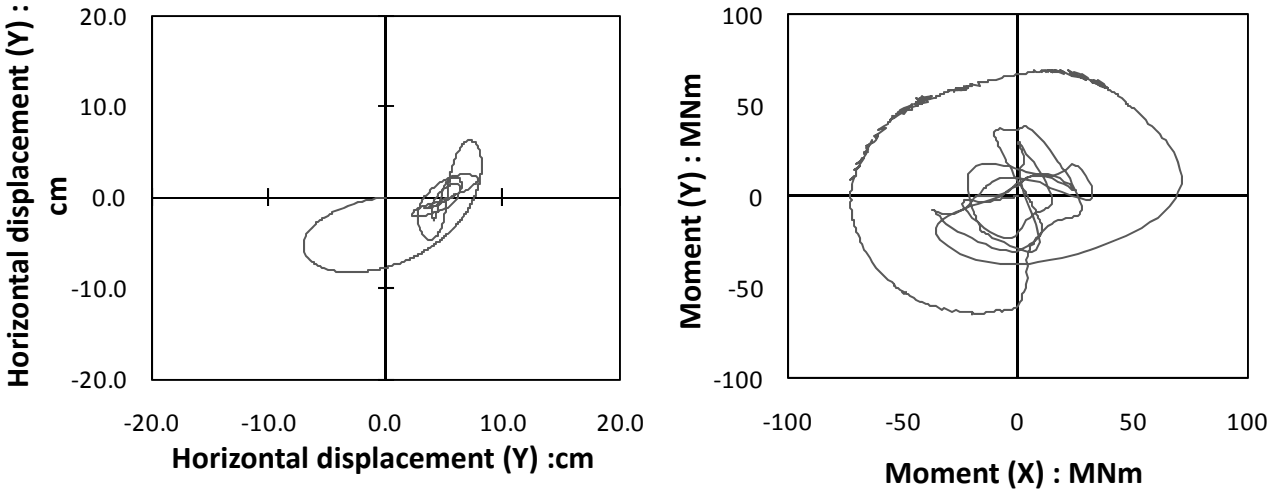

Figure 5.105. **a)** Orbit of center of mass in the X-Y plane.
b) Orbit in the M_X –M_Y plane.

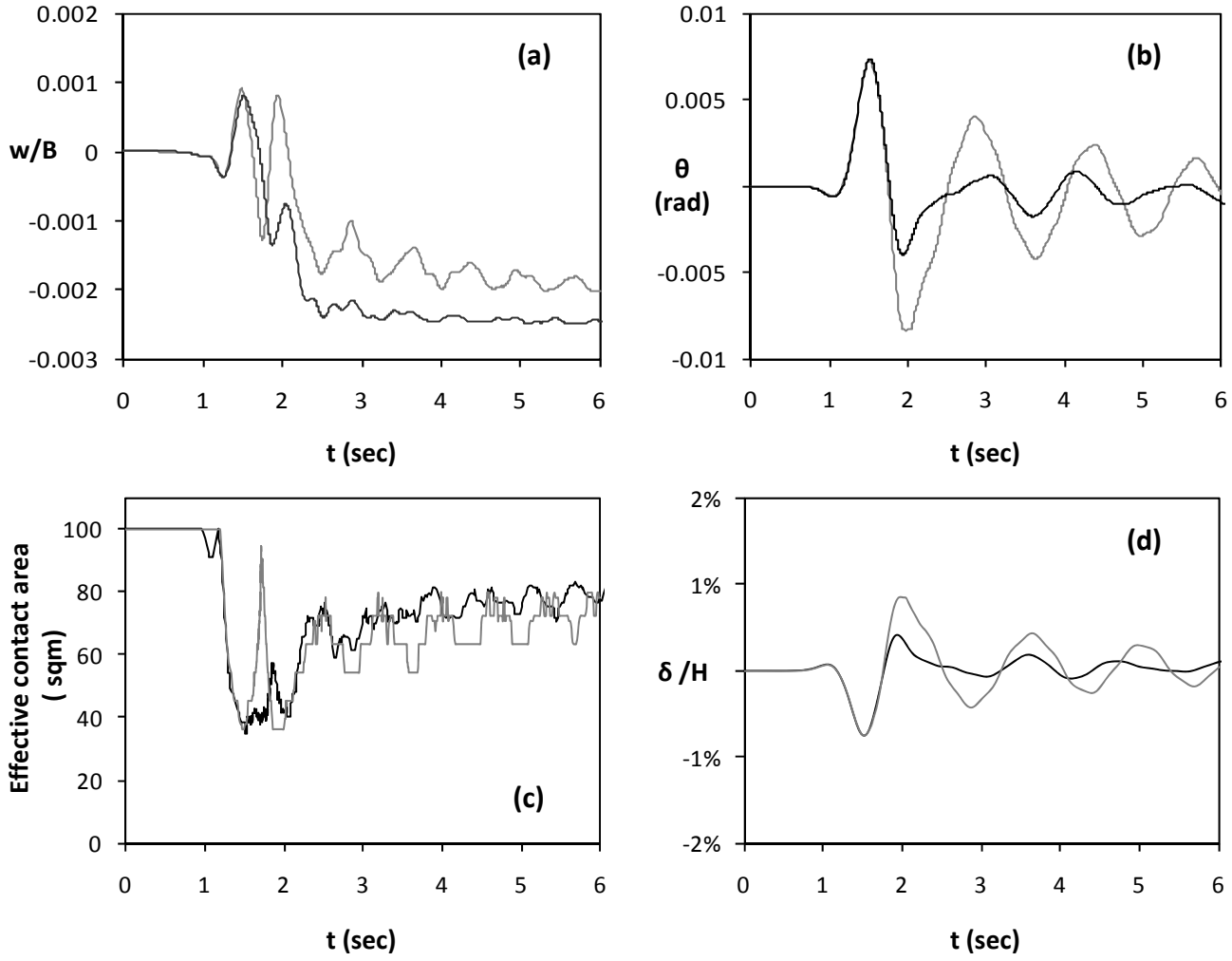

Figure 5.106. Seismic excitation in both directions, Ricker 1 A_x = 0.5 g and A_y = 0.5 g asynchronous and comparison with the single direction case.
Time histories of (a) Vertical settlement (b) Rotation ; (c) Effective contact area time ; (d) horizontal displacement normalized to height. (Black line represents excitation in both directions and grey line single direction excitation)

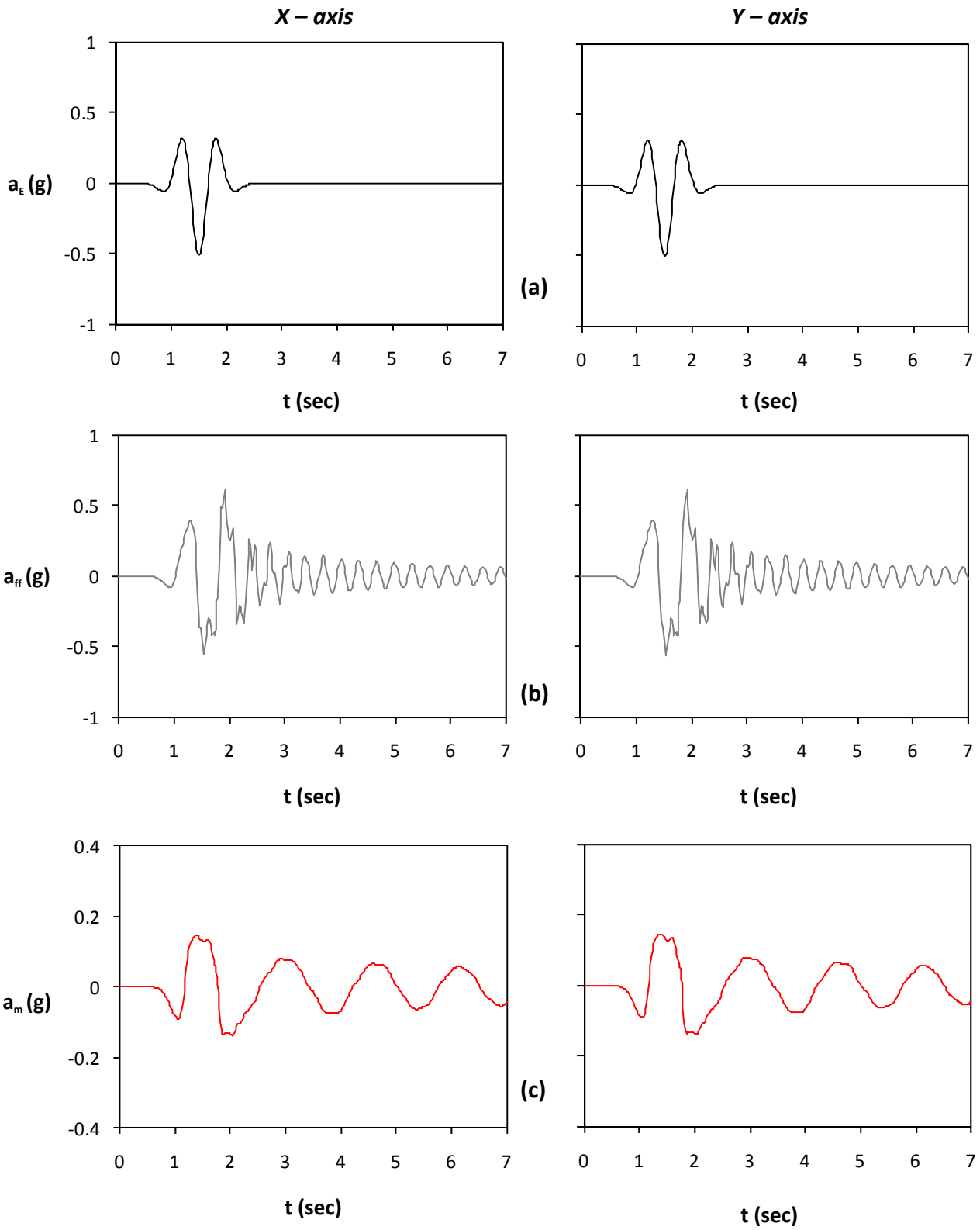

Figure 5.107. Seismic excitation in both directions, Ricker 1 A_x = 0.5 g and A_y = 0.5 g asynchronous : (a) acceleration time histories of bedrock excitation along the *x* axis (left) and the *y* axis (right) ; (b) acceleration time histories at the free field ; and (c) acceleration time histories of lumped mass.

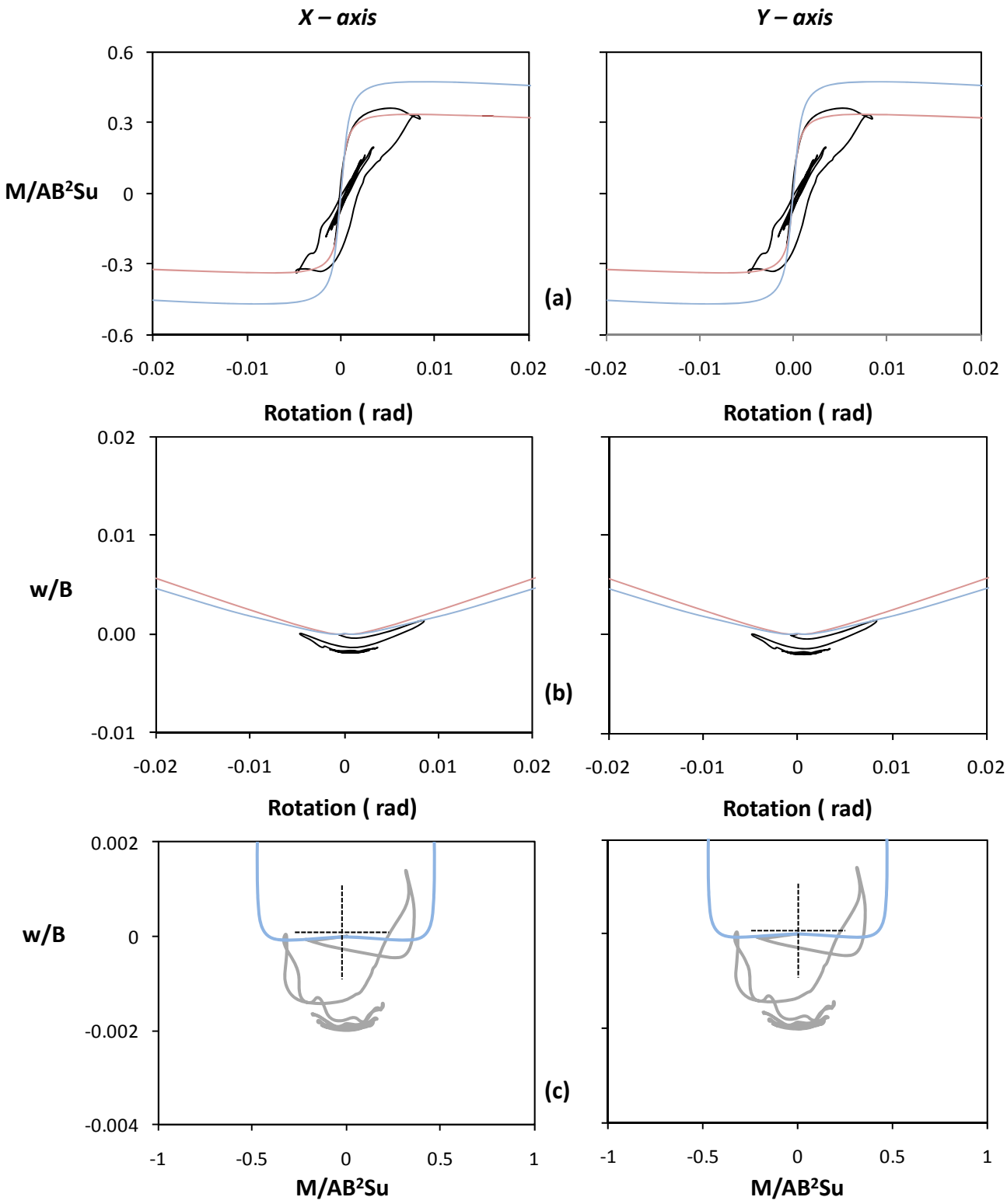

Figure 5.108. Seismic excitation in both directions, A_x = 0.5 g and A_y = 0.5 g asynchronous :
(a) Normalized moment versus rotation along the *x* axis (left) and the *y* axis (right) ;
(b) Normalized to width vertical settlement versus rotation ; and
(c) Normalized vertical settlement to moment along the *x* axis (left) and the *y* axis (right) .

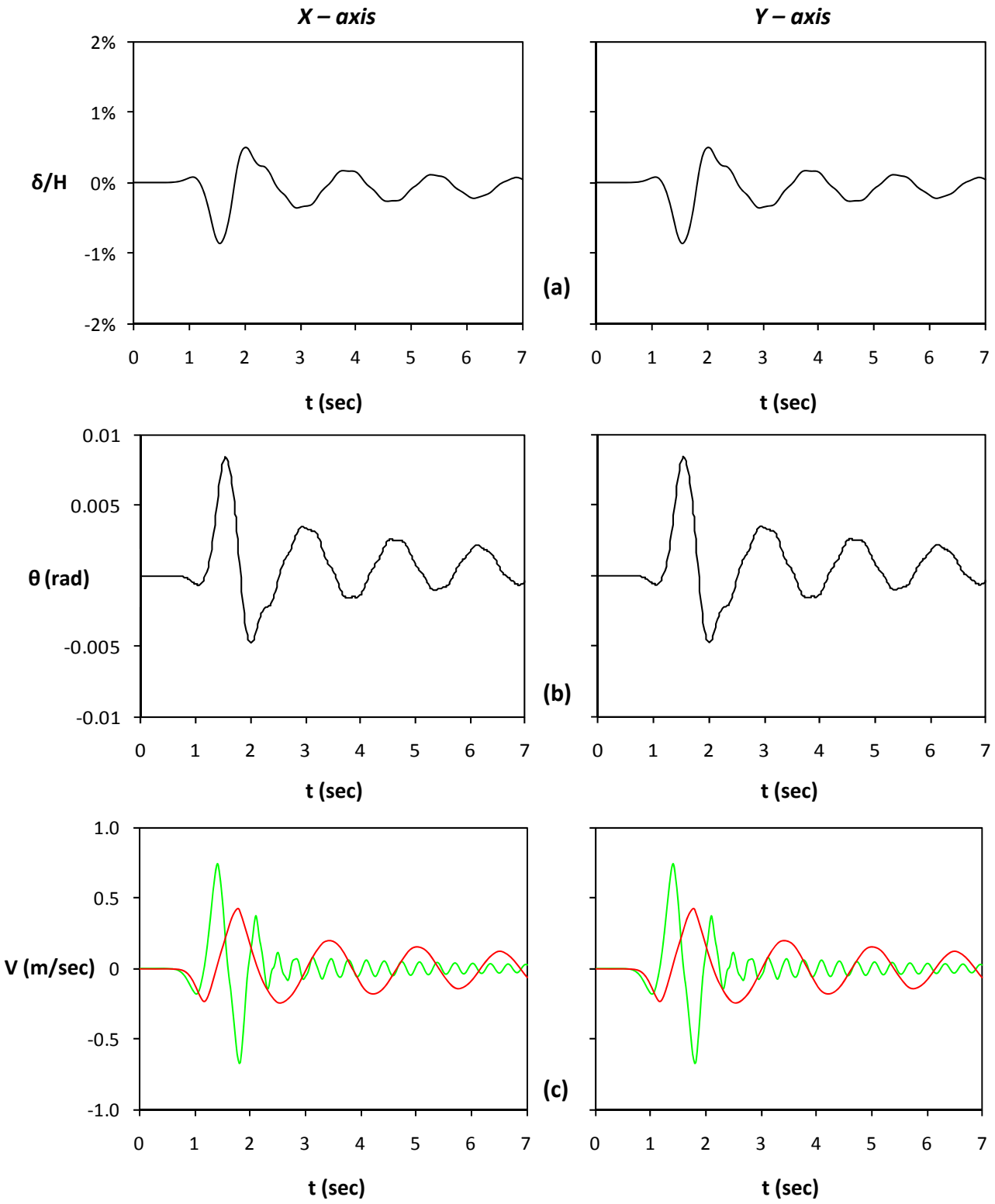

Figure 5.109. Seismic excitation in both directions, A_x = 0.5 g and A_y = 0.5 g asynchronous : (a)Horizontal displacement normalized to height time histories along the *x* axis (left) and the *y* axis (right) ; (b) rotation time histories along the *x* axis (left) and the *y* axis (right) ; (c) velocity time histories (Green line stands for free field motion and red line for lumped mass)

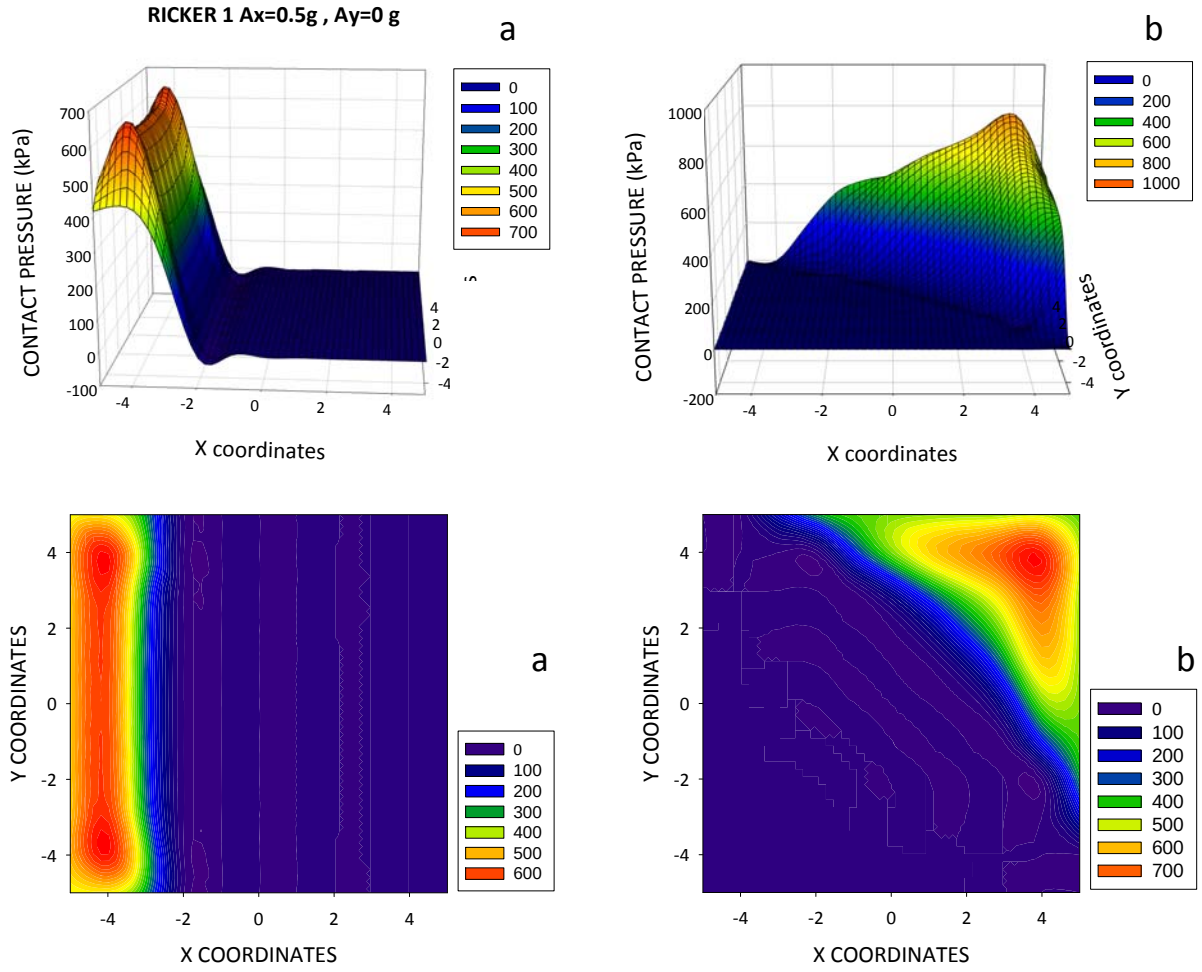

Figure 5.110. Seismic excitation in both directions, Ricker 1 A_x = 0.5 g and A_y = 0.5 g asynchronous : Distribution of pressures under the footing at the time increment when the maximum uplift occurs for excitation in a) one direction (left) b) both directions (right) .

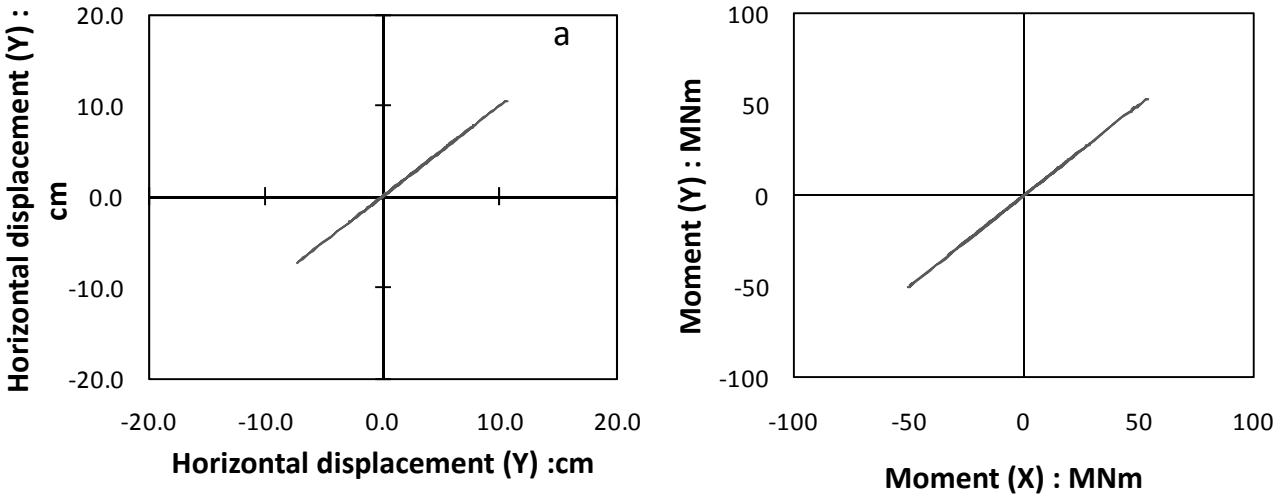

Figure 5.111. a) Orbit of center of mass in the X-Y plane.
b) Orbit in the M_X –M_Y plane.

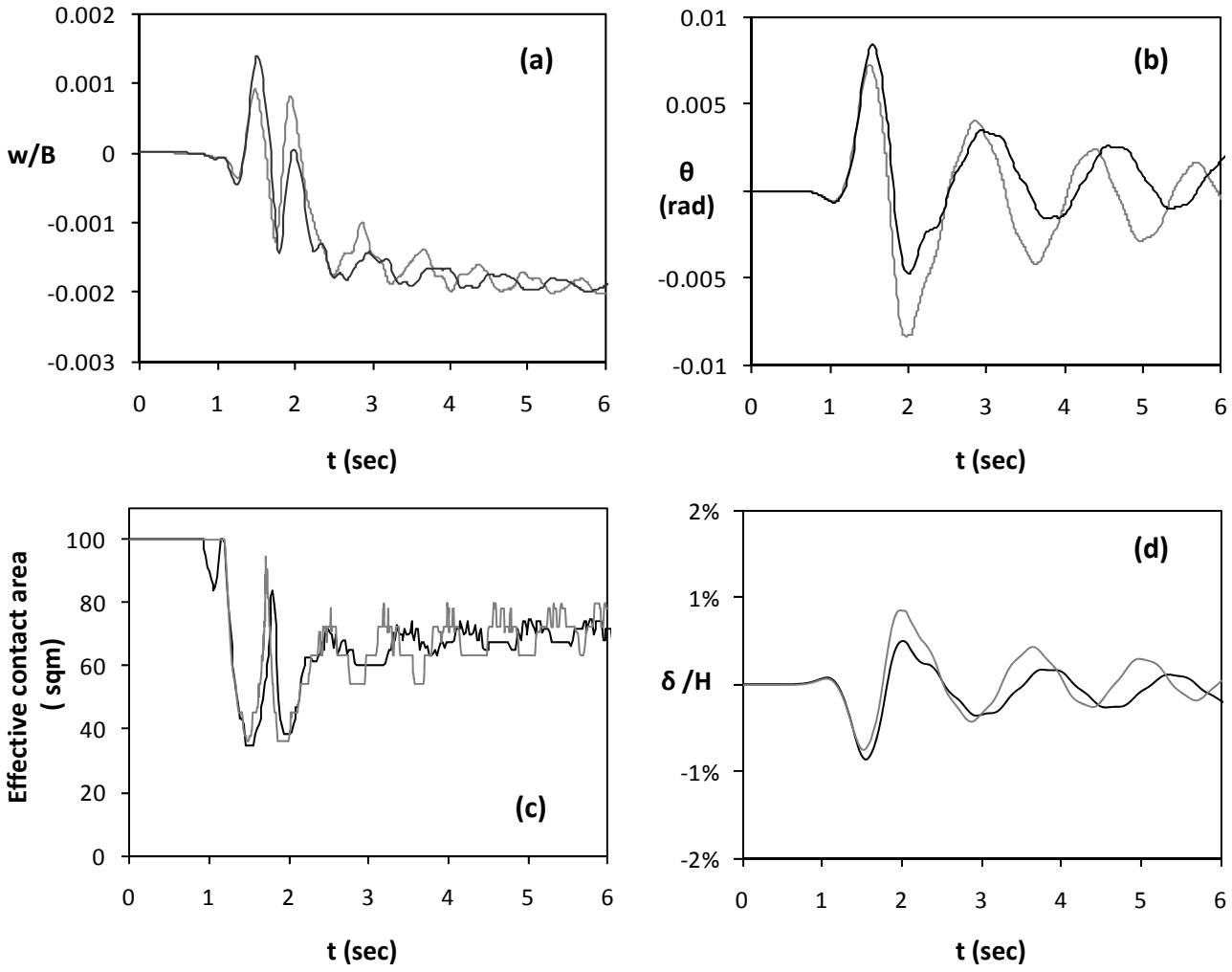

Figure 5.112. Seismic excitation in both directions, A_x = 0.5 g and A_y = 0.5 g asynchronous and comparison with the single direction case.
Time histories of (a) Vertical settlement (b) Rotation ; (c) Effective contact area time ; (d) horizontal displacement normalized to height. (Black line represents excitation in both directions and grey line single direction excitation)

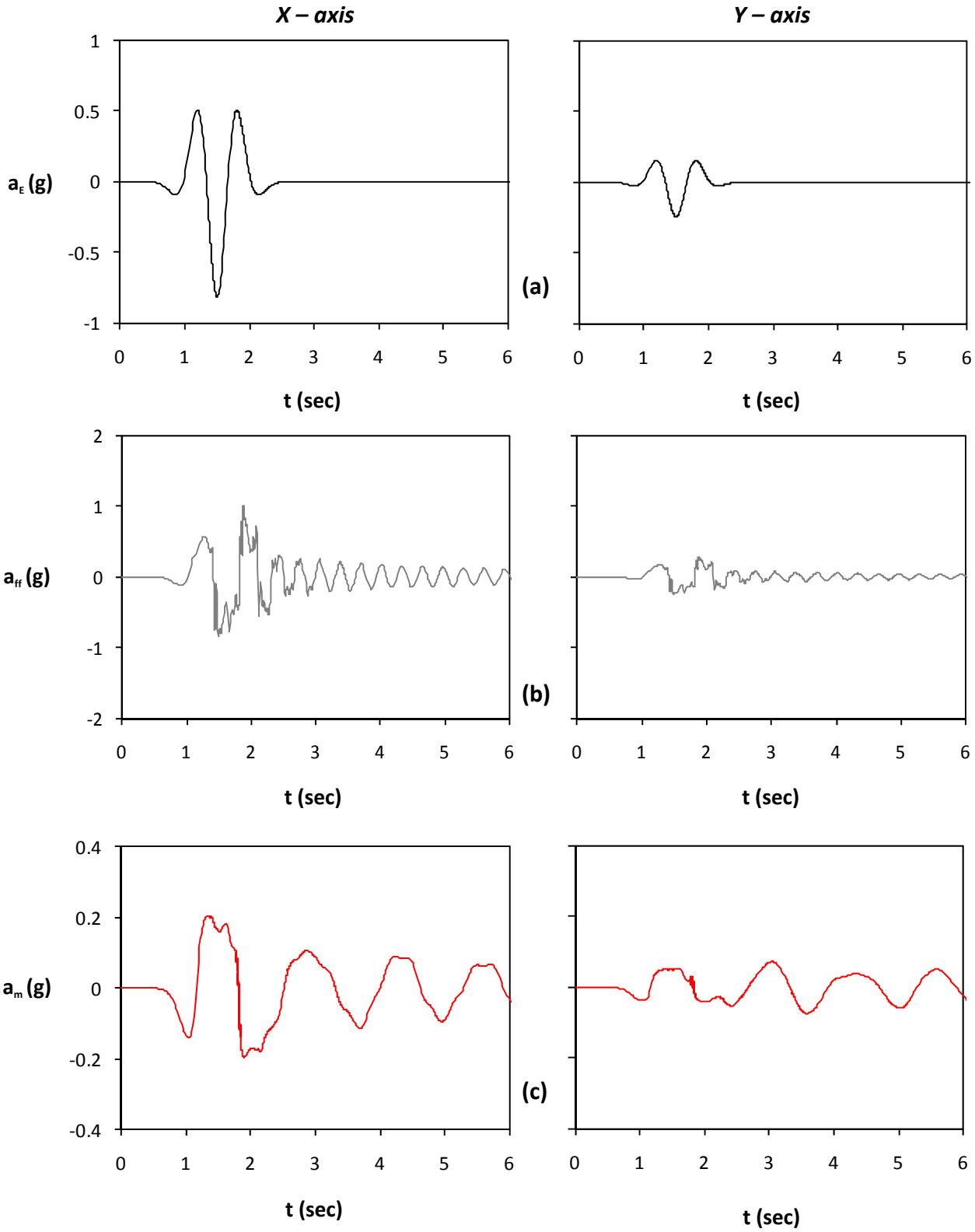

Figure 5.113. Seismic excitation in both directions, Ricker 1 A_x = 0.8 g and A_y =30% x 0.8 g: (a) acceleration time histories of bedrock excitation along the *x* axis (left) and the *y* axis (right) ; (b) acceleration time histories at the free field ; and (c) acceleration time histories of lumped mass.

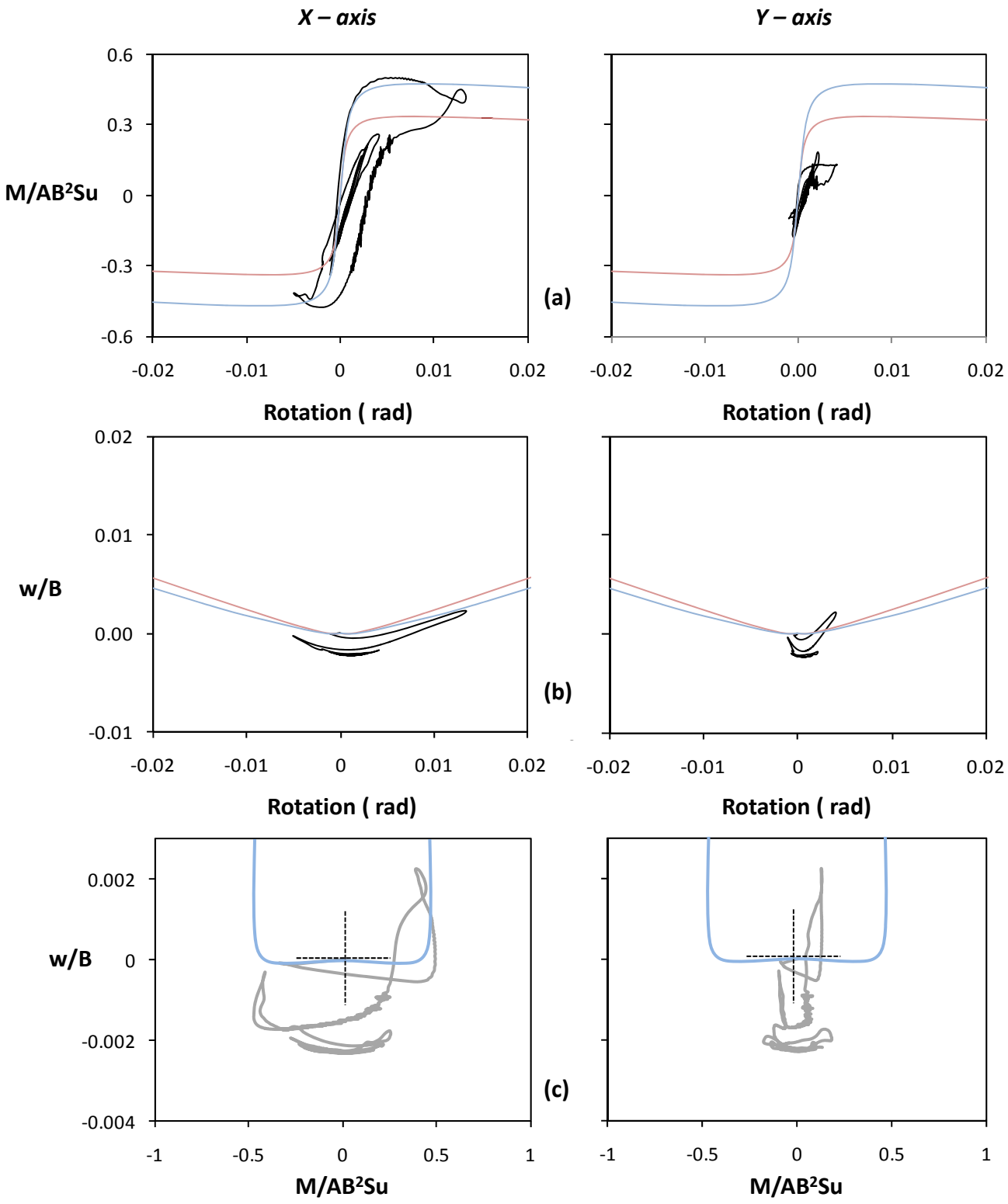

Figure 5.114. Seismic excitation in both directions, A_x = 0.8 g and A_y =30% x 0.8 g :
(a) Normalized moment versus rotation along the *x* axis (left) and the *y* axis (right) ;
(b) Normalized to width vertical settlement versus rotation ; and
(c) Normalized vertical settlement to moment along the *x* axis (left) and the *y* axis (right) .

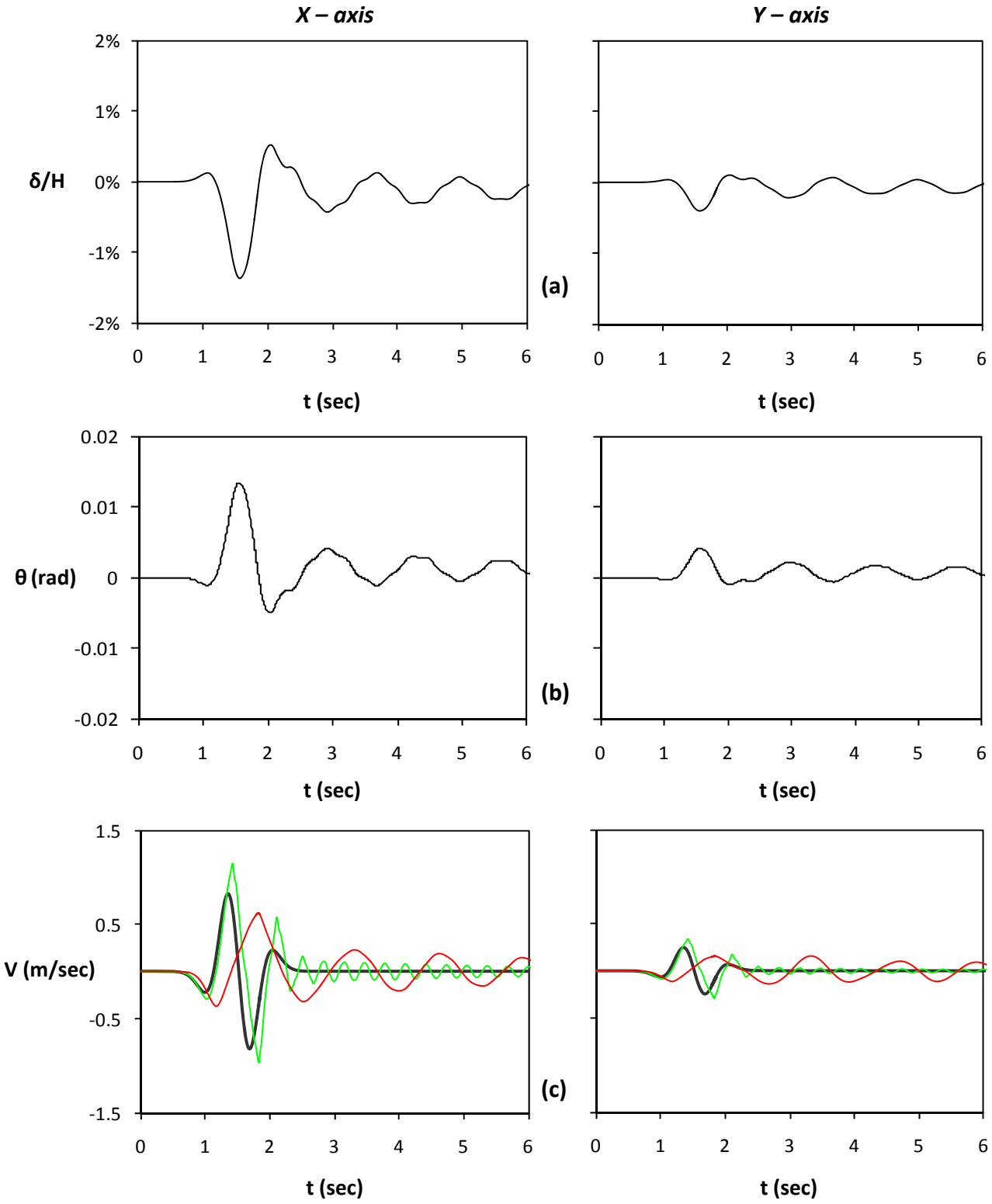

Figure 5.115. Seismic excitation in both directions, A_x = 0.8 g and A_y =30% x 0.8 g : (a) Horizontal displacement normalized to height time histories along the *x* axis (left) and the *y* axis (right) ; (b) rotation time histories along the *x* axis (left) and the *y* axis (right) ; (c) velocity time histories (Green line stands for free field motion and red line for lumped mass)

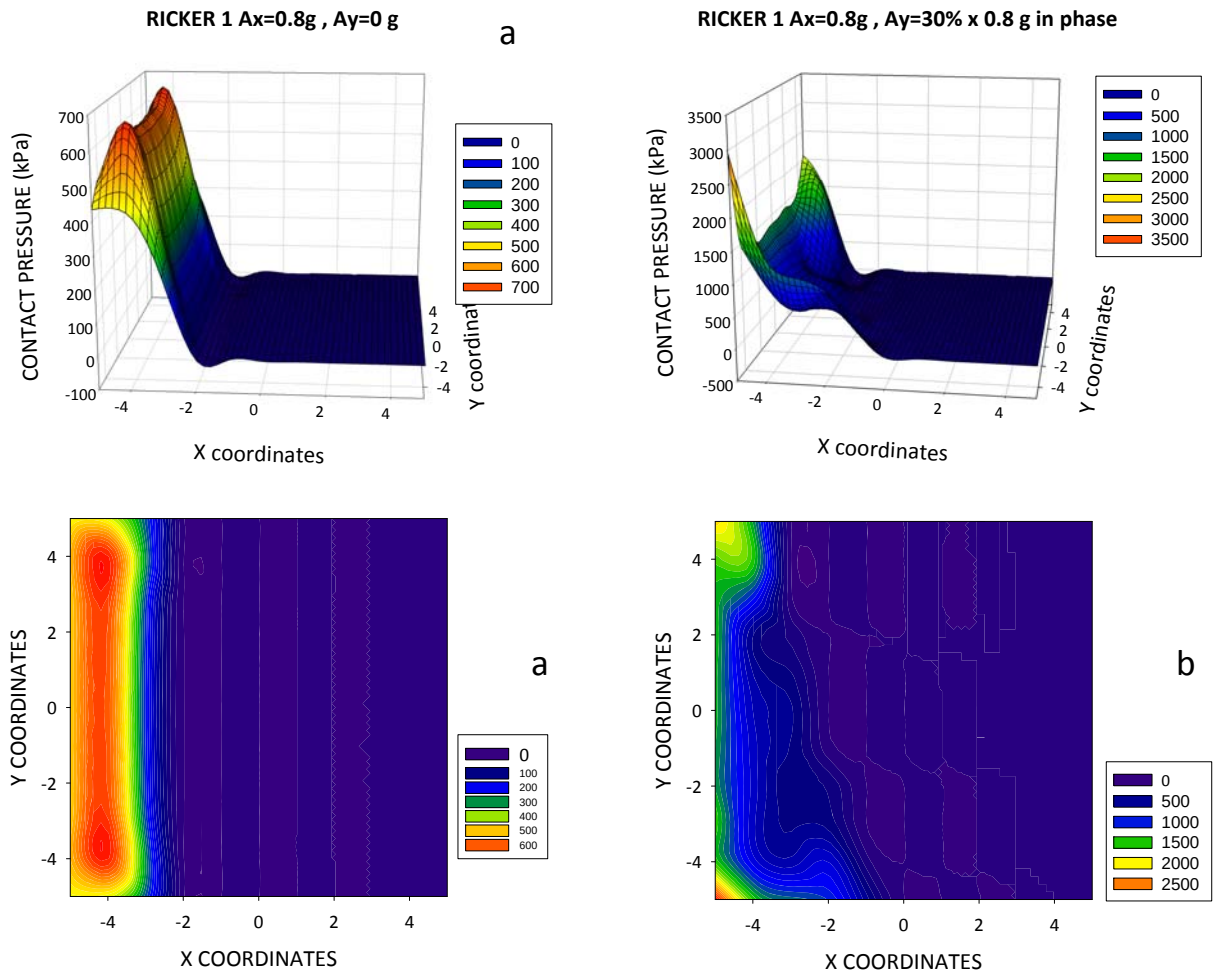

Figure 5.116. Seismic excitation in both directions, Ricker 1 A_x = 0.8 g and A_y =30% x 0.8 g : Distribution of pressures under the footing at the time increment when the maximum uplift occurs for excitation in a) one direction (left) b) both directions (right) .

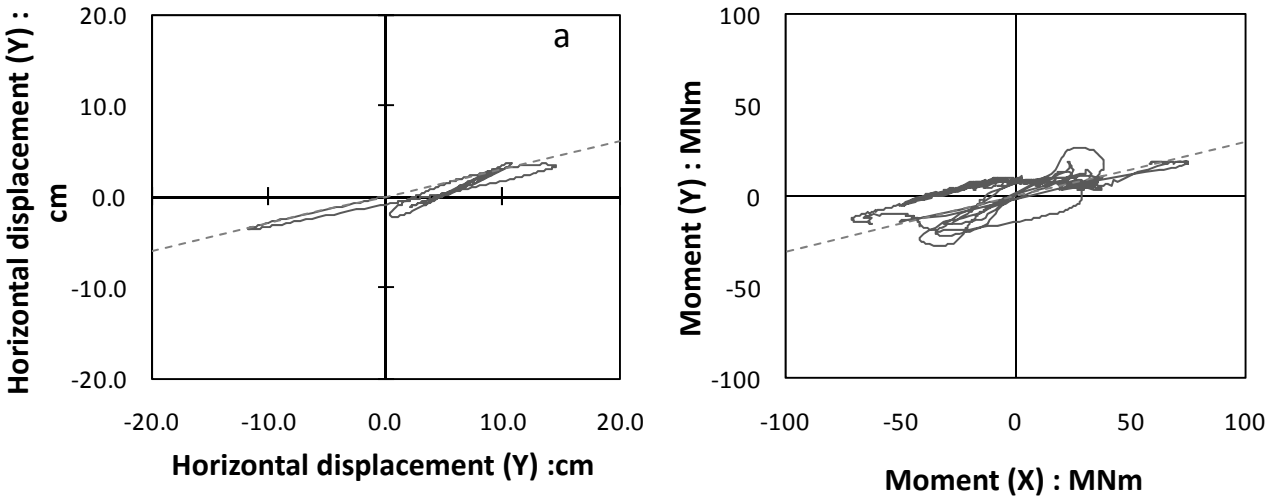

Figure 5.117. a) Orbit of center of mass in the X-Y plane.
b) Orbit in the M_X –M_Y plane.

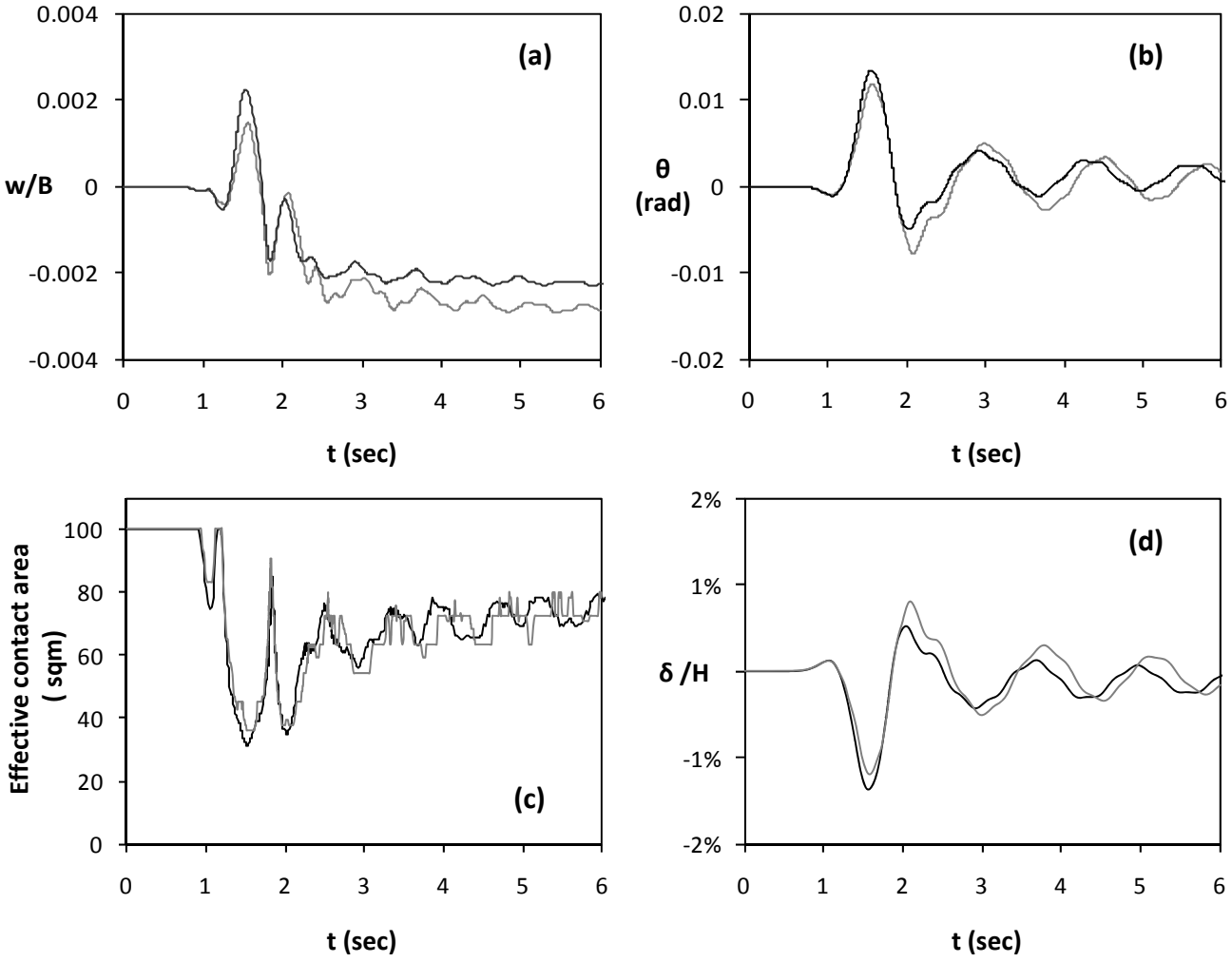

Figure 5.118. Seismic excitation in both directions, Ricker 1 A_x = 0.8 g and A_y = 30% x 0.8 g and comparison with the single direction case.
Time histories of (a) Vertical settlement (b) Rotation ; (c) Effective contact area time ; (d) horizontal displacement normalized to height. (Black line represents excitation in both directions and grey line single direction excitation)

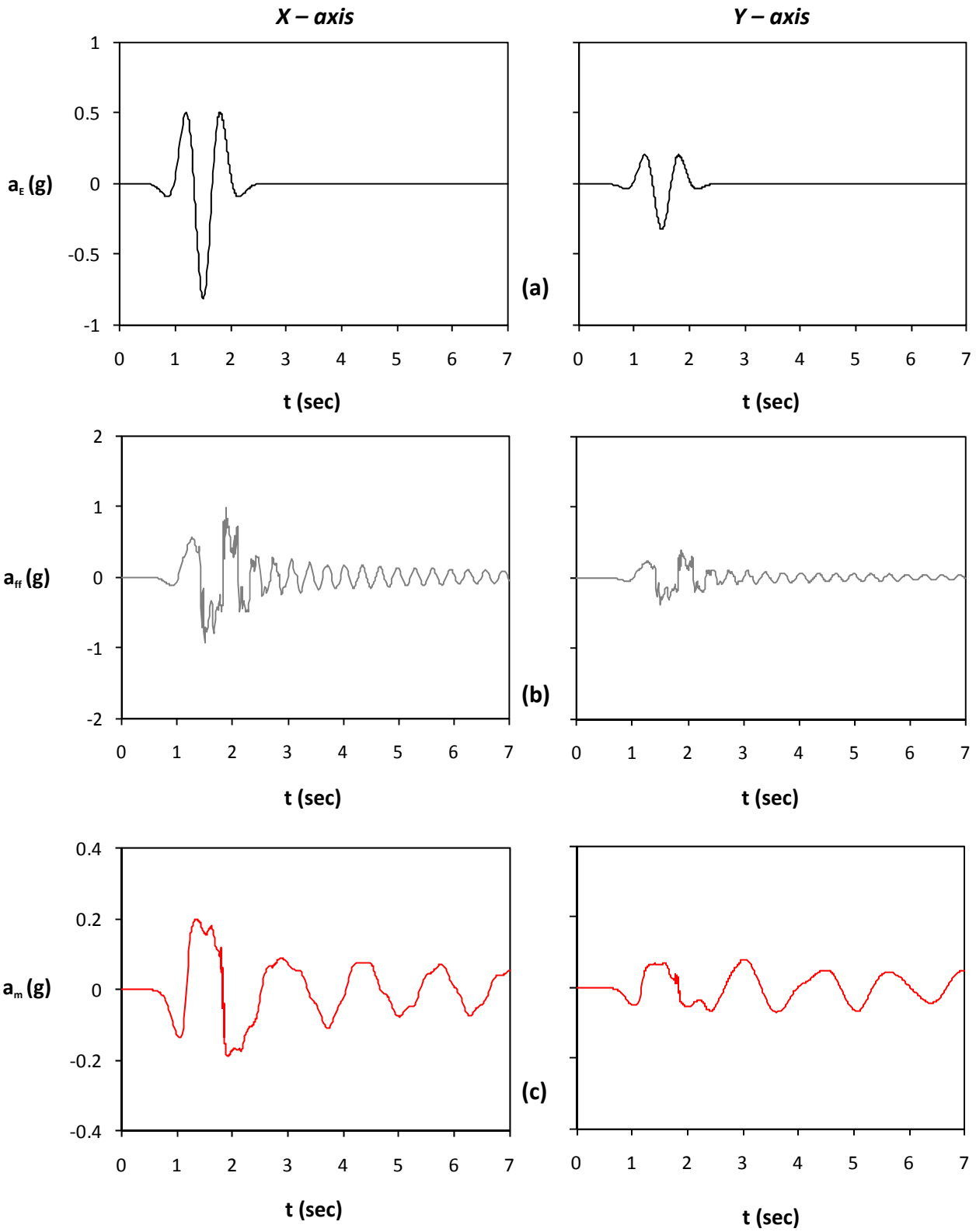

Figure 5.119. Seismic excitation in both directions, Ricker 1 A_x = 0.8 g and A_y =40% x 0.8 g : (a) acceleration time histories of bedrock excitation along the *x* axis (left) and the *y* axis (right) ; (b) acceleration time histories at the free field ; and (c) acceleration time histories of lumped mass.

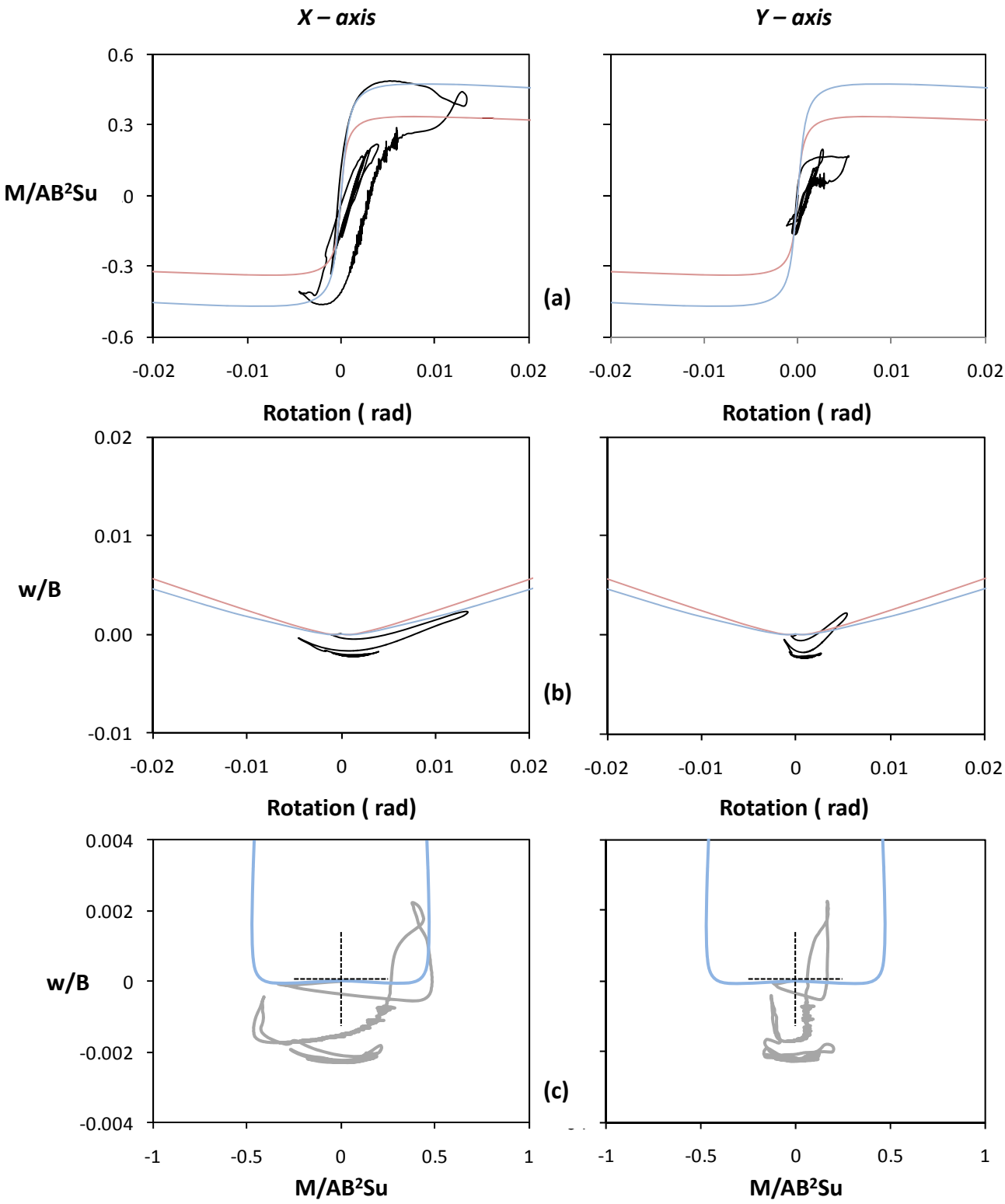

Figure 5.120. Seismic excitation in both directions, A_x = 0.8 g and A_y =40% x 0.8 g :
(a) Normalized moment versus rotation along the *x* axis (left) and the *y* axis (right) ;
(b) Normalized to width vertical settlement versus rotation ; and
(c) Normalized vertical settlement to moment along the *x* axis (left) and the *y* axis (right) .

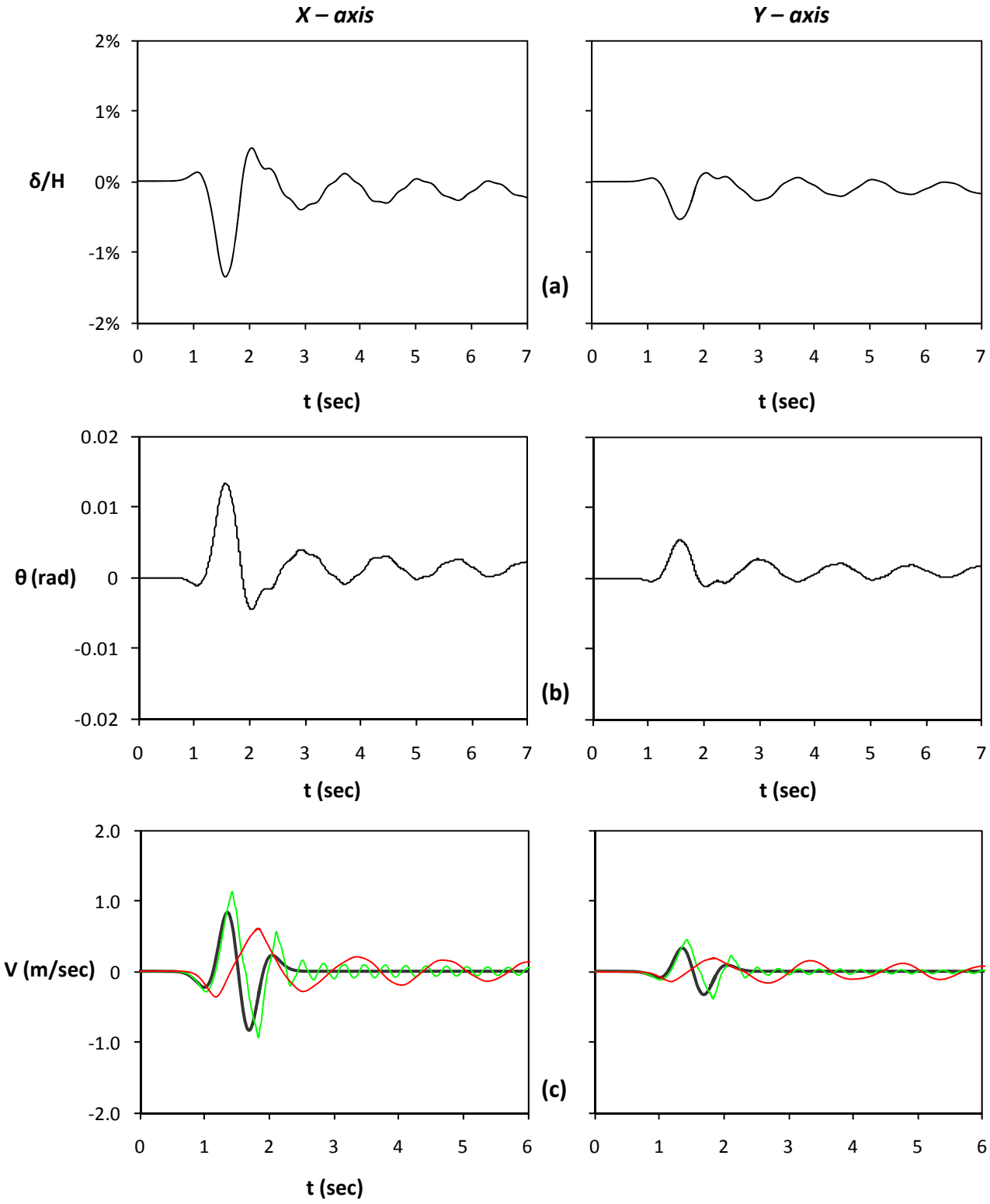

Figure 5.121. Seismic excitation in both directions, A_x = 0.8 g and A_y =40% x 0.8 g :
(a) Horizontal displacement normalized to height time histories along the *x* axis (left) and the *y* axis (right) ; (b) rotation time histories along the *x* axis (left) and the *y* axis (right) ; (c) velocity time histories (Green line stands for free field motion and red line for lumped mass)

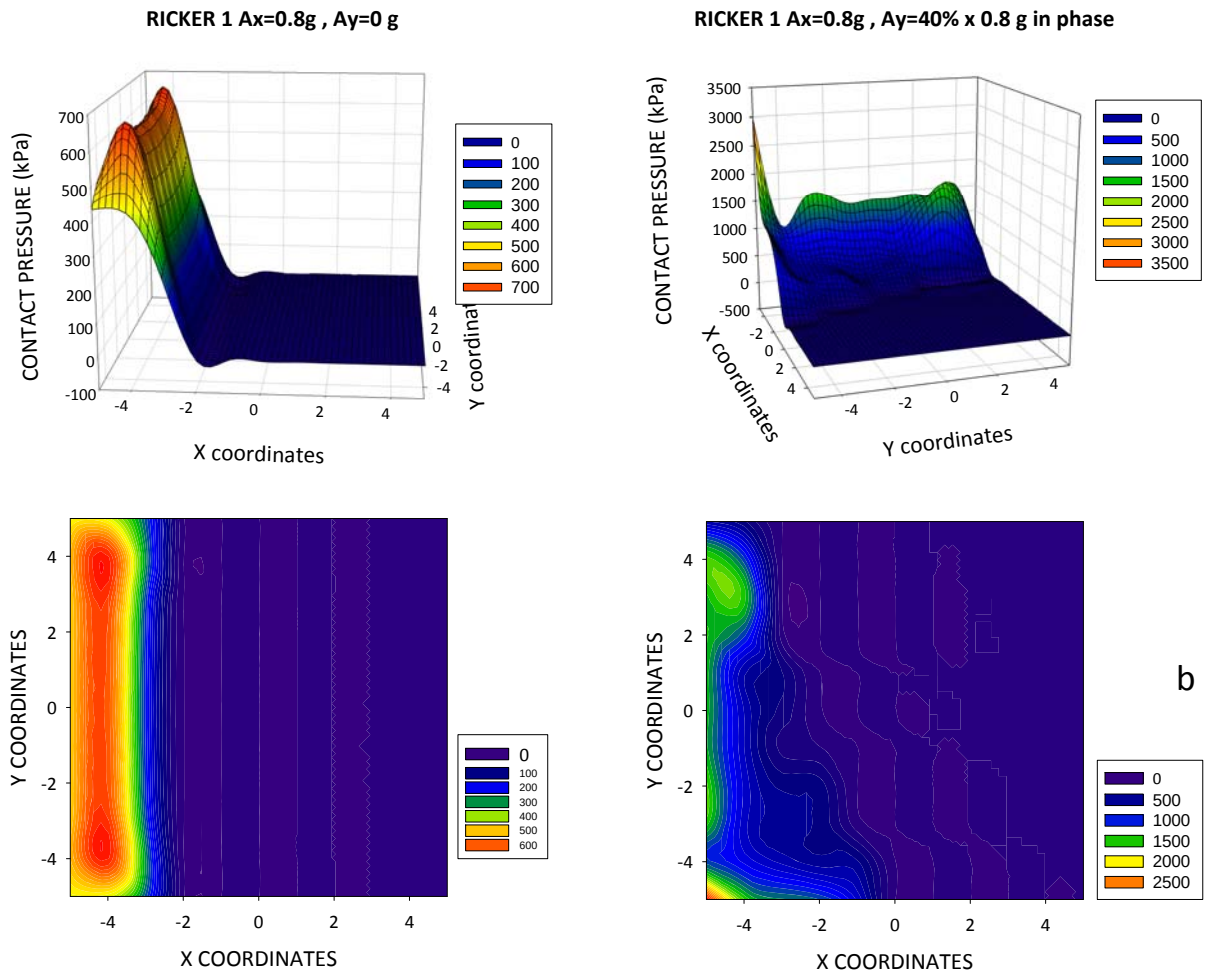

Figure 5.122. Seismic excitation in both directions, Ricker 1 A_x = 0.8 g and A_y = 40% x 0.8 g : Distribution of pressures under the footing at the time increment when the maximum uplift occurs for excitation in a) one direction (left) b) both directions (right) .

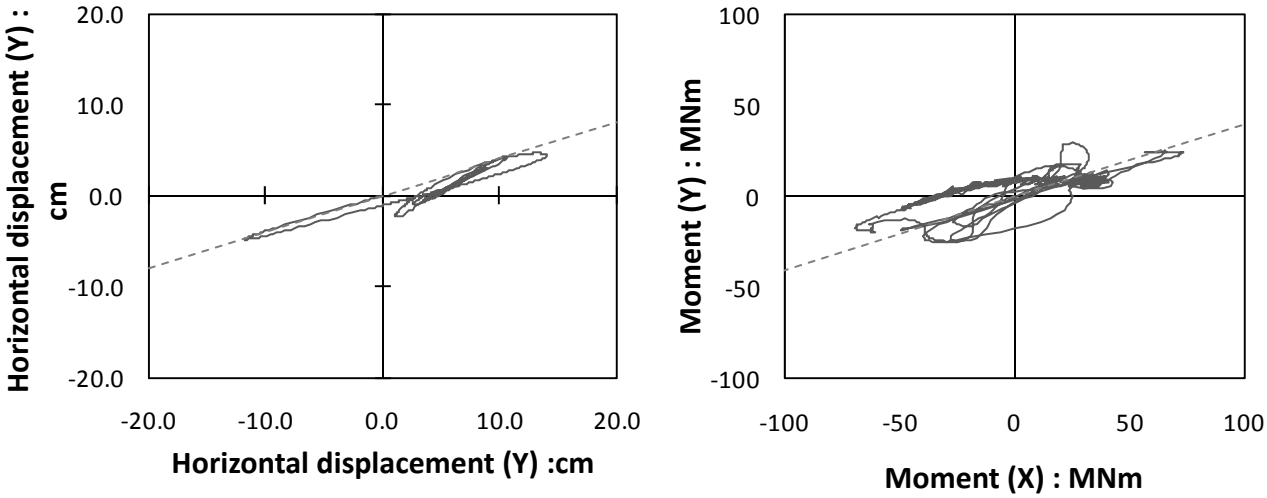

Figure 5.123. **a)** Orbit of center of mass in the X-Y plane.
b) Orbit in the M_X –M_Y plane.

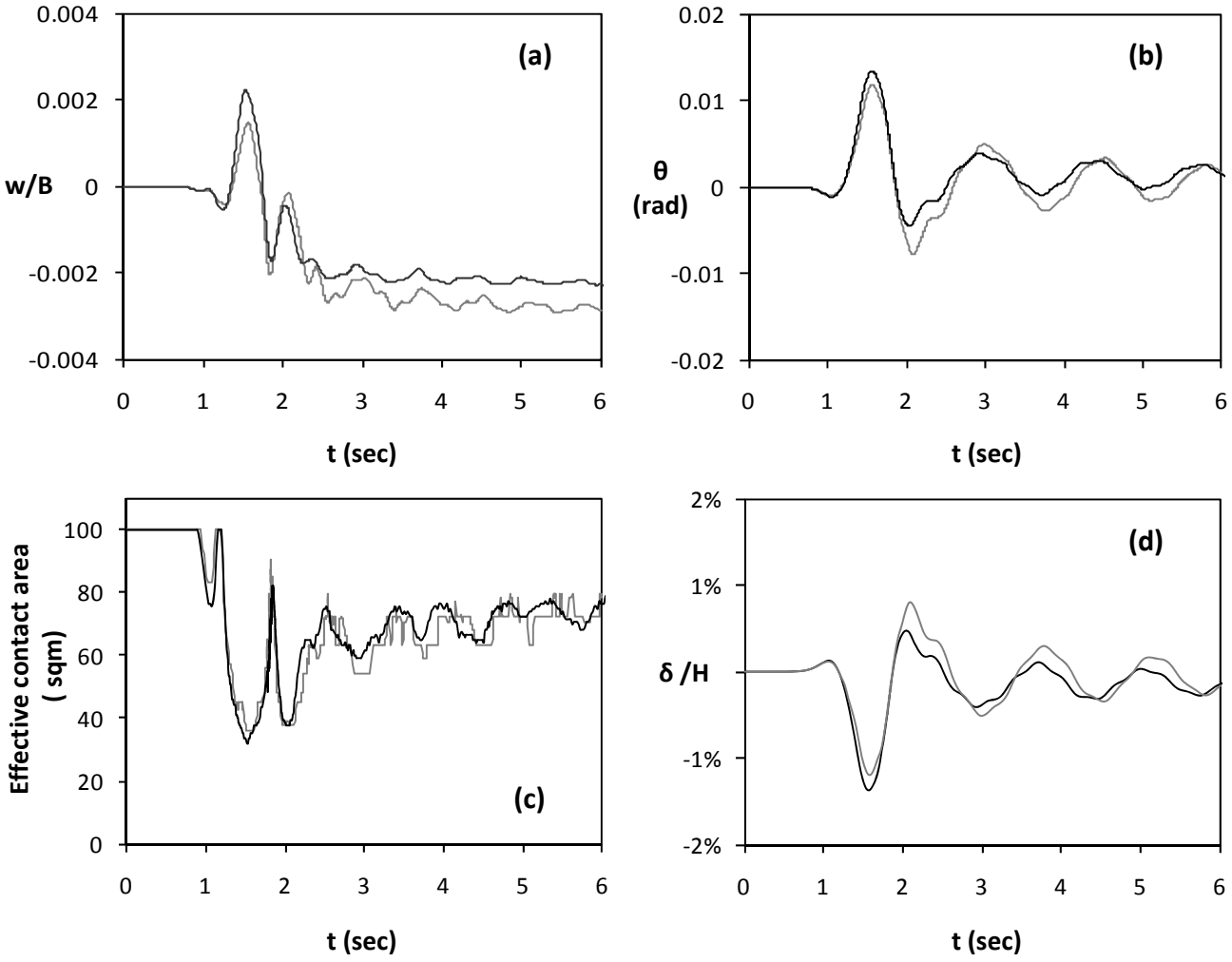

Figure 5.124. Seismic excitation in both directions, Ricker 1 A_x = 0.8 g and A_y =40% x 0.8 g and comparison with the single direction case.
Time histories of (a) Vertical settlement (b) Rotation ; (c) Effective contact area time ; (d) horizontal displacement normalized to height. (Black line represents excitation in both directions and grey line single direction excitation)

Sinusoidal pulses Loading

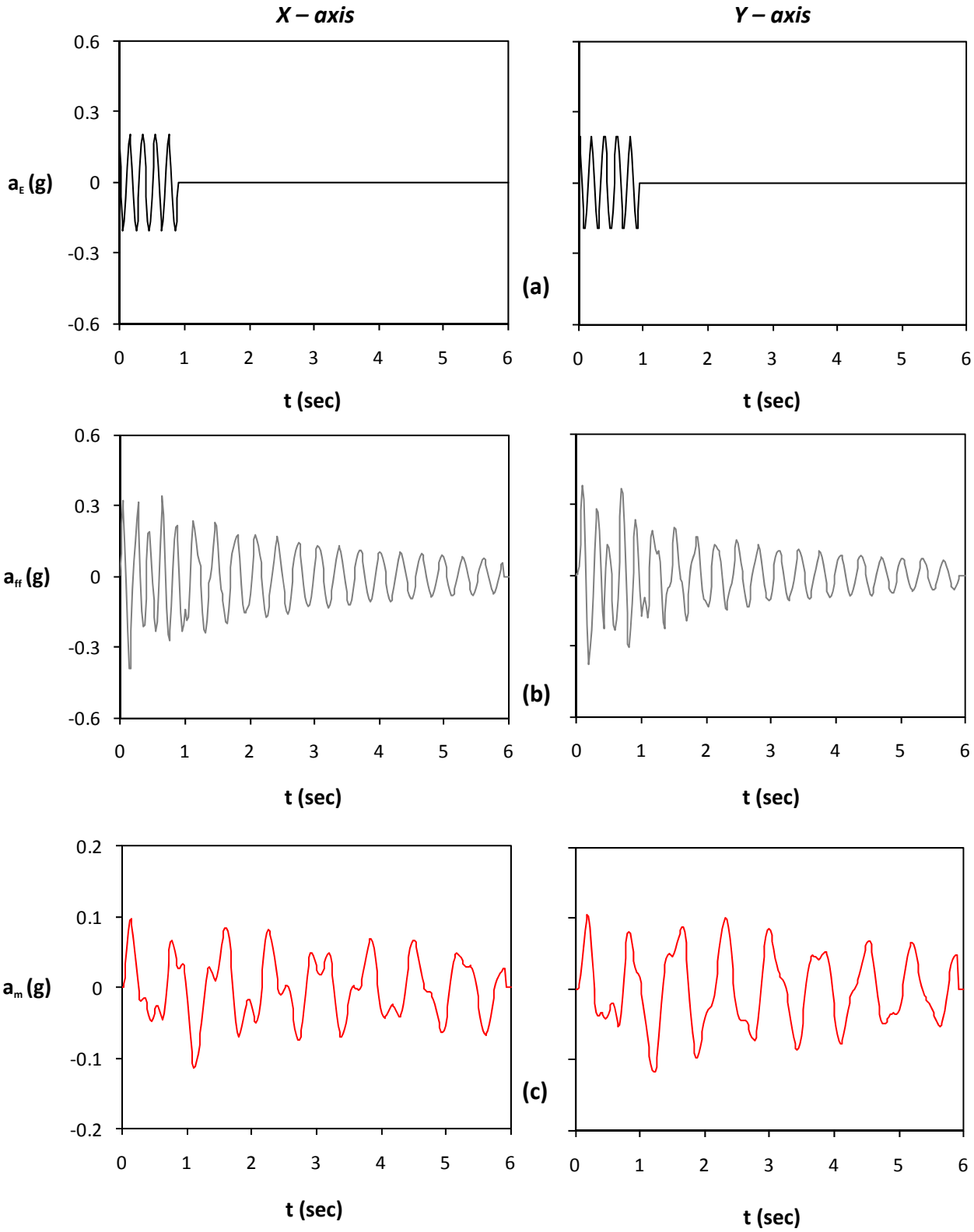

Figure 6.1. Harmonic excitation in both directions, sin02t A_x = 0.2 g and A_y = 0.2 g phase difference π/2 (5 cycles) : (a) acceleration time histories of bedrock excitation along the *x* axis (left) and the *y* axis (right) ; (b) acceleration time histories at the free field ; and (c) acceleration time histories of lumped mass.

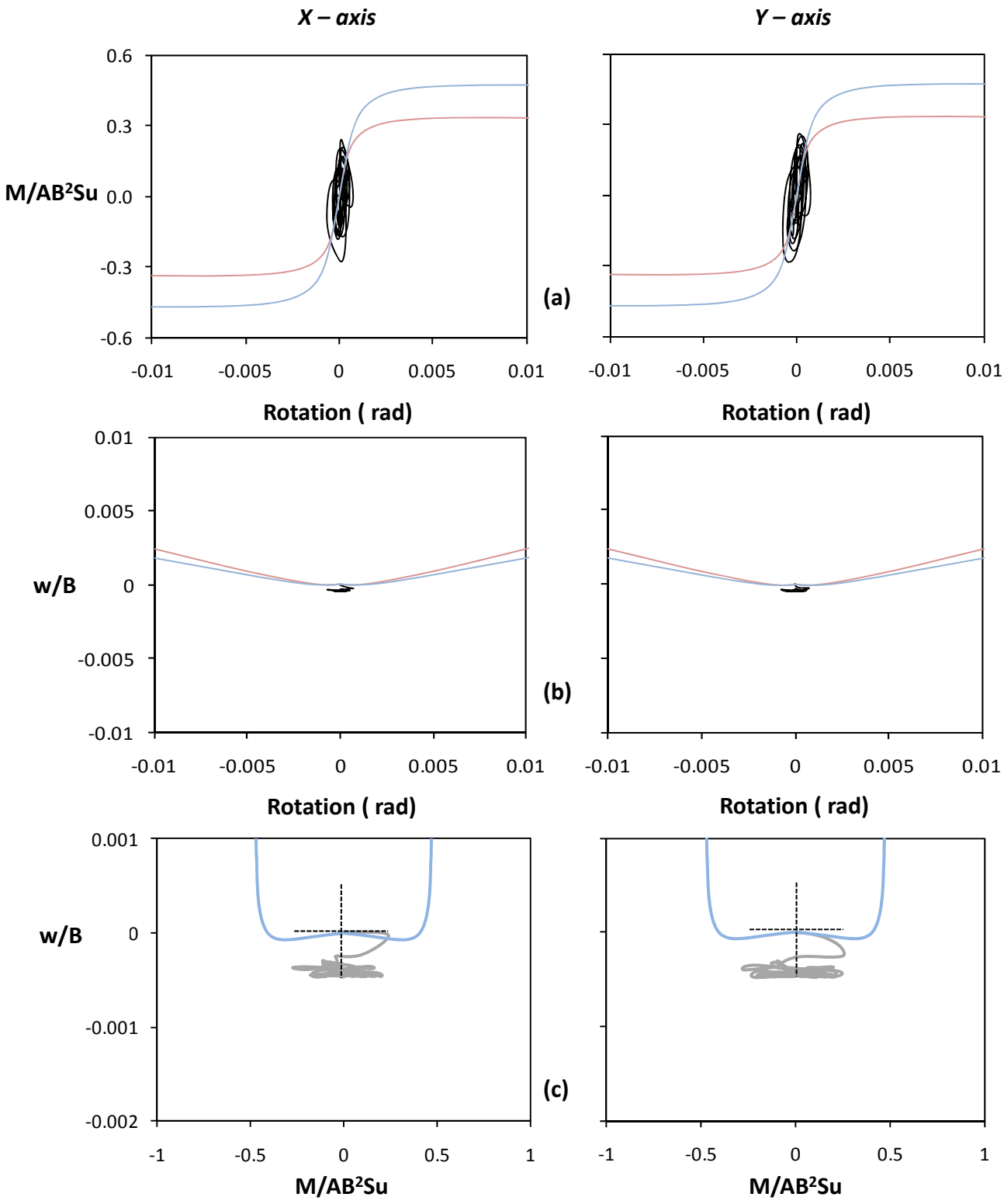

Figure 6.2. Harmonic excitation in both directions, sin02t (5 cycles) A_x = 0.2 g and A_y = 0.2 g phase difference π/2 :
(a) Normalized moment versus rotation along the *x* axis (left) and the *y* axis (right) ;
(b) Normalized to width vertical settlement versus rotation ; and
(c) Normalized vertical settlement to moment along the *x* axis (left) and the *y* axis (right) .

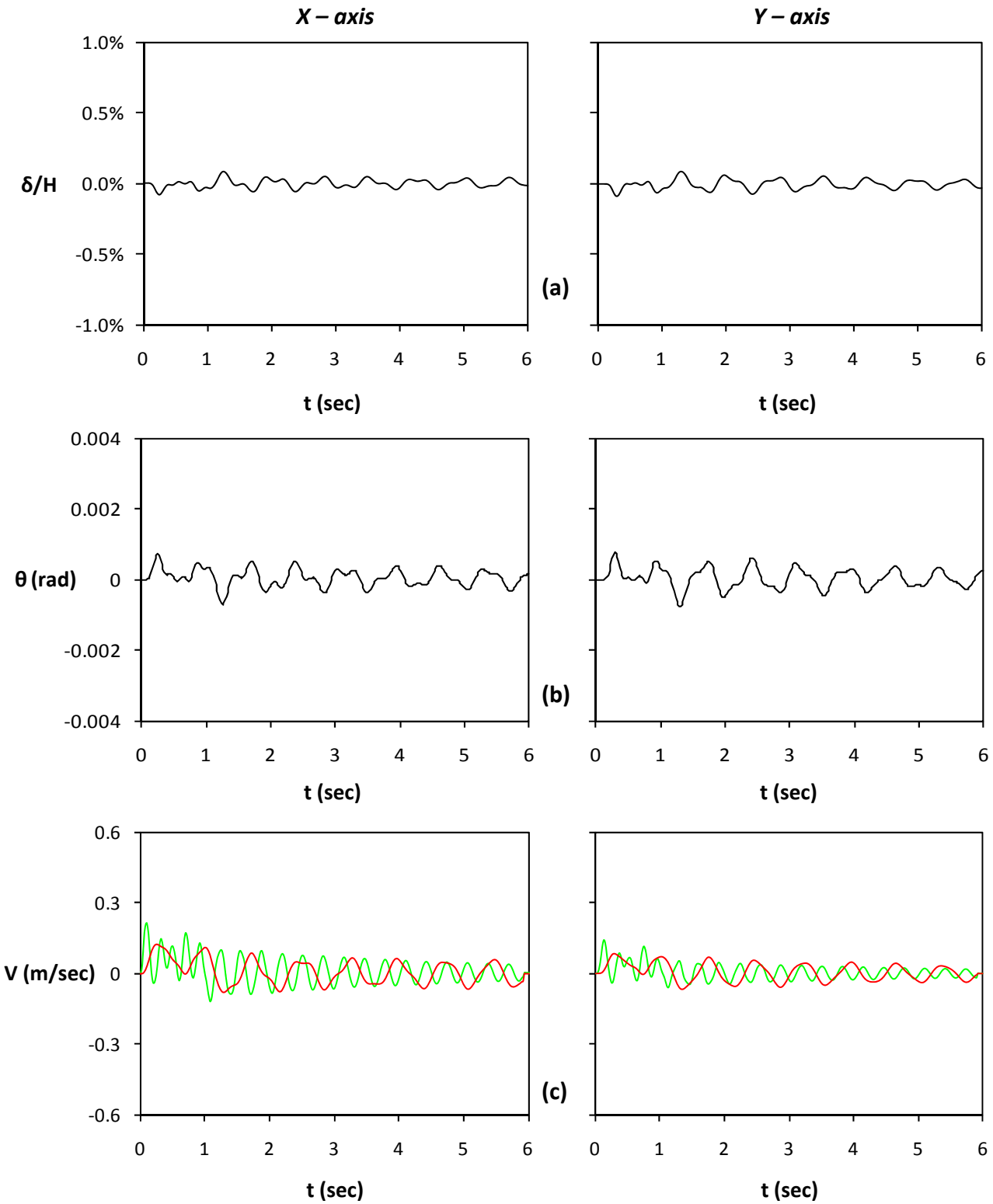

Figure 6.3. Harmonic excitation in both directions, sin02t A_x = 0.2 g and A_y = 0.2 g phase difference π/2 (5 cycles) :
(a) Horizontal displacement normalized to height time histories along the *x* axis (left) and the *y* axis (right) ; (b) rotation time histories along the *x* axis (left) and the *y* axis (right) ; (c) velocity time histories (Green line stands for free field motion and red line for lumped mass)

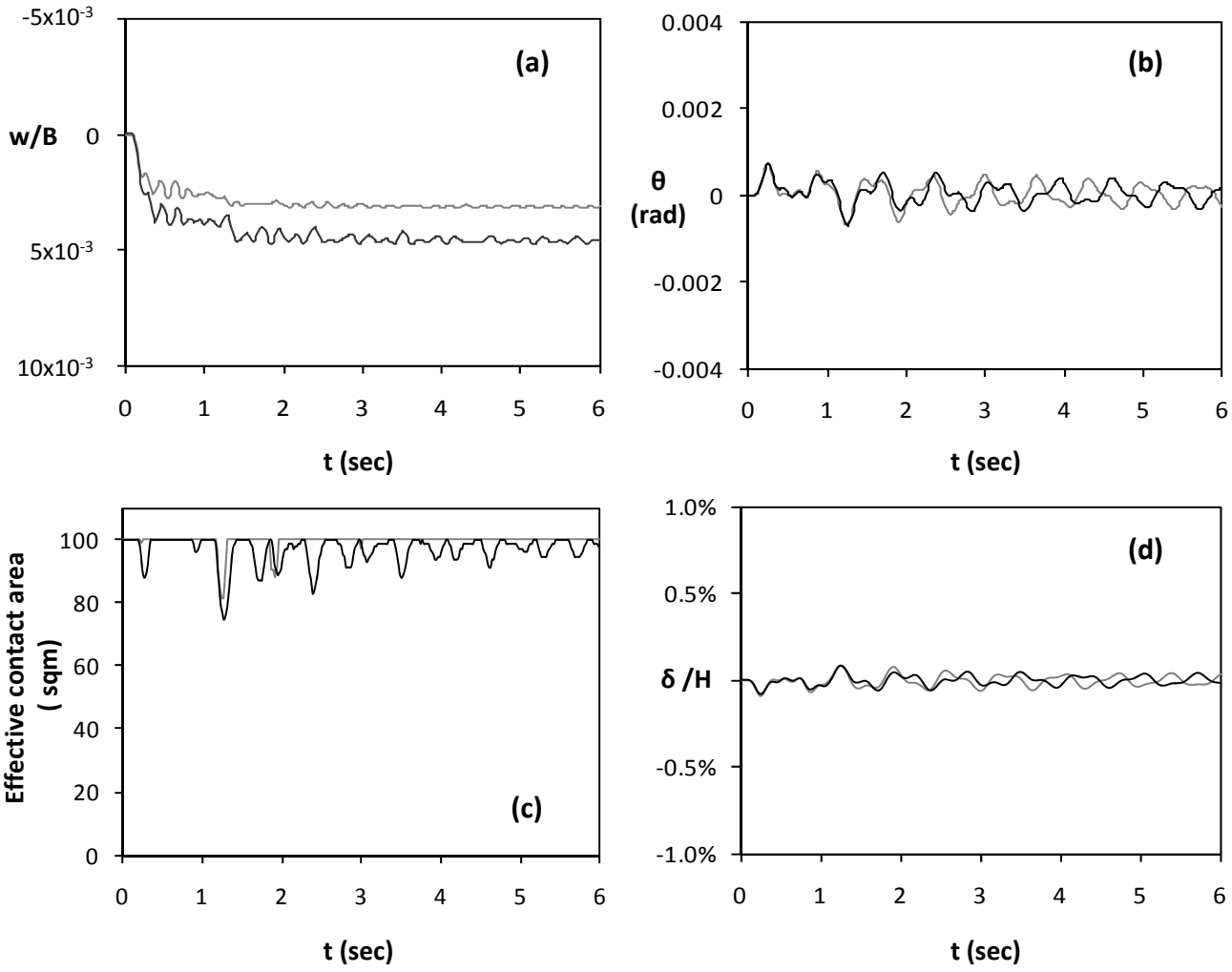

Figure 6.6. Harmonic excitation in both directions, sin02t (5 cycles) A_x = 0.2 g and A_y = 0.2 g time lag T/4 and comparison with the single direction case.
Time histories of (a) Vertical settlement (b) Rotation ; (c) Effective contact area time ; (d) horizontal displacement normalized to height. (Black line represents excitation in both directions and grey line single direction excitation)

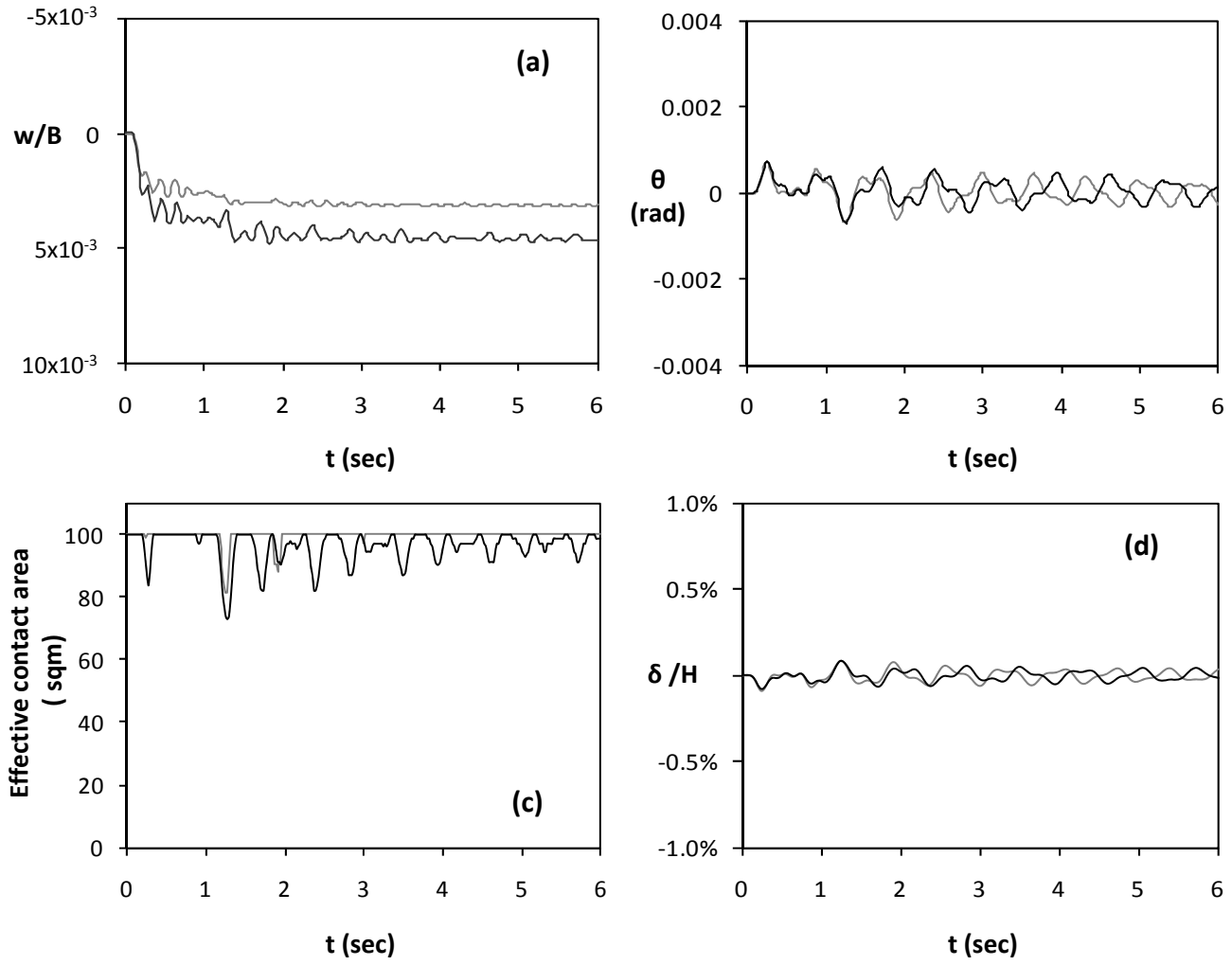

Figure 6.7. Harmonic excitation in both directions, sin02t (5 cycles) A_x = 0.2 g and A_y = 0.2 g phase difference π/3 and comparison with the single direction case.
Time histories of (a) Vertical settlement (b) Rotation ; (c) Effective contact area time ; (d) horizontal displacement normalized to height. (Black line represents excitation in both directions and grey line single direction excitation)

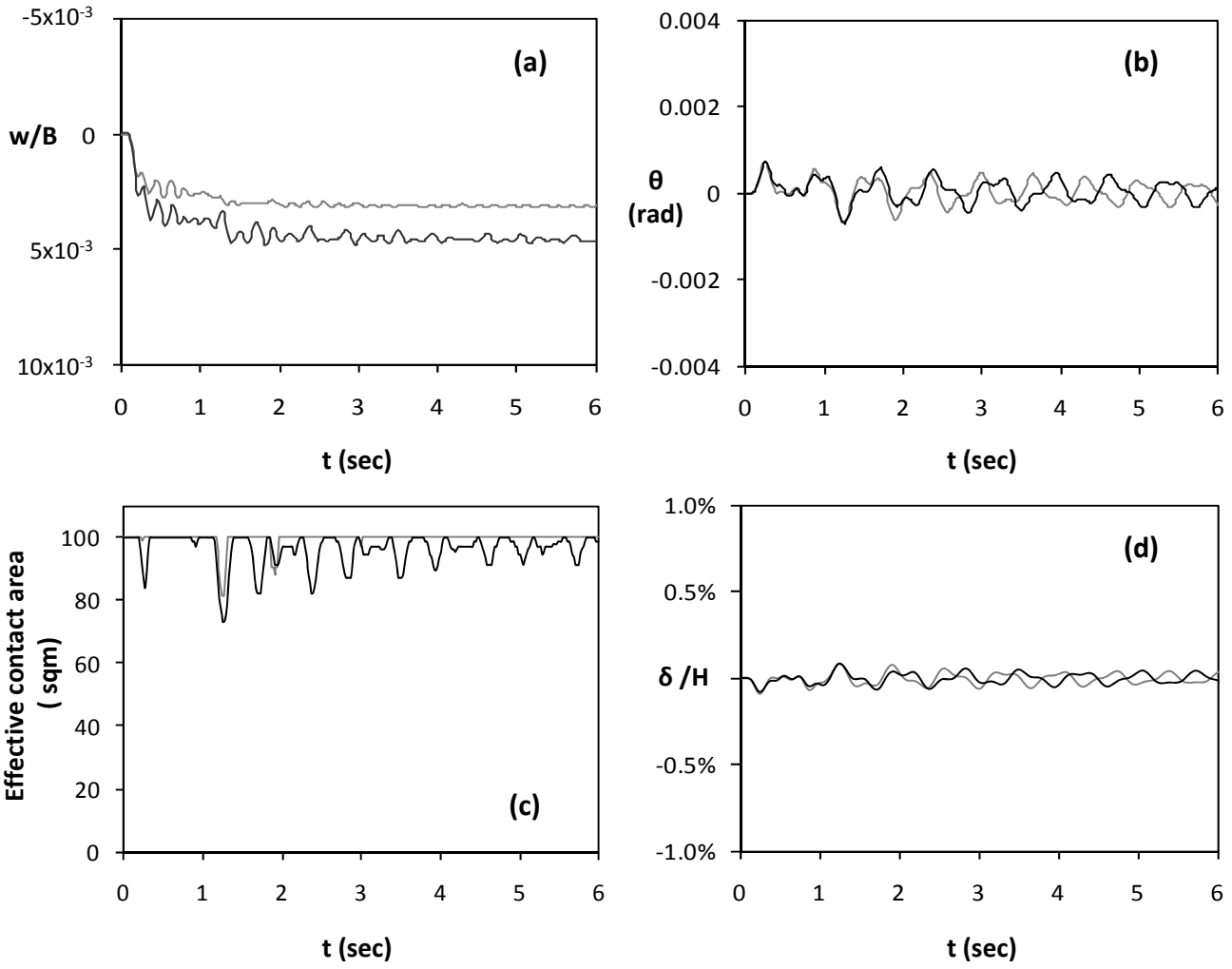

Figure 6.8. Harmonic excitation in both directions, sin02t (5 cycles) A_x = 0.2 g and A_y = 0.2 g phase difference $\pi/4$ and comparison with the single direction case.
Time histories of (a) Vertical settlement (b) Rotation ; (c) Effective contact area time ; (d) horizontal displacement normalized to height. (Black line represents excitation in both directions and grey line single direction excitation)

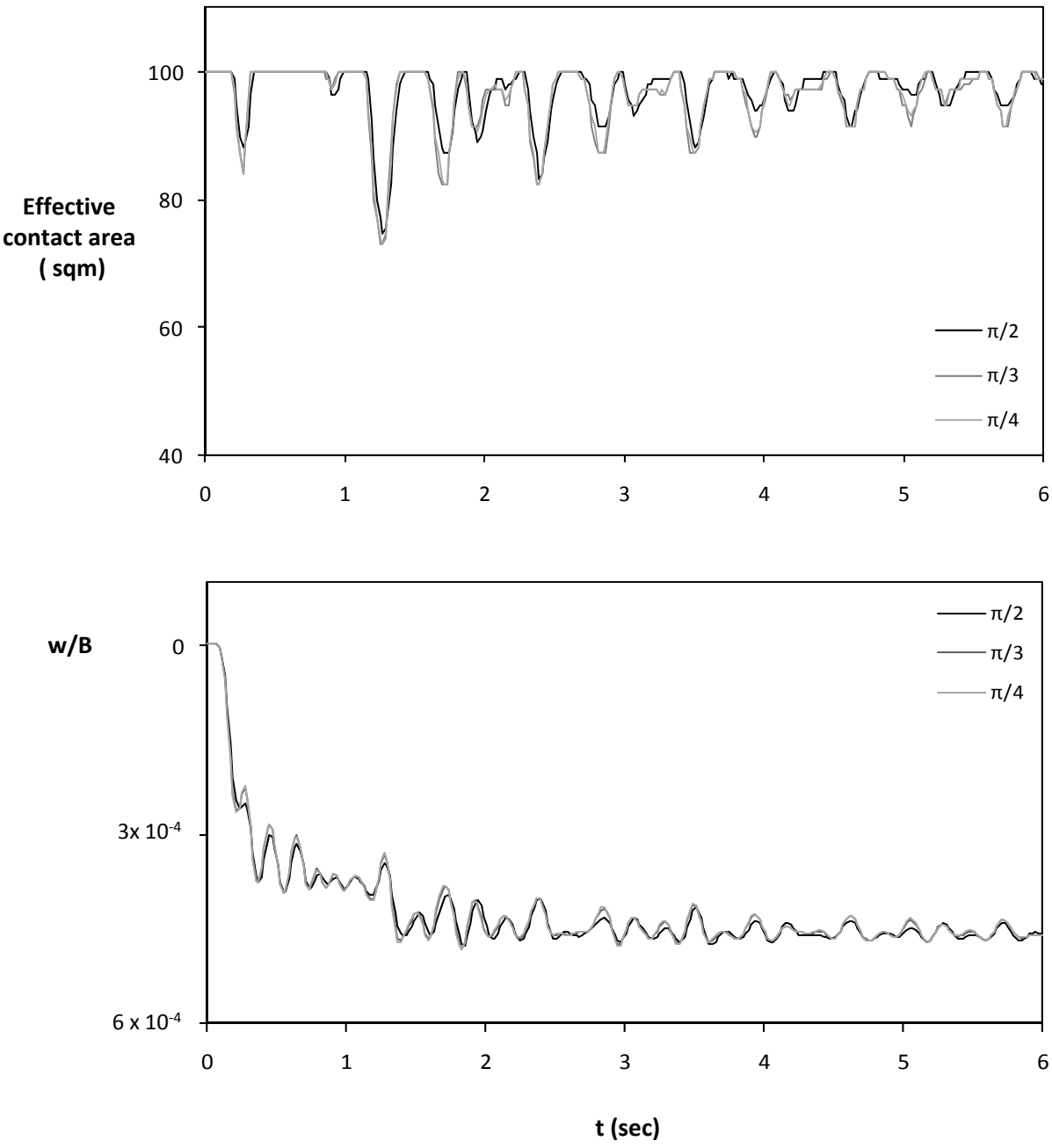

Figure 6.9. Harmonic excitation in both directions, sin02t (5 cycles) A_x = 0.2 g and A_y = 0.2 g with phase difference. Time histories of (a) Effective contact area ; (d) Vertical settlement normalized to width.

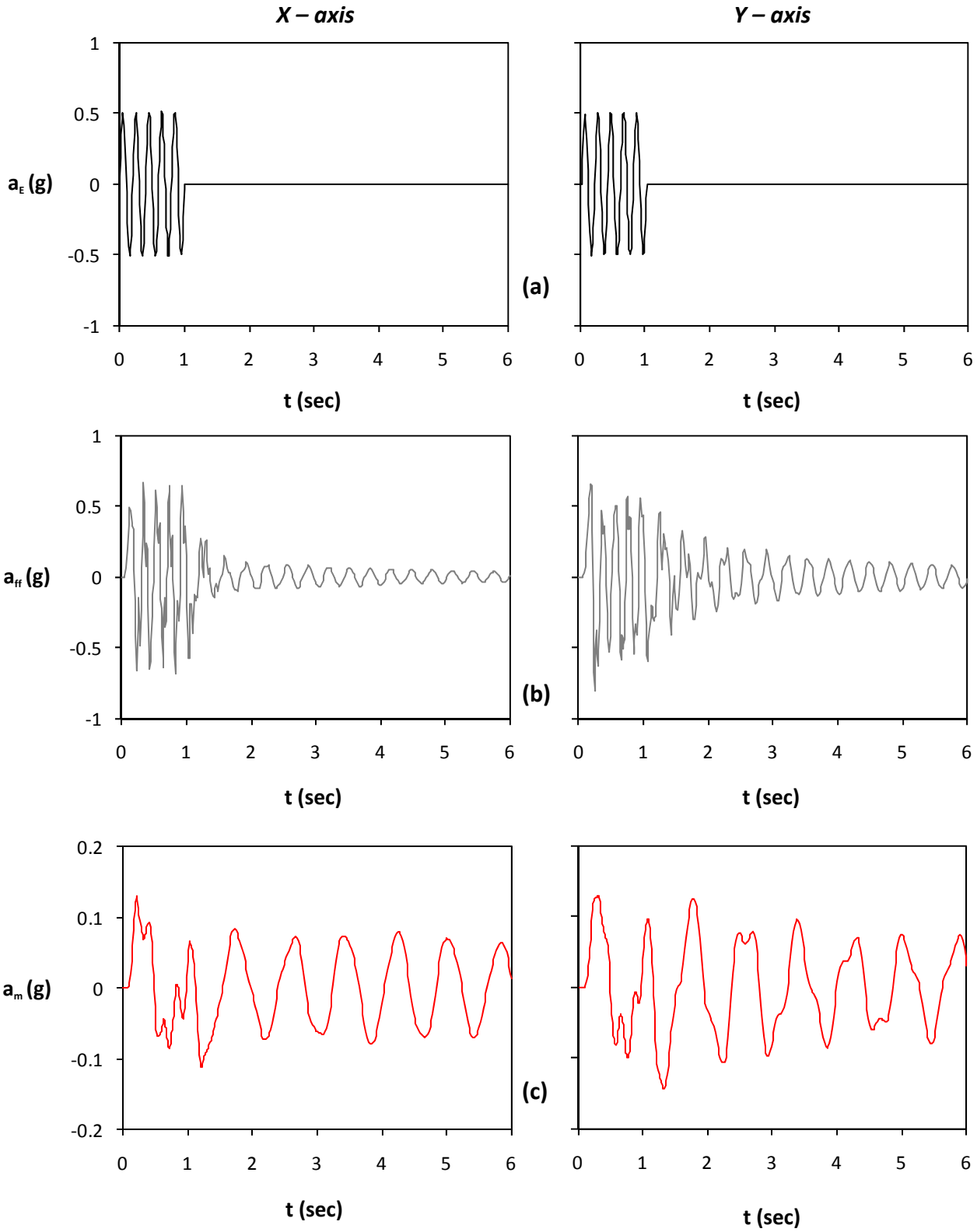

Figure 6.10. Harmonic excitation in both directions, sin02 (5 cycles) A_x = 0.2 g and A_y = 0.2 g phase difference π/4 : (a) acceleration time histories of bedrock excitation along the *x* axis (left) and the *y* axis (right) ; (b) acceleration time histories at the free field ; and (c) acceleration time histories of lumped mass.

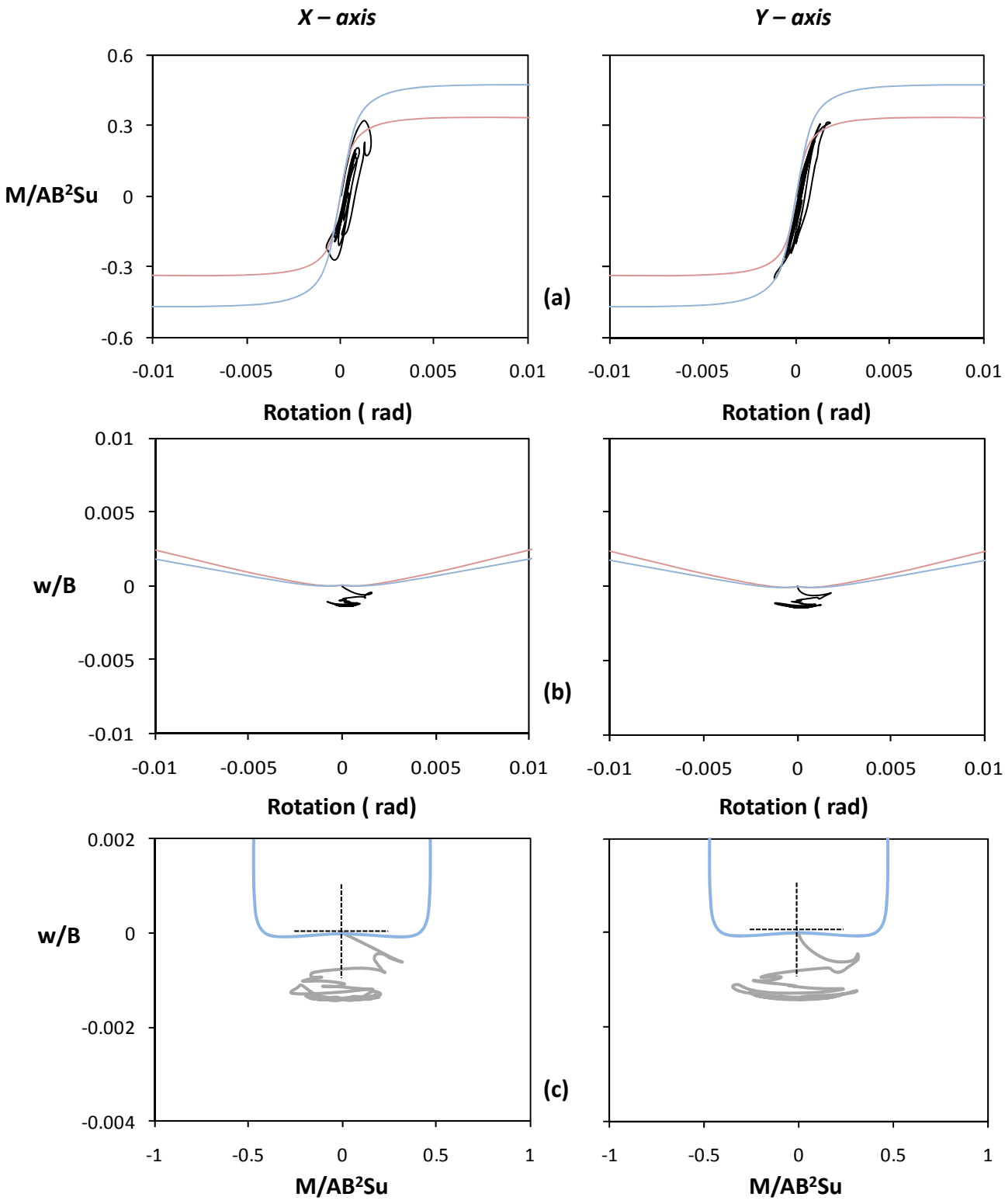

Figure 6.11. Harmonic excitation in both directions, sin02t (5 cycles) A_x = 0.5 g and A_y = 0.5 g phase difference π/4 :
(a) Normalized moment versus rotation along the *x* axis (left) and the *y* axis (right) ;
(b) Normalized to width vertical settlement versus rotation ; and
(c) Normalized vertical settlement to moment along the *x* axis (left) and the *y* axis (right) .

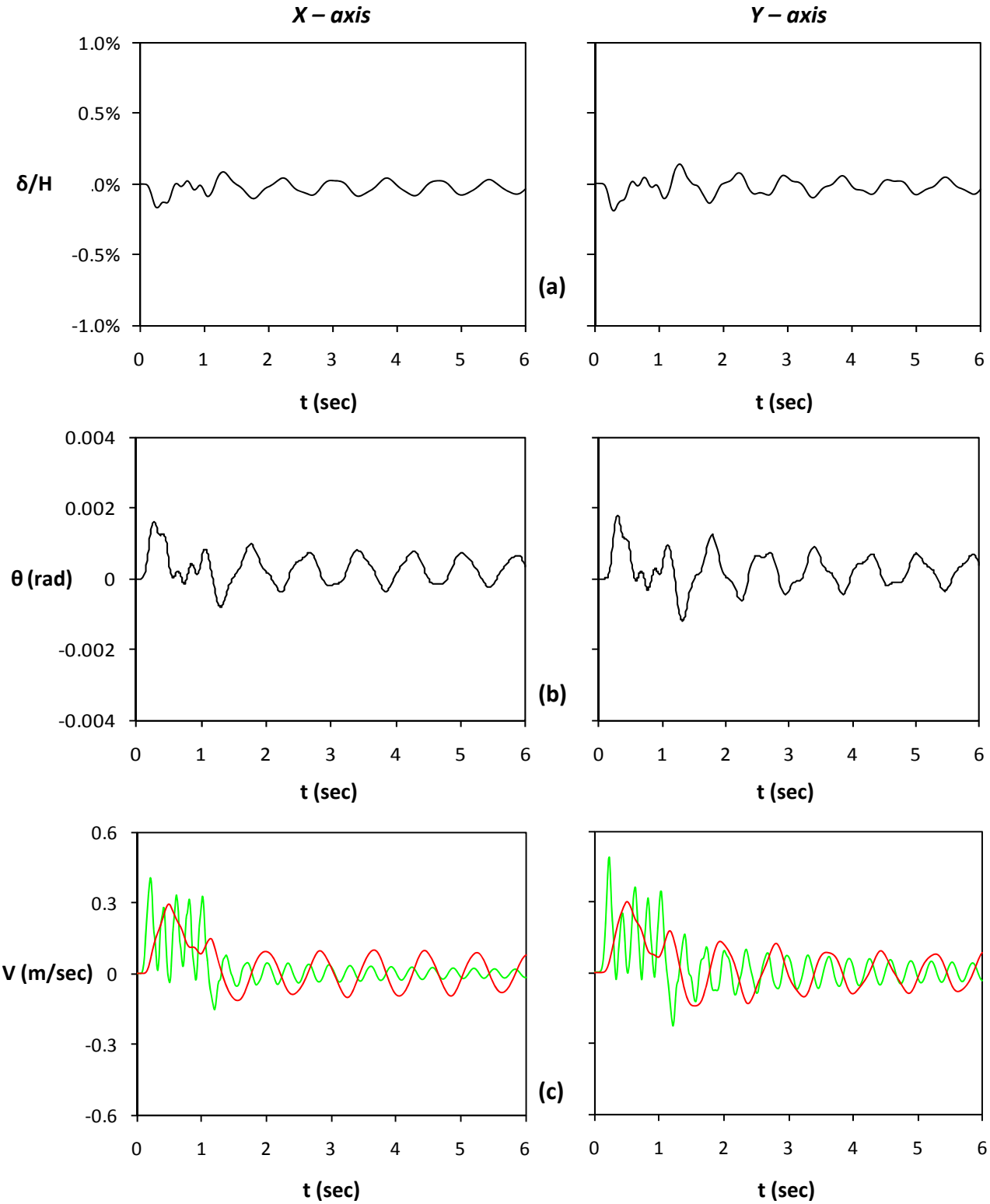

Figure 6.12. Harmonic excitation in both directions, sin02t (5 cycles) A_x = 0.5 g and A_y = 0.5g phase difference π/4 :
(a) Horizontal displacement normalized to height time histories along the *x* axis (left) and the *y* axis (right) ; (b) rotation time histories along the *x* axis (left) and the *y* axis (right) ; (c) velocity time histories (Green line stands for free field motion and red line for lumped mass)

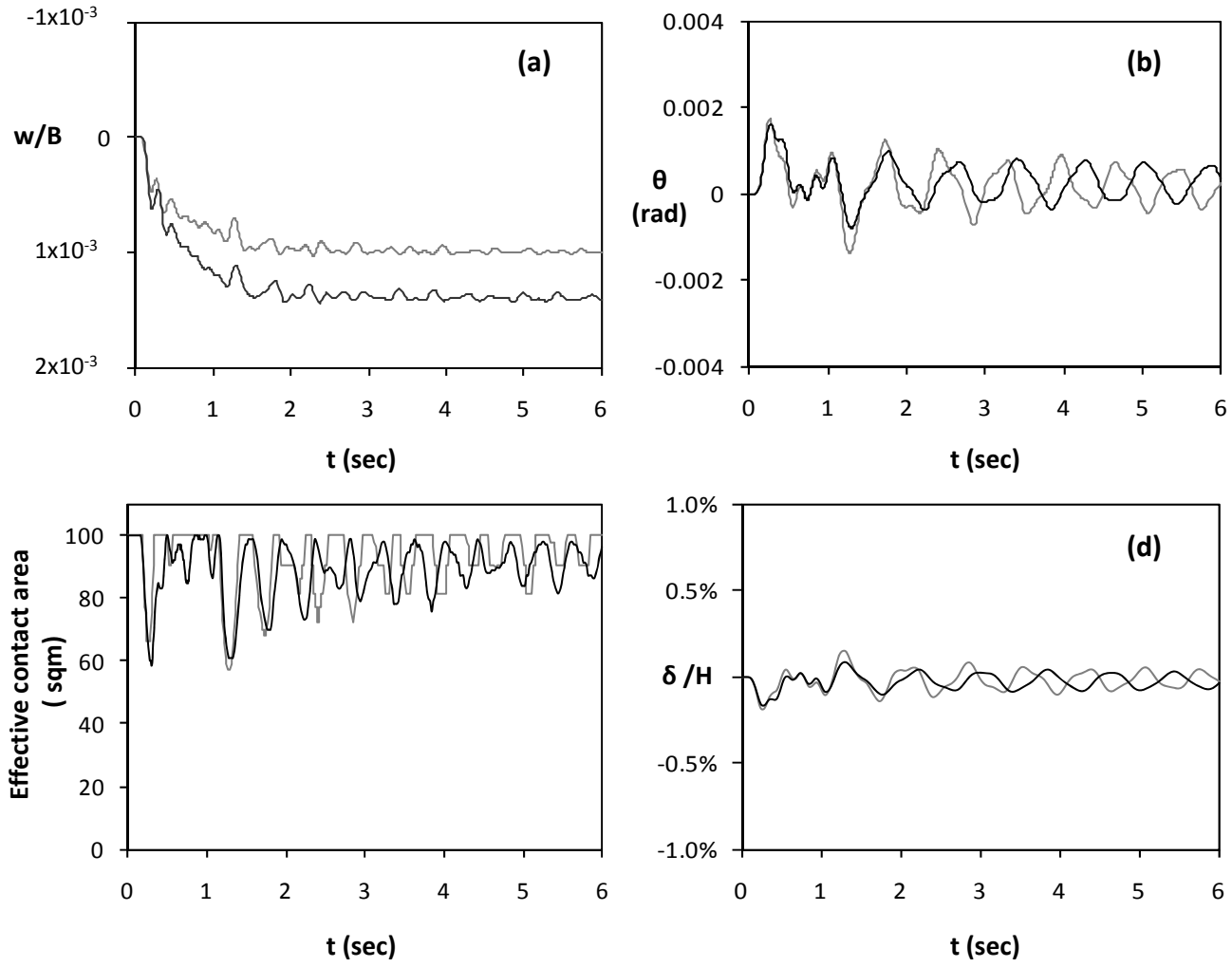

Figure 6.15. Harmonic excitation in both directions, sin02t (5 cycles) A_x = 0.5 g and A_y = 0.5 g phase difference π/4 and comparison with the single direction case.
Time histories of (a) Vertical settlement (b) Rotation ; (c) Effective contact area time ; (d) horizontal displacement normalized to height. (Black line represents excitation in both directions and grey line single direction excitation)

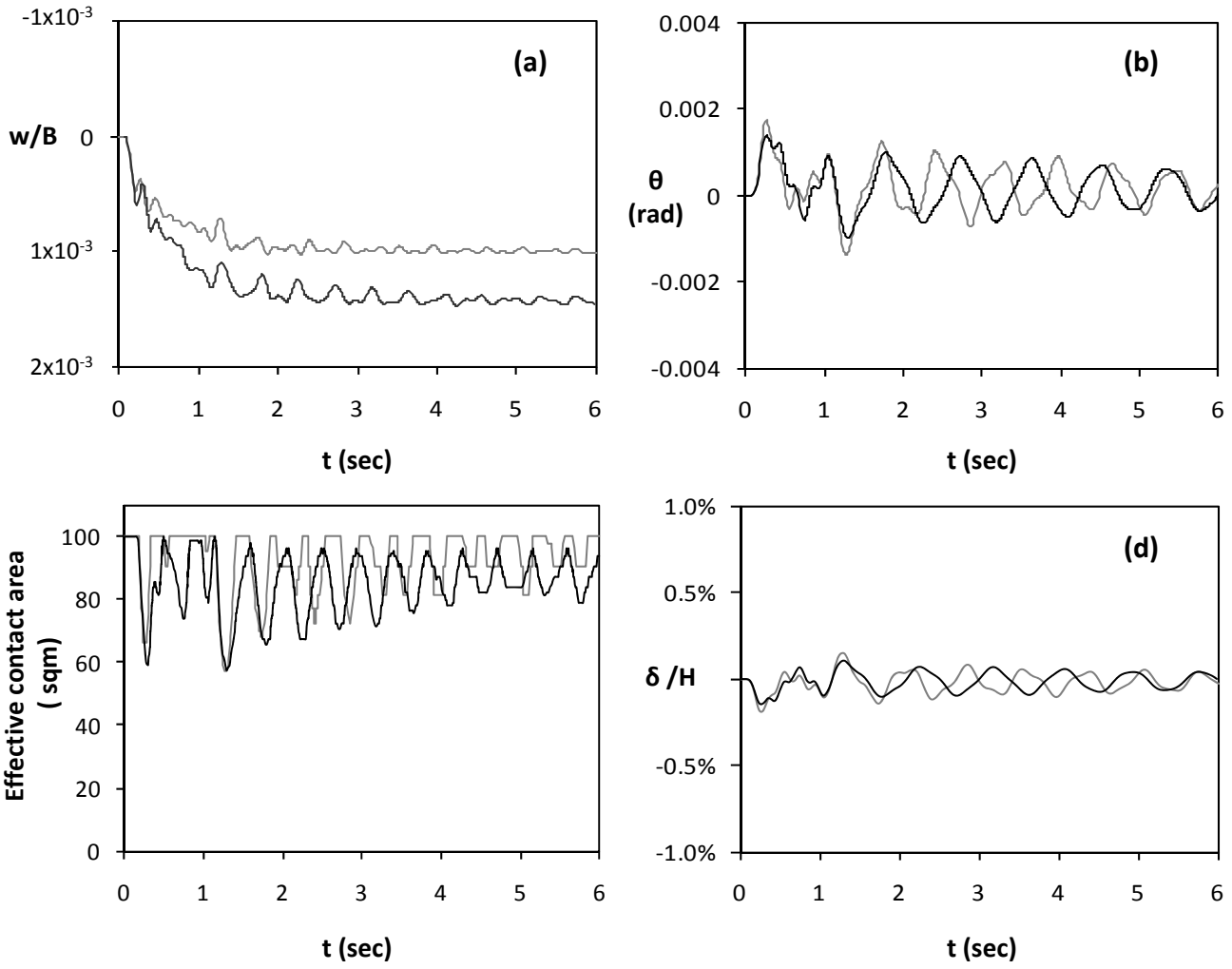

Figure 6.16. Harmonic excitation in both directions, sin02t (5 cycles) A_x = 0.5 g and A_y = 0.5 g phase difference π/3 and comparison with the single direction case.
Time histories of (a) Vertical settlement (b) Rotation ; (c) Effective contact area time ; (d) horizontal displacement normalized to height. (Black line represents excitation in both directions and grey line single direction excitation)

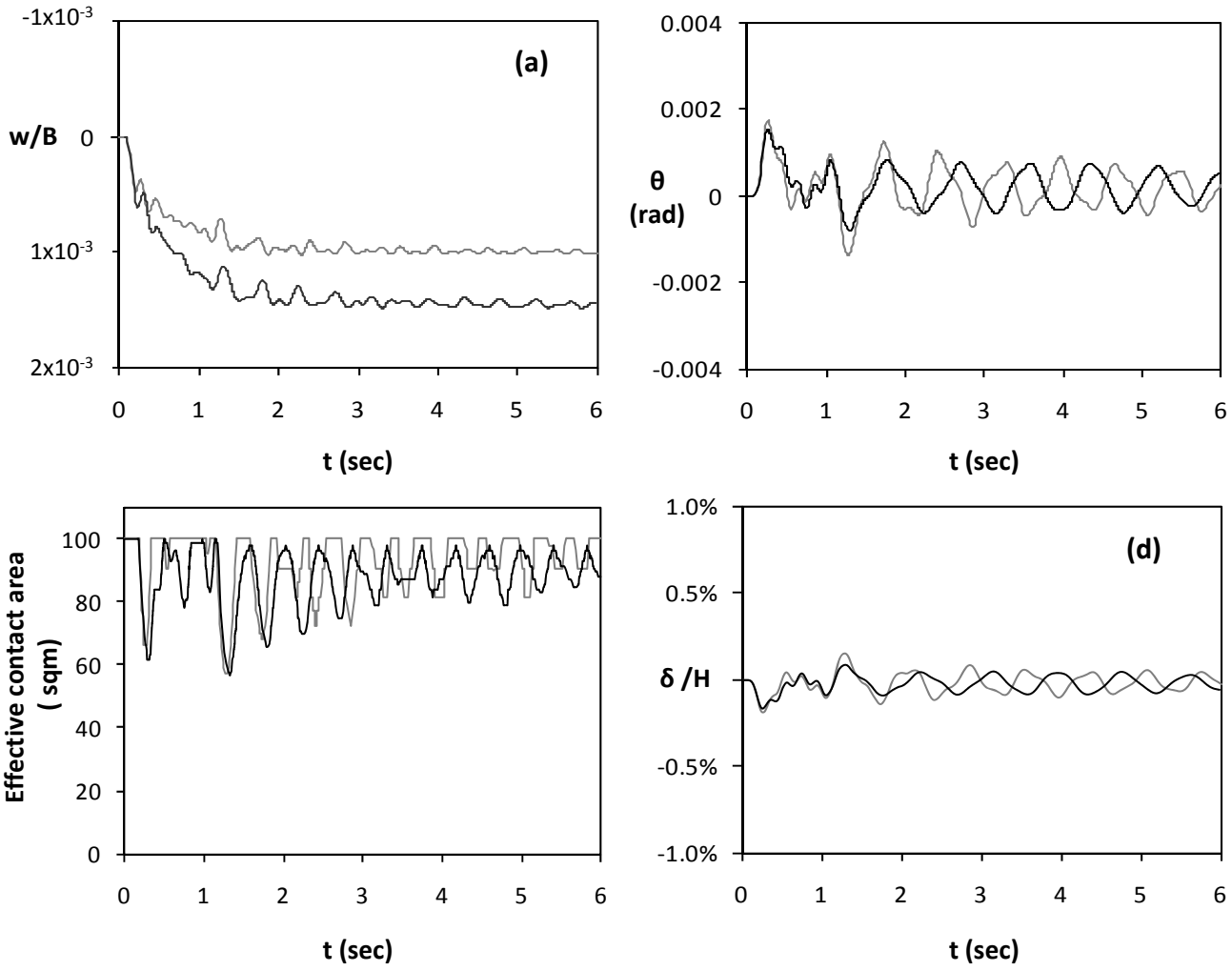

Figure 6.17. Harmonic excitation in both directions, sin02 A_x = 0.5 g and A_y = 0.5 g phase difference π/2 (5 cycles) and comparison with the single direction case.
Time histories of (a) Vertical settlement (b) Rotation ; (c) Effective contact area time ; (d) horizontal displacement normalized to height. (Black line represents excitation in both directions and grey line single direction excitation)

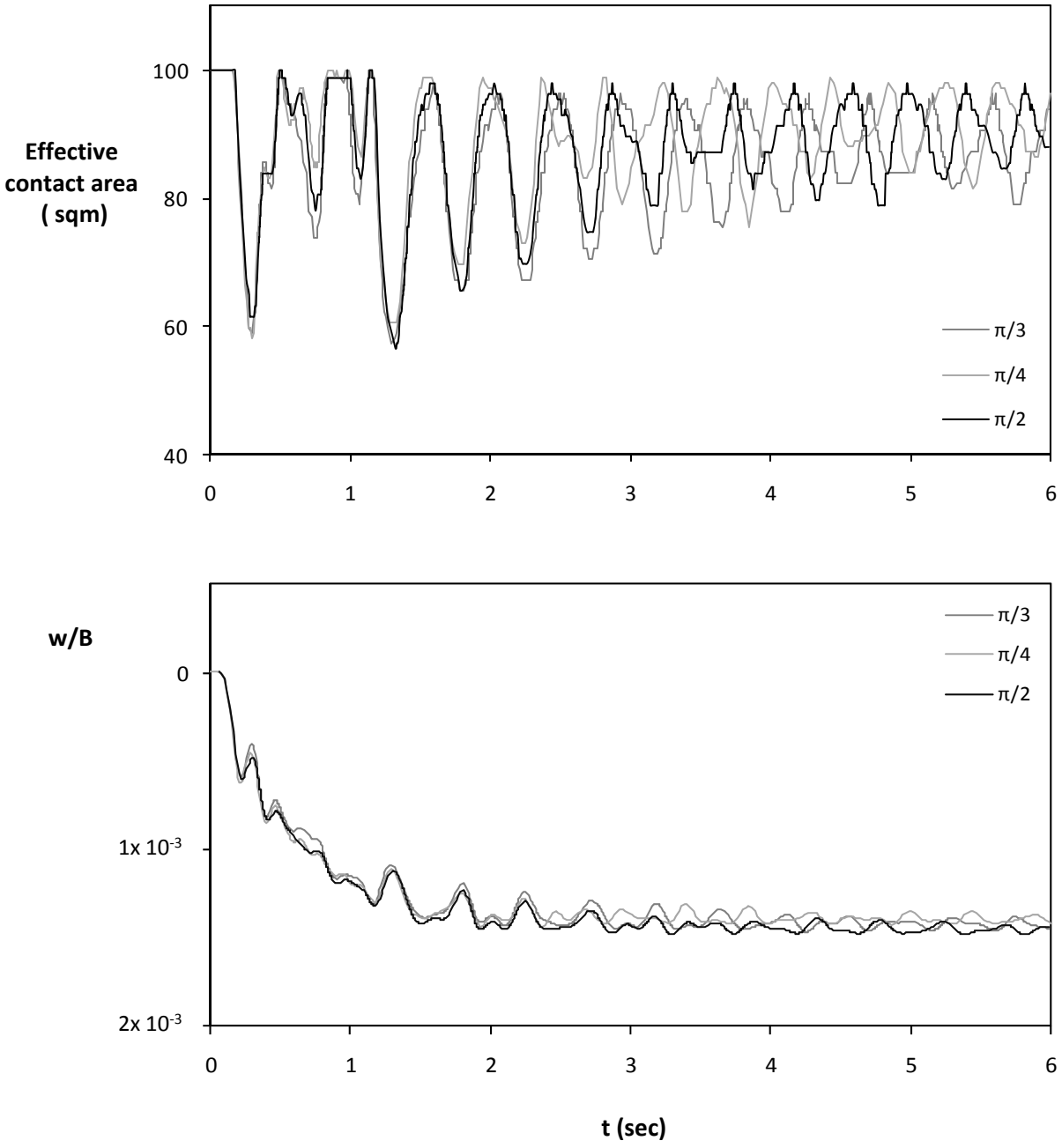

Figure 6.18. Harmonic excitation in both directions, sin02t (5 cycles) A_x = 0.5 g and A_y = 0.5 g with phase difference. Time histories of (a) Effective contact area ; (d) Vertical settlement normalized to width.

Harmonic Wavelets Loading

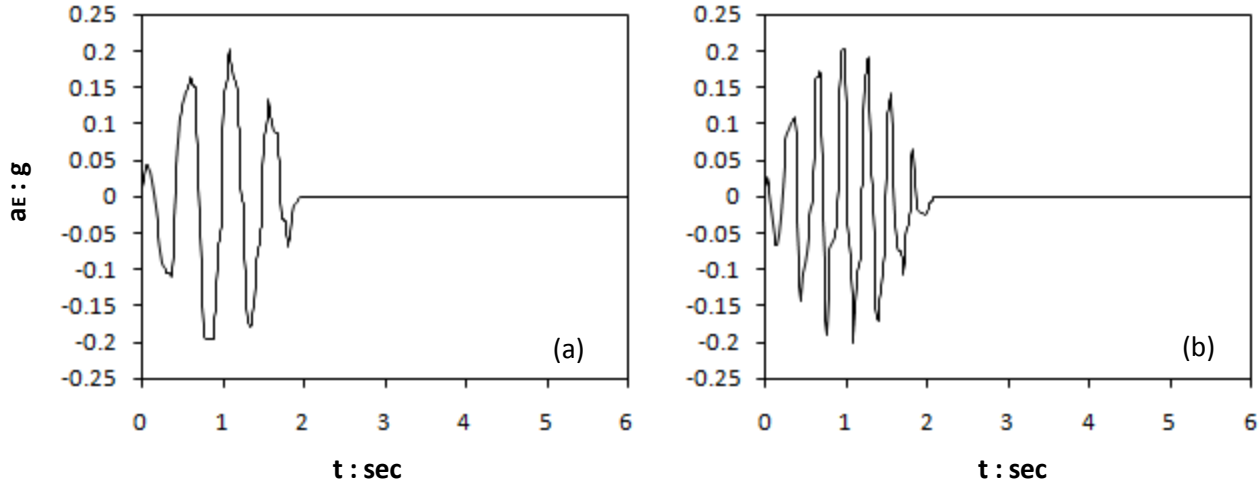

Figure 5.1:. Acceleration time histories of bedrock excitation along (a) x axis, (b) y axis .

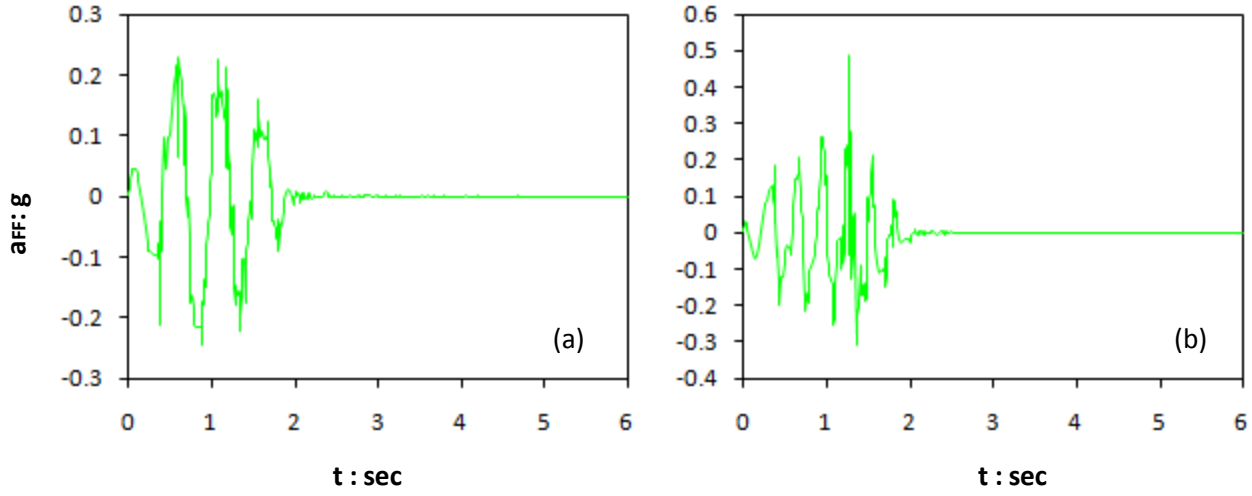

Figure 7.2: Acceleration time histories of free field along (a) x axis, (b) y axis

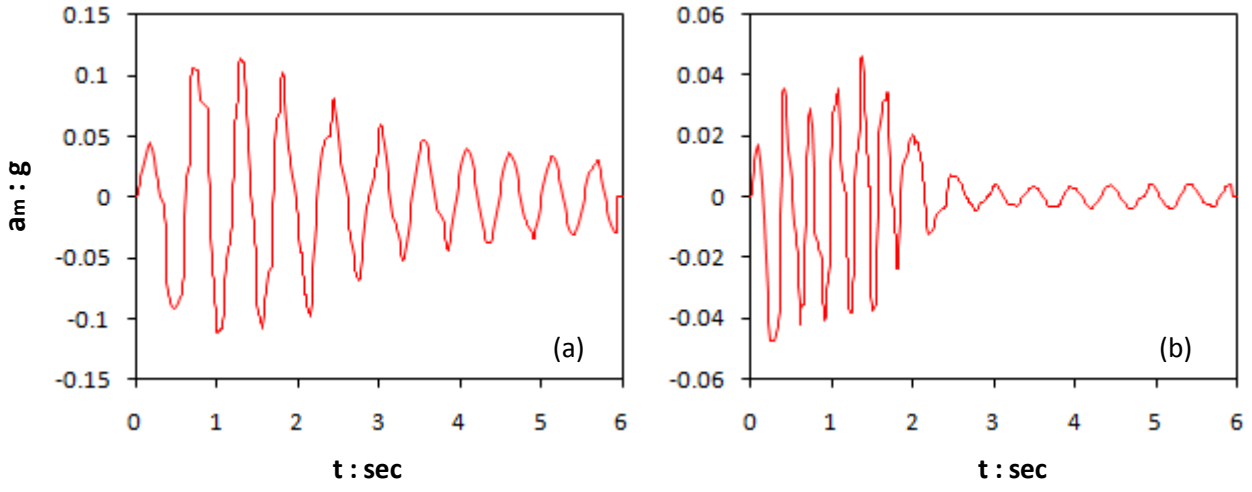

Figure 7.3 Acceleration time histories of lumped mass (bridge deck) along (a) x axis, (b) y axis .

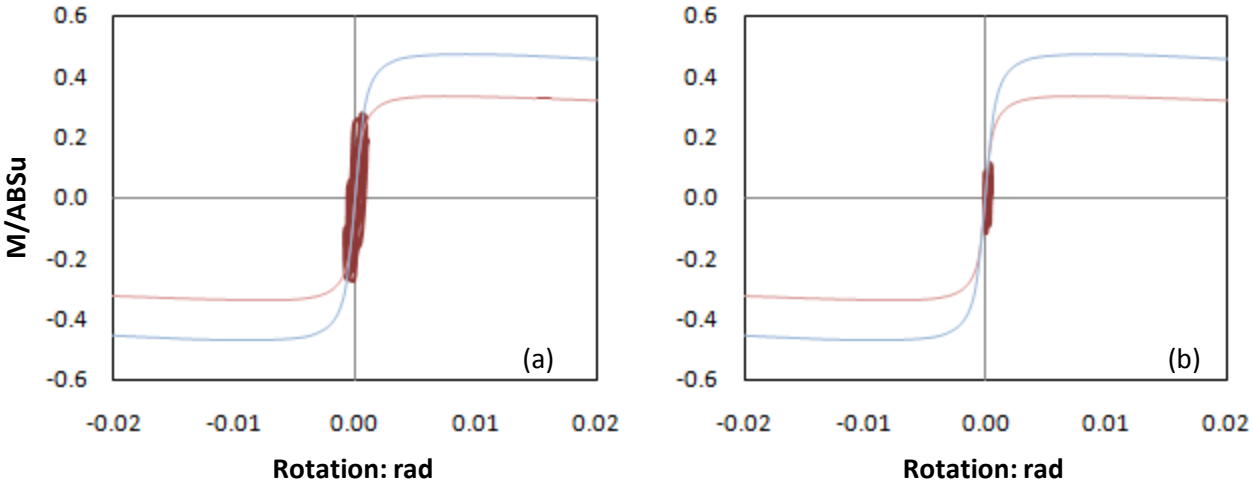

Figure 7.4 Normalized moment versus rotation loops in (a) X-Z plane, (b) Y-Z plane.

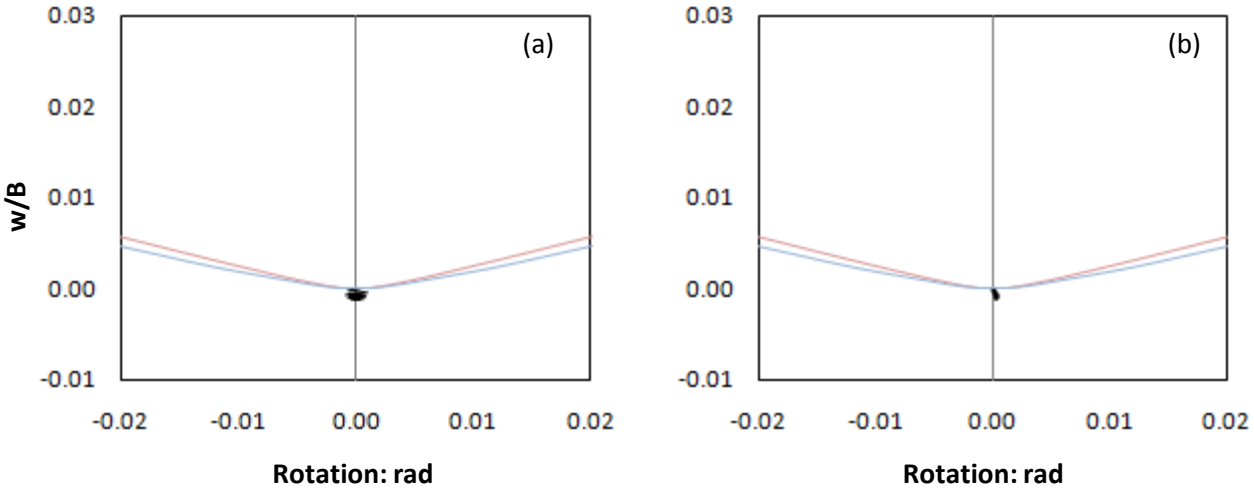

Figure 7.5 Normalized vertical settlement versus rotation loops n (a) X-Z plane, (b) Y-Z plane.. (Light blue line represents the static backbone curve for uni-axial loading, pink line represents bi-axial static loading .

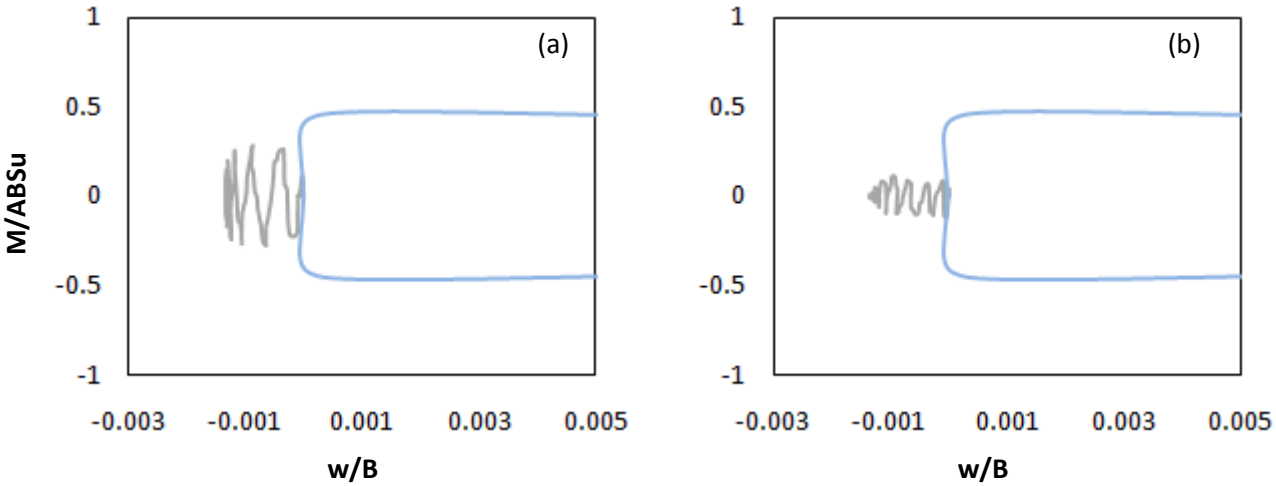

Figure 7.6 Normalized vertical settlement versus moment curves n (a) X-Z plane, (b) Y-Z plane. (The grey line stands for the dynamic response whereas the light blue line represents the static backbone curve)

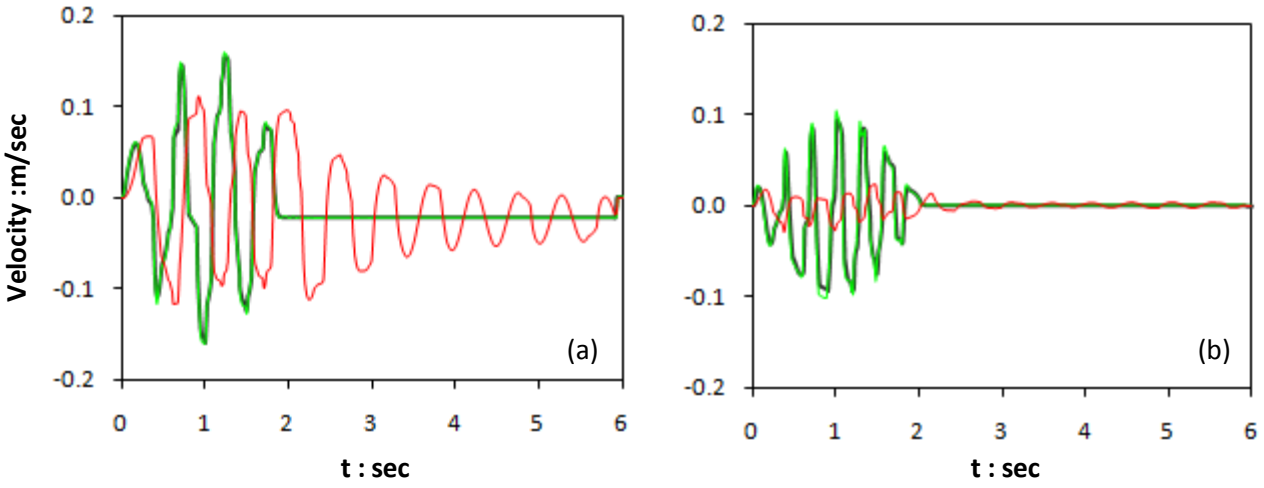

Figure 7.7 Velocity time histories of bedrock excitation along (a) x axis, (b) y axis . (black line represents bedrock, green line free field and red line the bridge deck)

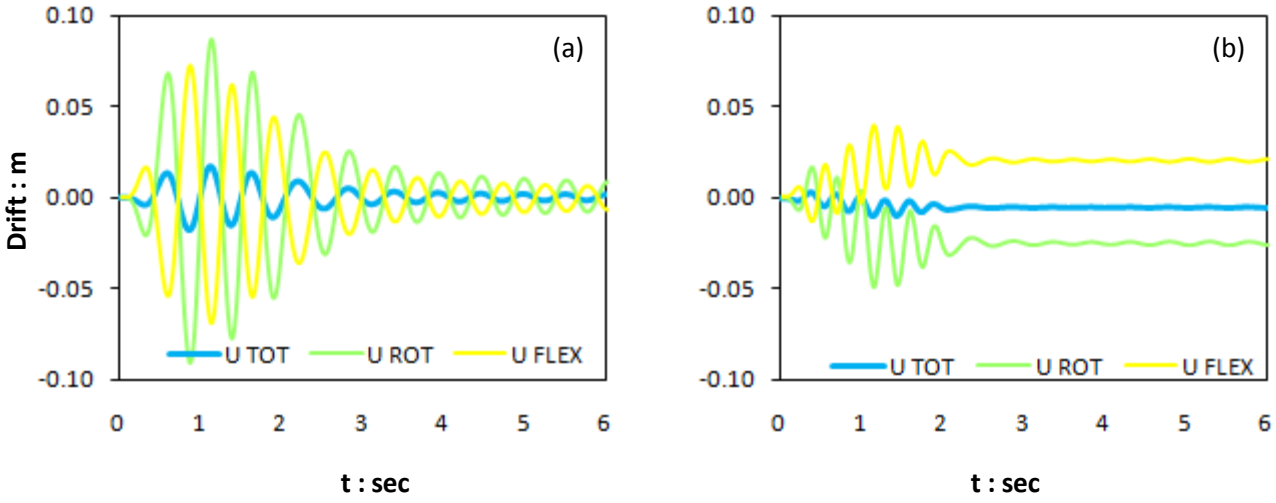

Figure 7.8 Horizontal displacement histories along (a) x axis, (b) y axis . (Blue line represents total drift, green line rotational component and yellow line flexural bending of pier.)

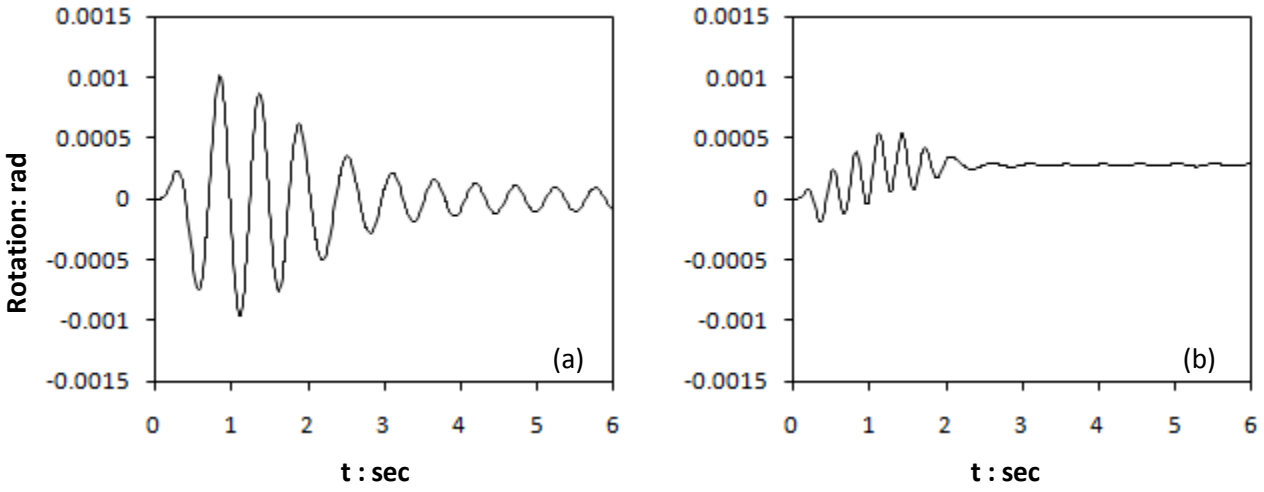

Figure 7.9 Rotation time histories of lumped mass (bridge deck) n (a) X-Z plane, (b) Y-Z plane.

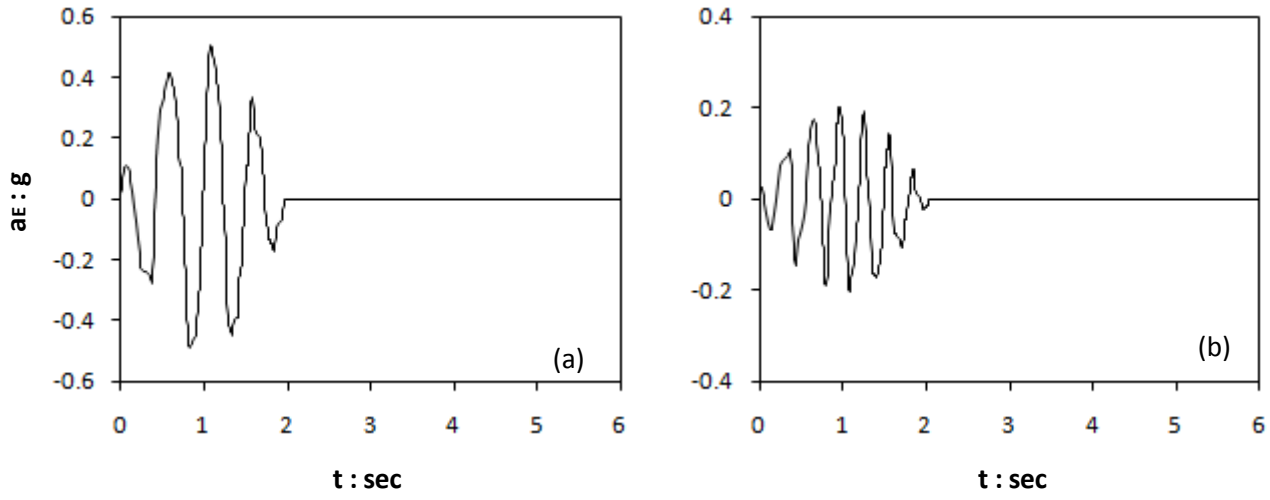

Figure 7.10 Acceleration time histories of bedrock excitation along (a) x axis, (b) y axis .

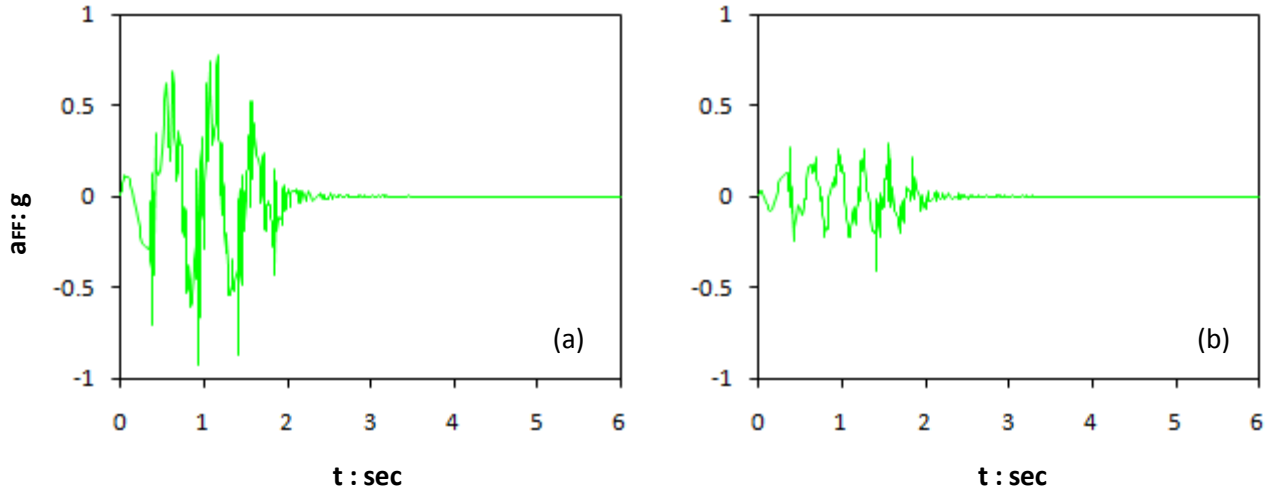

Figure 7.11 Acceleration time histories of free field along (a) x axis, (b) y axis

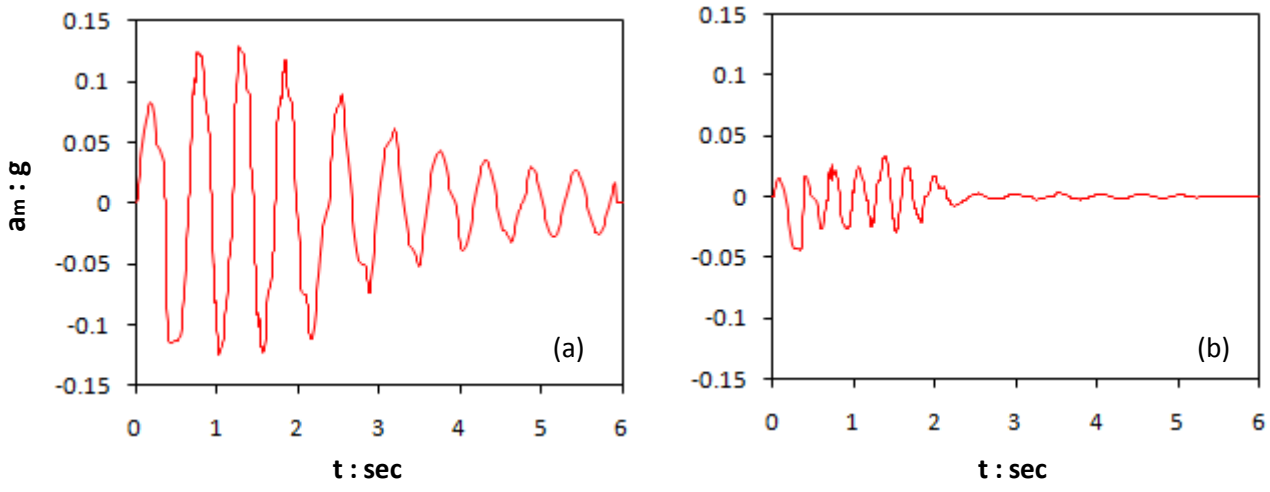

Figure 7.12 Acceleration time histories of lumped mass (bridge deck) along (a) x axis, (b) y axis .

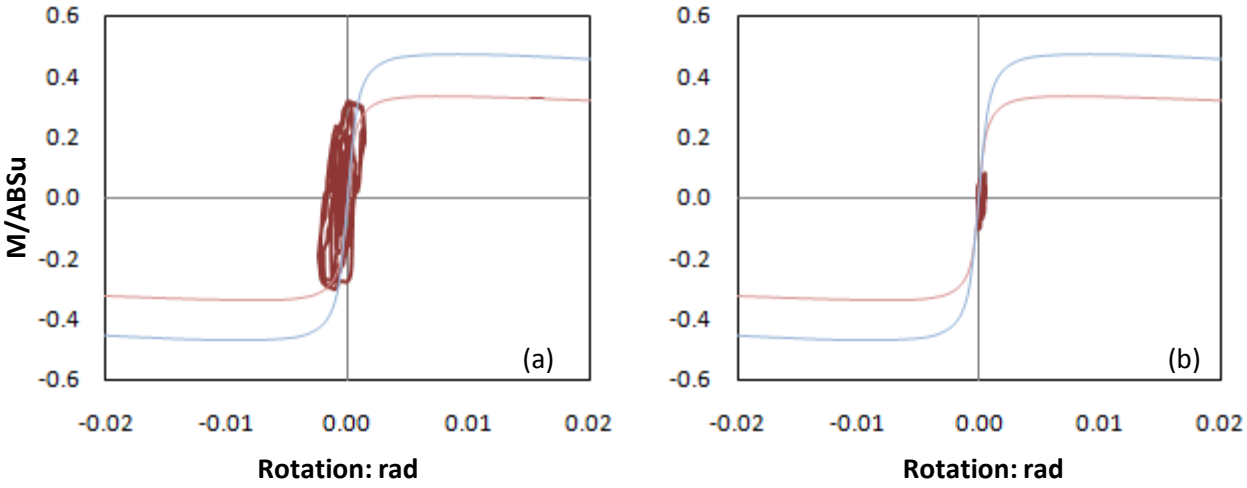

Figure 7.13 Normalized moment versus rotation loops in (a) X-Z plane, (b) Y-Z plane.

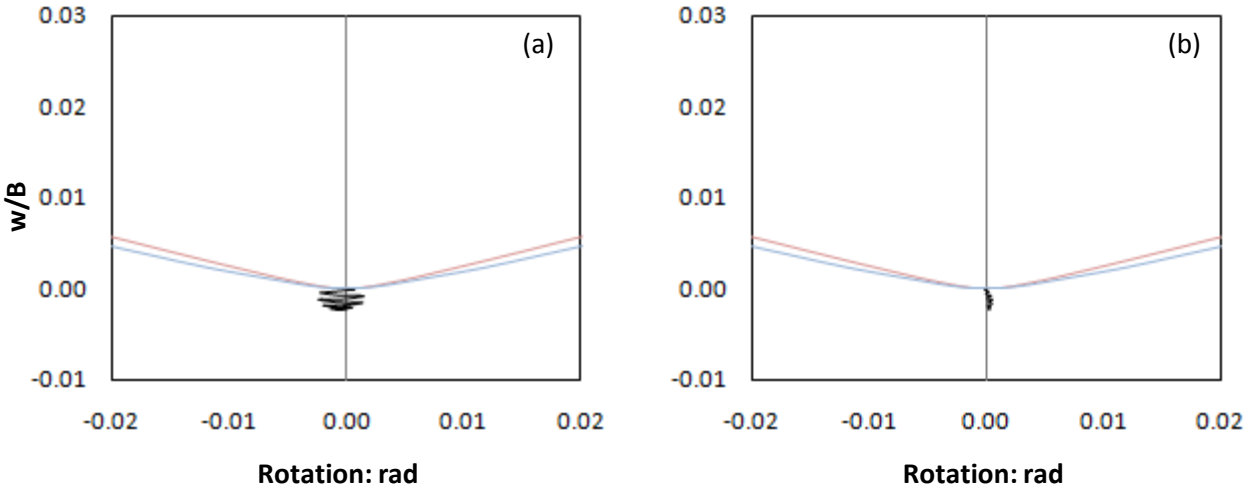

Figure 7.14 Normalized vertical settlement versus rotation loops n (a) X-Z plane, (b) Y-Z plane.. (Light blue line represents the static backbone curve for uni-axial loading, pink line represents bi-axial static loading .

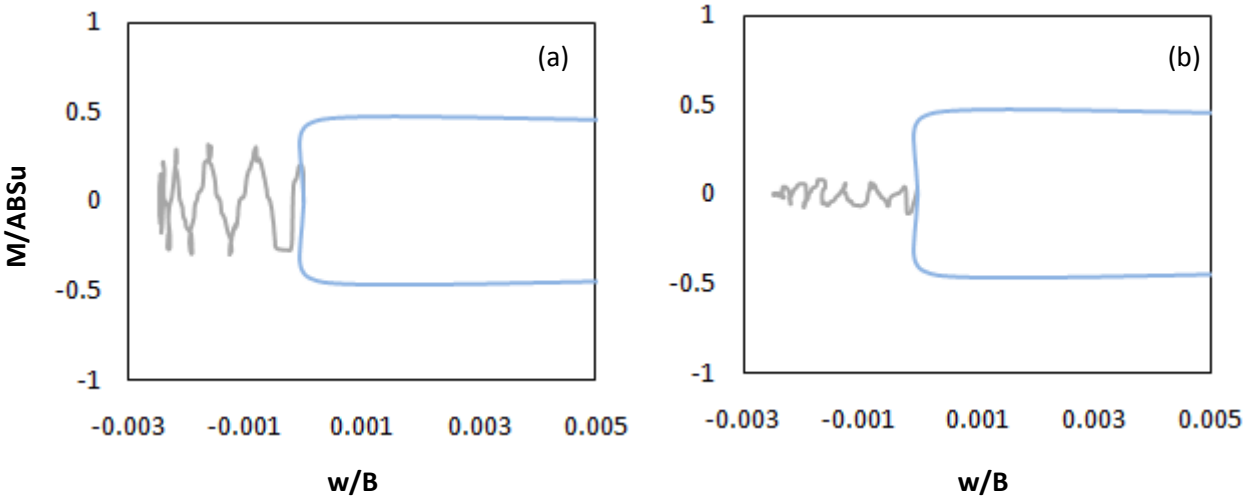

Figure 7.15 Normalized vertical settlement versus moment curves n (a) X-Z plane, (b) Y-Z plane. (The grey line stands for the dynamic response whereas the light blue line represents the static backbone curve)

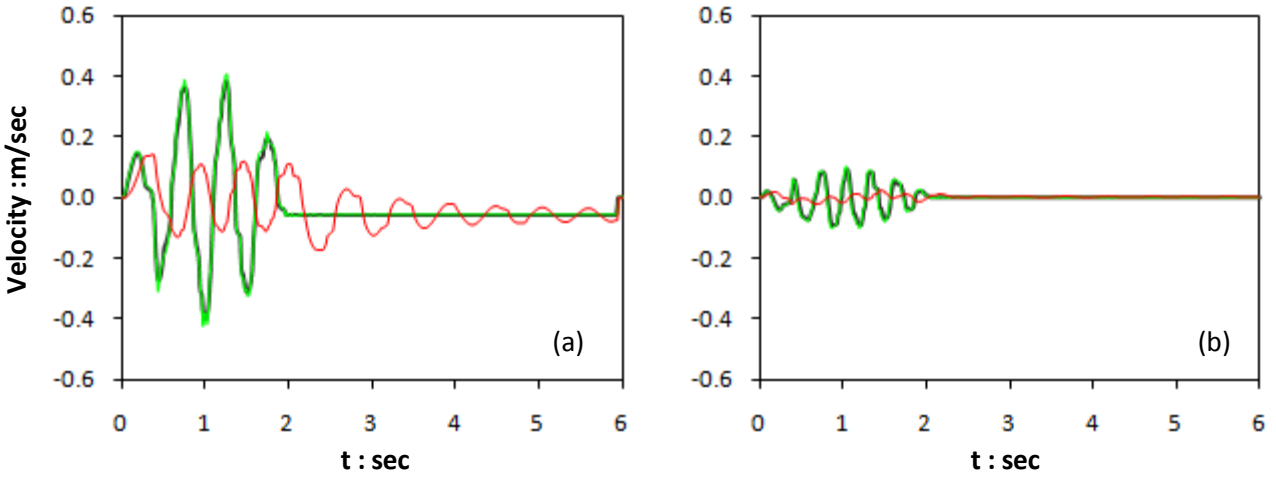

Figure 7.16: Velocity time histories of bedrock excitation along (a) x axis, (b) y axis . (black line represents bedrock, green line free field and red line the bridge deck)

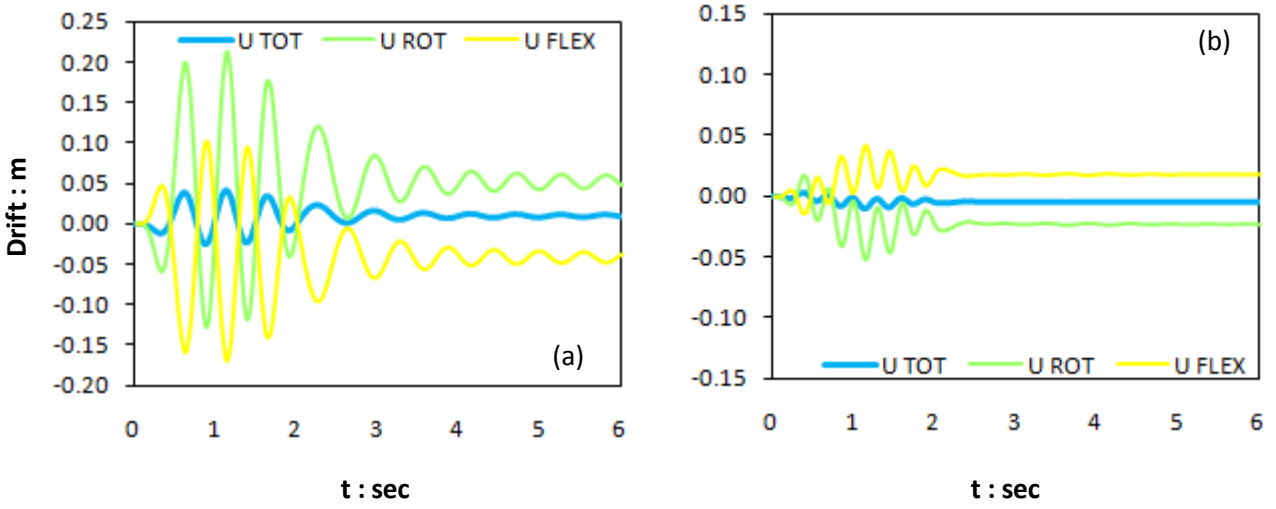

Figure 7.17: Horizontal displacement histories along (a) x axis, (b) y axis . (Blue line represents total drift, green line rotational component and yellow line flexural bending of pier.)

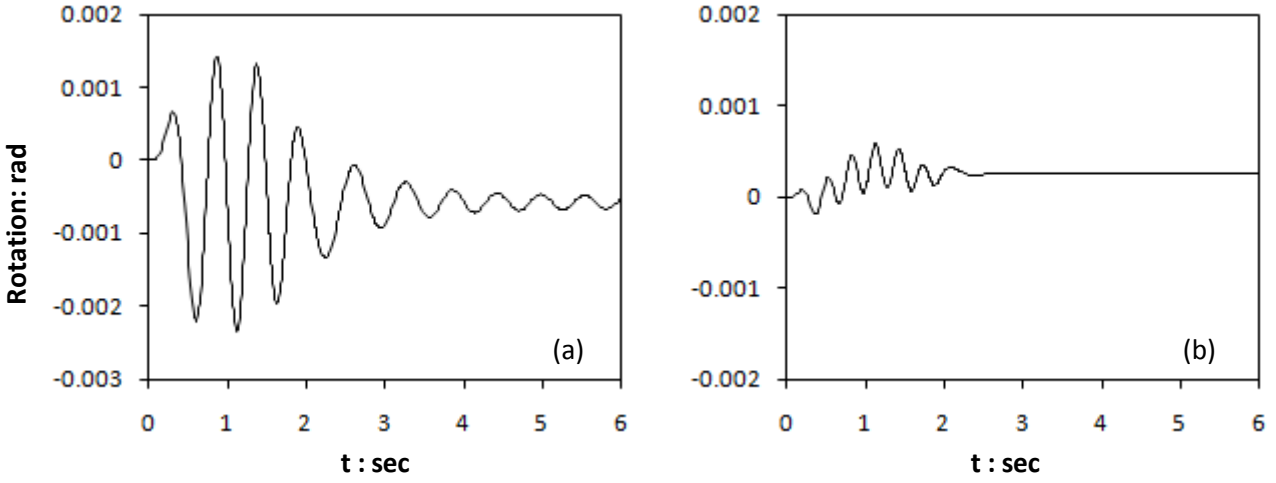

Figure 7.18: Rotation time histories of lumped mass (bridge deck) n (a) X-Z plane, (b) Y-Z plane.

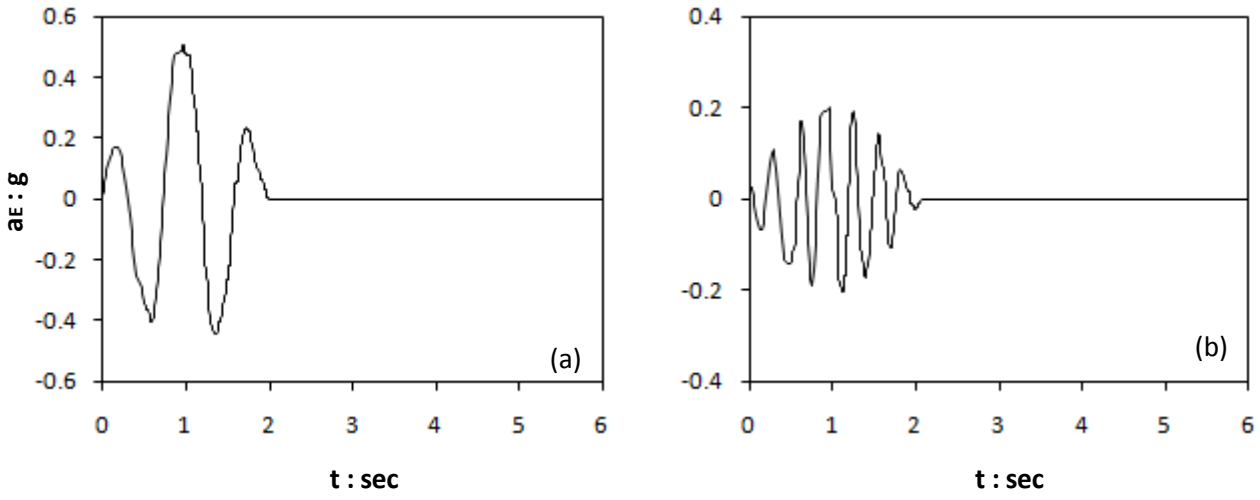

Figure 7.19. Acceleration time histories of bedrock excitation along (a) x axis, (b) y axis .

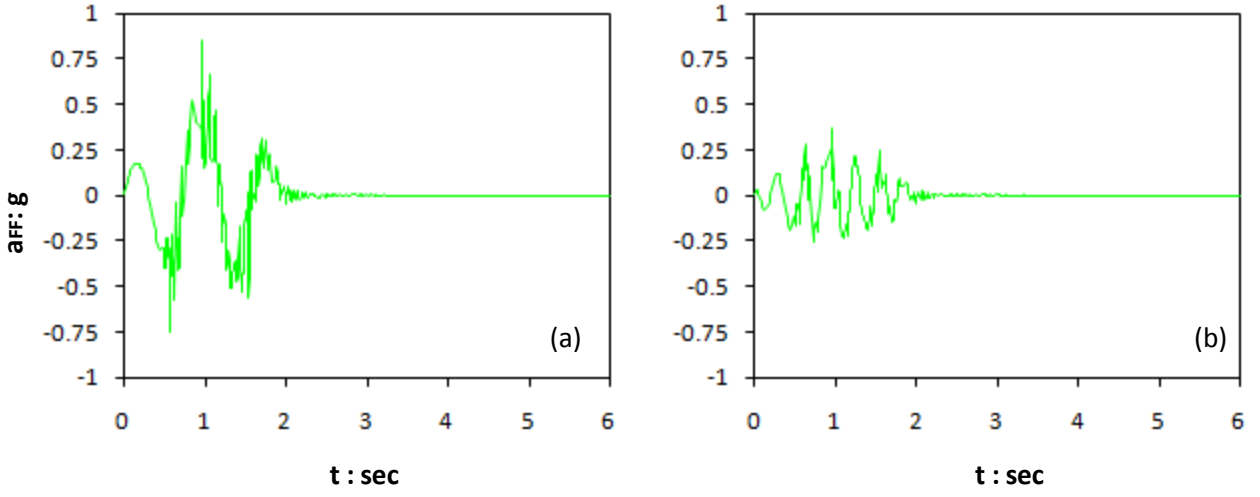

Figure 7.20: Acceleration time histories of free field along (a) x axis, (b) y axis

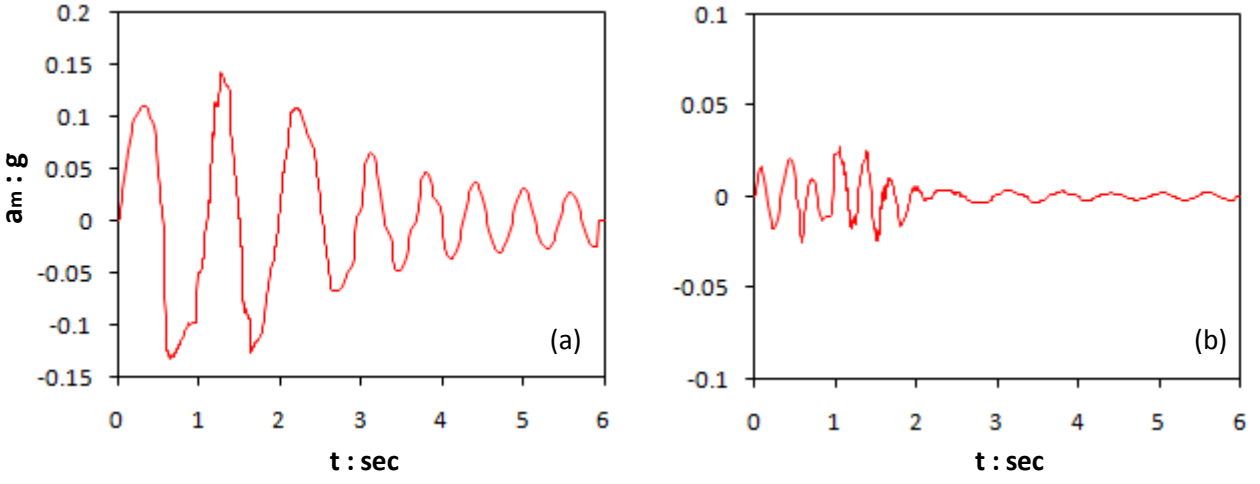

Figure 7.21: Acceleration time histories of lumped mass (bridge deck) along (a) x axis, (b) y axis .

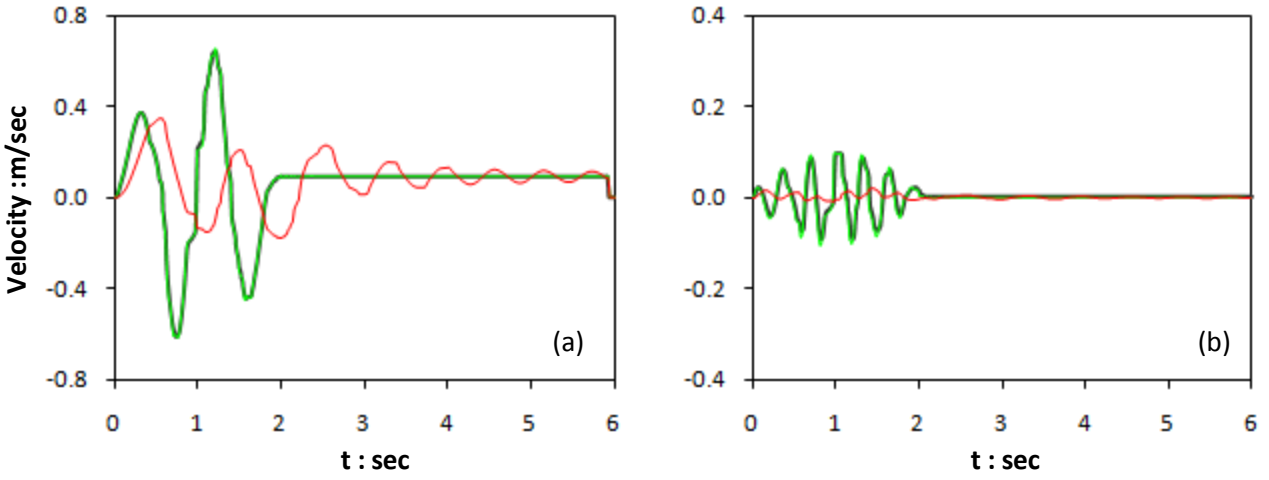

Figure 7.22: Velocity time histories of bedrock excitation along (a) x axis, (b) y axis . (black line represents bedrock, green line free field and red line the bridge deck)

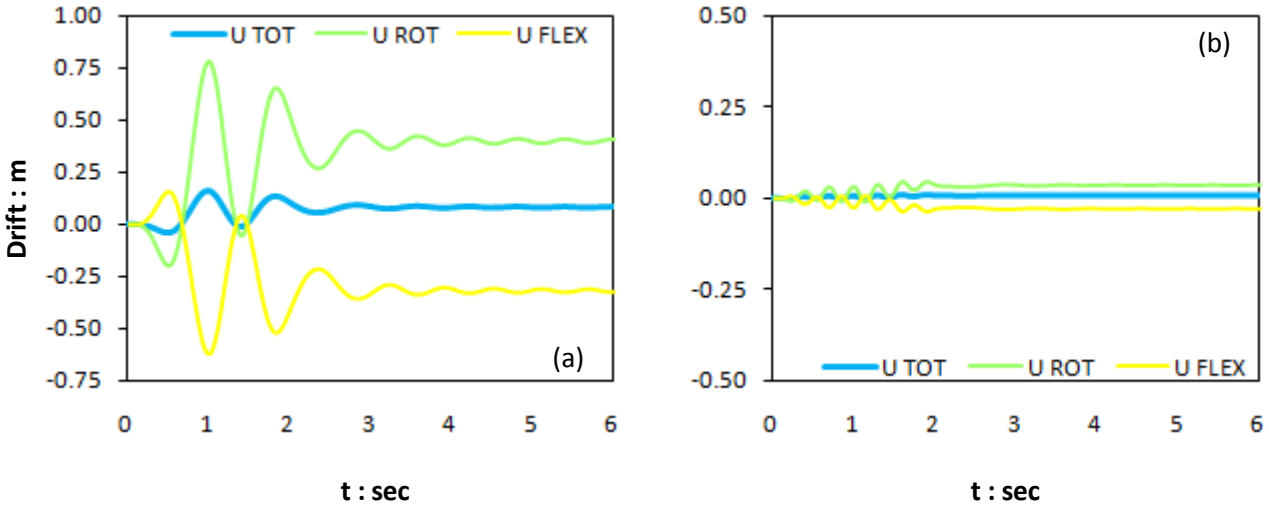

Figure 7.23: Horizontal displacement histories along (a) x axis, (b) y axis . (Blue line represents total drift, green line rotational component and yellow line flexural bending of pier.)

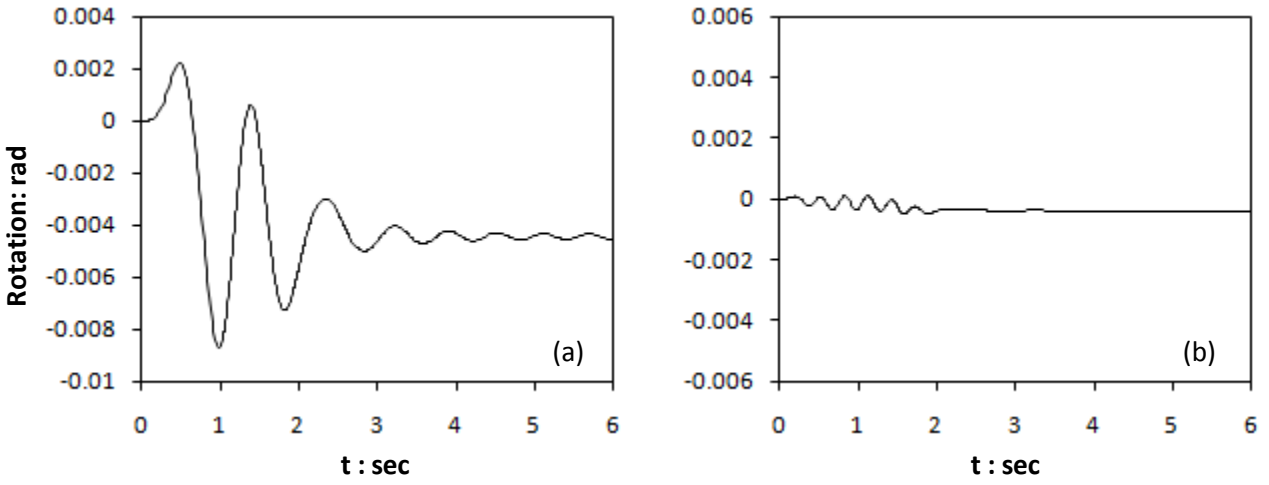

Figure 7.24: Rotation time histories of lumped mass (bridge deck) n (a) X-Z plane, (b) Y-Z plane.

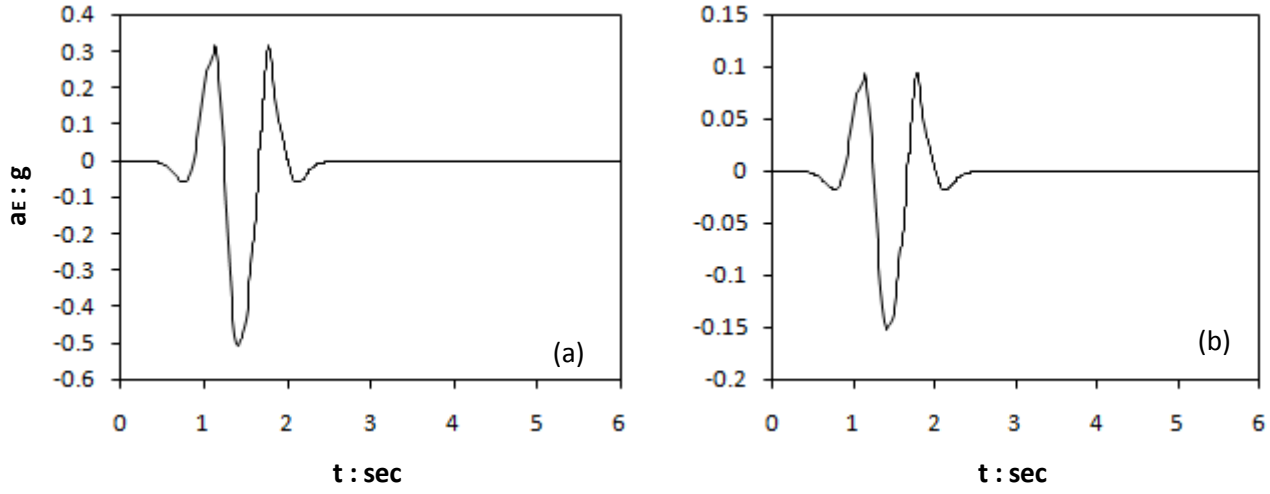

Figure 7.25. Acceleration time histories of bedrock excitation along (a) x axis, (b) y axis .

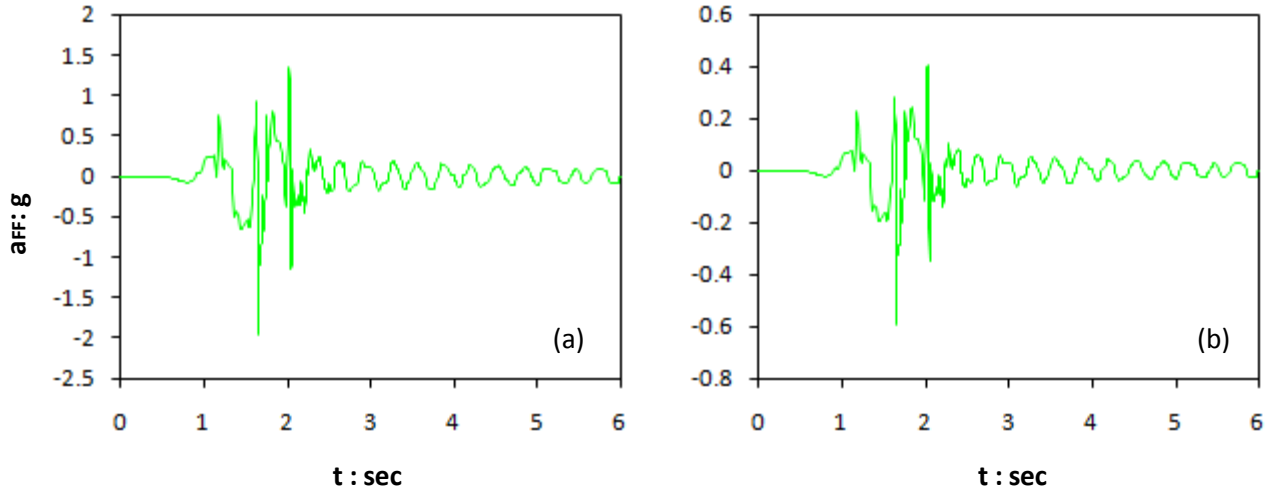

Figure 7.26: Acceleration time histories of free field along (a) x axis, (b) y axis

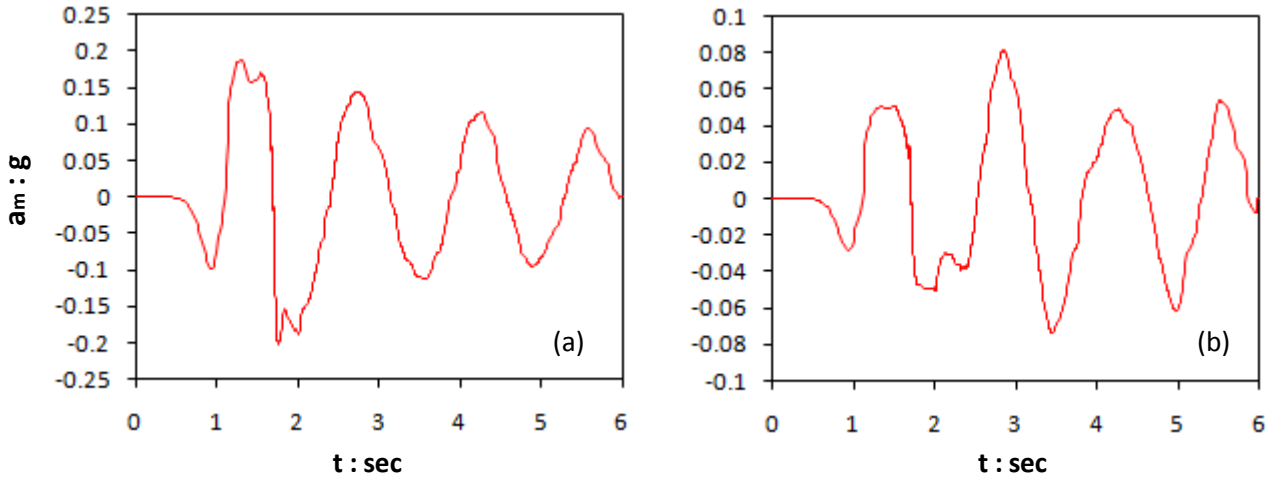

Figure 7.27: Acceleration time histories of lumped mass (bridge deck) along (a) x axis, (b) y axis .

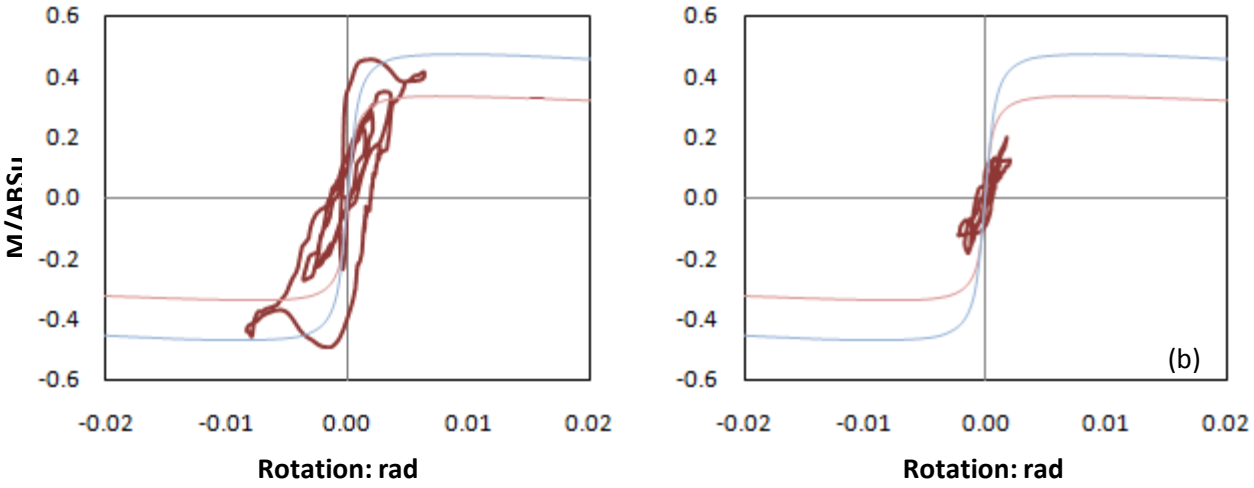

Figure 7.28: Normalized moment versus rotation loops in (a) X-Z plane, (b) Y-Z plane.

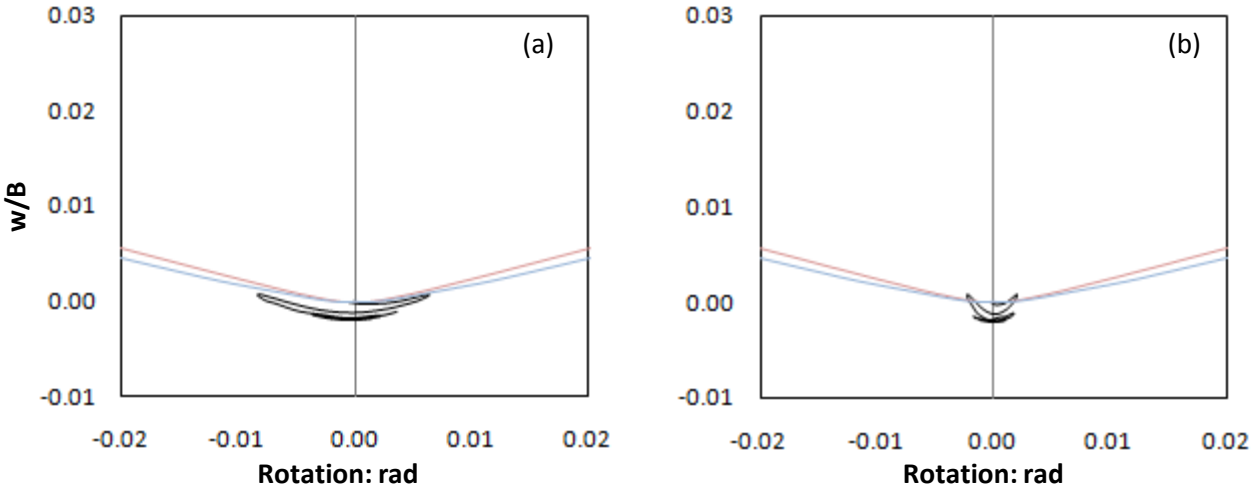

Figure 7.29: Normalized vertical settlement versus rotation loops n (a) X-Z plane, (b) Y-Z plane.. (Light blue line represents the static backbone curve for uni-axial loading, pink line represents bi-axial static loading .

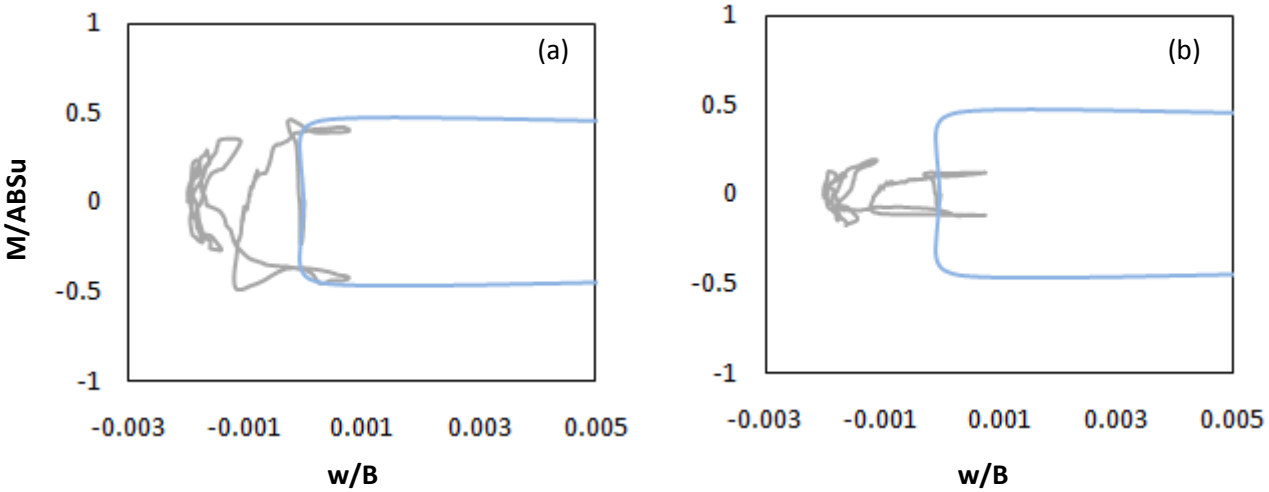

Figure 7.30: Normalized vertical settlement versus moment curves n (a) X-Z plane, (b) Y-Z plane. (The grey line stands for the dynamic response whereas the light blue line represents the static backbone curve)

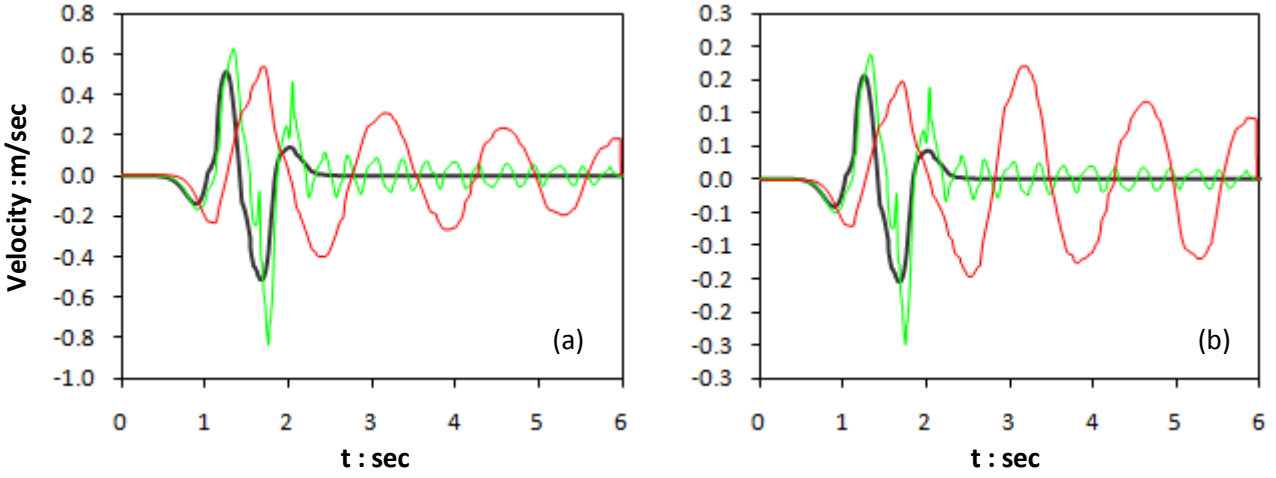

Figure 7.31: Velocity time histories of bedrock excitation along (a) x axis, (b) y axis . (black line represents bedrock, green line free field and red line the bridge deck)

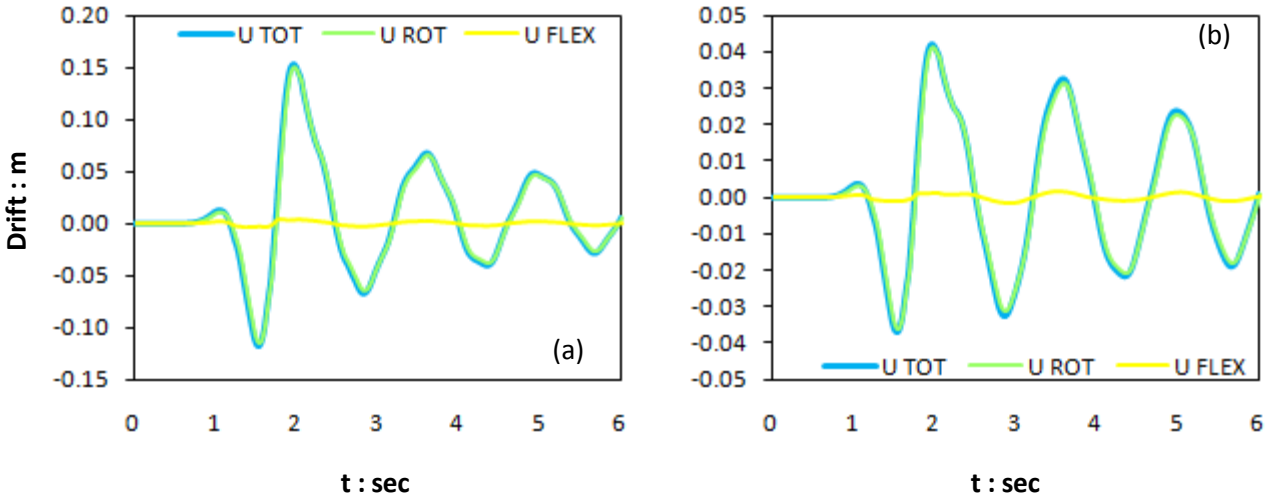

Figure 7.32: Horizontal displacement histories along (a) x axis, (b) y axis . (Blue line represents total drift, green line rotational component and yellow line flexural bending of pier.)

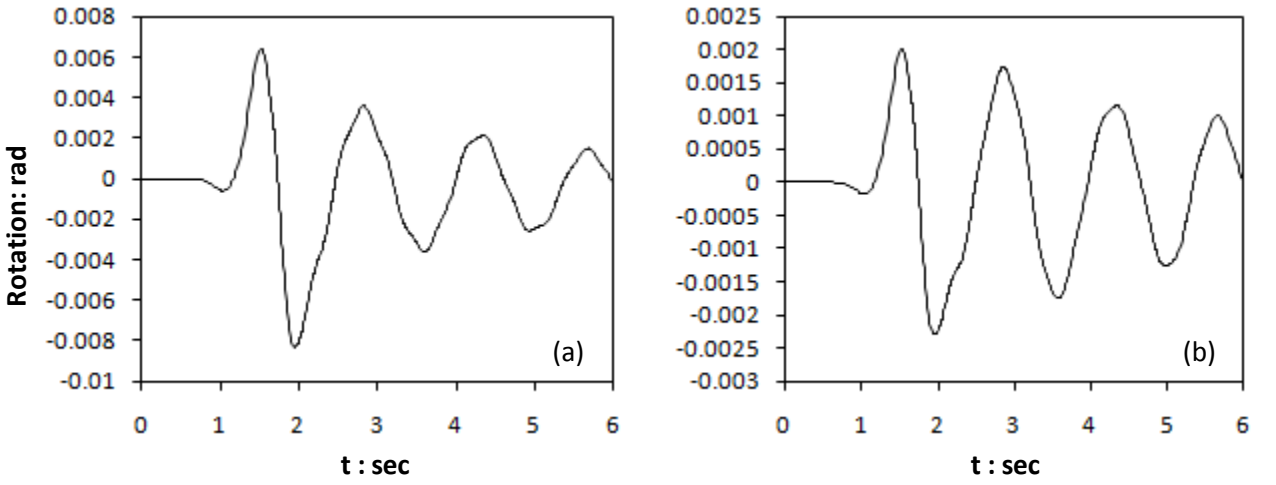

Figure 7.33: Rotation time histories of lumped mass (bridge deck) n (a) X-Z plane, (b) Y-Z plane.

Tsang pulses Loading

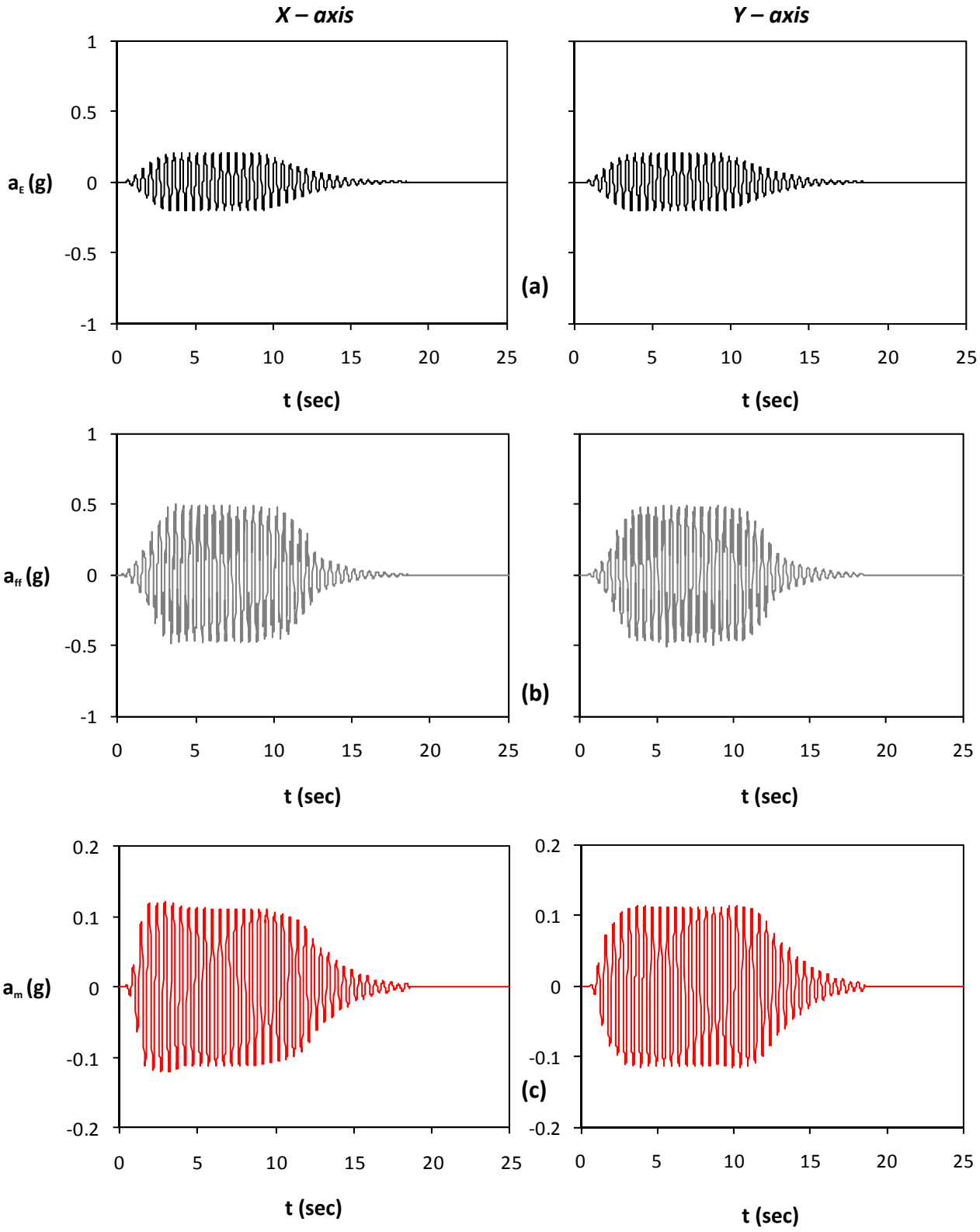

Figure 8.1. Seismic excitation in both directions, Tsang 2 A_x = 0.2 g and A_y = 0.2 g asynchronous : (a) acceleration time histories of bedrock excitation along the *x* axis (left) and the *y* axis (right) ; (b) acceleration time histories at the free field ; and (c) acceleration time histories of lumped mass.

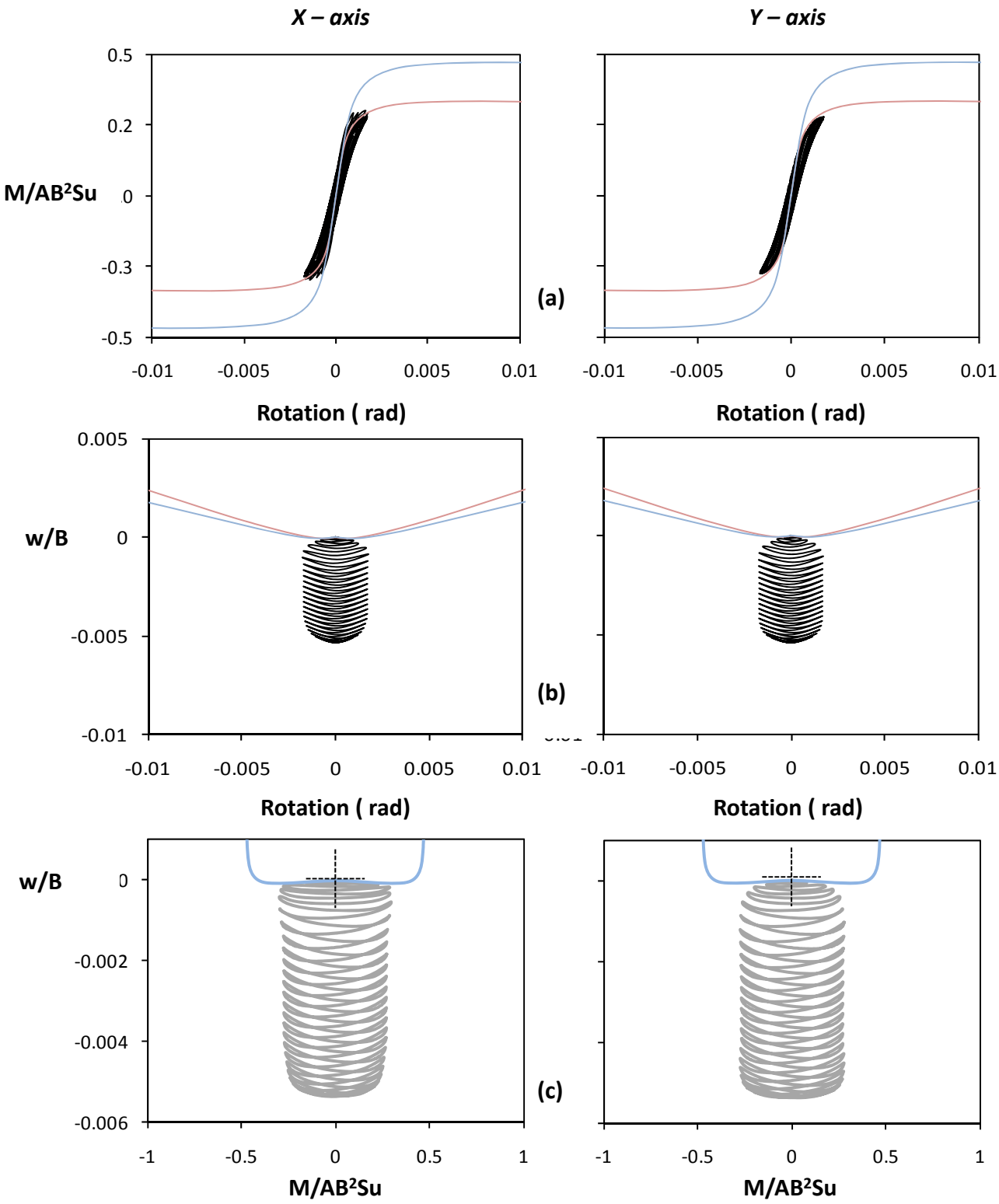

Figure 8.2. Seismic excitation in both directions, Tsang 2 A_x = 0.2 g and A_y = 0.2 g asynchronous :

(a) Normalized moment versus rotation along the *x* axis (left) and the *y* axis (right) ;

(b) Normalized to width vertical settlement versus rotation ; and

(c) Normalized vertical settlement to moment along the *x* axis (left) and the *y* axis (right) .

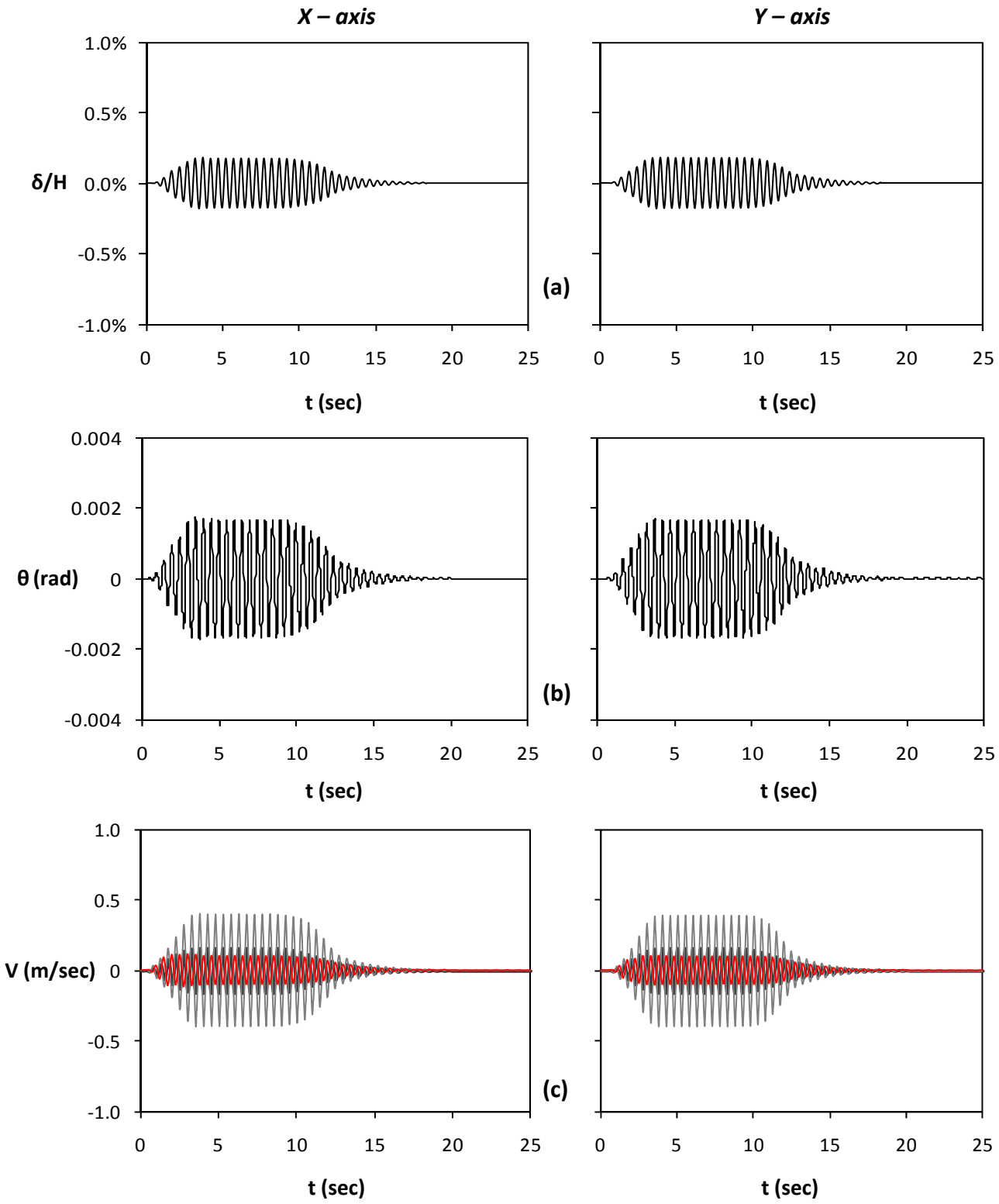

Figure 8.3. Seismic excitation in both directions, Tsang 2 A_x = 0.2 g and A_y = 0.2 g asynchronous :
(a) Horizontal displacement normalized to height time histories along the *x* axis (left) and the *y* axis (right) ; (b) rotation time histories along the *x* axis (left) and the *y* axis (right) ; (c) velocity time histories (Grey line stands for free field motion and red line for lumped mass)

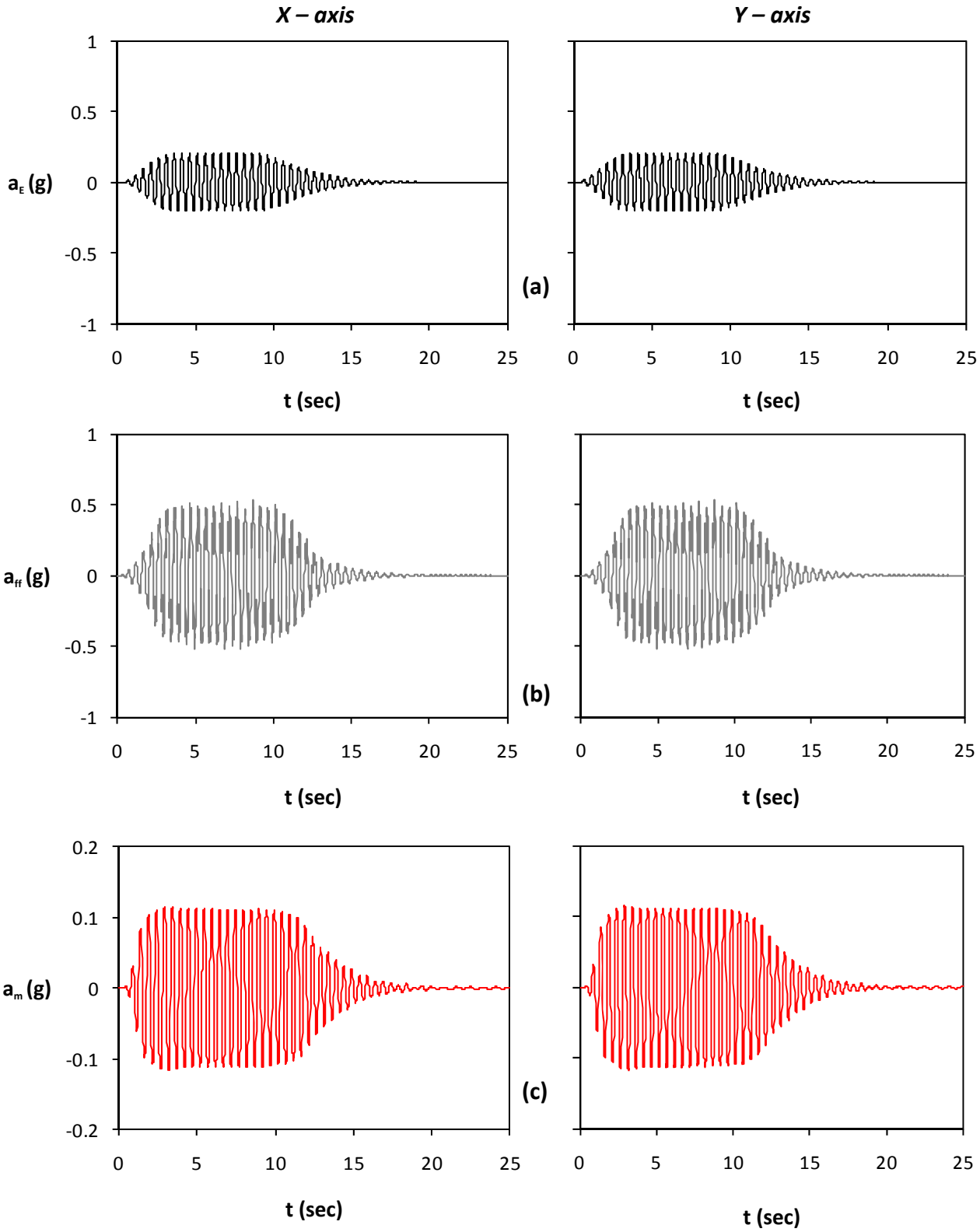

Figure 8.4. Seismic excitation in both directions, Tsang 2 A_x = 0.2 g and A_y = 0.2 g synchronous : (a) acceleration time histories of bedrock excitation along the *x* axis (left) and the *y* axis (right) ; (b) acceleration time histories at the free field ; and (c) acceleration time histories of lumped mass.

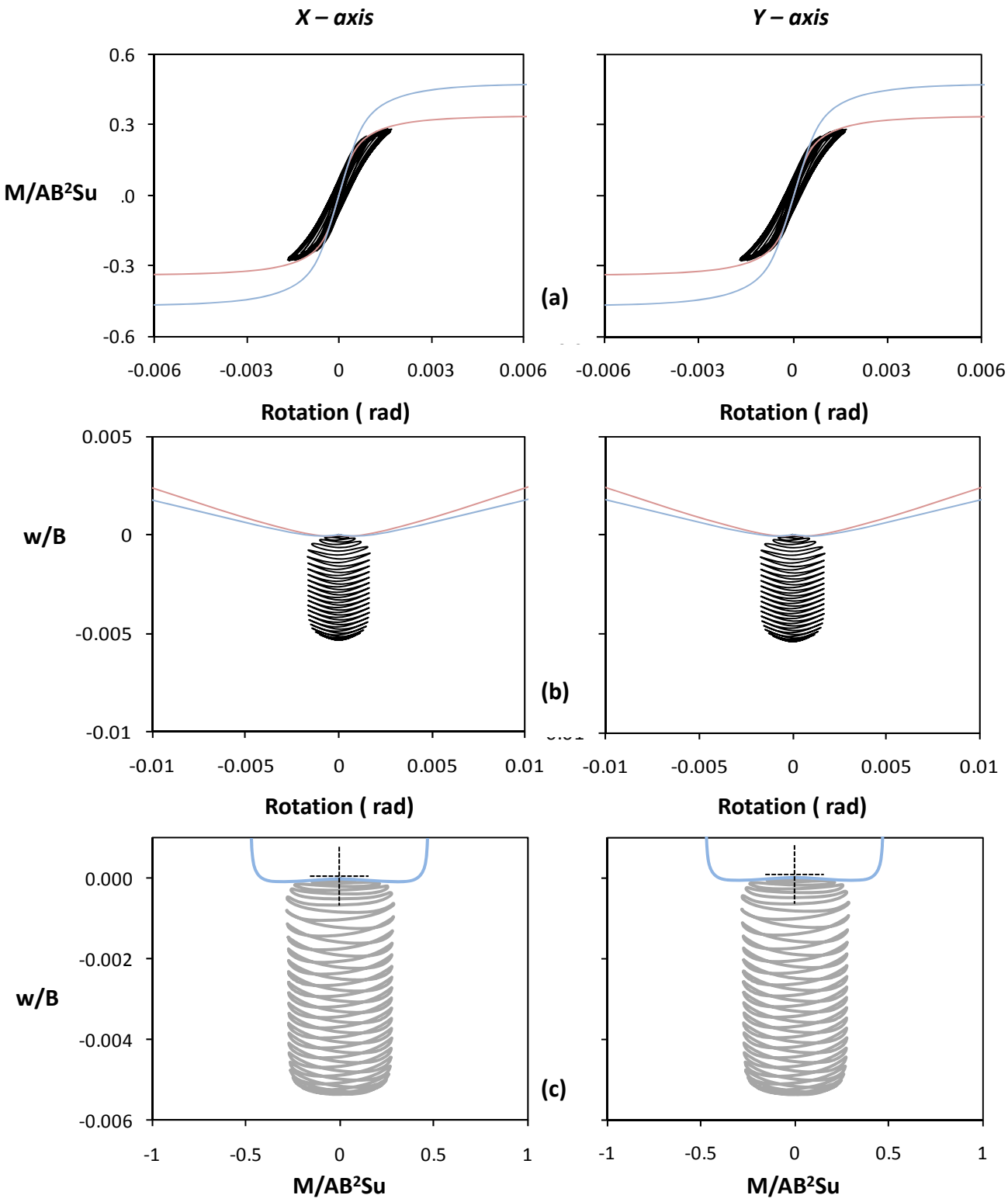

Figure 8.5. Seismic excitation in both directions, Tsang 2 A_x = 0.2 g and A_y = 0.2 g synchronous :

(a) Normalized moment versus rotation along the *x* axis (left) and the *y* axis (right) ;

(b) Normalized to width vertical settlement versus rotation ; and

(c) Normalized vertical settlement to moment along the *x* axis (left) and the *y* axis (right) .

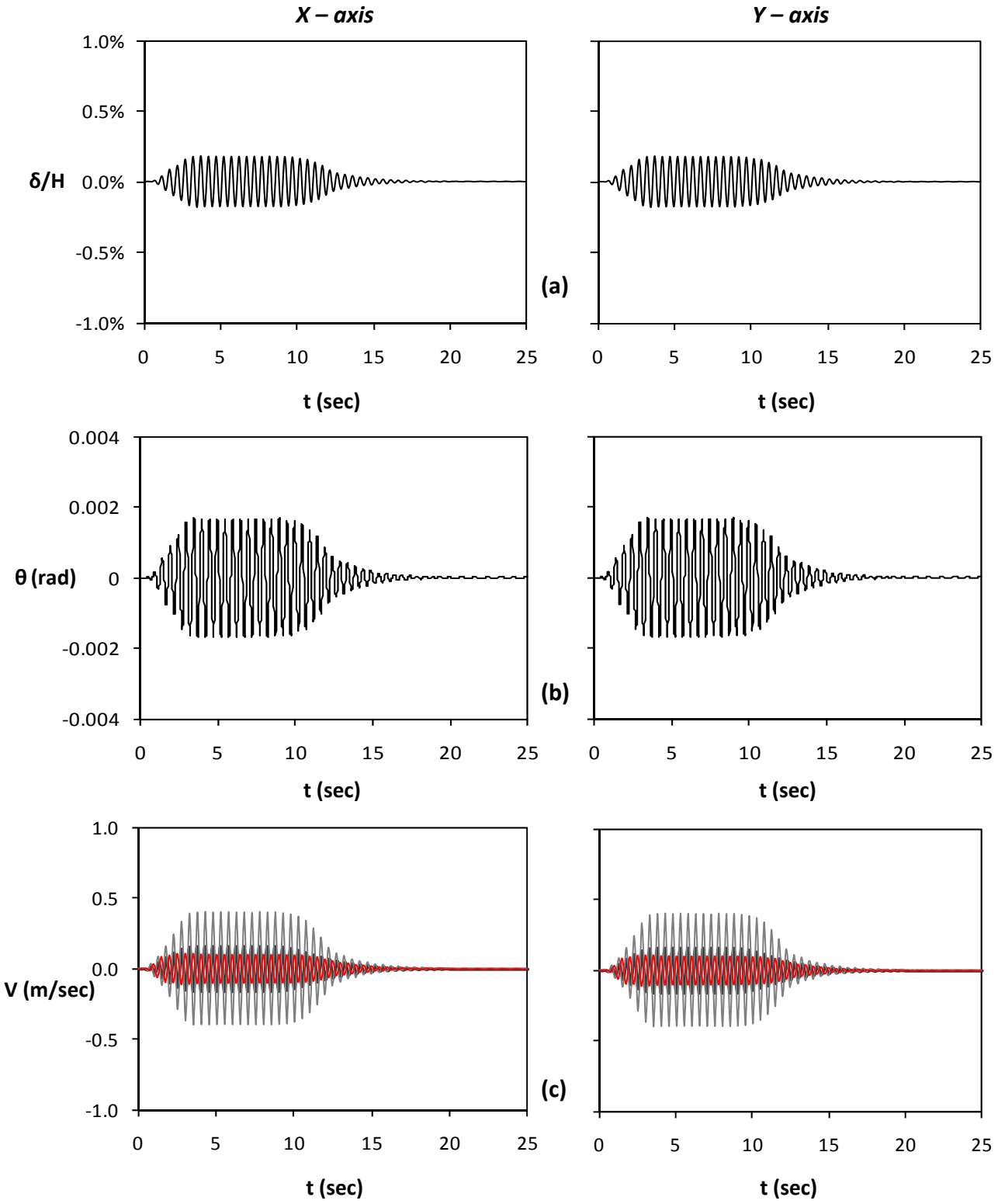

Figure 8.6. Seismic excitation in both directions, Tsang 2 A_x = 0.2 g and A_y = 0.2 g synchronous :
(a) Horizontal displacement normalized to height time histories along the *x* axis (left) and the *y* axis (right) ; (b) rotation time histories along the *x* axis (left) and the *y* axis (right) ; (c) velocity time histories (Grey line stands for free field motion and red line for lumped mass)

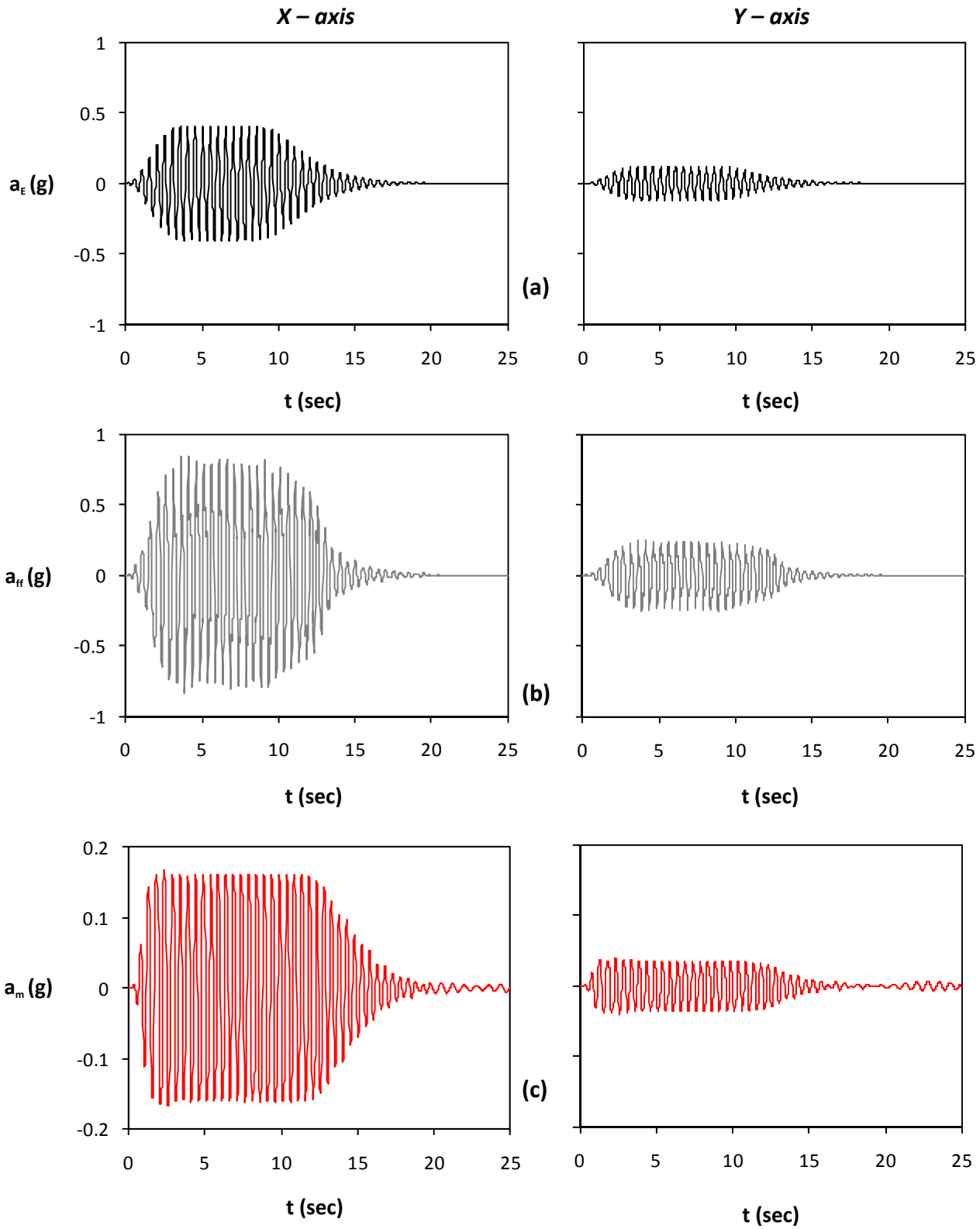

Figure 8.7. Seismic excitation in both directions, Tsang 2 A_x = 0.4 g and A_y =30% x 0.4 g : (a) acceleration time histories of bedrock excitation along the *x* axis (left) and the *y* axis (right) ; (b) acceleration time histories at the free field ; and (c) acceleration time histories of lumped mass.

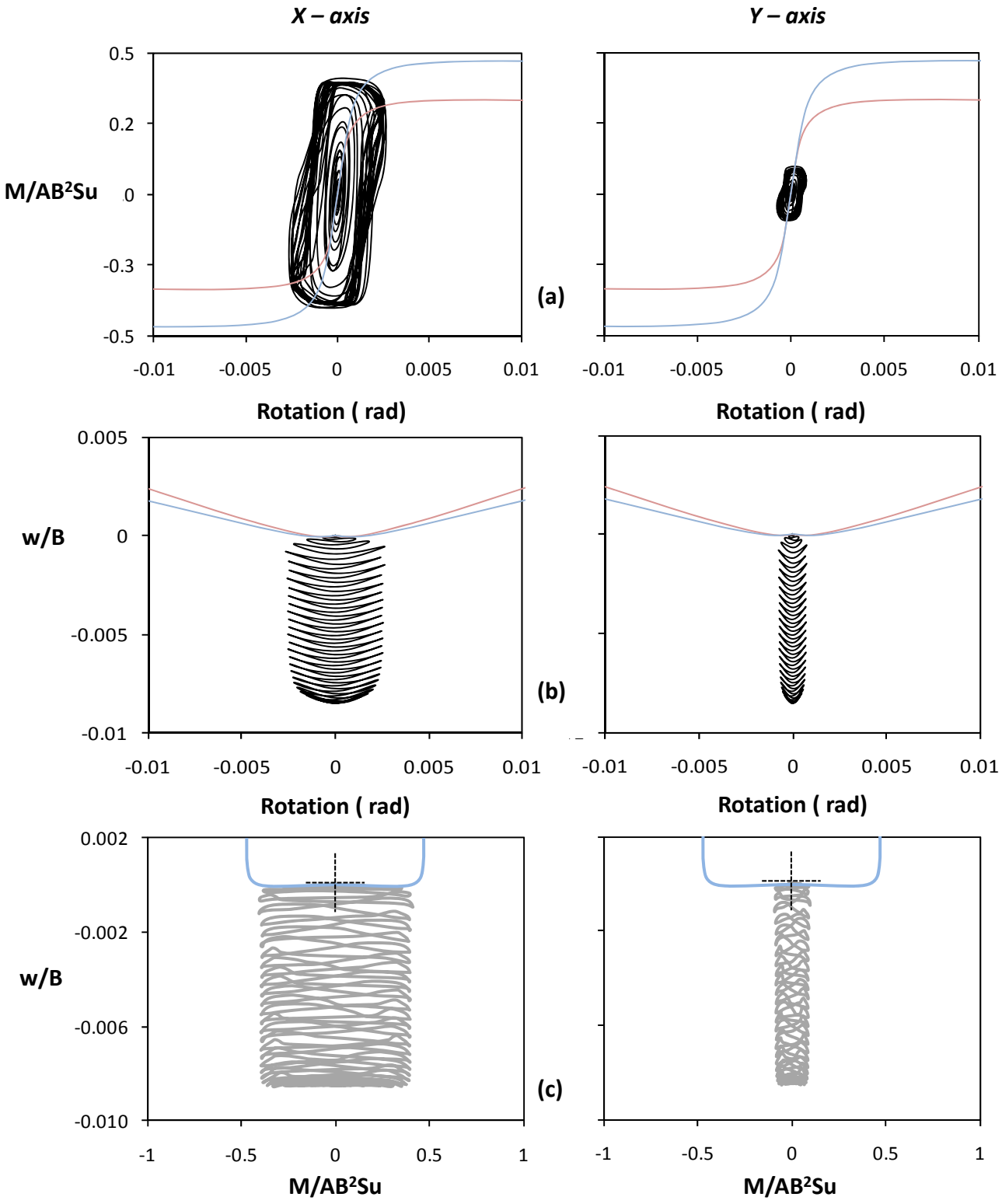

Figure 8.8. Seismic excitation in both directions, Tsang 2 A_x = 0.4 g and A_y =30% x 0.4 g :
(a) Normalized moment versus rotation along the *x* axis (left) and the *y* axis (right) ;
(b) Normalized to width vertical settlement versus rotation ; and
(c) Normalized vertical settlement to moment along the *x* axis (left) and the *y* axis (right) .

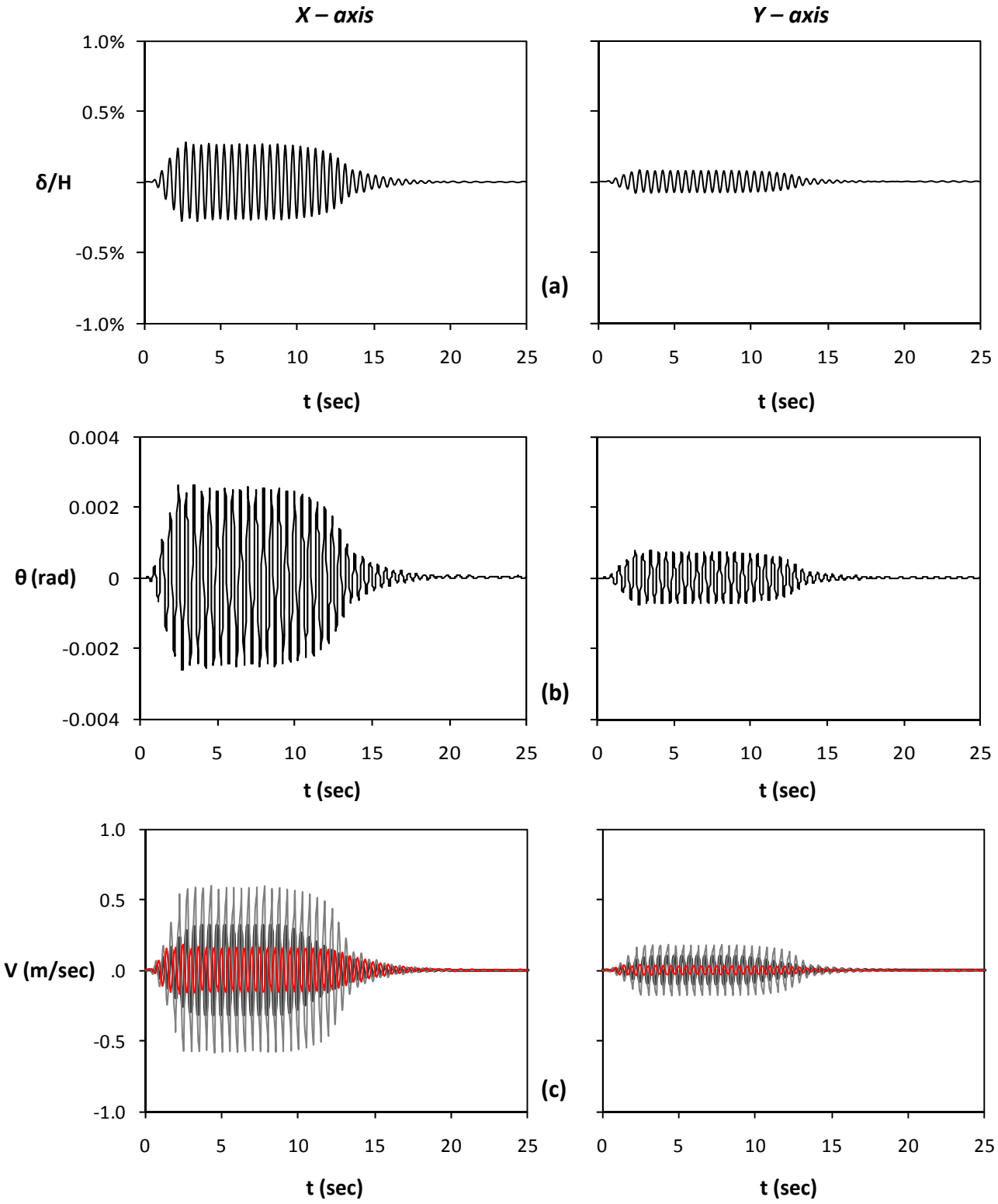

Figure 8.9. Seismic excitation in both directions, Tsang 2 A_x = 0.4 g and A_y =30% x 0.4 g : (a) Horizontal displacement normalized to height time histories along the *x* axis (left) and the *y* axis (right) ; (b) rotation time histories along the *x* axis (left) and the *y* axis (right) ; (c) velocity time histories (Grey line stands for free field motion and red line for lumped mass)

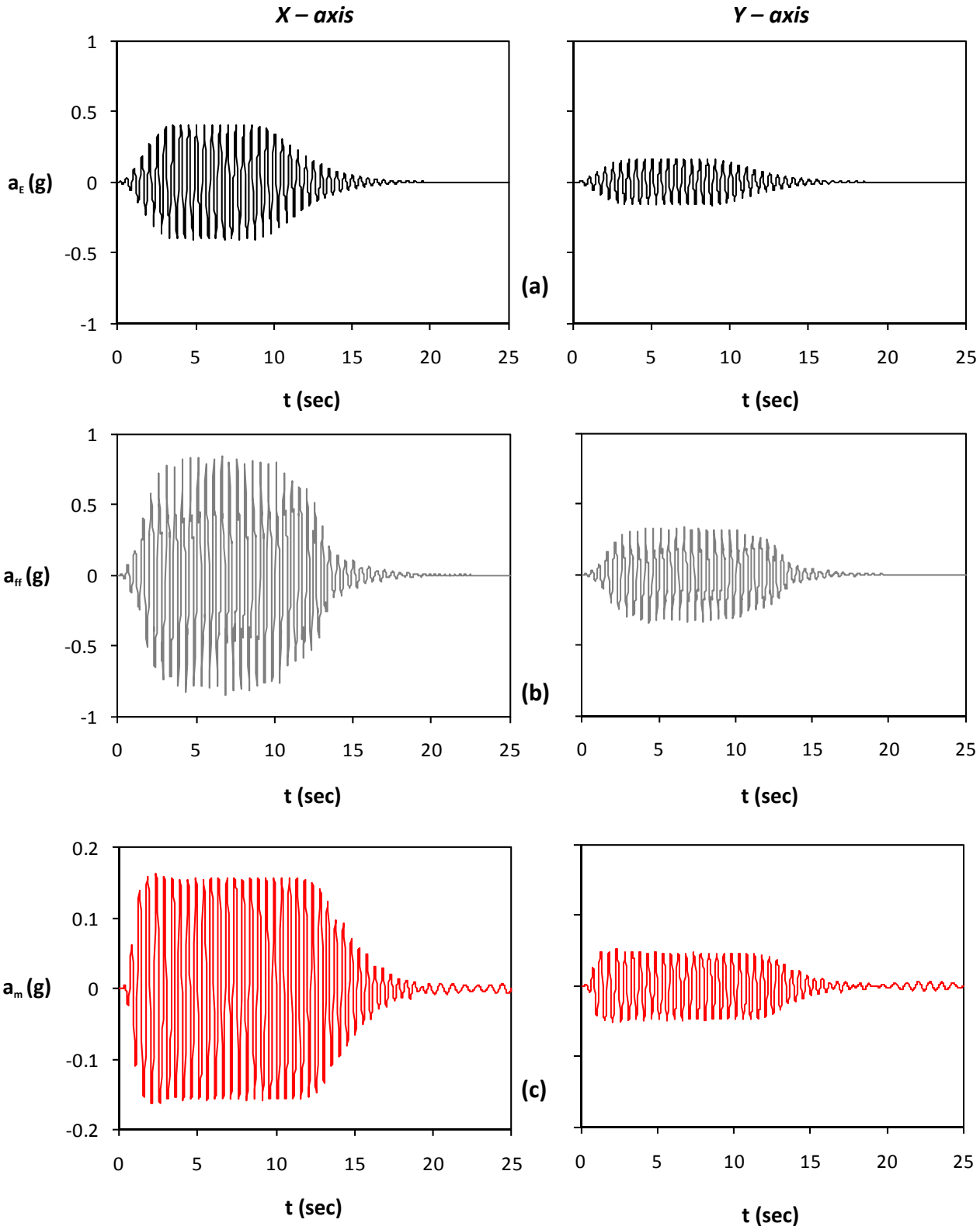

Figure 8.10. Seismic excitation in both directions, Tsang 2 A_x = 0.4 g and A_y = 40% x 0.4 g asynchronous : (a) acceleration time histories of bedrock excitation along the *x* axis (left) and the *y* axis (right) ; (b) acceleration time histories at the free field ; and (c) acceleration time histories of lumped mass.

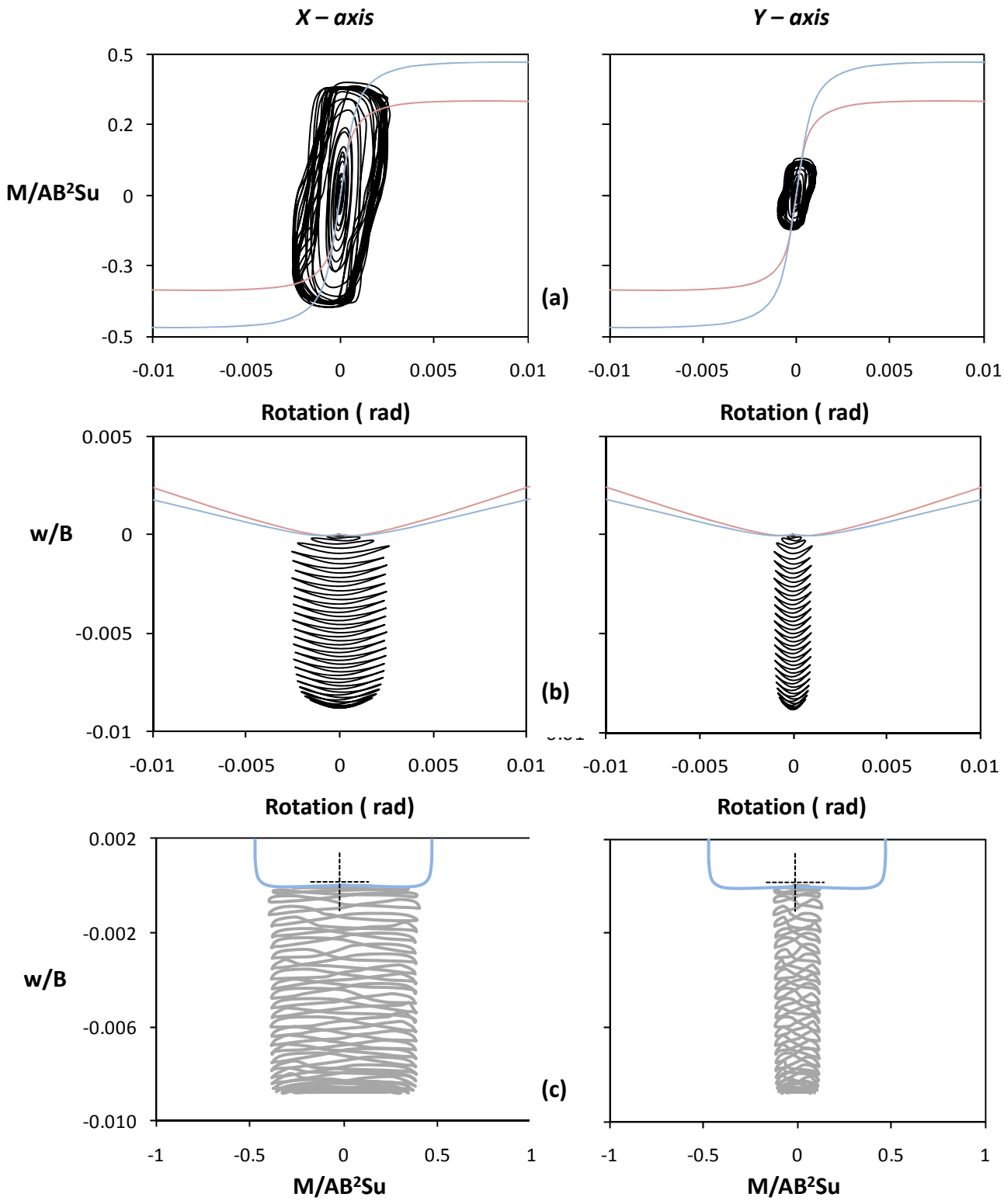

Figure 8.11. Seismic excitation in both directions, Tsang 2 A_x = 0.4 g and A_y = 40% x 0.4 g asynchronous :

(a) Normalized moment versus rotation along the *x* axis (left) and the *y* axis (right) ;

(b) Normalized to width vertical settlement versus rotation ; and

(c) Normalized vertical settlement to moment along the *x* axis (left) and the *y* axis (right) .

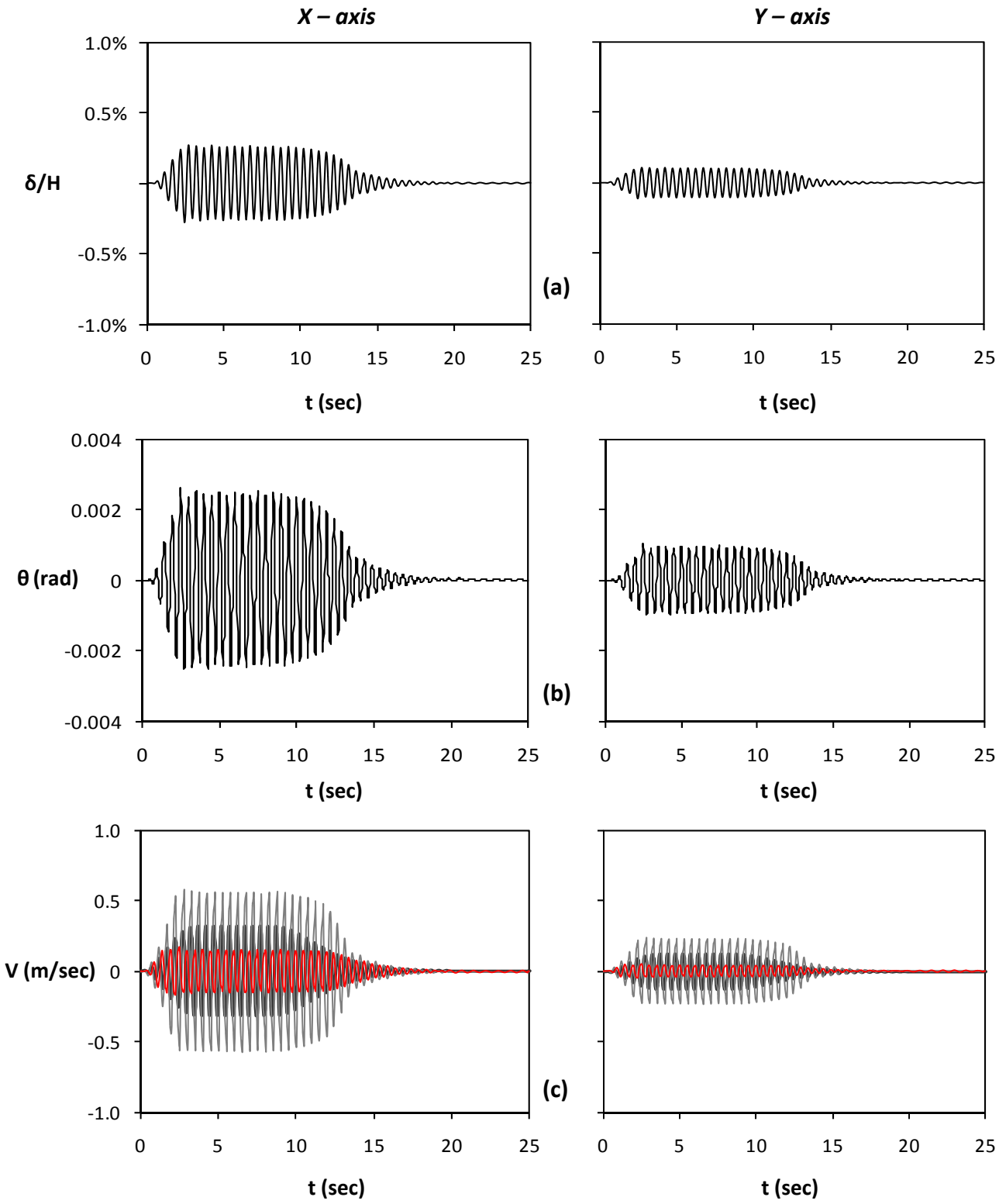

Figure 8.12. Seismic excitation in both directions, Tsang 2 A_x = 0.2 g and A_y =40% x 0.2 g asynchronous :
(a) Horizontal displacement normalized to height time histories along the *x* axis (left) and the *y* axis (right) ; (b) rotation time histories along the *x* axis (left) and the *y* axis (right) ; (c) velocity time histories (Grey line stands for free field motion and red line for lumped mass)

REFERENCES:

ROCKING

1. Anderson, D. L. (2003). "Effect of foundation rocking on the seismic response of shear walls." *Canadian Journal of Civil Engineering*, 30(2), 360-365.
2. Arze, E. (1993). "Seismic design of industrial facilities." *Tectonophysics*, 218(1-3),23-41.
3. Chopra, A. K., and Yim, S. C. S. (1985). "Simplified Earthquake Analysis of Structures with Foundation Uplift." *Journal of Structural Engineering*, 111(4), 906-930.
4. FEMA 356. (2000). "Prestandard and Commentary for the Seismic Rehabilitation of Buildings." Prepared by the American Society of Civil Engineers for the Federal
5. Gazetas, G., Apostolou, M., and Anastasopoulos, J. (2003). "Seismic uplifting of foundations on soft soil, with examples from Adapazari (Izmit 1999 earthquake)."*BGA International Conference on Foundations, Innovations, Observations, Design and Practice, Sep 2-5 2003*, Dundee, United Kingdom, 37-49.
6. Grant, D. N., Blandon, C. A., and Priestley, M. J. N. (2005). "Modelling InelasticResponse in Direct Displacement-Based Design." European School of Advanced Studies in Reduction of Seismic Risk, Pavia, Italy.
7. Hogan, S. J. (1989). "On the dynamics of rigid-block motion under harmonic forcing." *Proceedings of the Royal Society of London, Series A, Mathematical and Physical Sciences*, 425(1869), 441-476.
8. Hogan, S. J. (1992). "The Effect of Damping on Rigid Block Motion under Harmonic
9. Housner, G. W. (1963). "The behaviour of Inverted pendulum structures during earthquakes." *Bulletin of the Seismological Society of America*, 53(2), 403-417.
10. Huckelbridge, A. A., and Clough, R. W. (1978). "Seismic Response of Uplifting Building Frame." *ASCE J Struct. Div*, 104(8), 1211-1229.
11. Ichinose, T. (1986). "Rocking Motion of Slender Elastic Body on Rigid Floor."*Bulletin of the New Zealand National Society for Earthquake Engineering*, 19(1), 18-27.
12. Ikegami, R., and Kishinouye, F. (1946). "A Study on the Overturning of Rectangular Columns in the case of the Nankai Earthquake on December 21, 1946." *Bulletin of Earthquake Research Institute*, 24, 49-55.
13. Ikegami, R., and Kishinouye, F. (1947). "A Study on the Overturning of a Rectangular Column." *Bulletin of Earthquake Research Institute*, 25, 11-18.
14. Ikegami, R., and Kishinouye, F. (1950). "The Acceleration of Earthquake Motion Deduced from Overturning of the Gravestones in Case of the Imaichi Earthquake on Dec. 26 1949." *Bulletin of Earthquake Research Institute*, 28, 121-127.

15. Ishiyama, Y. (1982). "Motions of Rigid Bodies and Criteria for Overturning by Earthquake Excitations." *Earthquake Engineering & Structural Dynamics*, 10, 630-650.
16. Jennings, P. C., and Bielak, J. (1973). "Dynamics of building-soil interaction." *Bulletin of the Seismological Society of America*, 63(1), 9-48.
17. Kelly, J. M. (1986). "Aseismic base isolation: review and bibliography." *Soil Dynamics and Earthquake Engineering*, 5(4), 202-216.
18. Koh, A. S., Spanos, P. D., and Roesset, J. M. (1986). "Harmonic rocking of rigid block on flexible foundation." *Journal of Engineering Mechanics*, 112(11), 1165-1180.
19. Lin, H., and Yim, S. C. S. (1996). "Nonlinear rocking motions. I: Chaos under noisy periodic excitations." *Journal of Engineering Mechanics*, 122(8), 719-727.
20. Makris, N., and Konstantinidis, D. (2003). "The rocking spectrum and the limitations of practical design methodologies." *Earthquake Engineering and Structural Dynamics*, 32(2), 265-289.
21. Meek, J. W. (1975). "Effects of Foundation Tipping on Dynamic Response." *Journal of the Structural Division, ASCE*, 101(7), 1297-1311.
22. Milne, J. (1881). "Experiments in observational seismology." *Transactions of the Seismological Society of Japan*, 3, 12-64.
23. Milne, J. (1908). *Seismology*, Kegan Paul, Trench, Trubner, & Co. Ltd., London.
24. Milne, J., and Omori, F. (1893). "On the Overturning and fracturing of Brick and Other Columns by Horizontally Applied Motion." *Seismological Journal of Japan*,17, 59-86.-
25. Muto, K., Umemura, H., and Sonobe, Y. (1960). "Study of overturning vibration of slender structures." *2nd World Conference on Earthquake Engineering*, Tokyo, Japan,1239.
26. Ogawa, N. (1977). "A study on Rocking and Overturning of Rectangular Column."
27. *Report of the National Research Center for disaster Prevention*(18), 14.
28. *Publications of the Earthquake Investigation Committee in foreign language*, 4(2),13-24.
29. Omori, F. (1902). "On the Overturning and Sliding of Columns." *Publications of the Earthquake Investigation Committee in foreign language*, 12(2), 8-27.
30. Pampanin, S. (2006). "Controversial aspects in seismic assessment and retrofit of structures in modern times: Understanding and implementing lessons from ancient heritage." *Bulletin of the New Zealand Society for Earthquake Engineering*, 39(2),120-134.
31. Priestley, M. J. N., Calvi, G. M., and Kowalsky, M. J. (2007). *Displacement-based seismic design of structures*, IUSS Press : Fondazione Eucentre, Pavia.
32. Priestley, M. J. N., Evison, R. J., and Carr, A. J. (1978). "Seismic Response of Structures Free to Rock on their Foundations." *Bulletin of the New Zealand National Society for Earthquake Engineering*, 11(3), 10.
33. Priestley, M. J. N., and Grant, D. N. (2005). "Viscous Damping in Seismic Design and Analysis." *Journal of Earthquake Engineering*, 9 (Special Issue 2), 27.*PCI Journal*, 44(6), 42-67.

34. Psycharis, I. N. (1991). "Effect of base uplift on dynamic response of SDOF structures." *Journal of Structural Engineering*, 117(3), 733-754.
35. Psycharis, I. N. (2008). "Investigation of the dynamic response of rigid footings on tensionless Winkler foundation." *Soil Dynamics and Earthquake Engineering*, 28(7),577-591.
36. Psycharis , I. N., Papastamatiou, D. Y., and Alexandris, A. P. (2000). "Parametric investigation of the stability of classical columns under harmonic and earthquake excitations." *Earthquake Engineering & Structural Dynamics*, 29, 1093-1109.
37. Seed, H. B., and Idriss, I. M. (1970). "Soil Moduli and Damping Factors for Dynamic Response Analyses." *EERC 70-10*, Earthquake Engineering Research Center,University of California, Berkeley.
38. Sharpe, R. D., and Skinner, R. I. (1983). "The Seismic Design of an IndustrialChimney with Rocking Base." *Bulletin of the New Zealand Society for Earthquake Engineering*, 16(2), 98-106.
39. Shenton, H. W., and Jones, N. P. (1991). "Base excitation of rigid bodies. I.Formulation." *Journal of Engineering Mechanics*, 117(10), 2286-2306.
40. Spanos, P. D., and Koh, A.-S. (1984). "Rocking of rigid blocks due to harmonic shaking." *Journal of Engineering Mechanics*, 110(11), 1627-1642.
41. Toranzo, L. A., Carr, A. J., and Restrepo, J. I. (2001). "Displacement Based Design of Rocking Walls Incorporating Hysteretic Energy Dissipators." *7th International Seminar on Seismic Isolation, Passive Energy Dissipation and Active Control of Vibrations of Structures*, Assisi, Italy, 10.244
42. Veletsos, A. S., and Verbic, B. (1973). "Vibration of Viscoelastic Foundations."*Earthquake Engineering and Structural Dynamics*, 2(1), 87-102.
43. Wong, C. M., and Tso, W. K. (1989). "Steady state rocking response of rigid blocks part 2: experiment." *Earthquake Engineering & Structural Dynamics*, 18(1), 107-120.
44. Xu, C., and Spyrakos, C. C. (1996). "Seismic analysis of towers including foundation uplift." *Engineering Structures*, 18(4), 271-278.
45. Yim, C.-S., and Chopra, A. K. (1983a). "Effects of Transient Foundation Uplift on Earthquake Response of Structures." *UCB/EERC-83/09*, Earthquake Engineering Research Center, University of California, Berkeley.
46. Yim, C.-S., and Chopra, A. K. (1983b). "Effects of transient foundation uplift on earthquake response of structures." *UCB/EERC-83/09*, University of California,Berkeley.
47. Yim, S. C. S., and Chopra, A. K. (1984a). "Dynamics Of Structures On Two-Springs Foundation Allowed To Uplift." *Journal of Engineering Mechanics, ASCE*, 110(7),1124-1146.
48. Yim, S. C. S., and Chopra, A. K. (1984b). "Earthquake Response of Structures with Partial Uplift on Winkler Foundation." *Earthquake Engineering & Structural Dynamics*, 12, 263-281.
49. Yim, S. C. S., and Chopra, A. K. (1985). "Simplified Earthquake Analysis Of Multistory Structures With Foundation Uplift." *Journal of Structural Engineering*,111(12), 2708-2731.

50. Yim, S. C. S., Chopra, A. K., and Penzien, J. (1980). "Rocking Response of Rigid Blocks to Earthquakes." *Earthquake Engineering & Structural Dynamics*, 8, 565-587.
51. Zhang, J., and Makris, N. (2001). "Rocking response of free-standing blocks under cycloidal pulses." *Journal of Engineering Mechanics*, 127(5), 473-483.

COMBINATIONAL RULES

52. International Conference of Building Officials (ICBO). Uniform Building Code, Vol. 2, Structural Engineering Design Provisions, Whittier, CA, 1997; 492.
53. American Society of Civil Engineers. Seismic Analysis of Safety Nuclear Structures and Commentary on Standard for Seismic Analysis of Safety Related Nuclear Structures, New York, 1986; 91.
54. Nutt RV. ATC—32: Provisional recommendations for the seismic design of bridges. Proceedings of the 4th Caltrans Seismic Workshop, California Department of Transportation, Sacramento, CA, 1996.
55. Newmark NM. Seismic design criteria for structures and facilities, trans-Alaska pipeline system. Proceedings of the U.S. National Conference Earthquake Engineering, EERI, 1975; 94–103.
56. Building Seismic Safety Council. NEHRP recommended provisions for seismic regulations for new buildings. FEMA302, Washington, DC, 1997.
57. California Department of Transportation (Caltrans). Bridge Design Specifications, Sacramento, CA, June 1990.
58. Rosenblueth E, Contreras H. Approximate design for multicomponent earthquakes. Journal of Engineering Mechanics, ASCE, 1977; 103:895 –911.
59. Smeby W, Der Kiureghian A. Modal combination rules for multicomponent earthquake excitation. Earthquake Engineering and Structural Dynamics, 1985; 13:1–12.
60. Lopez OA, Torres R. The critical angle of seismic incidence and the maximum structural response. Earthquake Engineering and Structural Dynamics 1997;26:881–894.
61. Menun C, Der Kiureghian A. A replacement for the 30%, 40% and SRSS rules for multi-component seismic analysis, Earthquake Spectra 1998; 14(1):153 –156.
62. Anastassiadis K. Directions sismiques defavorables et combinaisons defavorables des efforts. Annales de I'I.T.B.T.P., No. 512, Mars–Avril, 1993; 83–99 (in French).
63. Anastassiadis K, Avramidis IE, Panetsos PK. Earthquake resistant design of structures under three-component orthotropic seismic excitation. Proceedings of the XIth European Conference on Earthquake Engineering, Paris, France, 6–11 September, 1998.
64. Lopez OA, Chopra AK, Hernandez JJ. Critical response of structures to multicomponent earthquake excitation. Earthquake Engineering and Structural Dynamics 2000; 29(12):1759 –1778.
65. Penzien J, Watabe M. Characteristics of 3-dimensional earthquake ground motion. Earthquake Engineering and Structural Dynamics 1975; 3:365 –374.

66. Chopra AK. Dynamics of Structures: Theory and Applications to Earthquake Engineering (2nd edn). Prentice- Hall: SaddleRive r, NY, 2001.
67. Newmark NM, Hall WJ. Vibration of Structures Induced by Ground Motion. Shock and Vibration Handbook (2nd edn). McGraw Hill: New York, 1976.
68. Clough, R. W. and Penzien, J. *Dynamic of Structures*, 2nd ed., McGraw Hill, New York [1993].
69. Correnza, J. C. and Hutchinson, G. L. [1994] "Effect of transverse load resisting elements on inelastic response of eccentric-plan buildings," *Earthquake Engineering and Structural Dynamics* **23**, 75–89.
70. De Steffano, M. and Faella, G. [1996] "An evaluation of the inelastic response of systems under biaxial seismic excitations," *Engineering Structures* **18**(9), 724–731.
71. Der Kiureghian, A. [1981] "A response spectrum method for random vibration analysis of MDOF systems," *Earthquake Engineering and Structural Dynamics* **9**, 419–435.
72. Gao, L. and Haldar, A. [1995] "Nonlinear seismic response of space structures with PR connections," *International Journal of Microcomputers in Civil Engineering* **10**, 27–37.
73. Haldar, A. and Mahadevan, S. [2000] "*Probability, Reliability and Statistical Methods in Engineering Design*, John Wiley and Sons, New York.
74. Hernández, J. J. and López, O. A. [2003] "Evaluation of combination rules for peak response calculation in three-component seismic analysis," *Earthquake Engineering and Structural Dynamics* **32**, 1585–1602.